

THERMOMECHANICAL PROPERTIES OF POLYHEDRAL OLIGOMERIC SILSESQUOXANE – POLY(METHYL METHACRYLATE) NANOCOMPOSITES

by

EDWARD THOMAS KOPESKY

Bachelor of Chemical Engineering
Department of Chemical Engineering and Materials Science
University of Minnesota, Minneapolis, MN, 2000

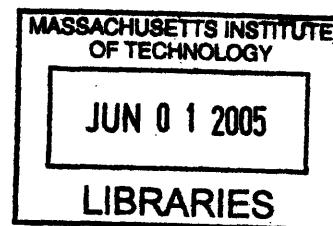
Submitted to the Department of Chemical Engineering
in partial fulfillment of the requirements for the degree of

DOCTOR OF PHILOSOPHY IN CHEMICAL ENGINEERING

at the

MASSACHUSETTS INSTITUTE OF TECHNOLOGY

JUNE 2005



© 2005 Massachusetts Institute of Technology. All rights reserved.

Signature of Author: _____
Department of Chemical Engineering
May 3, 2005

Certified by: _____
Robert E. Cohen
St. Laurent Professor of Chemical Engineering
Thesis Advisor

Certified by: _____
Gareth H. McKinley
Professor of Mechanical Engineering
Thesis Co-Advisor

Accepted by: _____
Daniel Blankschtein
Professor of Chemical Engineering
Chairman, Committee for Graduate Students

ARCHIVES

Thermomechanical Properties of Polyhedral Oligomeric Silsesquioxane-Poly(methyl methacrylate) Nanocomposites

by
Edward Thomas Kopesky

Submitted to the Department of Chemical Engineering on May 4, 2005
in partial fulfillment of the requirements for the degree of
Doctor of Philosophy in Chemical Engineering

Abstract

Poly(methyl methacrylate)s (PMMA) containing polyhedral oligomeric silsesquioxane (POSS) nanoparticles ($d \approx 1.5$ nm) were subjected to rheological, mechanical, and morphological tests to determine the effects that POSS has on the melt-state and solid-state properties of this commercially important amorphous polymer.

The effect of POSS on the rheological properties varied depending on the type of POSS cage and whether the POSS was covalently tethered to the PMMA backbone. A highly miscible acrylic-POSS species plasticizes PMMA, decreasing the glass transition temperature by approximately 10°C at a loading of 10 vol%. An essentially immiscible POSS species (cyclohexyl-POSS) does not alter the T_g of PMMA but is able to decrease slightly the zero shear-rate viscosity at low loadings. Incorporating a POSS filler (isobutyl-POSS) into an isobutyl-POSS-PMMA copolymer causes a significant increase in viscosity at all loadings.

The addition of POSS fillers to PMMA leads to an enhancement in the toughness in both slow-speed tension (strain rate = $3.3 \times 10^{-3} \text{ s}^{-1}$) and high rate split-Hopkinson pressure bar tests (strain rate = 1000 s^{-1}). In particular, the combined addition of two distinct POSS species – one miscible, one immiscible – led to the greatest enhancement in toughness and excellent reproducibility. A four-fold increase in tensile toughness was observed through the use of these two disparate POSS species.

Polyhedral oligomeric silsesquioxane macromers were copolymerized separately with a glassy polymer [PMMA, $T_g = 104^\circ\text{C}$] and a rubbery polymer [Poly(*n*-butyl acrylate), $T_g = -52^\circ\text{C}$] to determine the effect of the polymer glass transition temperature on the ultimate properties of an acrylic copolymer. Copolymers of POSS and PMMA show a significant decrease in T_g . Conversely, copolymers of POSS and poly(*n*-butyl acrylate) have significantly higher glass transition temperatures than the pure PBA. These also exhibit a more than two order of magnitude increase in the room temperature modulus measured in DMA and tensile tests. The increase in modulus was due to nanocrystallites of POSS within the butyl acrylate matrix.

Thesis Supervisors: Robert E. Cohen, St. Laurent Professor of Chemical Engineering
Gareth H. McKinley, Professor of Mechanical Engineering

Acknowledgements

I first would like to acknowledge and thank my advisors: Bob Cohen and Gareth McKinley. They've helped guide me to a successful five-year completion of my doctorate. They've encouraged more often than they've badgered, they've given me confidence when I've needed it, and they've taught me not to equivocate, in speech or in print. I hope this work does only minimal damage to their reputations as great teachers and scholars.

I'd also like to thank the members of my thesis committee, Karen Gleason and Ken Beers, for giving of their time and knowledge, and Mary Boyce for her intellectual and financial support. I'd like to thank my collaborators: Dr. Tim Haddad at Edwards Air Force Base, and Dr. Alex Hsieh at the Institute for Soldier Nanotechnologies via the Army Research Lab. Without them, I would not be graduating for a while longer.

I would also like to thank the members of the Cohen group who made my time at MIT more fun and all the others who helped me with my experiments. Some of these people are, in no particular order, Michelle, Ben, Ryan, Sharon, Roger, Adam N., Adam M., Franco, Greg, among others. I'd also like to thank some of the friends I made outside of work: Wes and Lucy, Cynthia, Ken, Amy, David, Muiyiwa, Brian B., Steve, Brian Mahoney, and all whom I've forgotten. I'd also like to thank the Carrolls at the Salvation Army.

I'd like to acknowledge the professors who helped shape me at the undergraduate level: Ron Bieniek at Missouri-Rolla, whose Engineering Physics recitations scared me to death but also taught me the need for a correlation between performance and reward; Skip Scriven, whom I never dared call Skip as a lowly undergrad, for allowing a shy undergrad to have my name attached to his; Rina Tannenbaum, who pushed me to apply to graduate school when I had no plans of doing so; and Chris Macosko, the man whose Polymers class was most influential in directing my graduate course of study, for showing that you can be a world-class scientist and a sincere Christian.

My family has always been the most important thing in my life. My grandparents, Russ and Dorothy Nelson, have always been there for me and for that I am grateful. My grandpa's sense of humor inspires me, and my grandma's nurturing spirit has blessed all of us grandchildren immensely. I remember my grandmother Mary Kopesky, who passed away in 2002, for her gentleness and for the special bond she shared with my dad. My aunt and uncle John and Mary Helland have been two of the most important people in my life from the time I was born and I will always be thankful for their presence and their prayers. Tim, Shelly, and Sarah Helland, thanks for all the memories. I'd also like to thank my aunt Diane Kopesky, my aunt and uncle Mike and Beth Nelson, my aunt Sue El-Eid, and my cousins Christine, Mary, and Jeff(Seth) Lund.

I'd also like to acknowledge those to whom I'm not related by blood, but who I consider family in my heart. Bert and Cindy Schmitt, Dave and Anne Johnson, Jon and Marilyn Buesing, thanks for all the good times.

My three primary inspirations in life are music, humor, and sports. Musicians who've touched my soul are: Eric Johnson, Lindsey Buckingham, Ty Tabor; David Zaffiro, Les Carlsen("You plugged your ears, you chicken!"), Michael "Rock Star" Bloodgood; Bob Hartman and John Schlitt of Petra; Michael W. Smith; the guys from Stryper: Michael Sweet ("I'm not singing this ..."), Oz Fox, Robert Sweet, and even Tim Gaines; Geddy Lee and Alex Lifeson of Rush; Gordon Lightfoot, Mark Knopfler, Peter Gabriel, Dave Mustaine, Ken Tamplin, Bruce Hornsby, and Neil Diamond ("Forever in blue jeans, babe...").

Comedians who've enriched my life include: Rodney Dangerfield, Peter Sellers, Brian Regan, Laurel and Hardy, The Three Stooges; Michael Richards, Jason Alexander, Jerry Seinfeld et al. (*Seinfeld*); The Simpsons, Chevy Chase, Phil Hartman, Arnold Schwarzenegger (unintentionally funny), Dana Carvey, Chris Farley; Christopher Guest, Michael McKean, and Harry Shearer (*Spinal Tap*); Kelsey Grammer and John Ratzenberger; Weird Al Yankovic; G.W.

Bailey, George Gaynes, the late David Graf, Bobcat Goldthwait, Lance Kinsey(*Police Academy*); Robert Carradine, Donald Gibb, Curtis Armstrong (*Revenge of the Nerds*); Gene Wilder, Zero Mostel, Kenneth Mars, and Mel Brooks (*The Producers*); Madeline Kahn; and M. Emmet Walsh for his role in *The Jerk*.

Sports figures who've made life more fun have been: Kirby Puckett for Game 6 '91, Kent Hrbek for Game 6 '87 and for pulling Ron Gant off first in Game 2 '91, Gary Gaetti for putting "JESUS IS LORD" on his batting glove during introductions to the All-Star Game in 1988; Frank Viola for '87; Dan Gladden for the broken-bat double in Game 7 '91, Gene Larkin and Jack Morris for obvious reasons, and Randy Bush for the pinch-hits in '91; Bobby Jackson for the trip to the Final Four (yes, NCAA, it did happen), Willie Burton; Randy Moss for rebelling against the idiocy at Winter Park; Gary Anderson for being a class act after the devastating miss in 1999; Joey Browner, Keith "My arms are stronger than your gun" Millard, Scott Studwell; Dino Ciccarelli, for signing autographs for us at the car dealer in North Branch in the early 80s; Dan Nystrom for the kick against Penn State in 1999; Matt Koalska and Grant Potulny for the goals at the end of the title game against Maine in 2002. Special thanks to Denny Green for ending his torturous, dictatorial run as Vikings head coach in 2001.

Most importantly, I'd like to thank my immediate family. Thanks to my siblings – my older brother Andy, the one with whom I've shared the most Vikings-related sorrow and the person with whom I've seen dozens of great concerts (Stryper at Cornerstone 2001, King's X on the Dogman Tour, Megadeth at Roy Wilkins) and a few lousy ones (e.g. Metallica at Target Center, Tourniquet at Sonshine); my younger sister Emily, who should be commended for surviving with three brothers like us, and the person whose love for the late 80s-early 90s Saturday Night Live shows we all share; and my younger brother Jim, my co-architect of the most revolutionary idea in the history of mankind: The Jerk List – for all their encouragement through the years. At times I've been a good brother, often times not, but we're all grown up now and we're still speaking so that says something in itself.

Of course, how could I have ever become so great without the help of two great parents. Mom("The University of Kansas is in Kansas, right?") and Dad("We're Packers fans now"), I've never really told you, but I wouldn't trade you for any parents in the world (although I'd trade your bank accounts for Bill Gates's). You've always wanted what's best for all of us kids, and you've given more time than most parents would even dream. You took us on vacations (the Griswold-esque trip to CA in 1990), took us to sporting events (Twins games, high school hockey, Gopher sports), coached our lousy Parks & Rec teams when nobody else would, fed us, spanked us, watched *Office Space* with us for the first time more than once, raised us in a Christian home and instilled in us the importance of being a good steward of your faith. And Dad, you've even shown me that it's possible for a good and reasonably sane person to vote for a democrat (occasionally). Thanks for putting up with the webpage and all the fun I (and others) have had with it at your expense.

Last, of course, I'd like to thank my Minnie, my future wife, the only love of my life, Darlene. I'm glad I kept after you the first two times you told me to get lost. Third time's a charm, I guess. I can't wait to start our new life with little Macy in our new home. Here's to the future and all it holds for us. Since I'm part Scottish (of the McClellan clan), I'll use the words William Wallace spoke in *Braveheart*: "I love you. Always have. I'm going to marry you." Here's to many years of chicken fajitas, Chardonnay, and chocolate-covered strawberries.

I've read confusing fiction, and lived a contradiction, and I've wondered where on earth I've been.
I've known a love forever, a Truth I couldn't sever, a chord that flows a free as wind.
I've stood on the mountain and drank from the fountain and poured it all out on the floor.
Turned my back to the glory and walked the tenth story and come back to knock on Your door.
On...my life going by

"Life Going By" by Ty Tabor

TABLE OF CONTENTS

<i>List of Figures</i>	8
<i>List of Tables</i>	13
CHAPTER 1: Introduction	14
1.1 Filled Polymers: From the micro to the nano	14
1.2 Silicones	18
1.2.1 Silicone Resins.....	18
1.2.2 Silsesquioxanes.....	20
1.2.3 Polyhedral Oligomeric Silsesquioxanes.....	21
1.3 The Present Study	23
References	24
CHAPTER 2: Thermomechanical Properties of Poly(methyl methacrylate)s Containing Crystallizable Polyhedral Oligomeric Silsesquioxanes (POSS)	28
2.1 Introduction	28
2.2 Experimental Section	32
2.2.1 Synthesis of High Molecular Weight Polymers.....	32
2.2.2 Additional Materials	34
2.2.3 Blend Preparation	35
2.2.4 X-ray Diffraction	35
2.2.5 Differential Scanning Calorimetry.....	36
2.2.6 Rheological Characterization.....	36
2.3 Results	36
2.3.1 Thermal and Morphological Characterization of POSS-Homopolymer Blends.....	36
2.3.2 Thermal and Morphological Characterization of POSS-PMMA Copolymers and Copolymer Blends.....	41
2.3.3 Rheology.....	46
2.4 Discussion	51
2.4.1 Time-Temperature Superposition (TTS)	61
2.5 Conclusions	67
References	69
CHAPTER 3: Miscibility and Viscoelastic Properties of Acrylic Polyhedral Oligomeric Silsesquioxane-Poly(methyl methacrylate) Blends	72
3.1 Introduction	72
3.2 Experimental Section	75
3.2.1 Materials	75
3.2.2 Hydrogenation of (Methacryloxypropyl) _n (SiO _{3/2}) _n	75
3.2.3 Solution Blending and Sample Preparation	76
3.2.4 Thermal and Morphological Characterization	76
3.2.5 Rheological Characterization.....	77
3.3 Results and Discussion	77
3.3.1 Differential Scanning Calorimetry.....	77
3.3.2 Wide Angle X-ray Diffraction.....	82

3.3.3 Rheology.....	84
3.3.4 Time-Temperature Superposition and Free Volume.....	88
3.3.5 Thermomechanical Analysis.....	91
3.4 Conclusions	96
References	97
<i>CHAPTER 4: Rheological Properties of Blends Containing an Acrylic Polyhedral Silsesquioxane and an Acrylic Oligomer</i>	<i>100</i>
4.1 Introduction	100
4.2 Experimental Section	101
4.2.1 Oligomer Synthesis.....	101
4.2.2 Blending.....	103
4.2.3 Differential Scanning Calorimetry.....	104
4.2.4 Rheology.....	104
4.3 Results	104
4.3.1 Differential Scanning Calorimetry.....	104
4.3.2 Linear Viscoelastic Properties	106
4.3.3 Viscometric Properties.....	109
4.4 Discussion	111
4.5 Conclusions	121
References	121
<i>CHAPTER 5: Mechanical Properties of POSS-PMMA Nanocomposites</i>	<i>123</i>
5.1 Introduction	123
5.2 Experimental Section	125
5.2.1 Notes on nomenclature	125
5.2.2 Materials	126
5.2.3 Blending and Sample Properties.....	126
5.2.4 Mechanical Tests	127
5.3 Results	127
5.3.1 Slow-speed tension tests of PMMA and POSS-filled PMMA.....	127
5.3.2 Reproducibility of stress-strain results.....	135
5.3.3 Split-Hopkinson Pressure Bar and Notched IZOD Impact Testing	137
5.4 Discussion	141
5.5 Conclusions	155
References	156
<i>CHAPTER 6: In-situ Polymerized Acrylates Containing Isobutyl-POSS: Effect of Glass Transition Temperature on Self-Assembly and Properties</i>	<i>158</i>
6.1 Introduction	158
6.2 Experimental Section	160
6.2.1 Polymer Synthesis	160
6.2.2 Polymer Characterization	161
6.3 Results	161
6.3.1 In-situ polymerization of POSS-Poly(methyl methacrylate) copolymers.....	161
6.3.2 Wide angle x-ray Diffraction of POSS-PMMA copolymers	164

6.3.3 Thermomechanical Properties of POSS-PMMA copolymers.....	165
6.3.4 In-situ polymerization POSS-poly(<i>n</i> -butyl acrylate) copolymers.....	169
6.3.5 Wide angle x-ray diffraction of POSS-PBA copolymers.....	170
6.3.6 Thermomechanical Properties of POSS-PBA copolymers	171
6.3.7 Tensile Properties of POSS-PBA copolymers	174
6.4 Discussion.....	177
6.5 Conclusion.....	181
References	182
<i>CHAPTER 7: Conclusions and Future Work.....</i>	<i>184</i>
7.1 Conclusions	184
7.2 Future Work.....	185
7.2.1 Optimization of Mechanical Properties	185
7.2.2 Use of POSS in Elastomers for Shape Memory Applications	185
7.2.3 Adhesive Applications	187
<i>Appendices.....</i>	<i>188</i>
A.1 Stress-strain Properties of a Cyclohexyl-POSS-PMMA copolymer containing cyclohexyl-POSS filler.....	188
A.2 Rheological Properties of PMMA containing Trisilanol-Phenyl-POSS	191

LIST OF FIGURES

Figure 1.1 Size scales in filled polymers.....	14
Figure 1.2 Interparticle spacing in particle-filled polymers.	15
Figure 1.3 Schematic of POSS self-assembly.	17
Figure 1.4 Silicon-oxygen bonds in silicone resins.....	18
Figure 1.5 Schematic of Q, T, and D resins.	19
Figure 1.6 Structure of silesquioxanes.	21
Figure 1.7 Incompletely-condensed POSS cage.	23
Figure 2.1 Ternary composition diagram for POSS filler, POSS-PMMA copolymer, and PMMA homopolymer.	29
Figure 2.2 Wide angle x-ray diffraction (WAXD) patterns of cyclohexyl-POSS–PMMA blends.	37
Figure 2.3 DSC curves for PMMA homopolymer containing isobutyl-POSS.....	38
Figure 2.4 Heats of fusion per gram of isobutyl-POSS in POSS-PMMA blends.	39
Figure 2.5 WAXD patterns for isobutyl-POSS powder at 30°C and 110°C.....	40
Figure 2.6 WAXD patterns for isobutyl-POSS in a copolymer containing 25 wt% isobutyl-POSS on the chain.....	42
Figure 2.7 Transmission electron micrographs for blends of isobutyl-POSS in a copolymer containing 25 wt% isobutyl-POSS on the chain.....	43
Figure 2.8 Storage moduli G' and loss tangent for POSS-PMMA copolymers.....	45
Figure 2.9 Storage moduli G' and loss moduli G'' in filled copolymer blends.	48
Figure 2.10 Storage moduli G' and loss moduli G'' for PMMA homopolymer and for blends containing 5 vol% isobutyl-POSS and 5 vol% cyclohexyl-POSS.	49
Figure 2.11 Storage moduli G' for blends containing between 0 and 30 vol% cyclohexyl-POSS in PMMA homopolymer.	50
Figure 2.12 Normalized plateau moduli for the blend systems analyzed in the study.	52

Figure 2.13 Normalized zero shear-rate viscosities for the blend systems analyzed in the study.	53
Figure 2.14 Concentration shift factors for the different blend systems.	56
Figure 2.15 Schematic of reptating chain in a filled copolymer blend.....	60
Figure 2.16 Loss tangent for a 10 vol% cyclohexyl-POSS blend (a) unshifted; (b) shifted.	62
Figure 2.17 WLF plots for (a) cyclohexyl-POSS filled PMMA homopolymer; (b) filled copolymer.....	64
Figure 3.1 (a) Picture of a T ₁₀ methacryl-POSS cage; (b) clarity of blends containing 20 vol% methacryl POSS (hydrogenated and unhydrogenated).....	74
Figure 3.2 DSC curves for methacryl-POSS–PMMA blends (hydrogenated and unhydrogenated).....	78
Figure 3.3 Glass transition temperatures for methacryl-POSS–PMMA blends (hydrogenated and unhydrogenated).	80
Figure 3.4 WAXD patterns for (a) unmodified and (b) hydrogenated methacryl-POSS–PMMA blends.	82
Figure 3.5 Storage moduli G' and loss moduli G'' for unmodified methacryl POSS–PMMA blends.	85
Figure 3.6 Storage moduli G' and loss moduli G'' for hydrogenated methacryl-POSS–PMMA blends.	85
Figure 3.7 Shifted storage modulus curves for unmodified methacryl-POSS–PMMA blends.	86
Figure 3.8 Log-log plot of horizontal shift factor b_ϕ against the quantity $(1-\phi)$	88
Figure 3.9 Fractional free volume at $T_0 = 170^\circ\text{C}$ and at T_g for methacryl-POSS–PMMA blends.	90
Figure 3.10 Dynamic mechanical analysis of unmodified methacryl-POSS–PMMA blends: (a) E' ; (b) tan delta.....	92
Figure 3.11 Coefficient of Thermal Expansion (CTE) data for unmodified methacryl-POSS–PMMA blends.....	94
Figure 4.1 Size-exclusion chromatography curve for oligomeric methyl methacrylate.	102

Figure 4.2 DSC curves for methacryl-POSS–oligomeric MMA blends.	104
Figure 4.3 Glass transition temperatures of methacryl-POSS–oligomeric MMA blends.	105
Figure 4.4 Storage moduli G' and loss moduli G'' at $T = 0^\circ\text{C}$ for methacryl-POSS–oligomeric MMA blends.	106
Figure 4.5 Loss tangent at $T = 0^\circ\text{C}$ for methacryl-POSS–oligomeric MMA blends.	108
Figure 4.6 Storage moduli G' and loss moduli G'' at $T = -40^\circ\text{C}$ for methacryl-POSS.	109
Figure 4.7 Viscosity vs. shear rate at $T = 0^\circ\text{C}$ for methacryl-POSS–oligomeric MMA blends.	109
Figure 4.8 Viscosity vs. temperature for methacryl-POSS–oligomeric MMA blends.	110
Figure 4.9 Viscosity vs. volume fraction ϕ of POSS at $T = 20^\circ\text{C}$	111
Figure 4.10 $\log a_T$ vs. $1/T$ for methacryl-POSS–oligomeric MMA blends (inset shows flow activation energy ΔH).	112
Figure 4.11 Zero shear-rate viscosity vs. T_g/T for methacryl-POSS–oligomeric MMA blends.	113
Figure 4.12 Fits to the VFTH equation (Eq. 8) for methacryl-POSS and oligomeric MMA liquids.	114
Figure 4.13 Zero shear-rate viscosity vs. T_g/T plotted within the Angell framework for fragile and strong glass-forming liquids.	116
Figure 4.14 WLF plot $T_0=20^\circ\text{C}$ for methacryl-POSS–oligomeric MMA blends.	118
Figure 4.15 Normalized values of the fractional free volume f_0 for both oligomeric MMA and entangled PMMA.	120
Figure 5.1 Stress-strain behavior of PMMA modified with alumina nanoparticles (taken from Ash et al. 2004, <i>Macromolecules</i>).	124
Figure 5.2 Stress-strain behavior of unfilled PMMA in tension.	128
Figure 5.3 Optical Properties of POSS-PMMA blends.	129
Figure 5.4 Stress-strain behavior (in tension) of blends containing (a) cyclohexyl-POSS; (b) methacryl-POSS; (c) trisilanol-phenyl-POSS.	130
Figure 5.5 Dogbone samples after tensile testing.	131

Figure 5.6 Stress-strain behavior (in tension) of blends containing both cyclohexyl-POSS and methacryl-POSS.	133
Figure 5.7 Stress-strain properties (in tension) of (a) 5 wt% methacryl-POSS in PMMA; and (b) 5 wt% of both cyclohexyl-POSS and methacryl-POSS.....	136
Figure 5.8 Stress-strain behavior in Split-Hopkinson pressure bar high-rate tests.	137
Figure 5.9 True strain rate as a function of true strain in split-Hopkinson pressure bar tests.	138
Figure 5.10a Fraction of samples that yielded in split-Hopkinson pressure bar tests.	139
Figure 5.10b Notched IZOD impact energies of POSS-PMMA blends.....	140
Figure 5.11 Fracture surfaces for blends containing (a) 5 wt% methacryl-POSS and (b) 5 wt% trisilanol-phenyl-POSS.....	142
Figure 5.12 Side view of fracture dogbones containing (a) 5 wt% methacryl-POSS and (b) 5 wt% trisilanol-phenyl-POSS.	143
Figure 5.13 Fracture surfaces for blends containing (a) 5 wt% cyclohexyl-POSS and (b) 5 wt% of both cyclohexyl-POSS and methacryl-POSS.....	145
Figure 5.14 Wide angle x-ray diffraction patterns for blends containing only cyclohexyl-POSS and for blends containing both cyclohexyl-POSS and methacryl-POSS.	146
Figure 5.15 Side view of fracture dogbones containing (a) 5 wt% cyclohexyl-POSS and (b) 5 wt% of both cyclohexyl-POSS and methacryl-POSS.	148
Figure 5.16 Side view of more brittle blend containing 5 wt% of both cyclohexyl-POSS and methacryl-POSS.	149
Figure 5.17 (a) Fracture surface and (b) side view of a fracture dogbone containing 2.5 wt% of both cyclohexyl-POSS and methacryl-POSS.....	151
Figure 5.18 High magnification side views of fractured dogbones containing (a) 2.5 wt% of both cyclohexyl-POSS and methacryl-POSS and (b) 5 wt% of both cyclohexyl-POSS and methacryl-POSS.	152
Figure 5.19 Tensile properties of a 5 wt% cyclohexyl-POSS–PMMA blend compounded with 10 wt% of a cyclohexyl-POSS–PMMA copolymer.....	154
Figure 5.20 Fracture surface of a 5 wt% cyclohexyl-POSS–PMMA blend compounded with 10 wt% of a cyclohexyl-POSS–PMMA copolymer.....	154

Figure 6.1 Reaction scheme for in-situ polymerization of isobutyl-POSS–PMMA copolymers.	162
Figure 6.2 Optical clarity of 50 wt% isobutyl-POSS-PMMA copolymer.....	163
Figure 6.3 GPC curves for POSS-PMMA copolymers.	164
Figure 6.4 WAXD patterns for POSS-PMMA copolymers.	165
Figure 6.5 DSC curves for POSS-PMMA copolymers.	166
Figure 6.6 DMA curves for POSS-PMMA copolymers: (a) E' ; (b) loss tangent.	167
Figure 6.7 Arrhenius plot of frequency and beta transition temperature.....	168
Figure 6.8 Storage moduli G' and loss moduli G'' for POSS-PMMA copolymers.....	169
Figure 6.9 Reaction scheme for in-situ polymerization of isobutyl-POSS–PBA copolymers.	170
Figure 6.10 WAXD patterns for POSS-PBA copolymers.....	171
Figure 6.11 DSC curves for POSS-PBA copolymers.	172
Figure 6.12 Storage modulus E' as a function of temperature measured in dynamic mechanical analysis for POSS-PBA copolymers.	173
Figure 6.13 Loss tangent as a function of temperature measured in dynamic mechanical analysis for POSS-PBA copolymers.	174
Figure 6.14 Tensile stress-strain properties of POSS-PBA copolymers.	175
Figure 6.15 Qualitative pictures of deformation and recovery for POSS-PBA copolymers...	176
Figure 6.16 T_g as a function of POSS content in POSS-PMMA copolymers showing potential trajectories for more highly-filled copolymers.....	179
Figure 6.17 WAXD patterns for POSS-polyethylene copolymers (taken from Waddon and Coughlin, <i>Nano Letters</i> 2002).	181
Figure A.1 Tensile stress-strain behavior of cyclohexyl-POSS-filled copolymer.....	189
Figure A.2 Storage and loss moduli of PMMA containing trisilanol-phenyl-POSS.....	192

LIST OF TABLES

Table 1.1 Properties of Q, T, and D-type resins.	20
Table 2.1 Polymers Used in the Study.	34
Table 2.2 Quantitative DSC Results for POSS-filled PMMA homopolymer.	38
Table 2.3 Glass Transition Temperatures of POSS-PMMA copolymers.	41
Table 2.4 Glass transition temperatures and viscosities of POSS-copolymer blends.	44
Table 2.5 Rheological Properties of Unfilled, Entangled Polymers.	47
Table 2.6 WLF Parameters for POSS-homopolymer blends.	65
Table 2.7 WLF Parameters for POSS-copolymer blends.	65
Table 3.1 Properties of Methacryl-POSS-PMMA blends.	88
Table 4.1 Fragility parameters.	114
Table 4.2 WLF parameters for methacryl-POSS–oligomeric MMA blends.	118
Table 5.1 Nomenclature of POSS-PMMA nanocomposites.	126
Table 5.2 Tensile properties of POSS-PMMA nanocomposites.	134
Table 6.1 Composition and properties of POSS-PMMA copolymers.	162
Table 6.2 Beta transition temperatures measured in dielectric analysis for POSS-PMMA copolymers.	168
Table A.1 WLF Parameters for PMMA containing trisilanol-phenyl-POSS.	193

Chapter 1: Introduction

1.1 – Filled Polymers: From the micro to the nano

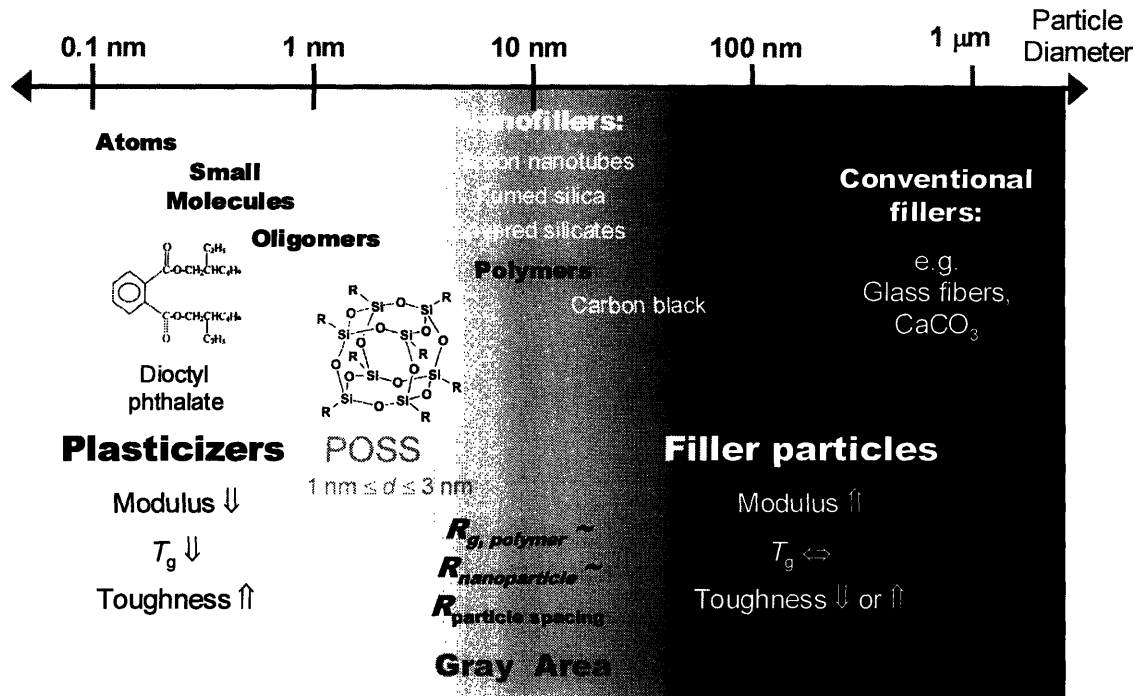


Figure 1.1 Schematic diagram showing important size scales in polymer-particle systems

In general, the mechanical properties of polymers are deliberately altered by two disparate types of additives: fillers and plasticizers. Classical fillers are composed of particles that are much larger than the polymer chain and act as reinforcing agents while plasticizers are molecular in nature and soften polymer matrices. (Rubber particles are another important toughening agent, however the present discussion is concerned with particles with stiffnesses at least as large as a typical glassy or semi-crystalline polymer matrix [$E \geq 1$ GPa].) Rigid fillers and plasticizers are usually thought of in black and white terms. Only recently has the transition between these two extremes been extensively studied.¹⁻⁷

In Figure 1.1 a scale diagram of the relevant sizes for polymer additives is shown. At the high end of the length scale ($d \geq 0.5 \mu\text{m}$) are classical fillers like glass fibers and mineral fillers like calcium carbonate. These are often added to polymers to increase their stiffness, reduce their cost and, in some cases, improve their toughness.⁸ Carbon black is a smaller-sized filler ($10 \text{ nm} \leq d \leq 50 \text{ nm}$) that is also a well-studied reinforcing agent, famous for its ability to bind rubber chains,⁹ imparting stiffness, tear resistance, and electrical conductivity.¹⁰ Other nanofillers listed in the gray area of Figure 1.1, which have received a vast amount of attention in academia and industry in recent years, have shapes that range from spheres (fumed silicas), to tubes (carbon nanotubes), to platelets (layered silicates). These fillers are utilized for their extremely small dimension(s) in order to dramatically increase the volume of polymer in the interfacial region (the “interphase”).

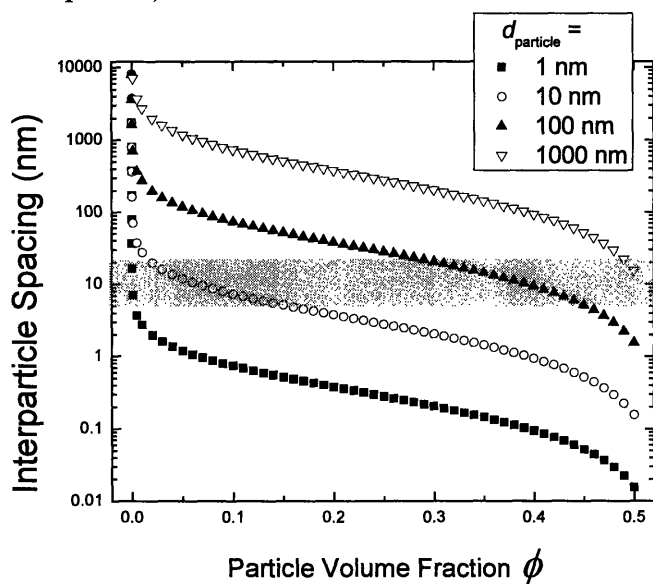


Figure 1.2
Interparticle spacing as a function of particle volume fraction for spherical particles on a simple cubic lattice. Data are plotted for four different particle sizes.

Figure 1.2 is a plot of the interparticle spacing d_{space} as a function of particle volume fraction ϕ in a composite system for spherical particle sizes ranging from $1 \text{ nm} \leq d \leq 1000 \text{ nm}$ (simple cubic lattice). The effect of particle size is obvious when one

observes the gray box denoting the normal range for the radius of gyration R_g for polymer chains ($5 \text{ nm} \leq R_g \leq 20 \text{ nm}$). For particles with $d = 1000 \text{ nm}$, the interparticle spacing is at least an order of magnitude larger than R_g up to a very high volume fraction of $\phi = 0.40$. When d is reduced to 100 nm , the interparticle distances drop by an order of magnitude yet still remain fairly large ($d_{\text{space}} > 50 \text{ nm}$) for $\phi \leq 0.15$. Further reduction of particle size to $d = 10 \text{ nm}$ results in a dramatic change whereby at a filler volume fraction of only $\phi = 0.02$, the interparticle spacing is only 20 nm . Thus at very small loadings of filler a substantial amount of the matrix volume will be in the “interphase”, where it will be subject to confinement¹¹ and adsorption^{12,13} effects. Depending on the particle-matrix interaction (attractive, repulsive, or neutral), tremendous differences in properties will be observed. This effect is one of the main reasons nanofillers have drawn so much interest, the idea that very small amounts yield significant property enhancements. (The high cost of nanofillers also necessitates this.)

By further reducing the size of the particles to $d = 1 \text{ nm}$ the point is reached at which all reasonable filler loadings lead to interparticle spacings well below R_g . It is at this particle size that even rigid particles may behave like solvents, as has been observed by Roberts et al. for polydimethylsiloxanes (PDMS) containing silicate nanoparticles.⁵ The addition of silicates with average diameter $d = 4.4 \text{ nm}$ led to an increase in the viscosity with increasing particle loading, however the addition of much smaller particles ($d = 0.7 \text{ nm}$) caused the viscosity to decrease with increasing particle loading. The authors claimed that the smaller particles were too small to allow polymer chain to adsorb onto their surfaces. These smaller particles had a mass of only 500 g/mol , much less than that of the polymer chains themselves ($M_w = 5,200\text{-}12,200 \text{ g/mol}$), compared with the

larger particles ($M_w = 14,100$ g/mol), which had a mass comparable to that of the polymer chains. Mackay et al.¹⁴ further demonstrated the effect of very small particles by blending crosslinked poly(styrene) particles ($d = 6\text{--}10$ nm) with linear, entangled poly(styrene) [$R_g = 7.5\text{--}15$ nm]. They reported as much as a 70% decrease in viscosity with the addition of nanoparticles and also a decrease in the glass transition temperature T_g . This plasticizing effect was attributed to an increase in free volume and constraint release modification,^{2,15} however the precise mechanisms remain unclear.¹ They observed an Einstein-like increase in viscosity when they blended in micron-sized polystyrene particles instead.

Regardless of the specific causes, it is clear that the size of a particle plays an important role in whether it behaves as a filler or a plasticizer when the particle dimensions approach those of the host polymer. This gives rise to the gray area in Figure 1.1 in which there is a transition from filler to plasticizer behavior between 100 nm and 1 nm. In particular, we note that a class of materials called polyhedral oligomeric silsesquioxanes (POSS) fall in this gray area where interfacial effects are amplified. The hybrid structure of POSS particles, with a silica core and a variable organic shell, offers a precise way to vary the polymer–nanoparticle interaction and thereby achieve either plasticization or reinforcement, depending on the application. A wide variety of studies have been carried out on POSS-containing copolymers and POSS-homopolymer blends¹⁶, probing their thermal,¹⁷⁻²⁴ morphological^{17-19,23,25-32}, mechanical^{28,30,31,33,34}, and self-assembly^{17,35} properties (Figure 1.3). POSS materials will be discussed further below.

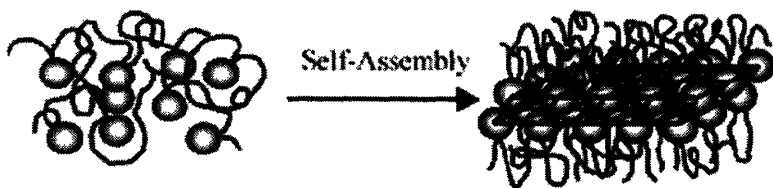


Figure 1.3
Schematic of POSS self-assembly (taken from Zheng, Coughlin et al., *Macromolecules*, 2004)

1.2 – Silicones

Many fillers are inorganic in nature; in particular, many are Si-O based. Most polymers, on the other hand, are carbon-based. Thus an inherent dissimilarity is present between many fillers and polymers. This has led to the development of hybrid organic-inorganic materials over the past fifty years.

1.2.1 – Silicone resins

The earth's crust is composed of 46.6 wt% oxygen and 27.7 wt% silicon. Not surprisingly, materials with a silicon-oxygen backbone are ubiquitous and have found practical uses in everyday life. Quartz, a crystalline form of silica (SiO_2), is the second most abundant mineral in the earth's crust (behind feldspar, which also contains mostly silicon and oxygen) and is often used in piezoelectric devices for precise timekeeping and weighing. Vitreous SiO_2 is optically transparent and is used in window glass.

Silicone resins, which are composed of a network of alternating atoms of silicon and oxygen with varying amounts of organic substituents (usually methyl or phenyl) attached to the silicon atoms, are among the most common commercially-produced silicon-oxygen materials. Figure 1.4 shows the different ways in which silicon atoms in a silicone resin can be bonded. The "Q" (silicate) and "T" (silsesquioxane) units represent silicon bonded to four and three

oxygens, respectively. Resins

with high Q and T content are

highly crosslinked, stiff

networks and are thermally and

dimensionally stable to very high

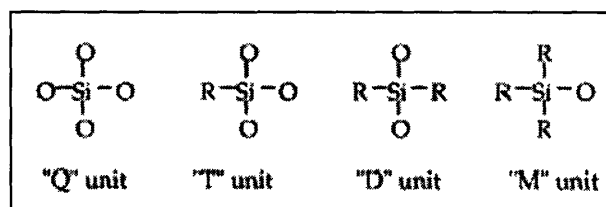


Figure 1.4 Terminology for silicon-oxygen bonding in silicone resins (image taken from Arkles et al., 2001)

temperatures. Silica is an all-Q resin. High D and M resins, on the other hand, are very flexible and, in many cases, liquids. An all D-resin with methyl R-groups is simply linear polydimethylsiloxane (PDMS). In Figure 1.5 a schematic of what a Q-resin, a T-resin, and a D-resin look like at the molecular level is shown.

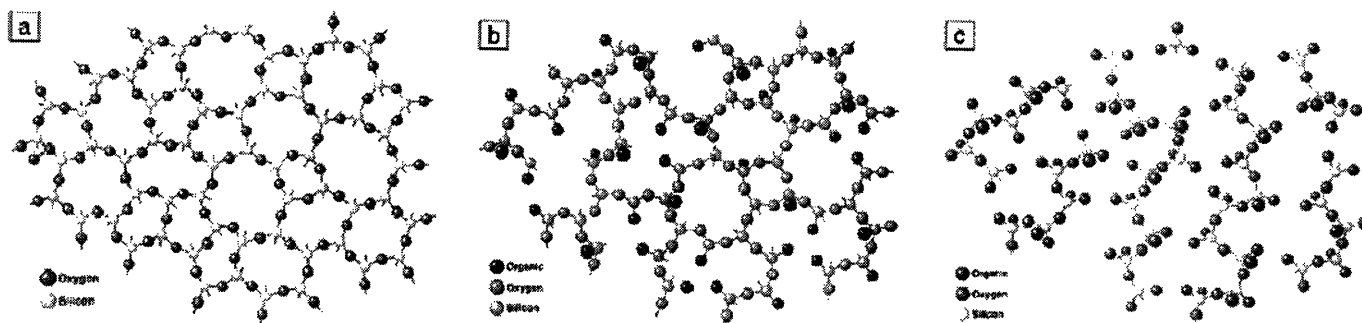


Figure 1. Hybrid organic–inorganic polymers can be visualized as successive organic substitutions of polyoxymetallates. (a) A “Q” structure, where four oxygen atoms are bound to a metal atom (silicon dioxide, or quartz in the example of silicon), gives rise to (b) a less rigid “T” resin when there is one organic substituent on each metal atom, and (c) linear “D” resins when there are two organic substituents on each metal atom (exemplified in the case of silicon by silicone oils).

Figure 1.5 Schematic diagram showing 2D representations of (a) a Q-resin (silicate); (b) a T-resin (silsesquioxane); and (c) a D-resin [image taken from Arkles, 2001].

Silicone resins have found widespread use as heat-, scratch-, and weather-resistant coatings, as separation media in high-performance liquid chromatography (HPLC) columns, and as pressure sensitive adhesives.³⁶ The relative amounts of Q, T, D, and M content can be varied in an almost limitless fashion to tailor the properties for the required application. In Table 1.1 the widely-varied properties for D, T, and Q-based materials can be observed. A pure D-resin, PDMS, has an extremely low T_g , very low room temperature modulus, and relatively high coefficient of thermal expansion. Poly(phenyl silsesquioxane), a ladder-like polymer made of T-linkages, has a high room temperature modulus, slightly lower coefficient of thermal expansion and it begins to degrade around 500°C before it passes through a glass transition. Amorphous silica, with

its Q linkages, is even stiffer, has a higher T_g , and has an extremely low coefficient of thermal expansion.

Name	Type	E [MPa]	T_g [°C]	CTE [°C ⁻¹ * 10 ⁻⁶]
Polydimethyl siloxane (PDMS)	D	0.2 - 0.36	-124	1000
Poly(phenyl silsesquioxane) (PPSQ)	T	1800	> 500	110
Vitreous SiO ₂	Q	72000	1173	9

1.2.2 – Silsesquioxanes

Silsesquioxanes (SSQs) are three-dimensional T-resins that contain one organic R-group per silicon atom. Figure 1.6 contains the different types of structures of SSQs. There are random SSQs, which have no perceivable order; ladder-like silsesquioxanes, such as poly(phenyl silsesquioxane)(PPSQ), which are rigid-rod chains; and caged silsesquioxanes, which have come to be known as polyhedral oligomeric silsesquioxanes (POSS, a trademark of Hybrid Plastics). Random SSQs are generally used in conjunction with D- and M-units for use in electrical-insulating coatings and pressure sensitive adhesives.³⁷ Ladder-like SSQs are used in photoresists and in interlayer dielectrics.³⁷ Caged SSQs (POSS) have yet to find a significant application but research in this area is extremely heavy at the moment. A high percentage of POSS studies have focused on using these nanoparticles to enhance the mechanical properties of polymers; in particular the mechanical properties of thermosets,³⁸⁻⁴⁷ but studies have also been undertaken on polyurethanes,^{48,49} polydimethylsiloxane networks,⁵⁰ poly(ethylene terephthalate),⁵¹ and immiscible blends of polystyrene and poly(methyl methacrylate).⁵²

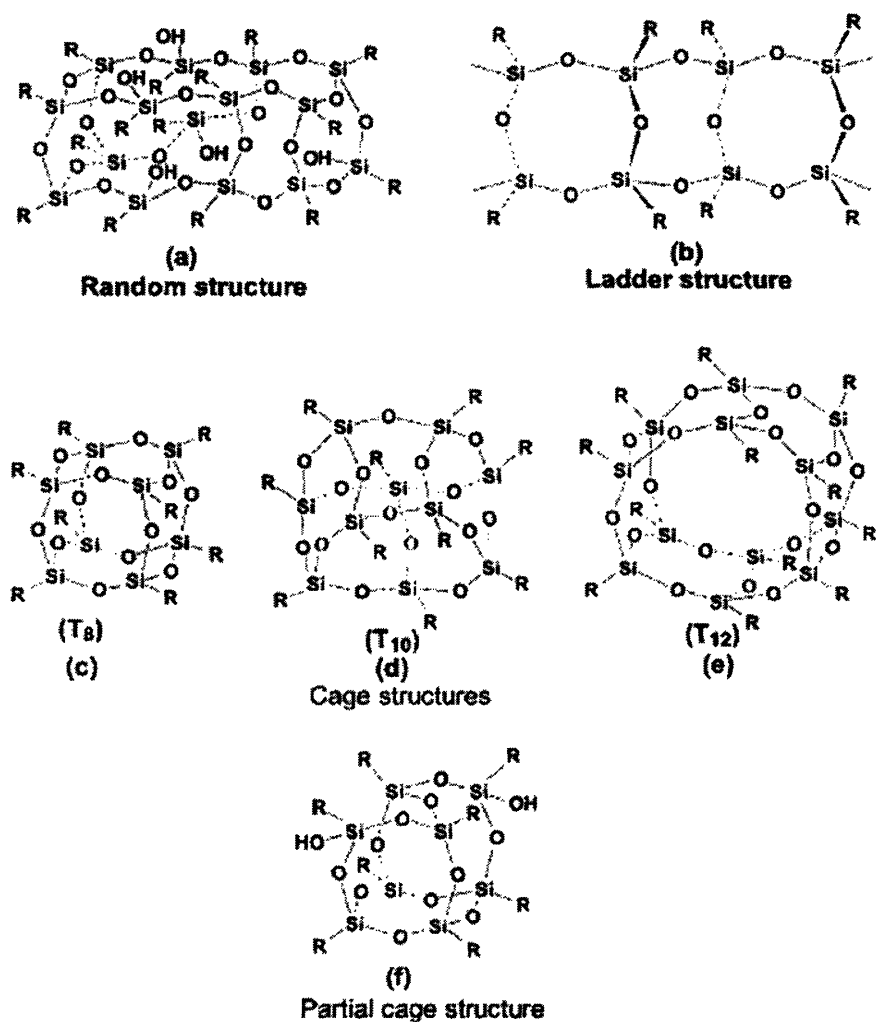


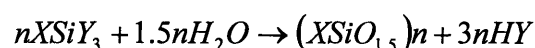
Figure 1.6 – Structure of silsesquioxanes
(taken from review by Li et al., 2001)

1.2.3. – Polyhedral Oligomeric Silsesquioxanes

Polyhedral oligomeric silsesquioxanes (POSS) are caged structures that vary in their cage size, the organic R-group positioned on the cage, and in whether the cage is fully condensed or not. They were first discovered by Scott⁵³ in 1946 and their caged structure was first identified through the crystallographic work of Barry et al. in 1955.⁵⁴ A surge of activity in this area has occurred in the past decade or so, with dozens of papers relating to POSS being published every year. These studies often focus on

specialized properties: in photoresists,⁵⁵ as components in PEO-electrolytes for rechargeable lithium batteries,^{56,57} as side-chain additives in electroluminescent polyfluorenes,^{58,59} as an intercalating agent in montmorillonite nanocomposites,⁶⁰ as components in low-dielectric polyimides,^{61,62} and as additives to resist atomic oxygen erosion.^{21,63}

In general, POSS cages are synthesized using trichlorosilanes according to the chemical reaction:⁶⁴



The synthesis often results in a variety of cage sizes and partially condensed cages which are then subjected to purification steps to obtain monodisperse lots of POSS particles.

The nomenclature for completely-condensed POSS cages is R_nT_n , where R represents the organic R-group, T represents the silsesquioxane linkage $SiO_{1.5}$, and n is the number of Si atoms in the cage. The most common cage size is T_8 ($d \approx 1.5$ nm), however T_6 , T_{10} , T_{12} , and T_{14} cages have also been identified.^{65,66} One can imagine the varied degrees of stiffness of the different T_n cages. A T_6 or a T_8 cage is very compact, with the Si-O core well-densified, resulting in a very stiff cage. T_8 cages typically are crystalline solids with high melting points ($T_m > 400^\circ C$). T_{10} and T_{12} cages are less stiff because of their less-compact nature. They have larger ring sizes and thus there is a non-trivial amount of free volume within these cages. A T_∞ cage may be approximately thought of as a ladder-like SSQ polymer like poly(phenyl silsesquioxane).

Polyhedral oligomeric silsesquioxanes are typically incorporated into a polymer matrix, and this can be done in two primary ways. The POSS cages may be either physically blended with a linear polymer or a thermosetting resin, or one corner of the POSS cage can be functionalized, thus allowing it to be incorporated into a copolymer. The choice of R-group is especially crucial in the former case, where POSS is known to phase separate into crystallites within the matrix.^{67,68} In the copolymer case, macromers containing functionalities including styryl,^{69,70} methacrylate,⁷¹ norbornyl,²⁸ among others have been produced. These macromers are produced from an incompletely condensed cage like the one shown in Figure 1.7, where one corner of a T₈ cage is open. A trichlorosilane with the desired functionality is reacted with this uncondensed cage to produce a POSS macromer¹⁷⁻²⁴ that can then be polymerized with the monomer of choice.

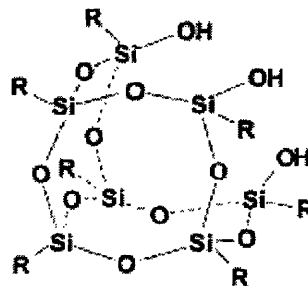


Figure 1.7 Incompletely-condensed POSS cage, often reacted with a trichlorosilane R'SiCl₃ to produce a functionalized POSS cage that can be incorporated into a polymer

1.3 – The Present Study

There is very little published work focusing on the effect POSS has on the melt-state properties of polymers. The void in the literature in this area was a major driving force in undertaking this study. A more specific aim of the study was to understand the way in which POSS cages impact the chain dynamics of polymers when incorporated as a tethered moiety, as an untethered filler, or when the two are combined. It is expected that these small particles, when well-dispersed, will create free volume and lead to some degree of plasticization, depending on the R-group. Chapter 2 reports on a study of the

rheological properties of PMMA containing both tethered and untethered crystallizable POSS species. The work in Chapter 3 analyzes a non-crystallizable POSS cage and its effect on the rheological and thermal properties of PMMA. The same non-crystallizable POSS species was blended with an oligomeric MMA ($M_w = 2190$ g/mol) and the properties of these blends are reported in Chapter 4.

There is also a dearth of published work on the solid state mechanical properties of POSS-filled thermoplastics, either glassy or semi-crystalline. Many studies in the past have attempted to toughen glassy polymers with other rigid fillers with minimal success. Whether POSS is able to toughen glassy PMMA will be reported in Chapter 5, along with the effects that different types of POSS (crystallizable or non-crystallizable) have on the stress-strain behavior of PMMA.

Finally, in Chapter 6, the in-situ polymerization of POSS-PMMA and POSS-(poly(*n*-butyl acrylates)) is presented in order to compare the effects that a low-melting POSS cage (isobutyl-POSS macromer, $T_m \approx 60^\circ\text{C}$) has on the thermomechanical properties of glassy PMMA ($T_g \approx 105^\circ\text{C}$) and rubbery PBA ($T_g \approx -55^\circ\text{C}$). The impact of the glass transition temperature of the matrix on the self-assembly properties of the POSS will be reported along with the resultant impact on the properties.

References

- (1) Glotzer, S. C. *Nature Materials* **2003**, *2*, 713.
- (2) Mackay, M. E.; Dao, T. T.; Tuteja, A.; Ho, D. L.; Van Horn, B.; Kim, H. C.; Hawker, C. J. *Nature Materials* **2003**, *2*, 762-766.
- (3) Cole, D. H.; Shull, K. R.; Baldon, P.; Rehn, L. *Macromolecules* **1999**, *32*, 771.
- (4) McCoy, J. D.; Curro, J. G. *Journal of Chemical Physics* **2002**, *116*, 9154.
- (5) Roberts, C.; Cosgrove, T.; Schmidt, R. G.; Gordon, G. V. *Macromolecules* **2001**, *34*, 538.
- (6) Starr, F. W.; Schroder, T. B.; Glotzer, S. C. *Macromolecules* **2002**, *35*, 4481.

- (7) Zhang, Q.; Archer, L. A. *Langmuir* **2002**, *18*, 10435.
- (8) Bartczak, Z.; Argon, A. S.; Cohen, R. E.; Weinberg, M. *Polymer* **1999**, *40*, 2347.
- (9) Leblanc, J. L. *Journal of Applied Polymer Science* **2000**, *78*, 1541.
- (10) Huang, J. C. *Advances in Polymer Technology* **2002**, *21*, 299.
- (11) Manias, E.; Chen, H.; Krishnamoorti, R.; Genzer, J.; Kramer, E. J.; Giannelis, E. P. *Macromolecules* **2000**, *33*, 7955.
- (12) Cosgrove, T.; Griffiths, P. C.; Lloyd, P. M. *Langmuir* **1995**, *11*, 1457.
- (13) Durning, C. J.; O'Shaughnessy, B.; Sawhney, U.; Nguyen, D.; Majewski, J.; Smith, G. S. *Macromolecules* **1999**, *32*, 6772.
- (14) Mackay, M. E.; Dao, T. T.; Tuteja, A.; Ho, D. L.; Van Horn, B.; Kim, H. C.; Hawker, C. J. *Nature Materials* **2003**, *2*, 762.
- (15) Mackay, M. E. *Personal communication*.
- (16) Phillips, S. H.; Haddad, T. S.; Tomczak, S. J. *Current Opinion in Solid State and Materials Science* **2004**, *8*, 21.
- (17) Carroll, J. B.; Waddon, A. J.; Nakade, H.; Rotello, V. M. *Macromolecules* **2003**, *36*, 6289.
- (18) Kopesky, E. T.; Haddad, T. S.; Cohen, R. E.; McKinley, G. H. *Macromolecules* **2004**.
- (19) Zheng, L.; Hong, S.; Cardoen, G.; Burgaz, E.; Gido, S. P.; Coughlin, E. B. *Macromolecules* **2004**, *87*, 8606.
- (20) Xu, H.; Kuo, S.-W.; Chang, F.-C. *Polymer Bulletin* **2002**, *48*, 469.
- (21) Gonzalez, R. I.; Phillips, S. H.; Hoflund, G. B. *Journal of Spacecraft and Rockets* **2000**, *37*, 463.
- (22) Huang, J. C.; He, C. B.; Xiao, Y.; Mya, K. Y.; Dai, J.; Siow, Y. P. *Polymer* **2003**, *44*, 4491.
- (23) Romo-Uribe, A.; Mather, P. T.; Haddad, T. S.; Lichtenhan, J. D. *Journal of Polymer Science Part B-Polymer Physics* **1998**, *36*, 1857.
- (24) Zheng, L.; Farris, R. J.; Coughlin, E. B. *Macromolecules* **2001**, *34*, 8034.
- (25) Zheng, L.; Waddon, A. J.; Farris, R. J.; Coughlin, E. B. *Macromolecules* **2002**, *35*, 2375.
- (26) Waddon, A. J.; Coughlin, E. B. *Chemistry of Materials* **2003**, *15*, 4555.
- (27) Waddon, A. J.; Zheng, L.; Farris, R. J.; Coughlin, E. B. *Nano Letters* **2002**, *2*, 1149.
- (28) Mather, P. T.; Jeon, H. G.; Romo-Uribe, A.; Haddad, T. S.; Lichtenhan, J. D. *Macromolecules* **1999**, *32*, 1194.
- (29) Larsson, K. *Arkiv for Kemi* **1960**, *16*, 209.
- (30) Hsiao, B. S.; White, H.; Rafailovich, M.; Mather, P. T.; Jeon, H. G.; Phillips, S.; Lichtenhan, J.; Schwab, J. *Polymer International* **2000**, *49*, 437.
- (31) Constable, G. S.; Lesser, A. J.; Coughlin, E. B. *Macromolecules* **2004**, *37*, 1276.
- (32) Barry, A. J.; Daudt, W. H.; Domicone, J. J.; Gilkey, J. W. *Journal of the American Chemical Society* **1955**, *77*, 4248.
- (33) Kim, G. M.; Qin, H.; Fang, X.; Sun, F. C.; Mather, P. T. *Journal of Polymer Science Part B-Polymer Physics* **2003**, *41*, 3299.
- (34) Zhang, W. H.; Fu, B. X.; Seo, Y.; Schrag, E.; Hsiao, B.; Mather, P. T.; Yang, N. L.; Xu, D. Y.; Ade, H.; Rafailovich, M.; Sokolov, J. *Macromolecules* **2002**, *35*, 8029.

- (35) Lamm, M. H.; Chen, T.; Glotzer, S. C. *Nano Letters* **2003**, *3*, 989.
- (36) Arkles, B. *MRS Bulletin* **2001**, *26*, 402.
- (37) Baney, R. H.; Itoh, M.; Sakakibara, A.; Suzuki, T. *Chemical Reviews* **1995**, *95*, 1409.
- (38) Lee, A.; Lichtenhan, J. *Macromolecules* **1998**, *31*, 4970.
- (39) Lee, A.; Lichtenhan, J. *Journal of Applied Polymer Science* **1999**, *73*, 1993.
- (40) Li, G. Z.; Wang, L. C.; Toghiani, H.; Daulton, T. L.; Koyama, K.; Pittman, C. U. *Macromolecules* **2001**, *34*, 8686.
- (41) Choi, J.; Yee, A. F.; Laine, R. M. *Macromolecules* **2003**, *36*, 5666.
- (42) Fu, B. X.; Namani, M.; Lee, A. *Polymer* **2003**, *44*, 7739.
- (43) Kim, G.-M.; Qin, H.; Fang, X.; Sun, F. C.; Mather, P. T. *Journal of Polymer Science Part B: Polymer Physics* **2003**, *41*, 3299.
- (44) Choi, J.; Yee, A. F.; Laine, R. M. *Macromolecules* **2004**, *37*, 3267.
- (45) Constable, G. S.; Lesser, A. J.; Coughlin, E. B. *Macromolecules* **2004**, *37*, 1276.
- (46) Matejka, L.; Strachota, A.; Plestil, J.; Whelan, P.; Steinhart, M.; Slouf, M. *Macromolecules* **2004**, *37*, 9449.
- (47) Strachota, A.; Kroutilova, I.; Kovarova, J.; Matejka, L. *Macromolecules* **2004**, *37*, 9457.
- (48) Fu, B. X.; Hsiao, B.; Pagola, S.; Stephens, P.; White, H.; Rafailovich, M.; Sokolov, J.; Mather, P. T.; Jeon, H. G.; Phillips, S.; Lichtenhan, J.; Schwab, J. *Polymer* **2001**, *42*, 599.
- (49) Liu, H.; Zheng, S. *Macromolecular Rapid Communications* **2005**, *26*, 196.
- (50) Pan, G.; Mark, J. E.; Schaefer, D. W. *Journal of Polymer Science Part B: Polymer Physics* **2003**, *41*, 3314.
- (51) Yoon, K. H.; Polk, M. B.; Park, J. H.; Min, B. G.; Schiraldi, D. A. *Polymer International* **2005**, *54*, 47.
- (52) Zhang, W. H.; Fu, B. X.; Seo, Y.; Schrag, E.; Hsiao, B.; Mather, P. T.; Yang, N. L.; Xu, D. Y.; Ade, H.; Rafailovich, M.; Sokolov, J. *Macromolecules* **2002**, *35*, 8029-8038.
- (53) Scott, D. W. *Journal of the American Chemical Society* **1946**, *68*, 356.
- (54) Barry, A. J.; Daudt, W. H.; Domicone, J. J.; Gilkey, J. W. *Journal of the American Chemical Society* **1955**, *77*, 4248-4252.
- (55) Eon, D.; Cartry, G.; Fernandez, V.; Cardinaud, C.; Tegou, E.; Bellas, V.; Argitis, P.; Gogolides, E. *Journal of Vacuum Science and Technology B* **2004**, *22*, 2526.
- (56) Maitra, P.; Wunder, S. L. *Electrochemical and Solid-State Letters* **2004**, *7*, A88.
- (57) Maitra, P.; Wunder, S. L. *Chemistry of Materials* **2002**, *14*, 4494.
- (58) Chou, C.-H.; Hsu, S.-L.; Dinakaran, K.; Chiu, M.-Y.; Wei, K.-H. *Macromolecules* **2005**, *38*, 745.
- (59) Lee, J.; Cho, H.-J.; Jung, B.-J.; Cho, N. S.; Shim, H.-K. *Macromolecules* **2004**, *37*, 8523.
- (60) Liu, H.; Zhang, W.; Zheng, S. *Polymer* **2005**, *46*, 157.
- (61) Leu, C. M.; Chang, Y. T.; Wei, K. H. *Macromolecules* **2003**, *36*, 9122.
- (62) Lee, Y. J.; Huang, J. M.; Kuo, S. W.; Lu, J. S.; Chang, F. C. *Polymer* **2005**, *46*, 173.

- (63) Brunsvold, A. L.; Minton, T. K.; Gouzman, I.; Grossman, E.; Gonzalez, R. *High Performance Polymers* **2004**, *16*, 303.
- (64) Li, G. Z.; Wang, L. C.; Ni, H. L.; Pittman, C. U. *Journal of Inorganic and Organometallic Polymers* **2001**, *11*, 123-154.
- (65) Franco, R.; Kandalam, A. K.; Pandey, R.; Pernisz, U. C. *Journal of Physical Chemistry B* **2002**, *106*, 1709.
- (66) Xiang, K. H.; Pandey, R.; Pernisz, U. C.; Freeman, C. *Journal of Physical Chemistry B* **1998**, *102*, 8704.
- (67) Blanski, R.; Phillips, S.; Chaffee, K. P.; Lichtenhan, J.; Lee, A.; Geng, H. P. *Polymer Preprints* **2000**, *41*, 585.
- (68) Kopesky, E. T.; Haddad, T. S.; Cohen, R. E.; McKinley, G. H. *Macromolecules* **2004**, *37*, 8992.
- (69) Haddad, T. S.; Lichtenhan, J. D. *Macromolecules* **1996**, *29*, 1996.
- (70) Haddad, T. S.; Viers, B. D.; Phillips, S. H. *Journal of Inorganic and Organometallic Polymers* **2001**, *11*, 155-164.
- (71) Lichtenhan, J. D.; Otonari, Y. A.; Carr, M. J. *Macromolecules* **1995**, *28*, 8435-8437.

*Chapter 2: Thermomechanical Properties of Poly(methyl methacrylate)s
Containing Crystallizable Polyhedral Oligomeric Silsesquioxanes
(POSS)*

[This work has been published previously, in slightly different form, in *Macromolecules* (2004)]¹

2.1 - Introduction

Polyhedral oligomeric silsesquioxanes (POSS) have drawn considerable interest due to their hybrid organic-inorganic structure which consists of a silica cage with organic R-groups on the corners.²⁻⁵ A generic POSS molecule ($R_8Si_8O_{12}$) is shown at the top of Figure 2.1. When covalently tethered to a polymer backbone, POSS has been shown to improve the thermo-oxidative stabilities of polymers,⁶ increase their glass transition temperatures,⁷⁻⁹ lower their zero-shear-rate viscosities,¹⁰ and increase the toughness of homopolymer blends.¹¹ POSS may be incorporated into a polymer matrix in two primary ways: chemically tethered to the polymer or as untethered filler particles, both of which are shown in Figure 2.1. (For brevity we will at times denote these limits as CO and F, respectively, to denote POSS copolymer and POSS filler.) In the copolymer case, one corner of the POSS macromer is functionalized, allowing it to be grafted onto the polymer backbone. Untethered POSS filler differs in that all corners of the cages have the same R-group and are non-reactive. The edges of the ternary composition diagram shown in Figure 2.1 indicate that there are three types of binary blends to consider: untethered POSS may be blended with either the homopolymer, poly(methyl methacrylate) (PMMA) in this case, or with a tethered-POSS-containing copolymer, which in this study has a PMMA backbone. The homopolymer and the copolymer may also be blended together. The interior of the triangular diagram represents the variety of ternary compositions that can be formulated. The present study focuses exclusively on the filler-homopolymer (F/HP) and the filler-copolymer (F/CO) sides of

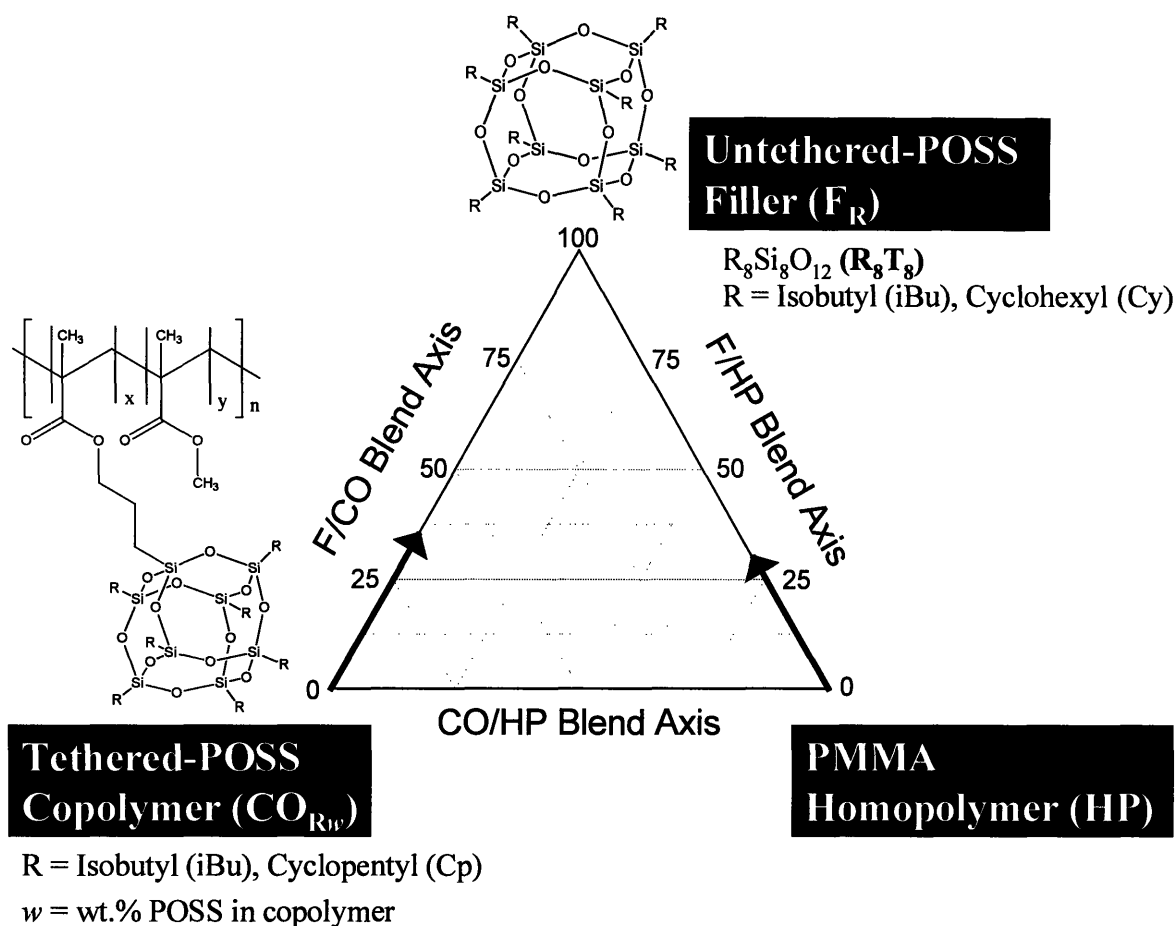


Figure 2.1 Ternary composition diagram for untethered-POSS filler (F), tethered-POSS containing copolymer with PMMA backbone (CO), and PMMA homopolymer (HP). The arrows represent the ranges of composition (in volume percent filler) analyzed in the present study.

the composition space in order to discern systematic differences, both quantitative and qualitative, between the thermomechanical properties of these two binary blend systems. The ranges of composition studied are indicated by the two arrows in Fig. 2.1.

A key factor in optimizing the properties of a POSS-polymer system is the thermodynamic interaction between the pendant R-group and the matrix. This controls the degree of dispersion of POSS in the matrix and thus the degree of property modification. Untethered POSS particles can disperse on a molecular scale (~1.5 nm) or as crystalline aggregates which can be on the order of microns in size.^{1,12} An important question is whether

both of these states of dispersion exist simultaneously, and to varying degrees, in a given POSS-polymer blend. Additional morphologies are possible when tethered-POSS particles are present. Their covalent attachment to the polymer backbone limits the length scale of association and, at high volume fractions, has been shown to lead to two-dimensional raft-like structures¹³ which are shaped similarly to clay platelets.¹⁴

Thermal and rheological characterization are important tools for comparing the behavior of the F/HP and the F/CO blend systems (Figure 2.1). Previous work on POSS rheology has been scarce, with few relevant publications.^{10,15,16} In a study by Romo-Urbe et al.(1998),¹⁰ poly(methyl styrenes) containing two different types of tethered-POSS [R = cyclopentyl (0-63 wt%) and R = cyclohexyl (0-64 wt%)] were tested in small amplitude oscillatory shear flow. One notable result was the appearance of a rubbery plateau ($\sim 10^3$ Pa) in the storage modulus G' at low frequencies for the 42 wt% cyclohexyl-POSS copolymer, indicating formation of a percolated network by the tethered-POSS particles. Low frequency plateaus in G' were not observed for copolymers containing 27 wt% cyclohexyl-POSS or 45 wt% cyclopentyl-POSS. For the 42 wt% cyclohexyl-POSS copolymer of molecular weight $M_w = 120,000$ g/mol and degree of polymerization $x_w = 420$, the viscosity was approximately half that of the homopolymer, which had M_w and x_w values of only 34,000 g/mol and 180, respectively. The study of Romo-Urbe et al. used only unentangled to very mildly entangled polymers, so no detailed information on plateau moduli and hence entanglement molecular weight (M_e) of the copolymers could be obtained.

A more recent study by Lee et al.¹⁵ used a novel synthetic technique to synthesize copolymers of styrene and vinyl-diphenylphosphine oxide that contained varied amounts of cyclohexyl-POSS (between 0 and 40 wt%) attached to the diphenylphosphine oxide units. These

polymers all had the same chain length. Contrary to the results of Romo-Urbe et al., this study showed an increase in the zero shear rate viscosity with increasing POSS content. In addition, the polymers also exhibited a higher plateau modulus with increasing POSS content. Unfortunately, no attempt was made by the authors to understand their results in light of the contrasting results of Romo-Urbe et al. In this chapter we will offer a possible explanation.

The rheological properties of blends of homopolymers and untethered-POSS were investigated by Fu et al.(2003)¹⁶ for ethylene-propylene copolymer containing 0, 10, 20 and 30 wt% methyl-POSS. At high frequencies, for loadings up to 20 wt%, the storage modulus G' remained essentially unchanged, only diverging at low frequencies, where a plateau of increasing magnitude ($10^2 - 10^3$ Pa) formed at high POSS loadings. Viscometric tests showed that the viscosity of the unfilled polymer and the 10 wt%-filled blend were virtually the same over a shear rate range of $10^{-4} - 10^{-1} \text{ s}^{-1}$, while the viscosities of the 20 wt% and 30 wt% blends were substantially higher over the same shear rate range. No information on rheological behavior at POSS loadings below 10 wt% was reported.

Studies of other (non-POSS) nanoparticles have demonstrated the unusual effect that very small (~ 10 nm) nanoparticles have on polymer matrices.^{17,18} In the work of Zhang and Archer (2002),¹⁷ poly(ethylene oxide) was filled with two types of 12 nm silica particles. In one case, the particles received no surface treatment, allowing them to hydrogen bond with the polymer matrix. Predictably, a dramatic enhancement in the linear viscoelastic properties was seen at very small loadings, with a low frequency plateau in the storage modulus G' appearing at a very small volume loading of particles $\phi \approx 2\%$. However, when the particles were treated with a PEO-like organosilane there was virtually no difference between the linear viscoelastic properties of the PEO and a 2 vol% blend. In fact, the loss moduli G'' were virtually indistinguishable between the

two samples in the terminal flow region, giving identical zero-shear-rate viscosities η_0 from linear viscoelasticity theory. This result suggests that polymers filled with very small nanoparticles ($d \sim 10$ nm) with weak polymer-filler interactions do not follow the classical theory for hard-sphere-filled suspensions.¹⁹

$$\eta_0(\phi) = \eta_0(0)\{1 + 2.5\phi + \dots\} \quad (1)$$

where ϕ is the particle volume fraction, which predicts a monotonic increase in viscosity with particle loading. This was further established by Mackay et al. (2003),¹⁸ who filled linear polystyrene melts with highly crosslinked 5 nm polystyrene nanoparticles. A substantial decrease in viscosity – more than 50% for some compositions – was reported, but no consistent trend in viscosity with increasing particle loading was found. The drop in viscosity was attributed to an increase in free volume and a change in conformation of the polystyrene chains in the matrix, although the precise mechanisms for these effects are still not well understood.²⁰

The present study seeks to determine if nanofilled polymer systems containing untethered POSS filler and tethered-POSS groups demonstrate similar unusual flow phenomena. The POSS nanoparticle-matrix interaction is different from those mentioned above in that there is the potential for molecularly dispersed nanoparticles, crystalline filler aggregates, and, in the filled copolymer case, nanoscopic POSS domains containing associated tethered and untethered-POSS groups. The combined effect of these states of dispersion is addressed in the present study.

2.2 - Experimental Section

2.2.1 - Synthesis of High Molecular Weight Polymers. The POSS

(R)₇Si₈O₁₂(propyl methacrylate) monomers, with R = isobutyl and cyclopentyl, were either synthesized according to existing literature procedures²¹⁻²⁴ or obtained from Hybrid Plastics (Fountain Valley, CA). Toluene (Fisher) was dried by passage through an anhydrous alumina

column, vacuum transferred and freeze-pump-thawed three times prior to use. Methyl methacrylate (Aldrich) was passed through an inhibitor-removal column (Aldrich), freeze-pump-thawed twice, vacuum transferred to a collection vessel and stored at -25°C in a glovebox under nitrogen. AIBN free radical initiator (TCI) was used as received. NMR spectra were obtained on a Bruker 400 MHz spectrometer and referenced to internal chloroform solvent (^1H and ^{13}C) or external tetramethylsilane (^{29}Si).

In a 500 mL jacketed reactor, (isobutyl) $_7\text{Si}_8\text{O}_{12}$ (propyl methacrylate) (40.0 g, 0.0424 mol), methyl methacrylate (120.0 g, 1.199 mol), 0.25 mole % AIBN (0.509 g, 3.10 mmol) and toluene (124 mL) were loaded under a nitrogen atmosphere to produce the isobutyl-POSS copolymer $\text{CO}_{2\text{iBu}25}$. The jacketed part of the reactor was filled with heating fluid maintained at 60°C and the reaction mixture stirred under a nitrogen atmosphere. Overnight the solution became very viscous. After 40 hours, the reactor was opened to air, diluted with CHCl_3 (200 mL) and allowed to stir overnight to form a less viscous solution. This was slowly poured through a small bore funnel into well-stirred methanol. A fibrous polymer was formed around the stir bar. After the addition was complete, the polymer was stirred for another hour before it was removed from the methanol/toluene mixture and dried overnight at 40°C under vacuum. A nearly quantitative yield of 158.1 grams of copolymer was isolated. A ^1H NMR spectrum was obtained to show that no residual unreacted POSS monomer was present (demonstrated by the absence of any peaks in the 5-6.5 ppm olefin region of the spectrum). Integration of the ^1H NMR spectra indicated that the mole % POSS in the copolymer (3.4 mole %) was the same as the % POSS in the monomer feed. The same synthesis procedure was used to produce the cyclopentyl version of the copolymer ($\text{CO}_{\text{Cp}25}$) and the high molecular weight homopolymer (HP2). The amounts of reagents used to synthesize $\text{CO}_{\text{Cp}25}$ were: (cyclopentyl) $_7\text{Si}_8\text{O}_{12}$ (propyl methacrylate) (40.0 g,

0.0389 mol), methyl methacrylate (120.0 g, 1.199 mol), 0.25 mole % AIBN (0.508 g, 3.09 mmol) and toluene (124 mL). A yield of 156.1 grams of copolymer was isolated. ¹H NMR spectra confirmed that the copolymer was monomer-free and that the mole % POSS in the copolymer (3.1 mole %) was the same as the % POSS in the monomer feed. The amounts of reagents used to synthesize the homopolymer HP2 were: methyl methacrylate (125.0 g, 1.249 mol), 0.25 mole % AIBN (0.513 g, 3.12 mmol) and toluene (125 mL). A yield of 123.4 grams of homopolymer was isolated. ¹H NMR spectra confirmed that the homopolymer was monomer-free. Molecular weight (M_w) and polydispersity (PDI) values for the copolymers and the homopolymer (Table 2.1) were determined using a Waters Gel Permeation Chromatograph (GPC) on a polystyrene standard with THF as eluent.

Table 2.1 Polymers Used in the Study

Polymer Name	POSS Type	Wt. % POSS	Mole % POSS	M_w (g/mol)	PDI	x_w
HP	---	0	0	80200	1.68	800
HP2	---	0	0	260000	1.89	2600
CO _{iBu15}	Isobutyl	15	2.1	205000	2.26	1740
CO1 _{iBu25}	Isobutyl	25	3.4	62700	1.73	490
CO2 _{iBu25}	Isobutyl	25	3.4	560000	2.64	4350
CO _{Cp25}	Cyclopentyl	25	3.1	720000	3.21	5590

2.2.2 - Additional Materials. A commercial PMMA resin from Atofina Chemicals (Atoglas V920, HP) was used for homopolymer blends due to its stability at high temperatures. A copolymerized PMMA containing 15 wt% tethered isobutyl-POSS (CO_{iBu15}) was purchased from Hybrid Plastics. A PMMA copolymer containing 25 wt% tethered isobutyl-POSS (CO1_{iBu25}) was purchased from Sigma-Aldrich for use in blend characterization. Molecular weight and polydispersity values for these polymers are reported in Table 2.1.

Two different POSS fillers [isobutyl-POSS (F_{iBu}) and cyclohexyl-POSS (F_{Cy})] were purchased from Hybrid Plastics. The molecular weights of these fillers are 873.6 and 1081.9

g/mol, respectively. The crystalline density of cyclohexyl-POSS was reported to be 1.174 g/cm³ by Barry et al.²⁵ The value for isobutyl-POSS has not been reported, but Larsson reported crystal densities for many POSS cages with similar structure.²⁶ For (n-propyl)-POSS, two crystal forms are present and the densities for these are 1.09 and 1.20 g/cm³. For isopropyl-POSS, a density of 1.20 g/cm³ was given, and for (n-butyl)-POSS a crystal density of 1.14 g/cm³ was reported. These data suggest that isobutyl-POSS should have a density at least as high as that of (n-butyl)-POSS. However, as is shown in the Results section, isobutyl-POSS has two crystal structures, which, if similar to (n-propyl)-POSS, would have different but similar densities. An estimate of 1.15 g/cm³ was thus taken as a reasonable median value for the density of the isobutyl-POSS filler. The density of the PMMA homopolymer HP was 1.19 g/cm³.

2.2.3 - Blend Preparation. Each of the filler species (cyclohexyl-POSS and isobutyl-POSS) was blended separately with the PMMA homopolymer HP in a DACA Instruments micro-compounder at 220°C for five minutes at compositions between 1 and 30 vol%. The isobutyl-POSS was also blended with the low molecular weight isobutyl-POSS copolymer CO1_{iBu25} at 175°C for five minutes at compositions between 2 and 35 vol%; the lower temperature was required to minimize thermal degradation of the copolymer. Rheological samples were made by compression-molding the extruded samples into disks 25 mm in diameter with a thickness of 2 mm. Molding temperatures were 190°C for the homopolymer blends and 150°C for the copolymer blends.

2.2.4 - X-ray Diffraction. Wide angle x-ray diffraction (WAXD) was carried out on two different diffractometers. Room temperature tests were performed on a Rigaku RU300 18kW rotating anode generator with a 250 mm diffractometer. Tests at room temperature and at an elevated temperature were performed in a Siemens 2D Small Angle Diffractometer configured in

Wide Angle mode using a 12kW rotating anode; these samples (powders mounted on Kapton tape) were tested in transmission. $\text{CuK}\alpha$ radiation was used in both cases.

2.2.5 - Differential Scanning Calorimetry (DSC). Thermal analysis was performed on a TA Instruments Q1000 DSC. Samples were heated at $5^\circ\text{C}/\text{min}$, cooled at the same rate, and then data were collected on the second heating ramp at the same heating rate. Glass transition temperatures (T_g) were determined from the inflection point in the heat flow vs. temperature curves. Melting points (T_m) and latent heats ($\Delta H/g_{\text{POSS}}$) of the isobutyl-POSS-filled homopolymer blends were determined from the peak and the area of each endotherm, respectively.

2.2.6 - Rheological Characterization. Rheological tests were performed on two separate rheometers. Linear viscoelastic tests on the high molecular weight homopolymer (HP2) and the high molecular weight copolymers ($\text{CO}_{\text{iBu}15}$, $\text{CO}_{\text{iBu}25}$ and $\text{CO}_{\text{Cp}25}$) were performed on a Rheometrics RMS-800 strain-controlled rheometer at strains between 0.1 and 1%, and at temperatures between 140°C and 220°C . All blend samples were rheologically characterized using a TA Instruments AR2000 stress-controlled rheometer. The filler-homopolymer blends were tested between 140°C and 225°C ; the filler-copolymer blends were tested between 120°C and 170°C . All rheology samples were tested in air using 25 mm parallel plates with gap separations of approximately 2 mm.

2.3 – Results

2.3.1 – Thermal and Morphological Characterization of POSS Homopolymer Blends (F/HP). X-ray diffraction patterns taken at room temperature for the cyclohexyl-POSS-filled homopolymer ($\text{F}_{\text{Cy}}/\text{HP}$) blend system are shown in Figure 2.2. It is clear that even at the lowest loading of 1 vol% filler ($1\text{F}_{\text{Cy}}/99\text{HP}$) appreciable POSS crystallinity is present in

the homopolymer blends. There is strong correspondence between the peak patterns of the blends and that of the pure cyclohexyl-POSS powder, and the peak locations agree with the results of Barry et al.²⁵ for cyclohexyl-POSS to within 0.01 nm. Sharp crystalline peaks were also observed at room temperature in the isobutyl-POSS–filled homopolymer blend system (F_{iBu}/HP) for all blend compositions. Thus at no point is complete molecular-level dispersion of either POSS species achieved.

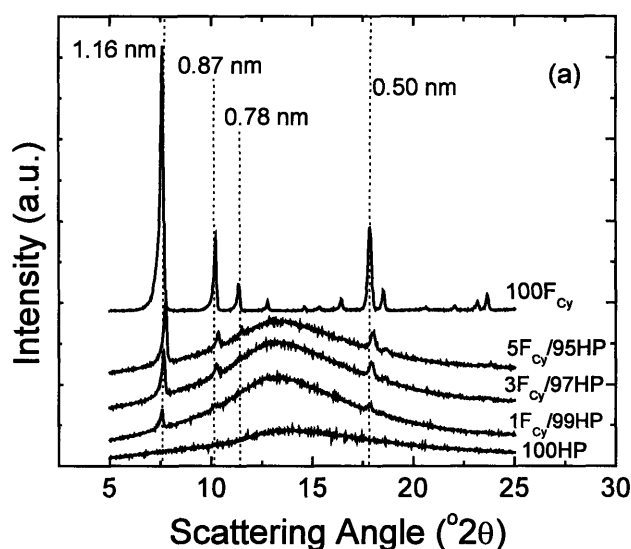


Figure 2.2. WAXD patterns for blends composed of cyclohexyl-POSS in PMMA homopolymer

The melting behavior of the POSS-homopolymer blends was quantified using DSC. In Table 2.2 the glass transition temperatures and, when applicable, melting point data are reported for both the cyclohexyl-POSS and the isobutyl-POSS blends with PMMA. The cyclohexyl-POSS-PMMA blends showed no melting transitions in the temperature range $30^{\circ}\text{C} \leq T \leq 225^{\circ}\text{C}$, only a single glass transition temperature of $T = 105^{\circ}\text{C}$ independent of cyclohexyl-POSS content. The isobutyl-POSS and its blends with PMMA showed more complex behavior. Representative DSC curves for the isobutyl-POSS–filled homopolymer system (F_{iBu}/HP) are reproduced in

Figure 2.3. In the pure isobutyl-POSS filler (100F_{iBu}), there are two endotherms: a sharp one at $T = 60^\circ\text{C}$ and a broader one at $T = 261^\circ\text{C}$. Similar results are seen in the F_{iBu}/HP blends, and the endotherms increase in magnitude with increasing POSS content. The locations and sizes of the endotherms for the F_{iBu}/HP system are reported in Table 2.2.

Table 2.2. Quantitative DSC results for POSS-filled PMMA Homopolymer

Blend	T_g ($^\circ\text{C}$)	T_m^1 ($^\circ\text{C}$)	ΔH_1 (J/g _{POSS})	T_m^2 ($^\circ\text{C}$)	ΔH_2 (J/g _{POSS})	$\Delta H_1/\Delta H_1^*$
100HP	105					
2.5F _{iBu} /97.5HP	105	51	1.34	---	0.00	0.11
5F _{iBu} /95HP	105	53	3.18	255	3.26	0.27
10F _{iBu} /90HP	103	54	4.90	263	11.4	0.42
30F _{iBu} /70HP	105	58	7.46	266	12.3	0.63
100F _{iBu}	106	60	11.8	261	16.1	1.00
1F _{Cy} /99HP	105					
3F _{Cy} /97HP	105					
5F _{Cy} /95HP	106					
10F _{Cy} /90HP	106					
20F _{Cy} /80HP	105					
30F _{Cy} /70HP ^b	106					

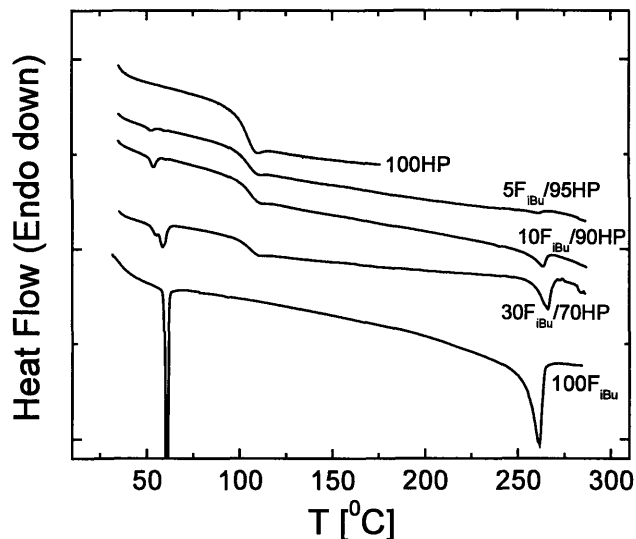


Figure 2.3. DSC curves for PMMA homopolymer filled with isobutyl-POSS. Two distinct endotherms are apparent in the more highly-filled samples, with the size of the endotherms proportionally larger at higher loadings.

In Figure 2.4 we plot the heat of fusion per gram of isobutyl-POSS filler in the F_{iBu}/HP samples as a function of POSS content. The horizontal dashed lines correspond to ΔH_1^* and ΔH_2^* , which are the latent heats for the isobutyl-POSS filler's low temperature transition ($T = 60^\circ\text{C}$) and high temperature transition ($T = 261^\circ\text{C}$), respectively. All points would fall on these lines if the isobutyl-POSS had the same degree of crystallinity in the blends as in its pure powder. However, the data show an increase in the heat of fusion per gram of POSS filler $\Delta H/g_{POSS}$ with increasing POSS content. The region of steepest increase is below 10 vol%. This indicates that at low loadings a large fraction of the POSS enters the polymer matrix as molecularly-dispersed nanoparticles. As the concentration of filler increases, a limiting value corresponding to the pure POSS powder is approached from below. This implies that a solubility limit of POSS nanoparticles exists in the PMMA matrix. Similar results were observed for the copolymer blend system's (F_{iBu}/CO_{1iBu25}) first endotherm, however the second endotherm of the filler ($T \sim 260^\circ\text{C}$) could be not be reached before extensive thermal degradation occurred. The cyclohexyl-POSS powder (F_{Cy}) showed no melting transition below 400°C .

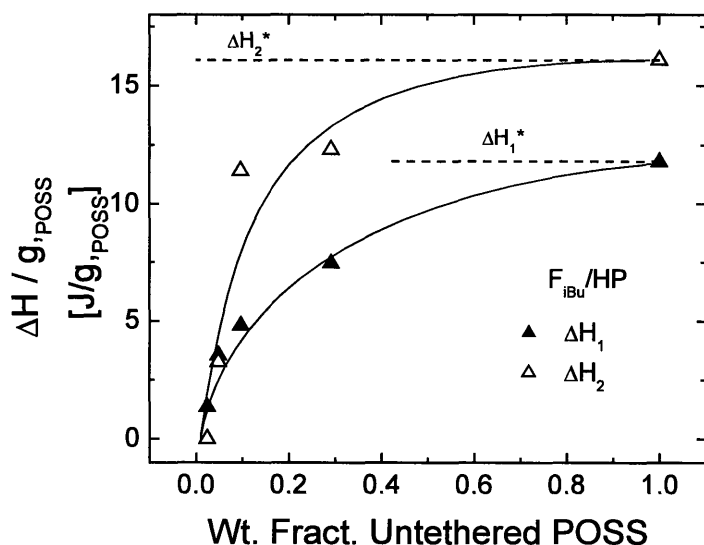


Figure 2.4. Heats of fusion per gram isobutyl-POSS in the sample for both thermal transitions of isobutyl-POSS–PMMA blends.

To determine the nature of the two endotherms in the isobutyl-POSS, the powder was heated in a sealed glass capillary from $T = 25^{\circ}\text{C}$ to $T = 280^{\circ}\text{C}$. There was no apparent change in the powder until 265°C , at which point the sample abruptly turned to liquid. Thus the high temperature transition corresponds to a melting point.

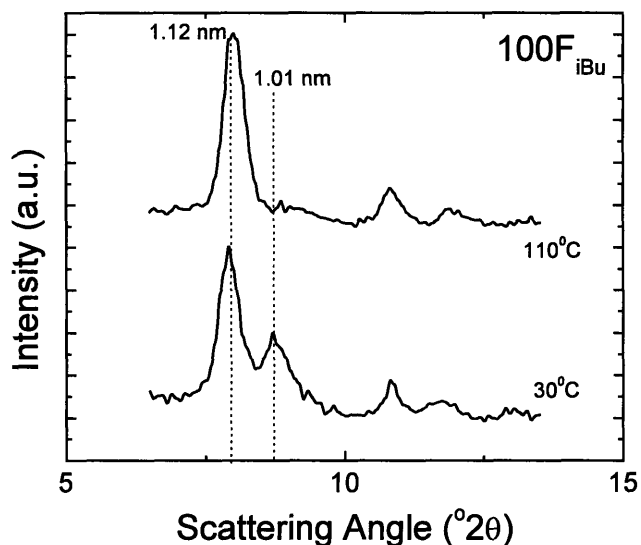


Figure 2.5. WAXD patterns for isobutyl-POSS powder taken below the first thermal transition of the powder (30°C) and also above (110°C).

Additional WAXD was performed on the isobutyl-POSS to examine the thermal transition at 60°C . A separate diffractometer equipped with a hot stage was used and diffraction patterns taken at 30°C and 110°C are shown in Figure 2.5. At 30°C two closely spaced peaks are present between $7^{\circ} < 2\theta < 10^{\circ}$. The smaller of these (at $d = 1.01 \text{ nm}$) is not present in the 110°C spectrum while the larger peak (at $d = 1.12 \text{ nm}$) has a slightly increased height and breadth at 110°C . This indicates that the thermal event at 60°C is likely a crystal-crystal transition, which have been observed in side-chain liquid crystalline polyacetylenes²⁷ and in various amphiphilic salts of ammonium, phosphonium, and pyridinium.²⁸⁻³⁰ The precise mechanism of this transition is unclear, however it appears that the isobutyl-POSS is present in two crystal forms below 60°C

and only one above that temperature. Larsson²⁶ reported two crystal forms for (n-propyl)-POSS, stating that the two forms differ in the packing of the propyl groups within the crystal.

Table 2.3
Glass Transition Temperatures of
POSS-PMMA Copolymers

Polymer	Wt.% POSS	T_g (C)
HP2	0	124
CO _{iBu15}	15	87
CO1 _{iBu25}	25	95
CO2 _{iBu25}	25	113
CO _{Cp25}	25	126

2.3.2 – Thermal and Morphological Characterization of POSS-PMMA Copolymers

(CO) and Copolymer Blends (F/CO). The glass transition temperatures measured in DSC of the synthesized PMMA and POSS-PMMA copolymers are reported in Table 2.3. In addition, two commercially purchased copolymers from Hybrid Plastics were tested. Two different R-groups were used: isobutyl and cyclopentyl. The isobutyl-POSS-PMMA copolymers show a decrease in the glass transition temperature T_g when compared with the pure PMMA, while the cyclopentyl-POSS-PMMA copolymer has a slightly higher glass transition temperature T_g . Mather et al. have shown a similar result for polystyrenes copolymerized separately with isobutyl-POSS and cyclopentyl-POSS.³¹ In the isobutyl-POSS case, the T_g decreased relative to the homopolymer, while in the cyclopentyl-POSS case, the opposite effect was observed. These contrasting effects are due to the relative melting temperatures of the POSS cages compared to the T_g of the polymer matrix. As is shown in Chapter 6, isobutyl-POSS cages tethered to a poly(*n*-butyl acrylate) backbone show the ability to self-assemble into nanocrystallites. These assemblies of POSS cages melt at approximately $T = 55^\circ\text{C}$. This melting point is far below the T_g of PMMA and should be nearly independent of the polymer backbone, thus one would expect

that isobutyl-POSS cages would be disordered as the PMMA matrix approaches its T_g (from below or above) and these disordered POSS cages not surprisingly plasticize the PMMA matrix, lowering the T_g . The cyclopentyl-POSS, on the other hand, has no discernible melting point below $T = 350^\circ\text{C}$ in DSC, and thus when tethered to a polymer chain it is likely to retain its POSS-POSS associations above the glass transition temperature of the PMMA. Thus the fact that the PMMA containing 25 wt% cyclopentyl-POSS retains its glass transition temperature while the one with 25 wt% isobutyl-POSS lowers the T_g is not surprising.

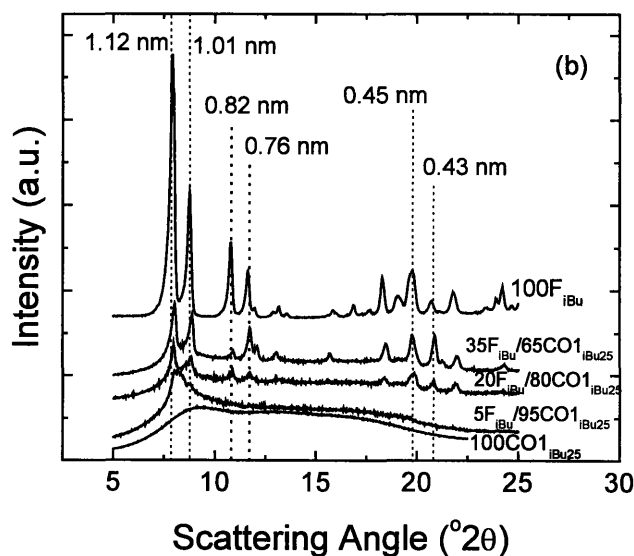


Figure 2.6. WAXD patterns for isobutyl-POSS in a copolymer containing 25 wt% isobutyl-POSS on the chain (CO1_{iBu25}).

The copolymer used in the blend studies was the relatively low molecular weight ($M_w = 63,000$ g/mol), but still mildly entangled, isobutyl-POSS-PMMA copolymer CO1_{iBu25}. The WAXD patterns for blends of isobutyl-POSS with CO1_{iBu25} are plotted in Figure 2.6. The diffraction pattern for the pure copolymer shows only a slight hump at $2\theta = 9.1^\circ$ ($d = 0.97$ nm). The absence of sharp peaks is consistent with previous WAXD studies of polymers containing tethered-POSS at comparable volume fractions.^{10,13} At 5 vol% isobutyl-POSS, a broad peak

forms which spans the 2θ range of the two highest peaks in the POSS powder spectrum ($7.5^\circ < 2\theta < 9^\circ$). At higher loadings, the peak pattern closely resembles that of the POSS powder. Based on sharper line widths in the spectrum of the 5 vol%-cyclohexyl-POSS-filled homopolymer ($5F_{Cy}/95HP$ in Figure 2.2) compared to those in the 5% isobutyl-POSS-filled copolymer ($5F_{iBu}/95CO1_{iBu25}$), it is clear that at low filler loadings there are substantially larger POSS crystals in the homopolymer blend. While the relative extents of crystallinity between the two types of blends are not easily determined from WAXD, the absence of any sharp peaks in the $5F_{iBu}/95CO1_{iBu25}$ blend indicates better nanodispersion of untethered-POSS at low loadings in the filled copolymer blend system compared to the filled homopolymer systems.

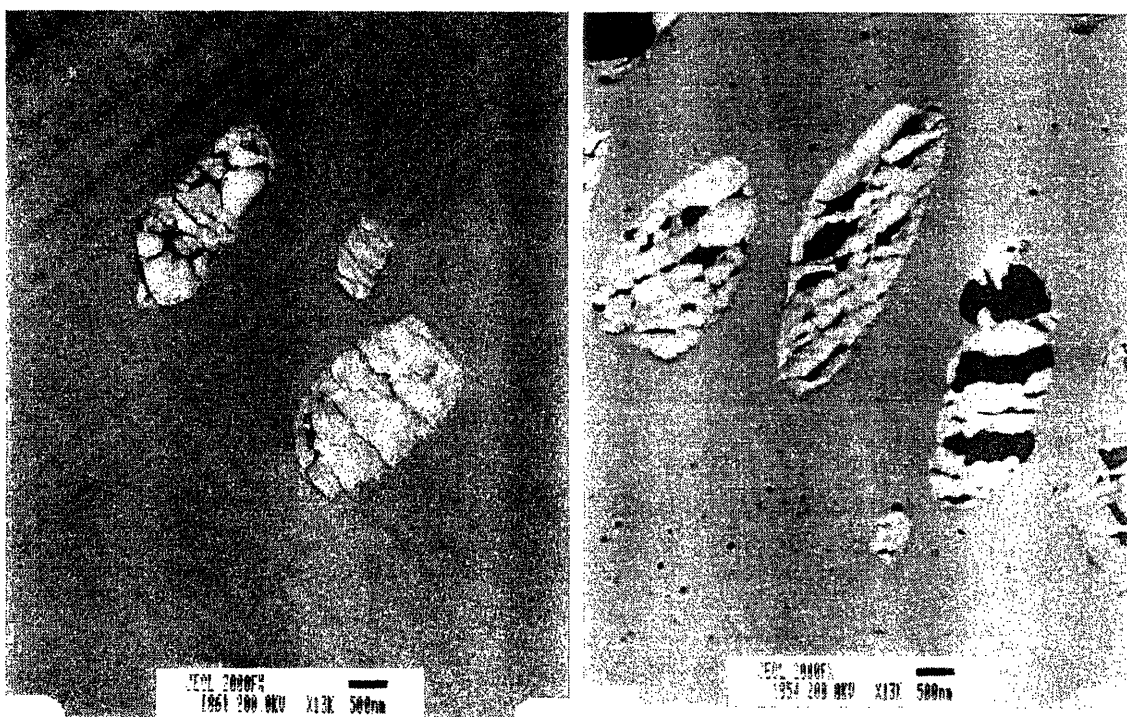


Figure 2.7 -- Transmission electron micrographs of blends containing isobutyl-POSS and the copolymer $CO1_{iBu25}$: (a) 12.5 wt% isobutyl-POSS filler; (b) 25 wt%

Transmission electron microscopy was performed on the filled copolymer blend system $F_{iBu}/CO1_{iBu25}$ in an attempt to observe the nanoscopic morphology. Figure 2.7 shows a TEM

micrograph for a 12.5 wt% blend and a 25 wt% blend of isobutyl-POSS in the copolymer CO1_{iBu25}. In Figure 2.7(a), there are sporadic potato-shaped domains ($d \approx 2 \mu\text{m}$) that are composed of crystalline isobutyl-POSS filler. These domains were not observed in a 5 wt% blend. At 25 wt% isobutyl-POSS filler, the domains are no longer sporadically distributed, but are instead regularly distributed throughout the matrix. In addition, small dark specks are visible in Figure 2.7(b). These domains of isobutyl-POSS filler, with diameters ranging from 10 to 75 nm, are not observed in Figure 2.7(a). This effect is consistent with a saturation of the matrix. At low loadings of POSS filler, the tethered-POSS on the copolymer chain greatly outnumbers the POSS filler cages (see Table 2.4). Thus, the copolymer allows the POSS filler to more completely disperse throughout the matrix. Above 20 wt% filler, the POSS filler outnumbers the POSS on the copolymer chain, causing the matrix to become saturated with dispersed filler. Above this point, the filler must necessarily start to phase separate into nanocrystallites, which are visible in Figure 2.7(b) but not in Figure 2.7(a). The presence of the micron-sized crystallites in Figure 2.7 may be due to incomplete distribution of the filler during the extrusion process.

Table 2.4. Glass Transition temperatures and viscosities in POSS-copolymer blends

Blend Composition	η_0 (Pa s)	T_g ($^{\circ}\text{C}$)	$N_{\text{Untethered}} /$
	($T_0 = 150^{\circ}\text{C}$)		$N_{\text{Tethered POSS}}$
100CO1 _{iBu25}	4.3×10^5	95	0.00
2F _{iBu} /98CO1 _{iBu25}	5.0×10^5	96	0.09
5F _{iBu} /95CO1 _{iBu25}	6.8×10^5	95	0.23
20F _{iBu} /80CO1 _{iBu25}	1.8×10^6	95	1.08
30F _{iBu} /70CO1 _{iBu25}	-----	103	1.85

Values of the glass transition temperature (T_g) were also obtained from DSC curves of the isobutyl-POSS-filled copolymer. Table 2.4 shows that there was no significant change in the glass transition temperature of the filled copolymer system (F_{iBu}/CO1_{iBu25}) for volume fractions ϕ

$\leq 20\%$ before an 8°C jump was observed in the 30 vol% blend. This is consistent with observations from the TEM showing evidence of matrix saturation above 20 wt%.

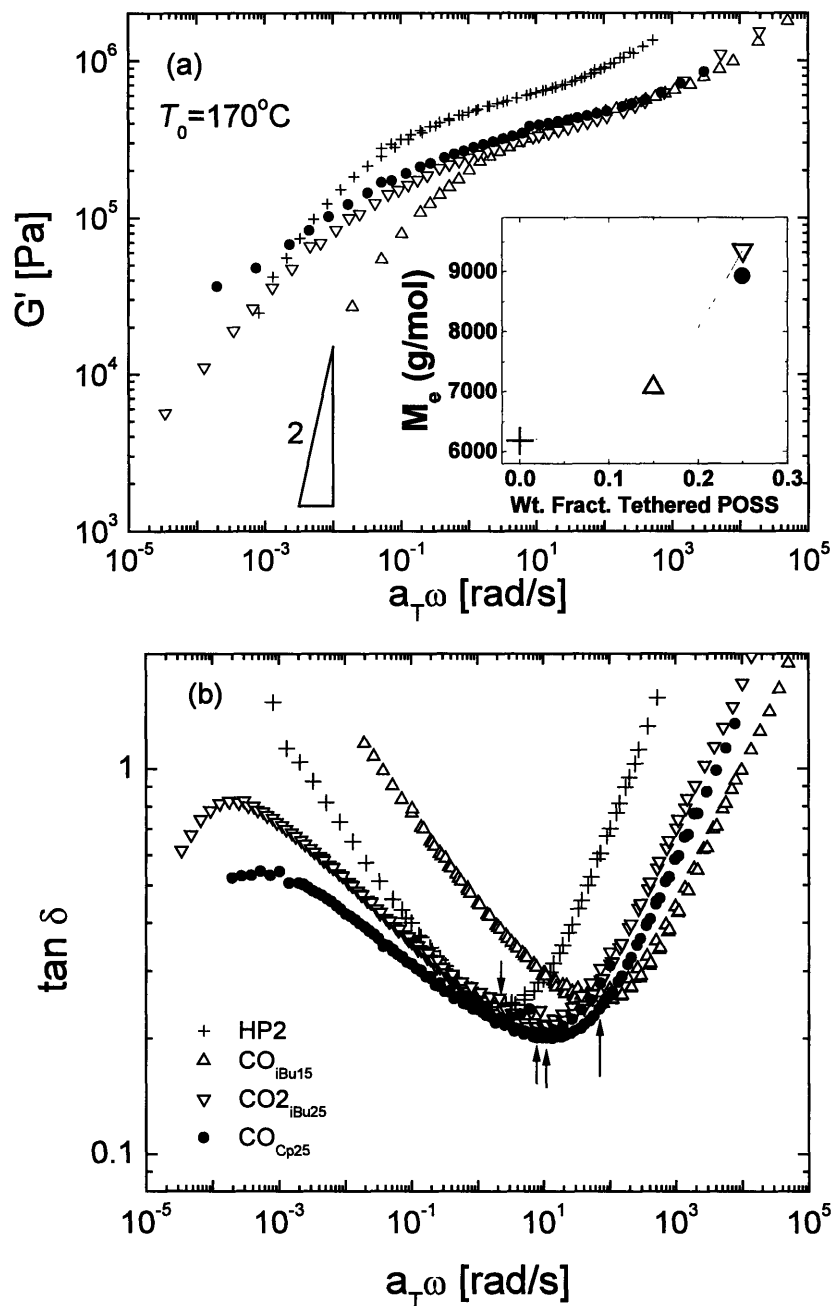


Figure 2.8 Master curves for (a) the storage modulus G' , and (b) the loss tangent $\tan \delta = G''/G'$ for entangled copolymers containing 15 and 25 wt% tethered-POSS on a PMMA backbone. Master curves for an entangled PMMA homopolymer (HP2) are also shown. The arrows in Fig. 6(b) correspond with the minima in the loss tangent curves ($T_0 = 170^\circ\text{C}$).

2.3.3 - Rheology. In Figure 2.8 master curves are plotted for the storage modulus G' and the loss tangent $\tan \delta = G''/G'$ at $T_0 = 170^\circ\text{C}$ for four unfilled polymers: the high molecular-weight homopolymer (HP2), and three highly entangled copolymers ($\text{CO}_{\text{iBu}15}$, $\text{CO}_{2\text{iBu}25}$, and $\text{CO}_{\text{Cp}25}$). The storage moduli show a significant shift downward and to the right with the addition of POSS to the chain. The magnitude of the storage modulus is similar for all three copolymers even though they exhibit significantly different glass transition temperatures (Table 3) that bracket the T_g of the homopolymer. Approximate plateau moduli (G_N^0) were calculated using the convention:^{32,33}

$$G_N^0 = (G'(\omega))_{\tan \delta \rightarrow \min} \quad (2)$$

where the plateau modulus G_N^0 is taken as the point in the storage modulus $G'(\omega)$ where the loss tangent $\tan \delta(\omega) = G''/G'$ passes through a minimum. These minima are noted by the arrows in Fig. 2.8(b). Values of the entanglement molecular weight, M_e , were then calculated from the expression:³⁴

$$M_e = \left(\frac{4}{5}\right) \frac{\rho RT}{G_N^0} \quad (3)$$

These values are tabulated in Table 2.5 along with $Z = M_w/M_e$, the number of entanglements per chain. The plateau modulus for PMMA ($G_N^0 = 5.2 \times 10^5$ Pa) at $T_0 = 170^\circ\text{C}$ agrees with the values reported by Fuchs et al.,³⁵ which ranged from $4.6 \times 10^5 \leq G_N^0 \leq 6.1 \times 10^5$ Pa at $T_0 = 190^\circ\text{C}$. The data reported by Fuchs et al. were for monodisperse PMMAs with the exception of the sample with the lowest plateau modulus, which was for a PMMA with a polydispersity $\text{PDI} = 2.0$, similar to that for HP2 in this study. The terminal region and zero-shear-rate value of the viscosity for these PMMA copolymers could not be readily accessed due to thermal instability at high temperatures: HP2, $\text{CO}_{\text{iBu}15}$ and $\text{CO}_{2\text{iBu}25}$ all depolymerized at temperatures above 200°C ,

leading to foaming of the samples; CO_{Cp25} crosslinked above 200°C, causing a low frequency plateau in the storage modulus G' and rendering the sample insoluble in THF.

Table 2.5 Rheological Properties of Unfilled, Entangled Polymers

Polymer	Wt.% POSS	G_N^0 (Pa) ($T_0 = 170^\circ\text{C}$)	M_e (g/mol)	$Z = M_w/M_e$	T_g (C)
HP2	0	5.2×10^5	6200	43	124
CO _{iBu15}	15	4.5×10^5	7100	29	87
CO _{2iBu25}	25	3.4×10^5	9400	60	113
CO _{Cp25}	25	3.7×10^5	8900	81	126

The poor thermal stability of these polymers for extended times at high temperature led to the use of different matrix materials for the blend portion of the study. In particular, a copolymer (CO_{1iBu25}) with substantially lower molecular weight ($M_w = 63,000$ g/mol) was used to study the effect of blending isobutyl-POSS filler with copolymer. In Figure 2.9 we show linear viscoelastic moduli for blends of isobutyl-POSS and copolymer ($F_{iBu}/\text{CO}_{1iBu25}$) at a reference temperature $T_0 = 150^\circ\text{C}$ for filler loadings between 0 and 30 vol%. The storage and loss moduli $G'(\omega)$ and $G''(\omega)$ increase monotonically but retain the same shape up to a filler loading of 20 vol%, with a noticeable change in the terminal slope for the 30 vol%-filled sample. This change in the relaxation spectrum of the blends is consistent with the discontinuity in the T_g values obtained from DSC (Table 2.4) and the morphological change apparent in Figure 2.7. There is also evidence of failure of time-temperature superposition (TTS) at low frequencies for the 30 vol%-filled sample. Zero-shear-rate viscosities were calculated from the relation:

$$\eta_0 = \lim_{\omega \rightarrow 0} \left(\frac{G''}{\omega} \right) \quad (4)$$

and are reported in Table 2.4. The five lowest-frequency points in G'' were used to determine η_0 for each blend sample. The average slope of $\log G''$ vs. $\log \omega$ in the terminal region for the

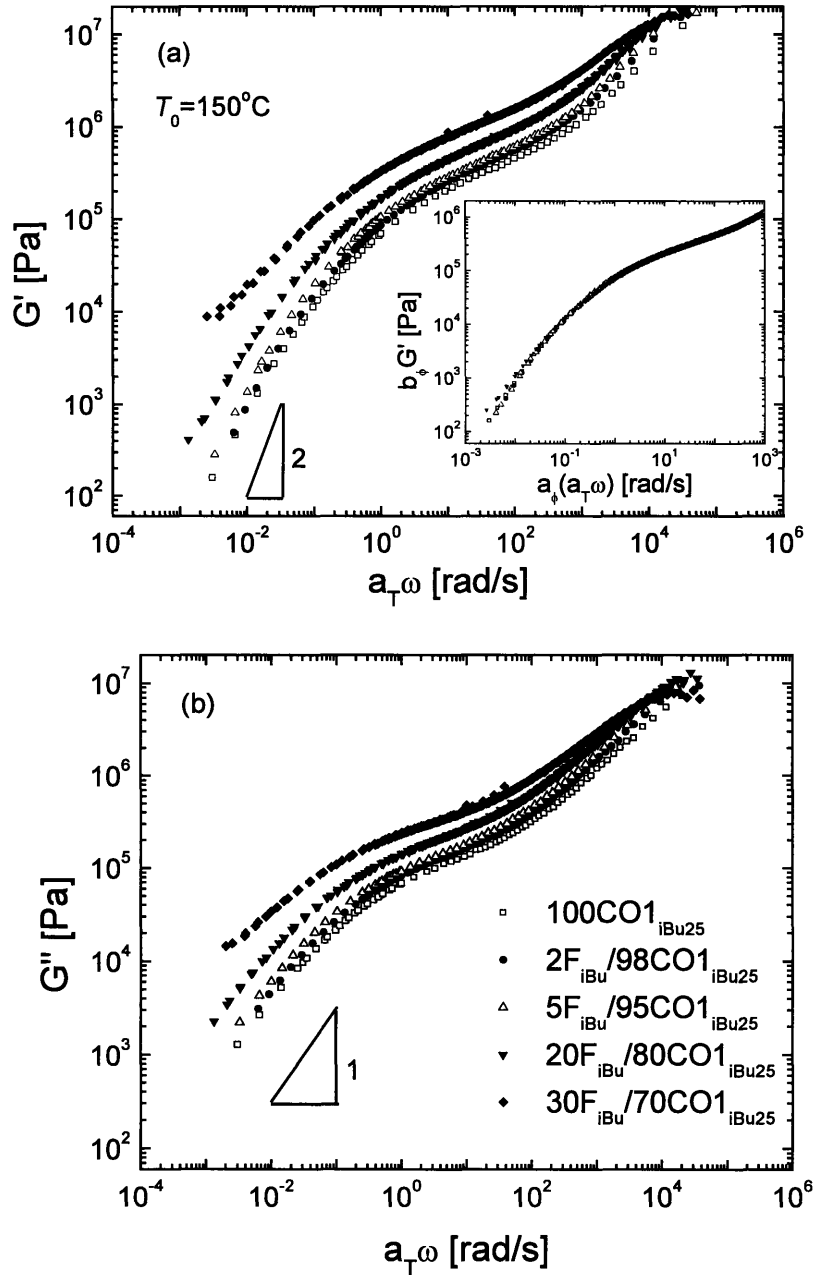


Figure 2.9. Master curves for (a) the storage modulus, and (b) the loss modulus for blends of isobutyl-POSS at between 0 and 30 vol% in a copolymer containing 25 wt% isobutyl-POSS on the chain (CO1_{iBu25}) ($T_0 = 150^\circ\text{C}$).

PMMA blends with reported viscosities was 0.997 ± 0.011 . It is apparent from Fig. 2.9(a) that the addition of POSS filler results in an additional, volume-fraction-dependent shift in the linear viscoelastic properties of these filled materials. The curves can thus be shifted by additional

factors (a_ϕ , b_ϕ) to generate a material master curve, as shown in the inset to Fig. 2.9(a). We discuss this further in the Discussion section below.

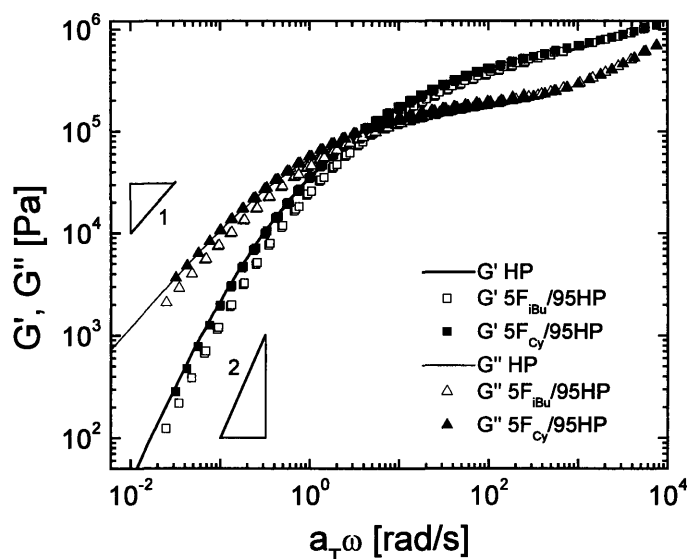


Figure 2.10. Master curves for the storage and loss moduli of three different samples: PMMA homopolymer, PMMA homopolymer containing 5 vol% cyclohexyl-POSS, and PMMA homopolymer containing 5 vol% isobutyl-POSS ($T_0 = 190^\circ\text{C}$).

In Figure 2.10 we show the linear viscoelastic moduli for the homopolymer HP and two blends of homopolymer with 5 vol% POSS filler ($5F_{iBu}/95HP$ and $5F_{Cy}/95HP$) at $T_0 = 190^\circ\text{C}$. In contrast to the response observed in the filled copolymer (Figure 2.8), there is very little change in the storage modulus G' or the loss modulus G'' of the 5 vol% cyclohexyl-POSS-filled homopolymer. The curves for the isobutyl-POSS-filled homopolymer exhibit a less-sustained plateau in G' than that observed in either the pure homopolymer or the 5% cyclohexyl-POSS-filled sample and thus the values of G' and G'' in the terminal region are noticeably lower for the isobutyl-POSS-filled homopolymer. As we discuss further below, the lack of reinforcement of the linear viscoelastic moduli at low loadings is indicative of substantial nanodispersion of the POSS in the PMMA matrix at low volume fractions of filler. This behavior

can be contrasted with that shown in Figure 2.11 for higher volume fractions of cyclohexyl-POSS ($\phi \geq 10\%$) at the same reference temperature $T_0 = 190^\circ\text{C}$. A substantial increase in G' is seen at these higher loadings, more indicative of conventional rigid filler behavior. The 30 vol% cyclohexyl-POSS–filled data appear to enter a plateau region at frequencies $a_T\omega < 10^{-1}$ rad/s. The isobutyl-POSS–filled homopolymer system exhibits qualitatively similar behavior at high filler loadings with a less substantial enhancement in the storage modulus. Fu et al.¹⁶ observed similar solid-like behavior at low frequencies in an ethylene-propylene copolymer filled with comparable amounts of methyl-POSS (20 and 30 wt%). The data in Figure 6 do not extend sufficiently into the terminal flow region (due to thermal degradation) to determine whether secondary plateaus would be present in any of the copolymers, however the results of Romo-Uribe et al.¹⁰ showed no solid-like behavior at low frequencies for loadings less than 42 wt% tethered-POSS. Thus it appears that untethered-POSS induces percolation in polymer melts at lower volume fractions than tethered-POSS, which is covalently bound to the entangled matrix.

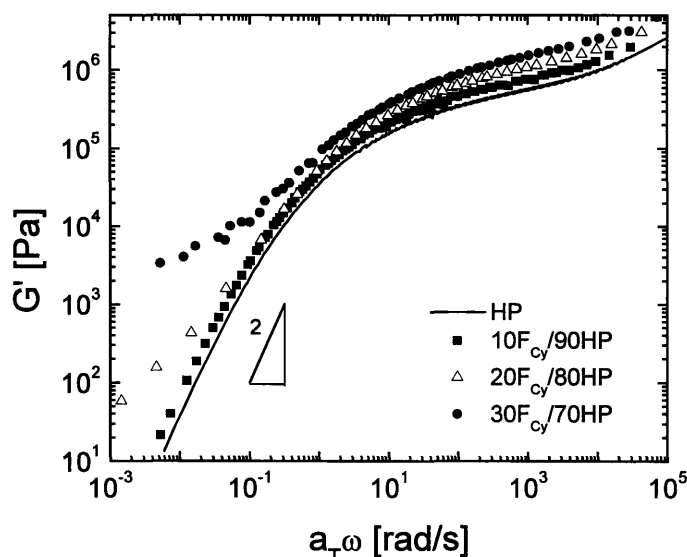


Figure 2.11. Master curves for the storage modulus of PMMA filled with between 0 and 30 vol% cyclohexyl-POSS ($T_0 = 190^\circ\text{C}$).

2.4 – Discussion

We now seek to understand the systematic trends observed in the thermal and rheological data with respect to the triangular composition diagram in Figure 2.1. Firstly, in the inset of Figure 2.8(a) we show a general trend of increasing entanglement molecular weight M_e with increasing POSS content based on plateau modulus values for the isobutyl-POSS copolymers CO_{iBu15} and CO_{2iBu25}. This trend is consistent with the results of Romo-Uribe et al.,¹⁰ who showed that tethered-POSS substantially decreases the zero-shear-rate viscosity of weakly entangled polymers at a given molecular weight. This suggests that tethered-POSS, due to its compact size ($d \sim 1.5$ nm) and relatively small molecular weight ($M_{\text{POSS}} \sim 1000$ g/mol), reduces the entanglement density in a manner that is analogous to short-chain branches in branched polymers.³⁶ In addition to reducing the linear viscoelastic moduli, tethered-POSS also shifts the curves to higher frequencies (shorter times), thereby accelerating chain relaxation processes. Our results, however, are opposite to the observations of Lee et al.¹⁵ for copolymers of styrene and vinyl-diphenylphosphine oxide that contained between 0 and 40 wt% cyclohexyl-POSS covalently attached to the vinyl-diphenylphosphine oxide segments. They observed an increase in viscosity and essentially no change in the plateau modulus with increasing POSS content. The opposing results are likely due to the nature of the attachment of the POSS to the polymer backbone. In our study, the POSS cages are attached to the backbone by a flexible propyl group (see Figure 2.1). In the study of Lee et al., the attachment group is a very rigid conjugated structure. Thus, using a flexible connecting group makes tethered-POSS act more like a melt plasticizer, while a rigid connecting group makes it act more as a nanoreinforcement.

In Figure 2.12 we show the variation in the plateau modulus values $G_N^0(\phi)$ [normalized by the homopolymer's plateau modulus $G_N^0(0)$], calculated using Eq. 2, for all three blend

systems. For the two filled homopolymer systems an essentially constant plateau modulus persists at low volume fractions of filler ($\phi \leq 5$ vol%) before an upturn appears at higher loadings. The values of the plateau moduli at higher loadings are greater for the cyclohexyl-POSS–filled homopolymer than in the equivalent isobutyl-POSS–filled homopolymer blends. The values are also compared to predictions for hard sphere fillers from the Guth-Smallwood Equation:³⁷

$$G_N^0(\phi) = G_N^0(0) \{1 + 2.5\phi + 14.1\phi^2\} \quad (5)$$

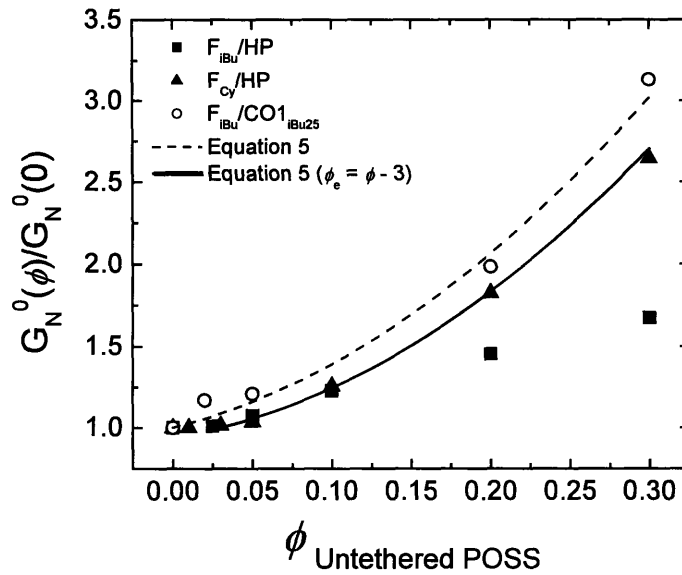


Figure 2.12. Plateau moduli for blends containing untethered-POSS, $G_N^0(\phi)$, normalized by the respective plateau modulus of the unfilled polymer, $G_N^0(0)$. Data are plotted for PMMA homopolymer filled with both cyclohexyl-POSS and isobutyl-POSS and for isobutyl-POSS in a copolymer containing 25 wt% isobutyl-POSS on the chain (CO1_{iBu25}). The lines represent fits to the Guth-Smallwood Equation (Eq. 5).

Although the data show similar trends with respect to Eq. 5, it is clear that the degree of enhancement is very sensitive to the chemical interaction between the pendant R-group and the PMMA matrix. Specifically, a superb fit was obtained for the cyclohexyl-POSS–filled

homopolymer system by defining an effective volume fraction to be $\phi_e = \phi - 3$. Thus the first 3 vol% of filler appears to have no apparent effect on the plateau modulus and above 3 vol% the filler behaves as a hard sphere. From Fig. 2.2 it is clear that there is some cyclohexyl-POSS crystallinity even at a loading of 1 vol%, however the nanodispersed portion of the filler at loadings $\phi \leq 5$ vol% softens the matrix to offset the reinforcement by the crystallites. The filled copolymer system ($F_{iBu}/CO1_{iBu25}$) exhibits a more conventional behavior, showing a monotonic increase in G_N^0 for all loadings. Thus the copolymer experiences a hard-sphere-like reinforcement when filled with untethered-POSS particles.

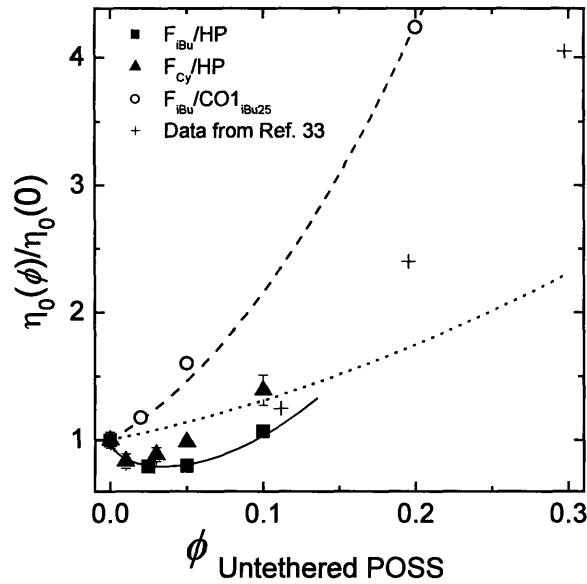


Figure 2.13. Zero-shear-rate viscosities for blends containing untethered-POSS, $\eta_0(\phi)$, normalized by the respective viscosity of the unfilled polymer, $\eta_0(0)$. Data are plotted for PMMA homopolymer filled with both cyclohexyl- and isobutyl-POSS and for isobutyl-POSS in a copolymer containing 25 wt% isobutyl-POSS on the chain ($CO1_{iBu25}$). The dotted line represents the prediction of the Einstein-Batchelor Equation (Eq. 6), while the dashed line is a plot of Eq. 6 for an effective volume fraction 2.75 times that of the actual filler value.

In Figure 2.13 we plot the normalized zero-shear-rate viscosities $[\eta_0(\phi)/\eta_0(0)]$ for the blends in an analogous fashion to the plateau moduli in Figure 2.12. The filled homopolymer systems show an initial *decrease* in the zero-shear-rate viscosity at loadings less than 5 vol%.

This result is significantly different from the prediction of the Einstein-Batchelor equation for hard sphere suspensions (shown by the dotted line in Fig. 2.13).³⁸⁻⁴⁰

$$\eta_0(\phi) = \eta_0(0) \{1 + 2.5\phi + 6.2\phi^2 + \dots\} \quad (6)$$

which predicts a monotonic increase in viscosity with increasing particle loading. A decrease in viscosity with particle loading has recently been shown in polystyrene melts filled with 5 nm crosslinked polystyrene particles by Mackay et al.;¹⁸ however, no clear trend in viscosity with increasing particle loading was apparent. The present data show a well-defined upwards curvature to the viscosity-filler loading curve for the filled homopolymer. For comparison, data from Poslinski et al.⁴¹ for a glass bead-filled thermoplastic are plotted in Fig. 2.13. The lowest loading investigated by Poslinski et al. ($\phi \sim 12\%$) is close to the prediction of Eq. 6, but the points at higher loading diverge upward from the curve. The data for the filled homopolymer blends (F_{Cy}/HP and F_{iBu}/HP) would likely show the same diverging behavior at moderate to high filler loadings, however neither linear viscoelastic nor viscometric tests were able to obtain zero-shear-rate viscosities for loadings above 10 vol%.

The decrease in viscosity at low loadings in the homopolymer blends and the eventual increase at higher loadings is again consistent with the combined presence of nanodispersed filler and crystallites. Initially an appreciable fraction of the POSS particles enter the matrix as amorphous, molecularly dispersed particles, and the remaining fraction forms crystalline aggregates. The nanodispersed particles act as a plasticizer, increasing the free volume due to the local mobility of the pendant R-groups and thereby decreasing the viscosity of the blend, but at higher loadings ($\phi \geq 5\%$) a saturation limit is reached regardless of compounding history. At this point any additional POSS filler agglomerates into crystallites, which increase the viscosity in a way analogous to hard spheres.

By contrast, the filled-copolymer blend system ($F_{iBu}/CO1_{iBu25}$) shows a substantial increase in the zero-shear-rate viscosity for all loadings (Figure 2.13). This enhancement is significantly greater than that predicted by Equation 6. However, an excellent fit is obtained if the effective volume fraction occupied by a POSS filler cage in the melt is allowed to exceed the actual volume fraction by a factor $\phi_e = 2.75\phi$ (indicated by the dashed line in Fig. 2.13). This result is not surprising when one considers that in the blend of 5% isobutyl-POSS with the copolymer ($5F_{iBu}/CO1_{iBu25}$), the mole ratio of untethered-POSS groups to tethered-POSS groups ($N_{Untethered}/N_{Tethered\ POSS}$) is only 0.23 (see Table 2.4), meaning the untethered-POSS filler constitutes only 19% of the total POSS contained in the blend. Therefore, the untethered-POSS is able to strongly associate with the tethered-POSS and increase the effective volume fraction of the filler, especially at low filler loadings. This internal amplification of the “effective matrix-filler interaction” leads to the factor of 2.75 multiplying the volume fraction in fitting the data to Equation 6.

To further illustrate the differences between the two types of blend systems, both horizontal and vertical concentration shift factors (a_ϕ and b_ϕ , respectively) were computed by shifting the master curves for the storage moduli of the blend samples onto the respective master curve of the unfilled polymer to generate a reduced modulus $G_r'(\omega_r) = b_\phi G'(a_\phi a_T \omega)$ with $b_\phi \leq 1$ and $a_\phi \geq 0.9$ for $\phi > 0$. Similar concentration-dependent shift factors have been used in the construction of universal master curves of semidilute and concentrated polymer solutions.^{42,43} The strong self-similarity of the material functions and the quality of the shifts for the filled copolymer system are shown in the inset to Fig. 2.9(a). In Figure 2.14 we plot the horizontal shift factors a_ϕ (filled symbols) and the vertical shift factors b_ϕ (open symbols) for both the filled homopolymer and the filled copolymer blend systems. No vertical shifts b_ϕ are required in the

filled homopolymer blends for $\phi \leq 5\%$, however the filled copolymer blends require vertical shifts at all filler loadings in order to superpose onto the master curve of the unfilled polymer. The reciprocal of the Guth-Smallwood equation is plotted as the dashed line in Fig. 2.14 to show that the vertical shifts correspond well with the plateau modulus values in Fig. 2.12. All blends above $\phi = 5\%$ require significant vertical shifts and thus the trend of increasing vertical shifts with filler loading is similar in the filled homopolymer blends and the filled copolymer blends. The behavior of the horizontal shift factors a_ϕ however, is distinctly different between the two types of blend systems. Only minimal horizontal shifting is required in the filled homopolymer blend systems, whereas in the filled copolymer a linear increase in a_ϕ with a slope of 7.5 is observed with increasing filler content. Thus for every 13 vol% of untethered-POSS added to the copolymer a subsequent one decade increase in relaxation time is observed.

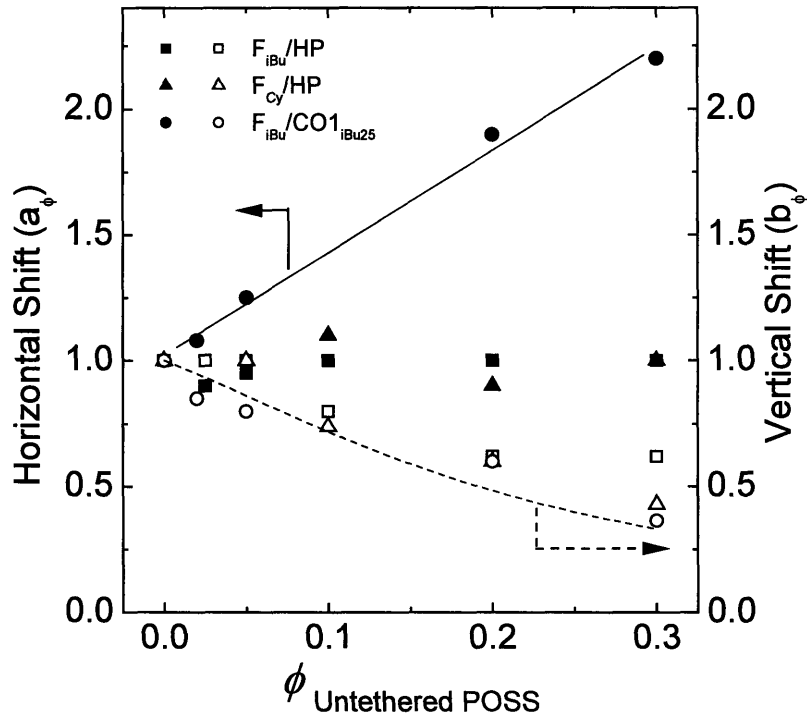


Figure 2.14. Horizontal (filled symbols) and vertical (open symbols) concentration shift factors for the three blend systems obtained by shifting the storage modulus curves downward and, if necessary, to the left or right onto the respective master curve of the unfilled polymer.

It is helpful at this point to utilize the Doi-Edwards scaling relation for the viscosity of unfilled, entangled polymers:⁴⁴

$$\eta_0 \cong G_N^0 \tau_{rep} \quad (7a)$$

where τ_{rep} is the reptation time of the unfilled polymer melt. This scaling relation may be altered to describe a filled polymer by writing:

$$\eta_0 = G_N^0(\phi) \tau_{rep}(\phi) = \left(\frac{G_N^0}{b_\phi} \right) (\tau_{rep} a_\phi) \quad (7b)$$

where a_ϕ and b_ϕ are the same concentration shift factors plotted in Fig. 2.14. To a first approximation, filler particles may be expected to reinforce a polymer melt, which leads to the factor $1/b_\phi$ in the modulus term of Eq. 7(b), and to retard chain motions, which leads to the term a_ϕ in the reptation term of Eq. 7(b). Overall, the reinforcement is more substantial in the filled copolymer systems (see Fig. 2.12), but both types of blend systems show a significant reinforcement effect which closely follows the prediction of the Guth-Smallwood equation (Eq. 5). The reptation term, which is directly related to the horizontal shift factor a_ϕ is not significantly affected in the untethered-POSS-homopolymer blend systems, but it linearly increases with filler loading in the copolymer blends. The rheological data in Figure 2.8 for unfilled copolymers show clearly that tethered-POSS, in the absence of untethered-POSS filler, does not retard chain relaxation processes, and in fact speeds them up (i.e. “plasticizes” them) relative to the homopolymer. Thus the additional slowdown in the dynamics of the filled copolymer reflected in the term $a_\phi > 1$ must be due to thermodynamic associations between tethered-POSS cages on the chain and untethered-POSS particles in the blend. This is the principal effect responsible for the large increase in the zero-shear-rate viscosity shown in Figure 2.13.

This combination of a retardation in the relaxation processes and an enhancement in the modulus in a well-entangled melt can be described by kinetic models such as the “sticky reptation” model of Liebler et al.⁴⁵ It has been previously conjectured by Romo-Uribe et al.¹⁰ that this model and other mechanisms are important in POSS-containing copolymers, however our results strongly indicate that it is the addition of POSS filler to a POSS-containing copolymer that results in the retardation, not simply the incorporation of tethered-POSS into a polymer chain. The horizontal shift factor a_ϕ is primarily related to the “stickiness” of the chains, which is characterized by the number of “stickers” (in this case, the number of tethered-POSS groups on the chain), the average lifetime for a sticker in the associated state, and the average fraction of stickers which are in the associated state, which is a function of both the tethered-POSS content and the untethered-POSS content. The filled homopolymer system experiences no significant horizontal shifts over the range of loadings examined because the chains contain no sticky groups. In the filled copolymer system, however, the sticky groups constitute 25 wt% of the polymer chains and lead to a rapid increase in relaxation time with particle loading. The vertical shift factor b_ϕ is also affected by the concentration of sticky groups on the chain, but it is affected by inert, rigid particles as well and thus a substantial increase in the plateau modulus G_N^0 with filler loading is present in both types of blend systems.

An unusual aspect of the linear viscoelastic results for the filled copolymer system is that the storage and loss moduli G' and G'' show virtually no change in shape up to 20 vol% filler loading (Fig. 2.9). In other filled systems with attractive matrix-filler interactions such as carbon-black-filled elastomers,⁴⁶ silica-filled poly(ethylene oxide),¹⁷ and clay-filled polystyrene-g-maleic anhydride,⁴⁷ a sustained plateau in the storage modulus, $G' \geq 10^4$ Pa typically persists at low frequencies for loadings $\phi \ll 20\%$. This is often attributed to a percolated network caused

by substantial chain adsorption onto the filler particles.¹⁷ There is ample evidence from the shape of the linear viscoelastic moduli and the glass transition temperatures indicating that percolation does not occur in the F_{iBu}/CO_{1iBu25} system until 30 vol% isobutyl-POSS filler is added; however, the linear increase in the horizontal shift factor a_ϕ is present at all loadings. This is because the adsorption effect is significantly different in the filled copolymer system of the present study, in which the polymer backbone has no strong attraction to the isobutyl-POSS filler (as evidenced by the plasticization at low loadings in the filled homopolymer). Thus the only portions of the copolymer chain which experience a thermodynamic attraction to the untethered-POSS are the tethered-POSS groups distributed randomly along the backbone, and though these groups constitute a substantial weight fraction of the copolymer CO_{1iBu25} they are incorporated in only 3.4 mol% of the repeat units. Thus only one out of approximately every 60 carbon atoms in the copolymer backbone contains a covalently-tethered isobutyl-POSS particle, and, at low loadings of untethered-POSS, hundreds of backbone carbon atoms will separate the tethered-POSS groups that are actively bound to a crystallite. This indicates that the retardation caused by the associations between the tethered and untethered isobutyl-POSS is a local effect restricted to isolated nanoscopic domains within the sample, rather than being caused by a global percolated network. The schematic in Fig. 2.15 further illustrates this postulate.

In Fig. 2.15(a), a reptating copolymer chain (represented by the dashed line) is close enough to a small (~ 5 nm) nanocrystallite of untethered-POSS that one of its tethered-POSS groups (represented by the gray-colored circle) has associated with the crystallite, forming a temporary crosslink. Very soon after [Fig. 2.15(b)], the bound tethered-POSS cage disassociates from the crystallite and the copolymer chain is again free to reptate along its contour length; however, before the chain has fully diffused away from the crystallite a new association is

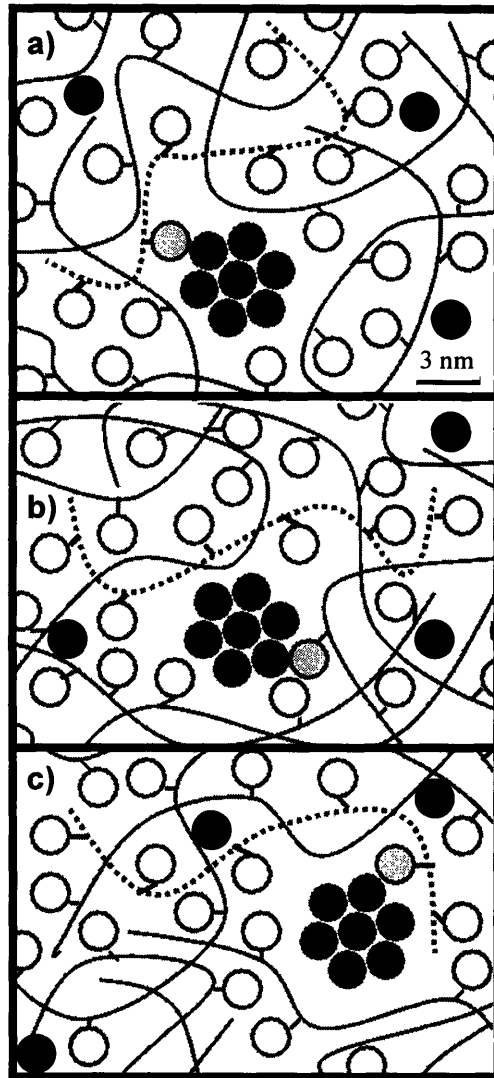


Figure 2.15. Schematic of the filled copolymer blend ($F_{iBu}/CO_{1-iBu25}$). At low loadings of untethered-POSS (black circles), most of the tethered-POSS groups are present in an unbound state (open circles). However, a kinetic exchange takes place whereby a particular chain (represented by the dashed line) may contain (a) an “active” tethered-POSS group (gray circle) which forms a thermodynamic association with a nanocrystallite of untethered-POSS. This temporary association may (b) break, thus allowing the chain to reptate freely before (c) a different tethered-POSS group on the same chain forms an association with the nanocrystallite. This kinetic exchange between an associated and a dissociated state leads to the dramatic slowdown in the relaxation processes in the copolymer matrix.

formed [Fig. 2.15(c)], this time with a different tethered-POSS group taking part in the association. Throughout this process the chain has been able to translate its center of mass in spite of the kinetic exchange between a bound and an unbound state. The associations

significantly delay the motion of the chain along its contour length (and thereby increase the reptation time, τ_{rep}); however, they do not significantly alter the mobility of the unbound segments (when the amount of untethered-POSS is small). In addition, the associations are short-lived ($\tau_{\text{assoc}} \ll \tau_{\text{rep}}$), allowing the shape of the linear viscoelastic moduli to remain the same for filler loadings $\phi \leq 20\%$. At filler loadings $\phi > 20\%$, the probability of a tethered-POSS cage taking part in an association surpasses a critical point and thereafter significant molecular mobility is lost due to the number of temporary crosslinks per molecule. This is responsible for the increase in the glass transition temperature observed in the filled copolymer at 30 vol% filler (Table 2.4). Furthermore, at this point the untethered-POSS becomes the dominant POSS species in the system and the tethered-POSS groups become saturated in their nanoscopic associations with untethered-POSS. This leads to the formation of large numbers of small crystallites (Figure 2.7) that percolate throughout the PMMA matrix.

2.4.1 – Time-Temperature Superposition.⁴⁸ The addition of unbound POSS nanofiller into an entangled polymer matrix may result in several competing effects. The high local mobility of the pendant R-groups on the Si_8O_{12} cages will create additional free volume and thus locally plasticize the matrix, leading to enhanced molecular mobility; conversely, the addition of a rigid filler (albeit nanoscale in characteristic dimension) is expected to result in enhanced local dissipation with a less clear effect on free volume. The TTS shift factors obtained experimentally were analyzed using the WLF framework⁴⁸ to further investigate the effect of POSS filler on free volume in the blends.

The time-temperature shift factors $a_T(T, T_0)$ used in constructing Figures 2.8 through 2.11 were obtained by shifting $\tan \delta$ curves obtained over a range of test temperatures to a reference temperature ($T_0 = 190^\circ\text{C}$ for the homopolymer, $T_0 = 135^\circ\text{C}$ for the copolymer). To illustrate the

quality of the TTS an example of original data is given in Figure 2.16. In Figure 2.16(a) we plot the unshifted $\tan \delta$ curves for the 10 vol% cyclohexyl-POSS-homopolymer blend and in Figure 2.16(b) we show the curves after shifting. No vertical shifting was required.

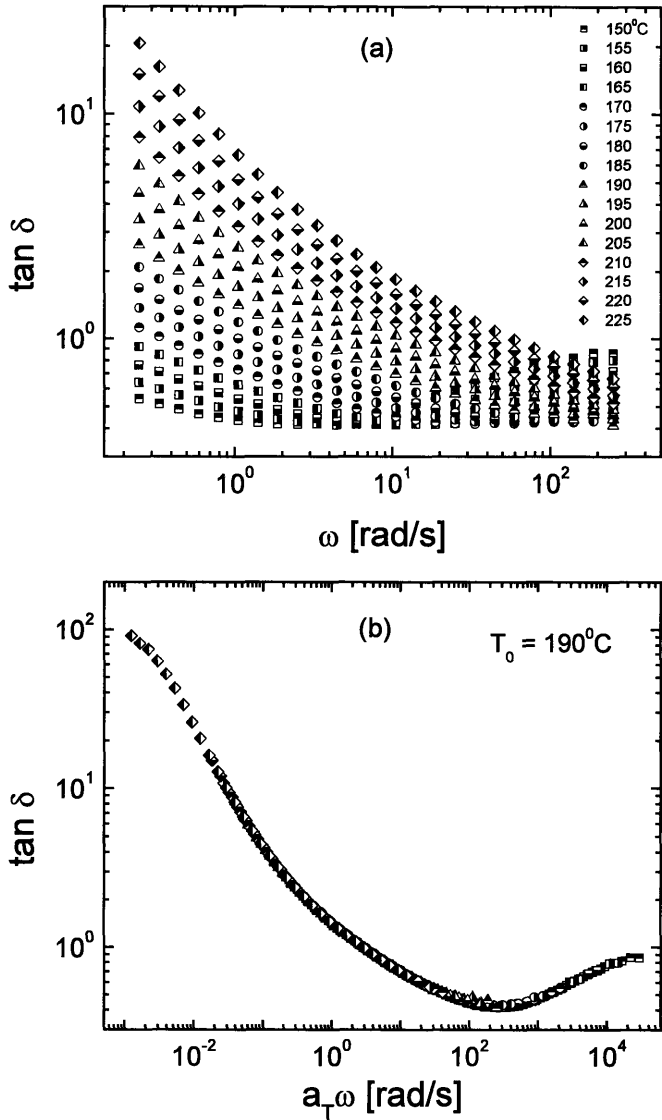


Figure 2.16. Loss tangent ($\tan \delta = G''/G'$) curves for PMMA filled with 10 vol% cyclohexyl-POSS: (a) unshifted frequency sweeps at different temperatures; (b) all curves shifted to a reference temperature of $T_0 = 190^\circ\text{C}$.

Initially, $\log a_T$ was plotted against the reciprocal of the absolute temperature to determine whether the rheology of the samples followed Arrhenius behavior; however, high

correlation coefficients were only obtained at high temperatures ($T \geq 190^\circ\text{C}$). Therefore, the WLF equation was employed in order to capture the temperature dependence of the shift factors over the entire temperature range:⁴⁸

$$\log a_T = \frac{-c_1^0(T - T_0)}{c_2^0 + (T - T_0)} \quad (8)$$

WLF coefficients were determined by plotting the quantity $-(T - T_0)/\log a_T$ against $(T - T_0)$;⁴⁸ the coefficient c_1^0 was obtained from the reciprocal of the slope, and the coefficient c_2^0 from the intercept. An example of the use of this method can be found in the work of Fetters et al. for polyisobutylene melts.⁴⁹ Values of the WLF coefficients are reported in Table 2.6 for all filler-homopolymer blends. The value of $c_1^0 = 8.6$ obtained for the PMMA homopolymer agrees well with values reported by Fuchs et al. for PMMA homopolymers ($8.6 \leq c_1^0 \leq 9.4$)³⁵ at the same reference temperature $T_0 = 190^\circ\text{C}$.

A representative WLF plot for the cyclohexyl-POSS–homopolymer blend system is shown in Figure 2.17(a), one set of data corresponding to the unfilled homopolymer and another for a blend containing 10 vol% cyclohexyl-POSS. There is a small but reproducible difference in the slope and the y -intercept of the two lines, indicating differences in the respective WLF coefficients. The c_1^0 values can be related to the fractional free volume f_0 using the relation:⁴⁸

$$f_0 = \frac{B}{2.303c_1^0} \quad (9)$$

where B is a constant usually assumed to be unity. Values of f_0/B are reported in Table 2.6 along with the zero-shear-rate viscosities for the homopolymer blends. Surprisingly, for filler loadings $\phi \leq 5\%$, the value of the fractional free volume of the unfilled homopolymer obtained from TTS ($f_0/B = 0.050$) is larger than that of the cyclohexyl-POSS–homopolymer system (0.048) but

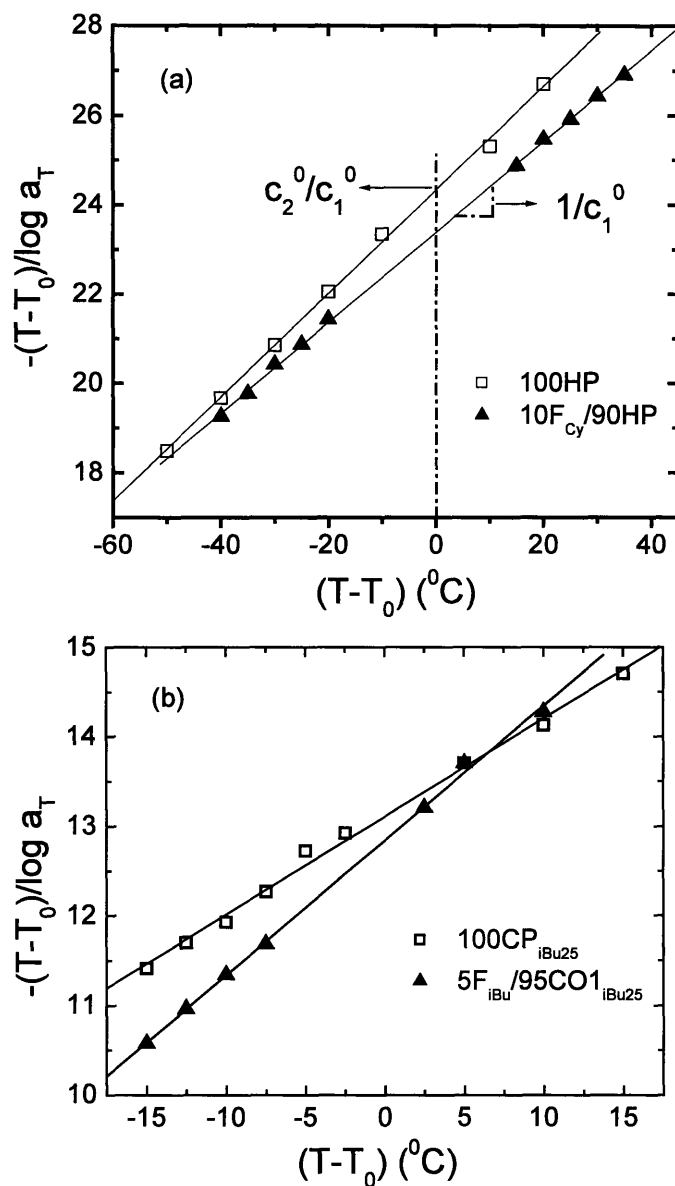


Figure 2.17. WLF plots for: (a) unfilled PMMA homopolymer and homopolymer containing 10 vol% cyclohexyl-POSS ($T_0 = 190^{\circ}\text{C}$); (b) unfilled copolymer containing 25 wt% isobutyl-POSS on the chain and respective copolymer containing 5 vol% isobutyl-POSS filler ($T_0 = 135^{\circ}\text{C}$).

smaller than that of the isobutyl-POSS–homopolymer system (0.051-0.052). The difficulty in developing clear trends lies in the above-mentioned competition between molecular dispersion and crystalline aggregation, which is present at all loadings (see Figure 2.2). The decrease in viscosity seen at low loadings in the filler-homopolymer system is almost certainly a result of

Table 2.6 WLF Parameters, Zero-shear-rate Viscosities and T_g values for Untethered-POSS-filled Homopolymer Blends

Blend Composition	c_1^0	c_2^0 (K)	f_0/B	f_g/B	η_0 (Pa s)	T_g ($^{\circ}$ C)
			($T_0 = 190^{\circ}$ C)	($T = T_g$)		
100HP	8.6	207	0.050	0.030	1.2×10^5	105
1F _{Cy} /99HP	8.7	208	0.050	0.030	9.6×10^4	105
3F _{Cy} /97HP	9.0	214	0.048	0.029	1.0×10^5	105
5F _{Cy} /95HP	9.0	213	0.048	0.029	1.1×10^5	106
10F _{Cy} /90HP	9.9	233	0.044	0.028	1.6×10^5	106
20F _{Cy} /80HP	7.6	176	0.057	0.030	a	105
30F _{Cy} /70HP ^b	---	---	---	---	d	106
2.5F _{iBu} /97.5HP	8.4	202	0.052	0.030	9.1×10^4	105
5F _{iBu} /95HP	8.6	205	0.051	0.030	9.2×10^4	105
10F _{iBu} /90HP	9.4	212	0.047	0.027	1.2×10^5	103
20F _{iBu} /80HP	7.4	175	0.059	0.030	c	105
30F _{iBu} /70HP ^b	---	---	---	---	d	106

a > 1.8×10^5 Pa s

b WLF fit was poor and the coefficients are considered unreliable

c > 1.9×10^5 Pa s

d Sample exhibited a yield stress

Table 2.7 WLF Parameters, Zero-shear-rate Viscosities and T_g values for Untethered-POSS-filled Copolymer Blends

Blend Composition	c_1^0	c_2^0 (K)	f_0/B	f_g/B	η_0 (Pa s)	T_g ($^{\circ}$ C)	$N_{Untethered} / N_{Tethered POSS}$
			($T_0 = 135^{\circ}$ C)	($T_0 = 150^{\circ}$ C)			
100CO1 _{iBu25}	9.1	120	0.048	0.032	4.3×10^5	95	0.00
2F _{iBu} /98CO1 _{iBu25}	6.6	90	0.066	0.037	5.0×10^5	96	0.09
5F _{iBu} /95CO1 _{iBu25}	6.6	85	0.065	0.035	6.8×10^5	95	0.23
20F _{iBu} /80CO1 _{iBu25}	8.3	110	0.053	0.033	1.8×10^6	95	1.08
30F _{iBu} /70CO1 _{iBu25} ^a	---	---	---	---	b	103	1.85

^a WLF fit was poor and the coefficients are considered unreliable

^b > 5.0×10^6 Pa s

additional free volume generated by the dispersed POSS nanoparticles, whose mobile, pendant R-groups are expected to create appreciable void space; the WLF coefficients in the F_{Cy}/HP system do not support this trend because of the complication caused by the crystallites, which reinforce the melt and thereby skew the WLF coefficients to values which suggest an opposing trend. The effect of the crystallites can be demonstrated by analyzing the coefficients obtained in

the F_{Cy}/HP system. Up to 10 vol% cyclohexyl-POSS filler, the first WLF coefficient shows a monotonic increase from $c_1^0 = 8.6$ for the homopolymer to $c_1^0 = 9.9$ for the 10%-filled sample. But the 20%-filled sample has a c_1^0 value of only 7.6, substantially smaller than the homopolymer's value, which leads to a higher calculated fractional free volume value ($f_0/B = 0.057$). Nothing in the linear viscoelastic data in Fig. 2.11 or in the T_g values in Table 2.6 predicts such a change in molecular arrangement. Future rheological studies on a POSS-filled system in which crystallization is entirely absent or at least greatly suppressed would help to clarify the interesting role of molecularly-dispersed POSS on the thermorheological properties.

In Figure 2.17(b) we show the WLF plot for the unfilled copolymer and the copolymer filled with 5 vol% isobutyl-POSS filler. Addition of untethered-POSS clearly has a stronger effect at low loadings ($\phi \leq 5\%$) on the time-temperature behavior in the copolymer blends. The slope of the 5F_{iBu}/95CO1_{iBu}25 line is notably larger, leading to smaller c_1^0 and c_2^0 values. The WLF coefficients for the filled copolymer system are reported in Table 2.7. In the range of isobutyl-POSS loadings $2\% \leq \phi \leq 20\%$, increasing the amount of POSS filler increases both the fractional free volume f_0 and the zero-shear-rate viscosity η_0 . In particular, at loadings of $\phi \leq 5\%$, which contain only small amounts of crystallite content [see Figure 2.6], the fractional free volume increases from $f_0/B = 0.048$ for the unfilled copolymer at $T_0 = 135^\circ\text{C}$ to $f_0/B = 0.065$ for the copolymer blended with 5 vol% isobutyl-POSS. That the free volume and viscosity should both increase concomitantly is counter to the concepts introduced by Doolittle which relate free volume in liquids to viscosity.⁵⁰ However, our result is not unreasonable, as the thermodynamic attraction between the well-dispersed isobutyl-POSS filler and the tethered-isobutyl-POSS groups in the copolymer chain could offset the increase in free volume observed in the system. The significant nanodispersion of the untethered-POSS in the copolymer system, evidenced both

by the X-ray pattern for the 5F_{iBu}/95CO_{1iBu25} blend in Figure 2.6 and the strong retardation of chain motion evident from the linear viscoelastic data, is responsible for the observed increase in free volume.

Tables 2.6 and 2.7 also report values of f_g/B , the fractional free volume at the glass transition temperature. These were calculated using a relation adapted from Ferry:⁴⁸

$$f_g = \frac{B(c_2^0 + T_g - T_0)}{2.303c_1^0 c_2^0} \quad (10)$$

where c_1^0 and c_2^0 are the WLF coefficients determined at T_0 . While no new trends or insights are obtained from this transformation, the numerical values of f_g provide support for the validity of the time-temperature superposition scheme, particularly for the POSS-filled homopolymer systems. According to Ferry, WLF coefficients, when referenced to the glass transition temperature, should lead to a numerical value of f_g in the range 0.025 ± 0.005 for all systems, and all but one of the highly loaded compounds in Table 4 conforms to this paradigm. The values of f_g for the compounds based on the copolymer CO_{1iBu25} lie somewhat above the universal range.

2.5 –Conclusions

Poly(methyl methacrylate)s containing both tethered and untethered polyhedral oligomeric silsesquioxanes (POSS) were investigated using wide-angle X-ray diffraction, differential scanning calorimetry, and rheological characterization. Entangled linear copolymers containing covalently-tethered-POSS showed a decrease in the plateau modulus compared to the homopolymer and this trend was nearly the same for two 25 wt% POSS copolymers with different organic R-groups. This behavior was attributed to the tethered-POSS behaving analogously to a short-chain branch, thereby reducing the entanglement density and softening the polymer in the melt state.

When untethered-POSS was blended with PMMA homopolymer, wide angle x-ray diffraction (WAXD) showed significant crystallinity of untethered-POSS even at loadings as low as 1 vol%, while significant crystallinity in the filled copolymer blends was not observed until greater than 5 vol% filler had been added. Melting endotherms from DSC suggest a regime at low loadings ($\phi \leq 5\%$) in which a large fraction of untethered-POSS enters the homopolymer in an amorphous state before a solubility limit is reached, at which point virtually all additional POSS filler is incorporated into crystallites.

Contrasting behavior was observed between the rheology of untethered-POSS-homopolymer blends and the untethered-POSS-copolymer blends. A minimum in the zero-shear-rate viscosity and a constant plateau modulus at loadings below 5 vol% were seen for both the isobutyl-POSS-filled and the cyclohexyl-POSS-filled homopolymer, indicating an initial plasticization of the matrix by the untethered POSS filler. However, at higher loadings these values increased in a way consistent with hard sphere fillers. Combining the thermal and rheological data leads to the conclusion that untethered-POSS distributes in two ways in a homopolymer matrix: as nanoscopically-dispersed particles and as crystallites. The copolymer blends showed a substantial increase in viscosity at all loadings. This was attributed to a substantial retardation of chain relaxation processes caused by significant association between the POSS cages on the chains and those in the blend. This thermodynamic attraction is particularly effective at retarding chain motions in nanoscopic domains while still allowing macroscopic relaxation of the sample.

Time-temperature superposition (TTS) was used to determine whether the decrease in viscosity in the untethered-POSS-homopolymer blends could be correlated with an increase in free volume. Linear regression fits to the WLF equation were excellent, however there was no

strong trend in the coefficients for the homopolymer blends. This was due to the POSS filler's tendency to form crystallites, which became dominant at filler loadings above 5 vol%. The untethered-POSS-copolymer blend system shows a significant decrease in the WLF coefficients upon the addition of small amounts of untethered-POSS filler, suggesting an increase in free volume with filler loading. Surprisingly, the viscosity also increases dramatically in this region; however, this counterintuitive result can be explained by the strong thermodynamic interaction between tethered and untethered-POSS moieties, which more than offsets the plasticization caused by the free volume increase.

References

- (1) Kopesky, E. T.; Haddad, T. S.; Cohen, R. E.; McKinley, G. H. *Macromolecules* **2004**, *37*, 8992.
- (2) Lichtenhan, J. D.; Vu, N. Q.; Carter, J. A.; Gilman, J. W.; Feher, F. J. *Macromolecules* **1993**, *26*, 2141-2142.
- (3) Schwab, J. J.; Lichtenhan, J. D. *Applied Organometallic Chemistry* **1998**, *12*, 707-713.
- (4) Lucke, S.; Stoppek-Langner, K. *Applied Surface Science* **1999**, *145*, 713-715.
- (5) Li, G. Z.; Wang, L. C.; Ni, H. L.; Pittman, C. U. *Journal of Inorganic and Organometallic Polymers* **2001**, *11*, 123-154.
- (6) Zheng, L.; Farris, R. J.; Coughlin, E. B. *Macromolecules* **2001**, *34*, 8034-8039.
- (7) Mather, P. T.; Jeon, H. G.; Romo-Uribe, A.; Haddad, T. S.; Lichtenhan, J. D. *Macromolecules* **1999**, *32*, 1194-1203.
- (8) Xu, H. Y.; Kuo, S. W.; Lee, J. S.; Chang, F. C. *Macromolecules* **2002**, *35*, 8788-8793.
- (9) Xu, H. Y.; Kuo, S. W.; Chang, F. C. *Polymer Bulletin* **2002**, *48*, 469-474.
- (10) Romo-Uribe, A.; Mather, P. T.; Haddad, T. S.; Lichtenhan, J. D. *Journal of Polymer Science Part B-Polymer Physics* **1998**, *36*, 1857-1872.
- (11) Zhang, W. H.; Fu, B. X.; Seo, Y.; Schrag, E.; Hsiao, B.; Mather, P. T.; Yang, N. L.; Xu, D. Y.; Ade, H.; Rafailovich, M.; Sokolov, J. *Macromolecules* **2002**, *35*, 8029-8038.
- (12) Blanski, R.; Phillips, S.; Chaffee, K. P.; Lichtenhan, J.; Lee, A.; Geng, H. P. *Polymer Preprints* **2000**, *41*, 585.
- (13) Zheng, L.; Waddon, A. J.; Farris, R. J.; Coughlin, E. B. *Macromolecules* **2002**, *35*, 2375-2379.
- (14) Vaia, R. A.; Giannelis, E. P. *MRS Bulletin* **2001**, *26*, 394.
- (15) Lee, A.; Xiao, J.; Feher, F. J. *Macromolecules* **2005**, *38*, 438.

- (16) Fu, B. X.; Gelfer, M. Y.; Hsiao, B. S.; Phillips, S.; Viers, B.; Blanski, R.; Ruth, P. *Polymer* **2003**, *44*, 1499-1506.
- (17) Zhang, Q.; Archer, L. A. *Langmuir* **2002**, *18*, 10435-10442.
- (18) Mackay, M. E.; Dao, T. T.; Tuteja, A.; Ho, D. L.; Van Horn, B.; Kim, H. C.; Hawker, C. J. *Nature Materials* **2003**, *2*, 762-766.
- (19) Einstein, A. *Ann. Phys. (Leipz.)* **1906**, *19*, 371.
- (20) Glotzer, S. C. *Nature Materials* **2003**, *2*, 713.
- (21) Brown Jr., J. F.; Vogt Jr., L. H. *Journal of the American Chemical Society* **1965**, *87*, 4313.
- (22) Feher, F. J.; Newman, D. A.; Walzer, J. F. *Journal of the American Chemical Society* **1989**, *111*, 1741.
- (23) Feher, F. J.; Budzichowski, T. A.; Blanski, R. L.; Weller, K. L.; Ziller, J. W. *Organometallics* **1991**, *10*, 2526.
- (24) Feher, F. J.; Terroba, R.; Ziller, J. W. *Chemical Communications* **1999**, *22*, 2309.
- (25) Barry, A. J.; Daudt, W. H.; Domicone, J. J.; Gilkey, J. W. *Journal of the American Chemical Society* **1955**, *77*, 4248-4252.
- (26) Larsson, K. *Arkiv for Kemi* **1960**, *16*, 209-214.
- (27) Kong, X.; Tang, B. Z. *Chemistry of Materials* **1998**, *10*, 3352.
- (28) Busico, V.; Corradini, P.; Vacatello, M. *Journal of Physical Chemistry* **1982**, *86*, 1033.
- (29) Sudholter, E. J. R.; Engberts, J. B. F. N.; de Jeu, W. H. *Journal of Physical Chemistry* **1982**, *86*, 1908.
- (30) Kanazawa, A.; Tsutsumi, O.; Ikeda, T.; Nagase, Y. *Journal of the American Chemical Society* **1997**, *119*, 7670.
- (31) Mather, P. T.; Wu, J.; Haddad, T. S. In *Society of Rheology Annual Meeting*: Pittsburgh, PA, 2003.
- (32) Wu, S. *Journal of Polymer Science Part B-Polymer Physics* **1989**, *27*, 723-741.
- (33) Lomellini, P.; Lavagnini, L. *Rheologica Acta* **1992**, *31*, 175-182.
- (34) Larson, R. G. *The Structure and Rheology of Complex Fluids*; Oxford University Press: Oxford, 1998.
- (35) Fuchs, K.; Friedrich, C.; Weese, J. *Macromolecules* **1996**, *29*, 5893-5901.
- (36) Dealy, J. M.; Wissbrun, K. F. *Melt Rheology and its Role in Plastics Processing: Theory and Applications*; Van Nostrand Reinhold: New York, 1990.
- (37) Smallwood, H. M. *Journal of Applied Physics* **1944**, *15*, 758.
- (38) Batchelor, G. K. *Journal of Fluid Mechanics* **1970**, *41*, 545.
- (39) Batchelor, G. K. *Journal of Fluid Mechanics* **1971**, *46*, 813.
- (40) Batchelor, G. K. *Journal of Fluid Mechanics* **1977**, *83*, 97.
- (41) Poslinski, A. J.; Ryan, M. E.; Gupta, R. K.; Seshadri, S. G.; Frechette, F. J. *Journal of Rheology* **1988**, *32*, 703.
- (42) Graessley, W. W. *Advances in Polymer Science* **1974**, *16*, 133.
- (43) Nakajima, N.; Varkey, J. P. *Journal of Applied Polymer Science* **1998**, *69*, 1727.
- (44) Doi, M.; Edwards, S. F. *The Theory of Polymer Dynamics*; Clarendon Press: Oxford, 1986.
- (45) Liebler, L.; Rubinstein, M.; Colby, R. H. *Macromolecules* **1991**, *24*, 4701.
- (46) Yurekli, K.; Krishnamoorti, R.; Tse, M. F.; McElrath, K. O.; Tsou, A. H.; Wang, H.-C. *Journal of Polymer Science Part B-Polymer Physics* **2000**, *39*, 256.

- (47) Lim, Y. T.; Park, O. O. *Rheologica Acta* **2000**, *40*, 220.
- (48) Ferry, J. D. *Viscoelastic Properties of Polymers*, 3 ed.; John Wiley & Sons: New York, 1980.
- (49) Fetters, L. J.; Graessley, W. W.; Kiss, A. D. *Macromolecules* **1991**, *24*, 3136-3141.
- (50) Doolittle, A. K.; Doolittle, D. B. *Journal of Applied Physics* **1957**, *28*, 901.

*Chapter 3: Miscibility and Viscoelastic Properties of Acrylic
Polyhedral Oligomeric Silsesquioxane–Poly(methyl methacrylate)
Blends*

(A summary of this work will appear in the journal *Polymer* in late Spring 2005.)

3.1 Introduction

Polymers filled with very small nanoparticles ($d < 15$ nm) have been studied both theoretically and experimentally in recent years and a number of unusual results have been reported.¹⁻⁸ While conventional fillers ($d \geq 50$ nm) reinforce polymer matrices regardless of the polymer-particle interaction, nanoparticles have shown the ability to either reinforce or plasticize polymer matrices depending on their size and the interfacial interaction between the polymer and the nanoparticle. Roberts et al.⁵ reported the effect of particle size in silicate particle–poly(dimethyl siloxane) blends. Very small particles ($d = 0.7$ nm) reduced the viscosity of poly(dimethyl siloxane) while larger silicate particles ($d = 4.4$ nm) increased the viscosity. Mackay et al.³ further demonstrated the effect of very small size by blending crosslinked poly(styrene) particles ($d = 6$ – 10 nm) with linear poly(styrene). They reported as much as a 70% decrease in viscosity with the addition of nanoparticles and also a decrease in the glass transition temperature T_g . Zhang and Archer⁶ reported the dramatic effect that polymer-particle interactions have on polymer-nanoparticle rheology. They observed solid-like behavior in the linear viscoelastic properties of poly(ethylene oxide) when bare silica nanoparticles ($d = 12$ nm) were added at a volume fraction of only $\phi = 0.02$, but there was no effect on the rheological properties when the polymer-nanoparticle interaction was essentially

athermal. Starr et al.^{7,8} performed a computational study that simulated a polymer chain near a nanoparticle ($d = 10$ nm) and calculated cases for which the polymer-nanoparticle interaction was either attractive or non-attractive. For the attractive case, the glass transition temperature T_g increased by approximately 6% for a particle loading of 8 wt% while for the non-attractive case the T_g decreased by a similar amount at the same loading. McCoy et al.⁴ reported similar results for polymers in confined geometries.

A class of nanoparticles that has drawn significant attention recently are polyhedral oligomeric silsesquioxanes (POSS). They are hybrid organic-inorganic nanoparticles with a cage structure R_xT_x , where R represents an organic group on each corner, T represents a silsesquioxane linkage $SiO_{3/2}$, and x commonly has values of 8, 10, or 12. An $R_{10}T_{10}$ POSS cage ($d \approx 2$ nm) with acrylic R-groups is shown in Figure 1(a). In light of the recent work on polymer-nanoparticle systems, the hybrid structure of POSS particles, with a silica core and a variable organic shell, offers a precise way to vary the polymer-nanoparticle interaction and thereby achieve either plasticization or reinforcement, depending on the application. A wide variety of studies have been carried out on POSS-containing copolymers and POSS-homopolymer blends,⁹ probing their thermal,¹⁰⁻¹⁷ morphological,^{10,13,14,17-25} mechanical,^{21,23,24,26,27} and self-assembly,^{10,28} properties. The rheological behavior of POSS-filled homopolymers has been studied by us¹³ and by others.²⁹ In both cases, the POSS filler tended to phase separate into microcrystallites, even at loadings as small as $\phi = 0.01$. Despite this phase separation, we observed a slight decrease in the viscosity for loadings $\phi < 0.05$.¹³ This decrease was attributed to a small amount of molecularly-dispersed POSS particles that plasticized the matrix in the melt state at small loadings; however we did not observe a decrease in either

T_g or an increase in the fractional free volume f_0 , which would be expected if plasticization were occurring.

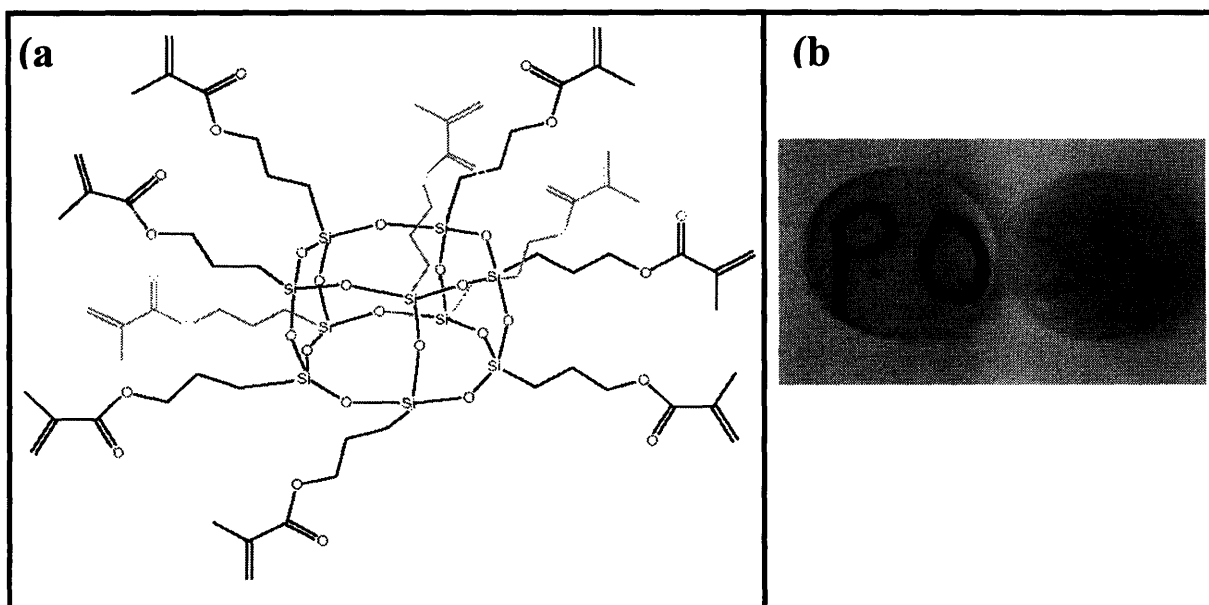


Figure 3.1 (a) Chemical structure of the unmodified acrylic-POSS used in the study. The hydrogenated form was the same but for the absence of any pendant carbon-carbon double bonds. (b) Comparison of clarity of two blends containing 20 vol% acrylic-POSS in PMMA. The clearer sample on the left contains the unmodified POSS pictured in Figure 3.1(a); the opaque sample on the right contains the hydrogenated form of the POSS in Figure 3.1(a), which contains no carbon-carbon double bonds.

The difficulty in suppressing crystallization of the POSS fillers when dispersed in homopolymers led to the selection of a non-crystallizable POSS species for the present study. To further improve the dispersion in PMMA, two POSS species with acrylic R-groups were chosen. One contained pendant carbon-carbon double bonds [pictured in Figure 3.1(a)] and the other was hydrogenated to reduce the double bonds to single bonds.

3.2 Experimental Section

3.2.1 Materials

The polymer used in the present study was a commercial poly(methyl methacrylate)(PMMA) resin obtained from Atofina Chemicals (Atoglas V920) with a weight average molecular weight $M_w = 80,200$ g/mol and a polydispersity $M_w/M_n = 1.7$. The PMMA was blended with two similar but distinct acrylic-POSS species: the first contained methacryloxypropyl R-groups (Hybrid Plastics Methacryl-POSS) and was used as received, the second was a hydrogenated form of the first that contained no carbon-carbon double bonds. Both types of POSS were mixtures of T₈, T₁₀, T₁₂, and T₁₄ cages, with the T₁₀ cages having the highest weight fraction (T₁₀ = 47.5 wt%; T₁₂ = 27.3 wt%; T₁₄ = 21.4 wt%; T₈ = 3.8 wt% as measured by NMR). The chemical structure of a T₁₀ cage of the unmodified acrylic-POSS is pictured in Figure 1. Both types of acrylic-POSS had a density $\rho = 1.19$ g/cm³.

3.2.2 Hydrogenation of (Methacryloxypropyl)_n(SiO_{3/2})_n

In a glass-lined PARR pressure vessel, 13 grams of (methacryloxypropyl)_n(SiO_{3/2})_n (Hybrid Plastics) was dissolved in 50 mL of dry toluene along with 50 mg of 5% palladium on carbon catalyst (Aldrich). The reactor was pressurized to 500 psi of hydrogen gas and heated to 70 °C for 14 hours. After cooling to room temperature, the reactor was reduced to atmospheric pressure and the solution was filtered through a short pad of silica to remove the catalyst. Removal of the toluene solvent produced the thick viscous product. Proton nmr spectroscopy showed the complete removal of starting material olefinic protons at 6.0 and 5.5 ppm. ¹H NMR (CDCl₃ referenced to residual CHCl₃ at 7.26 ppm) 3.99 (mult, 2H, CH₂O), 2.50 (sept, ³J_{H-}

$J_{\text{H-H}} = 6.8$ Hz, 1H, CH), 1.67 (mult, 2H, $\text{CH}_2\text{CH}_2\text{CH}_2$), 1.12 (d, $^3J_{\text{H-H}} = 6.8$ Hz, 6H, CH_3), 0.63 (mult, 2H, SiCH_2). $^{13}\text{C}\{^1\text{H}\}$ NMR (CDCl_3 referenced at 77.0 ppm; multiple peaks are observed due to the presence of a variety of POSS cages sizes with $n = 10$ and 12 the most abundant) 176.92 & 176.89 (C=O), 65.86 & 65.81 (OCH_2), 33.84 (CH), 22.35 & 22.22 ($\text{CH}_2\text{CH}_2\text{CH}_2$), 18.91 (CH_3), 9.02 & 8.50 (SiCH_2). $^{29}\text{Si}\{^1\text{H}\}$ NMR (referenced to external SiMe_4 at 0 ppm) -65.6, -66.6 (T_8), -67.5, -67.6, -67.7, -67.8, -68.1, -68.2 (T_{12}), -68.5 (T_{10}), -70.9 (T_{12}).

3.2.3 Solution Blending and Sample Preparation

Blends were prepared by dissolving PMMA and the acrylic-POSS at approximately 10 wt% in THF at room temperature. The solutions were poured into a partially-covered petri dish and the solvent was evaporated over a period of 24 hours. The cast films were then further dried in a vacuum oven at 110°C for 48 hours. Lower temperatures were insufficient to remove all of the solvent. Samples for rheological and dynamic mechanical analysis were molded in a Carver Press at a temperature $T = 190^\circ\text{C}$.

3.2.4 Thermal and Morphological Characterization

The blends were characterized using differential scanning calorimetry (DSC), dynamic mechanical analysis (DMA), and dynamic thermal analysis (DTA). The DSC tests were performed on a TA Instruments Q1000. Samples were heated to $T \geq T_g + 50^\circ\text{C}$ at a rate of 5°C/min, cooled to $T = -90^\circ\text{C}$ at the same rate, and data were collected on the second heating ramp at 5°C/min. Glass transition temperatures T_g were determined from the inflection point in the heat flow versus temperature curves. The DMA measurements were carried out on a TA Instruments Q800 using rectangular samples (50 mm \times 12 mm \times 3 mm) in a three-point bending geometry. Samples were cooled to $T = -80^\circ\text{C}$ and held

for five minutes before being subsequently heated to $T = 150^{\circ}\text{C}$ at a rate of $3^{\circ}\text{C}/\text{min}$.

DTA tests were performed on a Perkin-Elmer Diamond Thermomechanical Analyzer to determine the linear coefficient of thermal expansion. A quartz probe was used on cylindrical samples with dimensions diameter $d = 4$ mm and height $h = 6$ mm. The heating rate was $3^{\circ}\text{C}/\text{min}$.

Wide angle x-ray diffraction (WAXD) was performed on a Rigaku RU300 18kW rotating anode generator with a 250 mm diffractometer. Tests were carried out at 23°C using CuK_{α} radiation.

3.2.5 Rheological Characterization

Rheological tests were performed on a TA Instruments AR2000 controlled-stress rheometer. Samples were tested between 25 mm parallel plates in small amplitude oscillatory shear flow at strains between 0.1 and 2%. The average gap separation was 2 mm. Master curves of the storage modulus G' and the loss modulus G'' were generated using horizontal shift factors a_T determined from the loss tangent $\tan \delta = G''/G'$ over the temperature range $125^{\circ}\text{C} \leq T \leq 210^{\circ}\text{C}$. Subsequent vertical shift factors b_T were required to account for changes in density and variations in the gap separation with temperature.

3.3 Results and Discussion

3.3.1 Differential Scanning Calorimetry

In Figure 3.2(a) we plot differential scanning calorimetry (DSC) curves for the unmodified acrylic-POSS-PMMA blends. Loadings up to $\phi = 0.30$ lead to a decrease in the glass transition temperature T_g and a broadening of the glass transition region. In the $\phi = 0.30$ blend, a second glass transition event appears at $T = -55^{\circ}\text{C}$. This corresponds to the T_g of the pure POSS and indicates significant phase separation at this loading. This is

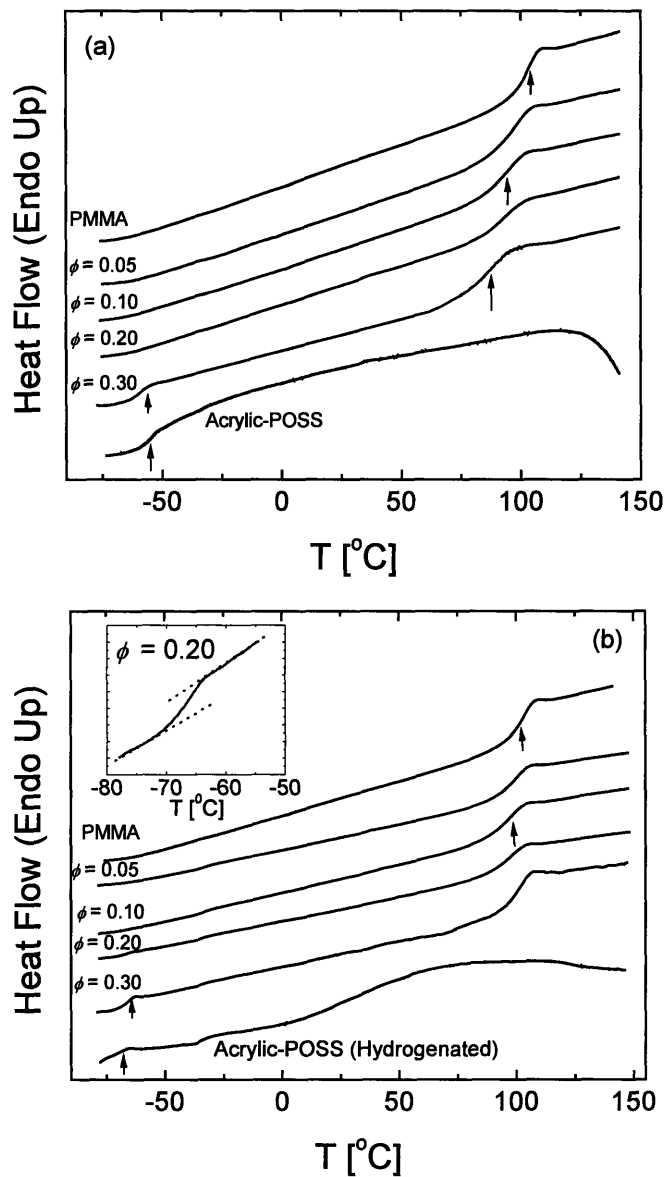


Figure 3.2 DSC curves for (a) unmodified acrylic-POSS in PMMA and (b) hydrogenated acrylic-POSS in PMMA. The inset in (b) is a close-up of the low- T region of the 20 vol% blend, showing evidence of phase separation.

also the point at which optical clarity of the unmodified acrylic-POSS blends is lost. The curve for the pure acrylic-POSS in Figure 3.2(a) shows the beginning of a large endotherm at $T = 120^{\circ}\text{C}$. This is due to crosslinking initiated by the pendant carbon-carbon double bonds on the corners of the acrylic-POSS cages. The only measured

composition to show evidence of this crosslinking in DSC was $\phi = 0.30$, which showed a very shallow endotherm beginning slightly above $T = 150^\circ\text{C}$, just outside the range of the data plotted in Figure 3.2.

In Figure 3.2(b) we show DSC curves for the hydrogenated form of the acrylic-POSS in PMMA. A similar trend of decreasing glass transition temperature T_g with increasing POSS loading is observed, however the drop in T_g is less substantial in the hydrogenated system [see Figure 3.3]. The decreased plasticization is also accompanied by much lower optical clarity when compared with the unmodified acrylic-POSS-PMMA blends at comparable POSS volume fractions. A comparison between the $\phi = 0.20$ blends in both the unmodified and the hydrogenated systems is shown in Figure 3.1(b). The unmodified POSS blend is nearly transparent and the hydrogenated blend is almost completely opaque. The hint of a second T_g due to phase separation is present in the $\phi = 0.20$ hydrogenated blend at $T \approx -68^\circ\text{C}$ [see inset to Figure 3.2(b)] and becomes obvious in the $\phi = 0.30$ blend. No sharp endotherm at temperatures above 150°C is observed in the hydrogenated POSS, nor in any of the blends, indicating that crosslinking does not occur in this system.

The values of the glass transition temperatures T_g extracted from the DSC scans in Figure 3.2 are plotted in Figure 3.3 for both the unmodified and the hydrogenated acrylic-POSS-PMMA blends. The magnitude of the drop in T_g is always larger in the unmodified acrylic-POSS-PMMA system, and the difference grows progressively greater at higher loadings. The hydrogenated acrylic-POSS ceases to further plasticize the PMMA matrix above $\phi = 0.10$, whereas at $\phi = 0.20$ the unmodified acrylic-POSS

continues to induce a modest decrease in T_g . For comparison, the well-known Fox equation³⁰ has also been plotted as the dotted line in Figure 3.3:

$$\frac{1}{T_g} = \frac{\phi}{T_{g,POSS}} + \frac{(1-\phi)}{T_{g,PMMA}} \quad (1)$$

where $T_{g,PMMA}$ and $T_{g,POSS}$ are the pure component glass transition temperatures of the PMMA (104°C) and the unmodified acrylic-POSS (-55°C).

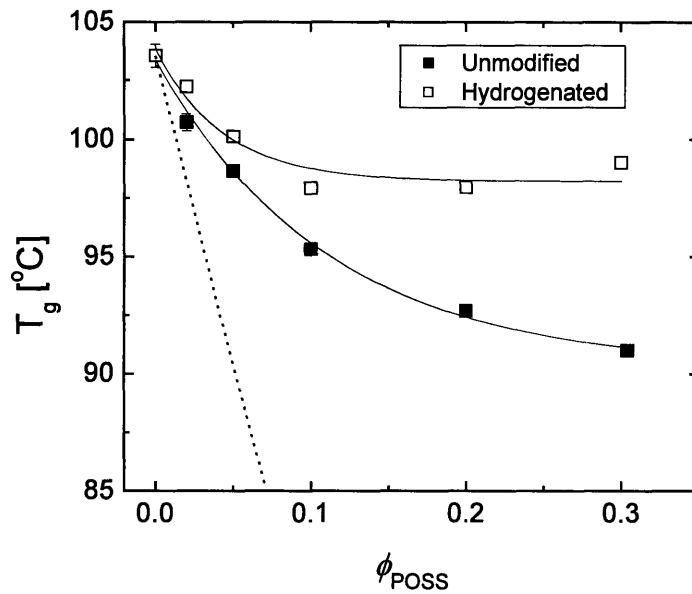


Figure 3.3 Glass transition temperatures measured in DSC for both types of acrylic-POSS—PMMA blends. The dotted line represents the prediction of the Fox Equation (Eqn. 1).

Neither blend system follows the prediction of the Fox equation; however, each system does have an approximately linear decrease in T_g at loadings $\phi \leq 0.10$ and they therefore follow the common relation for polymer-plasticizer blends at low concentrations of plasticizer:[31]

$$T_g = T_{g,PMMA} - k\phi \quad (2)$$

where k is a constant that typically ranges from 200°C to 500°C for plasticized polystyrene blends. By fitting the values of T_g at $\phi \leq 0.05$, k values of 98°C and 50°C are obtained for the unmodified and the hydrogenated acrylic-POSS–PMMA blends, respectively. These k values are well below the expected range for conventional plasticizers. It is likely that the relatively larger sizes of the POSS molecules ($V_{\text{POSS}} = 1297 \text{ cm}^3/\text{mol}$) compared with conventional plasticizers may be a primary cause for this disparity in k values. For comparison, we added dioctyl phthalate(DOP, $V_{\text{DOP}} = 403 \text{ cm}^3/\text{mol}$) to PMMA. At a DOP concentration $\phi = 0.05$, the measured T_g was 86.1°C and at $\phi = 0.10$ the T_g was 71.6°C., corresponding to a k value of 320°C, or approximately 3.2 times that observed in the unmodified acrylic-POSS–PMMA blends. At a plasticizer loading of $\phi = 0.05$, the actual number density of added plasticizer particles was much larger in the DOP–PMMA blend ($1.26 \times 10^{-4} \text{ mol per cm}^3$ of blend) than in the unmodified acrylic-POSS–PMMA blend ($0.39 \times 10^{-4} \text{ mol per cm}^3$ of blend). Therefore, adding 3.2 times as many DOP molecules per unit volume as acrylic-POSS molecules resulted in a comparably enhanced reduction in the T_g (reflected in the coefficient k in Equation 2) beyond that observed in the acrylic-POSS–PMMA blend. Therefore the lower degree of plasticization observed in the unmodified acrylic-POSS–PMMA blends at low loadings ($\phi \leq 0.10$) is a result of the larger size of the POSS molecules which, at a given volume fraction, leads to far fewer added POSS cages than in the DOP-PMMA blend. Consequently there is relatively less polymer-particle interface over which free volume can be generated in the POSS-modified blend, and hence the T_g reduction is correspondingly reduced.

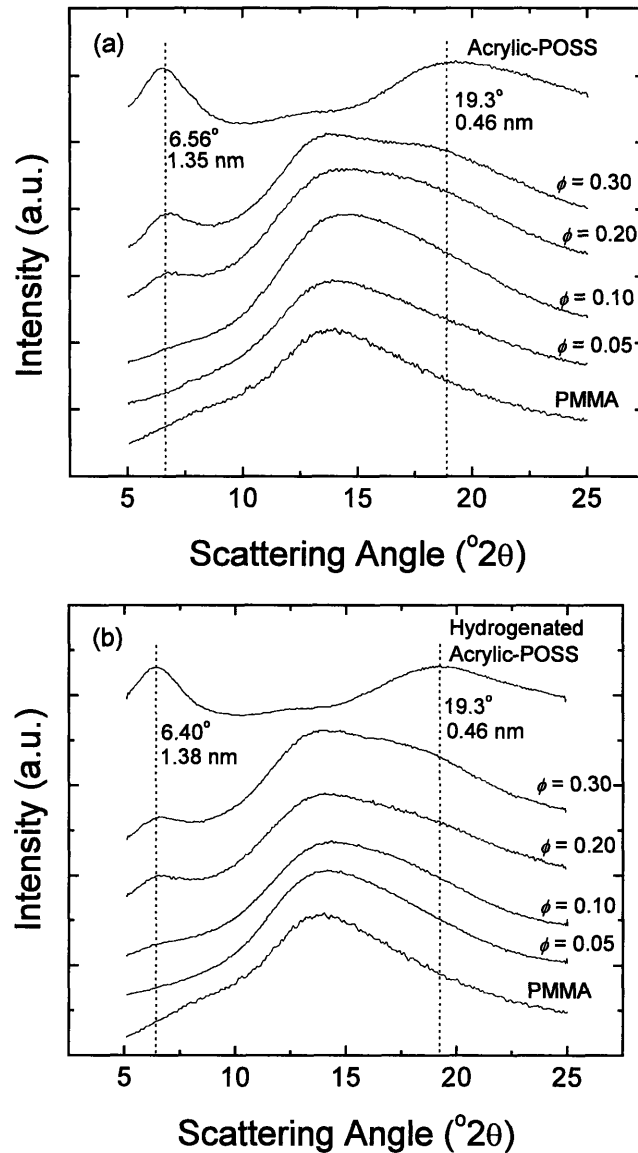


Figure 3.4 WAXD spectra for (a) unmodified acrylic-POSS in PMMA and (b) hydrogenated acrylic-POSS in PMMA.

3.3.2 Wide Angle X-ray Diffraction

Wide angle X-ray diffraction (WAXD) was used to further characterize the miscibility of the acrylic-POSS–PMMA blends. Diffraction patterns for the unmodified and the hydrogenated acrylic-POSS systems are shown in Figures 3.4(a) and 3.4(b), respectively. The characteristics of the WAXD patterns for the two blend systems are

similar at comparable loadings of POSS. In each case, the $\phi = 0.05$ and $\phi = 0.10$ diffraction patterns have only a broad amorphous peak at $2\theta \approx 14^\circ$, corresponding to the amorphous PMMA matrix peak. At $\phi = 0.20$, a shoulder matching the high-angle amorphous peak of the acrylic-POSS at $2\theta \approx 19.3^\circ$ appears, and becomes more prominent at $\phi = 30$. This corresponds to a spacing $d = 0.46$ nm, which is within the range $d = 0.4\text{--}0.5$ nm at which crystallizable POSS species and POSS-containing copolymers show a strong secondary peak.^{13,18-20,25} Broad peaks at $2\theta = 6.56^\circ$ in the $\phi = 0.20$ unmodified POSS blend and $2\theta = 6.40^\circ$ in the $\phi = 0.20$ hydrogenated POSS blend correspond to the low angle amorphous peaks in the pure POSS spectra. A spacing of $d = 1.35$ nm for the unmodified T₁₀ acrylic-POSS molecule of molecular weight 1544 g/mol is a reasonable center-to-center spacing; this would correspond to a mass density of 1.04 g/cm³ if the POSS were arranged on a simple cubic lattice (SC) and a mass density of 1.47 g/cm³ for a face-centered cubic lattice (FCC). The actual density of the non-crystalline acrylic-POSS at room temperature is 1.19 g/cm³, comfortably between the sparse SC limit and the close-packed FCC limit.

We would expect to see a shift in the location of the amorphous peak of the PMMA ($2\theta = 14.1^\circ$) if indeed POSS particles were distributed throughout the matrix. The nanoparticles would be expected to push chains apart and shift the peak to a higher d spacing (smaller 2θ angle). However, the POSS present in the blends tends to slightly shift the locations of the PMMA matrix peaks at loadings $\phi = 0.05$ and $\phi = 0.10$ in Figure 3.4 to higher 2θ values because of the very broad signal of the POSS centered at $2\theta = 19.3^\circ$. This does not allow the precise location of the matrix peak to be determined in these blends. However, the matrix peak and the POSS peak begin to separate at

$\phi = 0.20$ in both Figure 3.4(a) and Figure 3.4(b); at $\phi = 0.30$ it is possible to see both peaks. In the unmodified acrylic-POSS–PMMA blend spectra in Figure 3.4(a) at $\phi = 0.30$, the matrix peak location is $2\theta = 13.8^\circ$ ($d = 0.641$ nm), while in the hydrogenated blends in Figure 3.4(b) at $\phi = 0.30$ the matrix peak location is $2\theta = 14.0^\circ$ ($d = 0.632$ nm). These are both larger d spacings than in the pure PMMA ($d = 0.627$ nm), indicating penetration of the POSS nanoparticles between the PMMA chains. As expected, the unmodified acrylic-POSS [Figure 3.4(a)], which is more miscible than the hydrogenated form, shows a larger shift in the amorphous peak location.

3.3.3 Rheology

In Figures 3.5 and 3.6, we plot master curves of the storage and loss moduli for PMMA filled respectively with unmodified and hydrogenated acrylic-POSS at a reference temperature $T_0 = 170^\circ\text{C}$. All blends closely followed the principles of time-temperature superposition (TTS) with a lateral shift $a_T(T, T_0)$ and a vertical shift $b_T(T, T_0)$.³¹ The addition of POSS causes significant shifts downward and to the right in the storage modulus $G'(\omega)$ and the loss modulus $G''(\omega)$. The shifts are greatest at loadings $\phi \leq 0.10$, which is also the region of steepest decrease in the T_g shown in Figure 3.3. In the blends containing $\phi \geq 0.05$ unmodified acrylic-POSS in PMMA (Figure 3.5), the storage modulus measured at low frequencies deviates from the characteristic terminal slope of 2 expected for simple viscoelastic fluids; this is caused by crosslinking of the pendant carbon-carbon double bonds on the unmodified acrylic-POSS. The $\phi = 0.05$ blend and the $\phi = 0.10$ blend begin to show crosslinking effects at a reduced frequency $a_T\omega \approx 10^{-2}$ rad/s, whereas the $\phi = 0.30$ blend shows this effect close to $a_T\omega \approx 10^{-1}$ rad/s. Samples containing $\phi \geq 0.05$ unmodified acrylic-POSS could not be fully

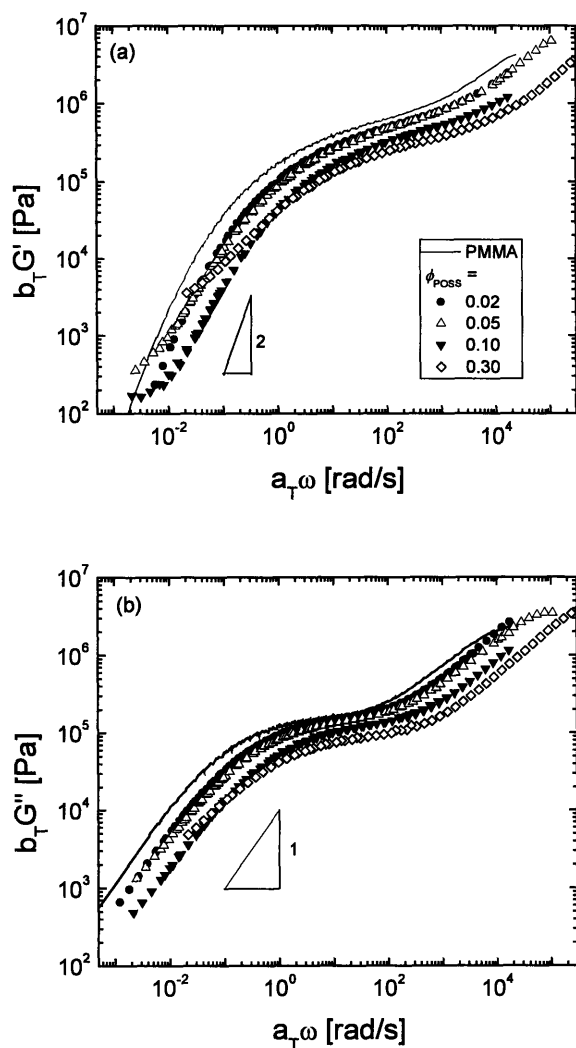


Figure 3.5 Master curves at $T_0 = 170^\circ\text{C}$ for (a) the storage modulus G' and (b) the loss modulus G'' of unmodified acrylic-POSS—PMMA blends.

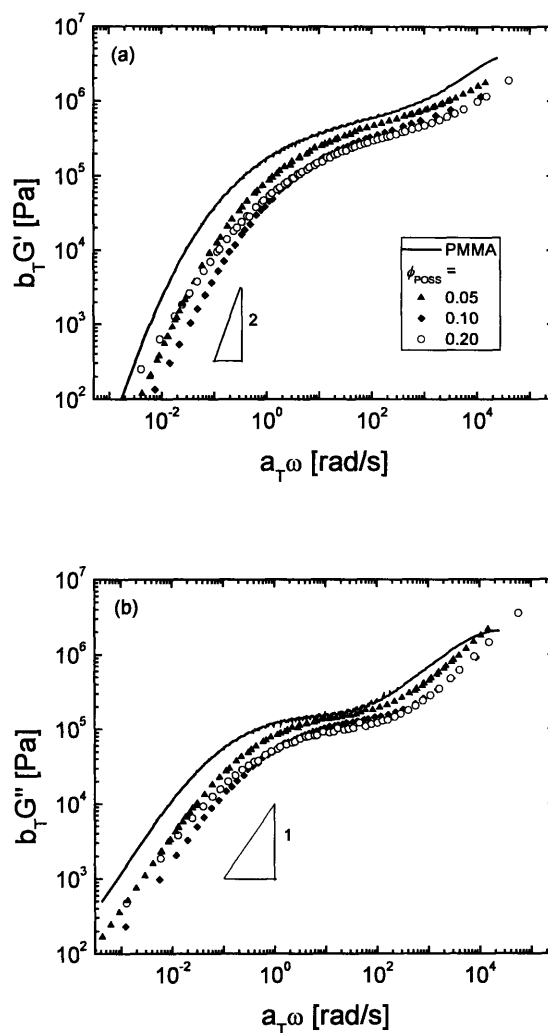


Figure 3.6 Master curves at $T_0 = 170^\circ\text{C}$ for (a) the storage modulus G' and (b) the loss modulus G'' of hydrogenated acrylic-POSS—PMMA blends.

redissolved in THF after testing, and GPC showed that no noticeable amount of the polymer was able to pass through a $0.45\ \mu\text{m}$ filter. The $\phi = 0.02$ blend does not show any effect of crosslinking in Figure 3.5(a). The concentration dependence of the onset of crosslinking provides a clear indication that it is initiated by POSS-POSS contacts in the melt. At very low loadings ($\phi < 0.05$), POSS-POSS interparticle contacts are rare and thus no crosslinked network is formed; however, at higher loadings, the POSS cages

contact each other regularly at high temperatures and are increasingly prone to react with each other to form a weakly crosslinked gel.

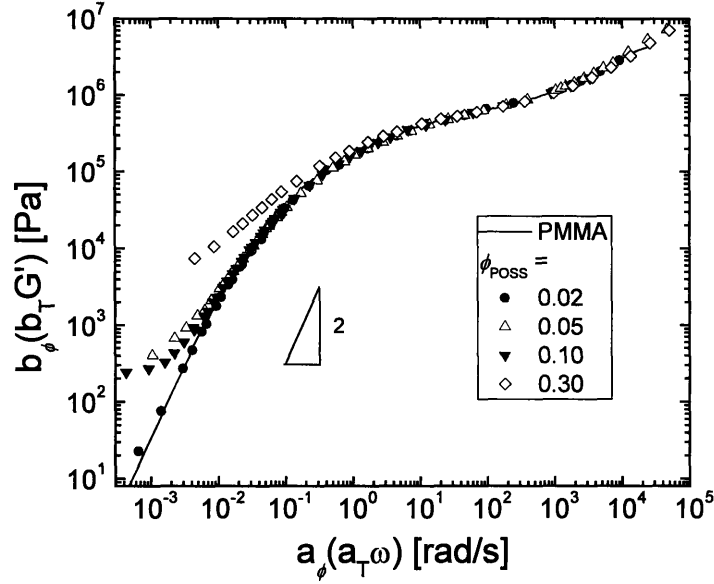


Figure 3.7 Storage modulus curves for the unmodified acrylic-POSS—PMMA blends after applying horizontal (a_ϕ) and vertical (b_ϕ) concentration-dependent shift factors to superpose all curves onto the storage modulus curve of the unfilled homopolymer.

A common way to quantify the effect of a plasticizer on the linear viscoelastic properties of a polymer melt is with the relation³²:

$$\frac{G_N^0\{\phi\}}{G_{N,unfilled}^0} = (1 - \phi)^n \quad (3)$$

where $G_N^0\{\phi\}$ and $G_{N,unfilled}^0$ are the rubbery plateau moduli for a polymer containing a volume fraction ϕ of plasticizer and an unfilled polymer respectively, and the exponent n is a constant. The plateau modulus of the unfilled polymer ($G_{N,unfilled}^0$) was determined using the convention³³⁻³⁵:

$$G_N^0 = (G'(\omega))_{\tan\delta \rightarrow \min} \quad (4)$$

so that the plateau modulus is taken as the point in the storage modulus at which the loss tangent $\tan \delta = G''/G'$ passes through a minimum. To determine the plateau moduli of the POSS–PMMA blends, the storage modulus curves for the blends were shifted manually by a horizontal factor a_ϕ and a vertical factor b_ϕ onto the G' curve of the unfilled polymer^{32,36}. These shifted curves are shown in Figure 3.7. The plateau modulus for each blend was then calculated as $G_N^0\{\phi\} = b_\phi G_{N,unfilled}^0$. These values of the plateau modulus are reported in Table 3.1. The quantity $-\log b_\phi$ is plotted against $-\log(1-\phi)$ in Figure 3.8. The slope of the linear fit to these data is equal to the exponent n in Equation 3. Many previous studies on polymer-plasticizer systems have reported values of n between 2.0 and 2.3.^{32,37-40} At POSS loadings $\phi \leq 0.10$, the value of n is 2.47 ± 0.28 for the unmodified acrylic-POSS–PMMA blends and 2.24 ± 0.10 for the blends containing hydrogenated acrylic-POSS. These values are, within experimental error, similar to previous results for plasticized polymers. This volume fraction dependence of the plateau modulus on the POSS nanoparticle content is in contrast to the results obtained for the reduction of the glass transition temperature for POSS loadings $\phi \leq 0.10$, where the reduction in the T_g was much less than that induced by the conventional plasticizer dioctyl phthalate. Above $\phi = 0.10$, the exponent n decreases significantly in the unmodified acrylic-POSS–PMMA blends to a value of 0.96 ± 0.05 due to the significant degree of phase separation of added POSS at these higher loadings.

Table 3.1 Properties of Methacryl-POSS-PMMA Blends ($T_0 = 170^\circ\text{C}$)

Vol% POSS	Hydrogenated	T_g [$^\circ\text{C}$]	G_N^0 (Pa)	c_1^0	c_2^0 [K]	f_0/B	f_g/B
0		103.6	5.15×10^5	9.5	187	0.046	0.029
2	No	100.7	4.78×10^5	8.4	162	0.052	0.030
5	No	98.7	4.62×10^5	7.7	148	0.057	0.029
10	No	95.3	3.97×10^5	6.8	141	0.064	0.030
20	No	92.7	3.47×10^5	7.0	153	0.062	0.030
30	No	91.0	3.08×10^5				
<hr/>							
5	Yes	100.1	4.62×10^5	9.3	189	0.046	0.029
10	Yes	97.9	4.05×10^5	8.1	173	0.053	0.031
20	Yes	98.0	3.35×10^5	8.4	172	0.052	0.030

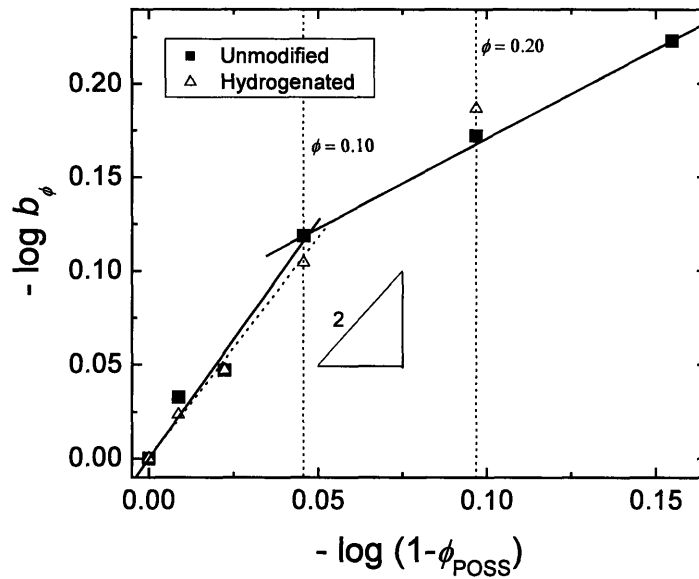


Figure 3.8 A log-log plot of the horizontal shift factor

$b_\phi = G_N^0\{\phi\} / G_{N,unfilled}^0$ against $(1-\phi_{POSS})$. The slope for conventional plasticizer-polymer systems typically lies between 2.0 and 2.3.

3.3.4 Time-Temperature Superposition and Free Volume

The TTS shift factors a_T obtained from the construction of the thermorheological master curves in Figures 3.5 and 3.6 were analyzed using the WLF equation³¹:

$$\log a_T = \frac{-c_1^0(T - T_0)}{c_2^0 + (T - T_0)} \quad (5)$$

where c_1^0 and c_2^0 are constants and T_0 is the reference temperature. Values of the constants c_1^0 and c_2^0 were determined by plotting the quantity $-(T - T_0)/\log a_T$ against $(T - T_0)$;^{31,41} the coefficient c_1^0 was obtained from the reciprocal of the slope, and the coefficient c_2^0 from the intercept. The WLF coefficients are reported in Table 3.1. The addition of unmodified acrylic-POSS leads to a strong decrease in c_1^0 and a significant increase in c_2^0 . Similar trends are observed in the hydrogenated system, however the changes are less substantial. An important parameter that can be obtained from these fits is the fractional free volume f_0 :

$$f_0 = \frac{B}{2.303c_1^0} \quad (6)$$

where B is a constant usually assumed to be unity³¹. These fractional free volume values are plotted in Figure 3.9. A clear trend is observed in the unmodified acrylic-POSS blend system. The free volume increases significantly for loadings $\phi \leq 0.10$ and appears to asymptote towards a maximum value for $\phi \geq 0.20$.

The differential between the fractional free volume of the unfilled PMMA ($f_0 = 0.046$) and the $\phi = 0.05$ blend ($f_0 = 0.057$) is $\Delta f_0 = 0.011$, or $1.1 \times 10^{19} \text{ nm}^3$ per cm^3 of the blend. At $\phi = 0.05$, there are 2.32×10^{19} POSS molecules per cm^3 of the blend (assuming all T_{10} cages); from these values we may infer that the amount of free volume generated per added POSS molecule is 0.47 nm^3 . The T_{10} acrylic-POSS cage has an approximate diameter of 2 nm, which corresponds to a hydrodynamic volume of 4.2 nm^3 . The dense silica core, which contains 10 silicon atoms and 15 oxygen atoms, takes up less than 10% of this volume but contains 34% of the mass. The volume of the shell containing the acrylic R-groups is more than 3.5 nm^3 . The density of the ten R-groups in this shell is

approximately 0.45 g/cm^3 , or half the bulk density of 0.9 g/cm^3 expected if the methacryloxypropyl R-groups were in their bulk state. This leaves approximately 1.75 nm^3 in the outer shell unfilled. The free volume increase per POSS molecule (0.47 nm^3) is approximately one-fourth this value and is quite reasonable when one considers the difficulty in fitting the relatively large polymer chains ($R_g \approx 15 \text{ nm}$) into the small spaces between R-groups ($< 0.5 \text{ nm}$). The values of the fractional free volume plateau at $\phi = 0.20$ because the POSS phase-separates and begins to pack in its bulk amorphous configuration.

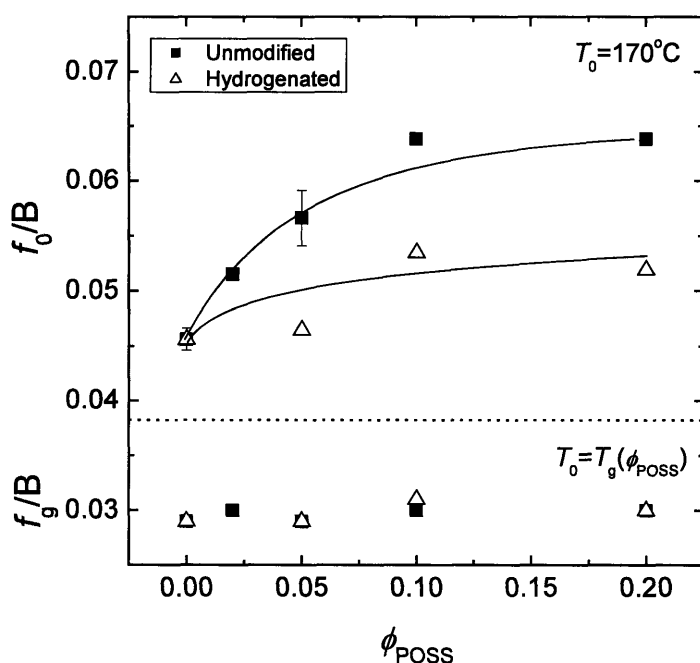


Figure 3.9 Variation of the fractional free volume f_0/B with increasing volume fraction of POSS nanoparticles at a reference temperature $T_0 = 170^\circ\text{C}$. Also shown is the fractional free volume f_g/B at the glass transition temperature of each blend (see Table 3.1). The error bars for the unfilled PMMA and the $\phi = 0.05$ blend in the unmodified acrylic-POSS system were determined by taking the standard deviation of three different samples.

The free volume data in Figure 3.9 help clarify our previous results for PMMA filled with crystallizable-POSS species.¹³ This earlier study reported that the POSS had a

strong tendency to phase-separate into crystallites, even at loadings of $\phi = 0.01$, and we could not find a clear trend in free volume with increasing POSS content. The present data show that molecularly-dispersed POSS nanoparticles can plasticize PMMA by increasing the free volume within the matrix.

The fractional free volume f_0 at the reference temperature T_0 may be converted to the fractional free volume f_g at the glass transition temperature T_g using the relation³¹:

$$f_g = \frac{f_0(c_2^0 + T_g - T_0)}{c_2^0} \quad (7)$$

Values of f_g/B are listed in Table 3.1 and plotted at the bottom of Figure 3.9. These values are approximately the same for all blends within experimental error. This indicates that, in these two blend systems, the glass transition is essentially an iso-free volume condition, and long range molecular relaxation occurs only when the free volume reaches the same critical level regardless of blend composition. The differential increase in free volume $\Delta f_0(\phi)$ arising from the addition of POSS therefore serves to lower the temperature at which the total available free volume within the blends reaches this critical level, which is $f_g = 0.030 \pm 0.001$ for this set of PMMA-based materials. This result is in good agreement with the range of values reported by Ferry for conventional thermoplastics, which tend to fall in the range $0.025 \leq f_g \leq 0.035$.³¹

3.3.5 Thermomechanical Analysis

We have shown that acrylic-POSS has a significant softening effect on the melt-state properties of PMMA (Figures 3.5 and 3.6). The effect on the solid-state properties is also interesting in that it can reveal how the materials will behave at room temperature and below. Dynamic mechanical analysis was performed on the unmodified acrylic-

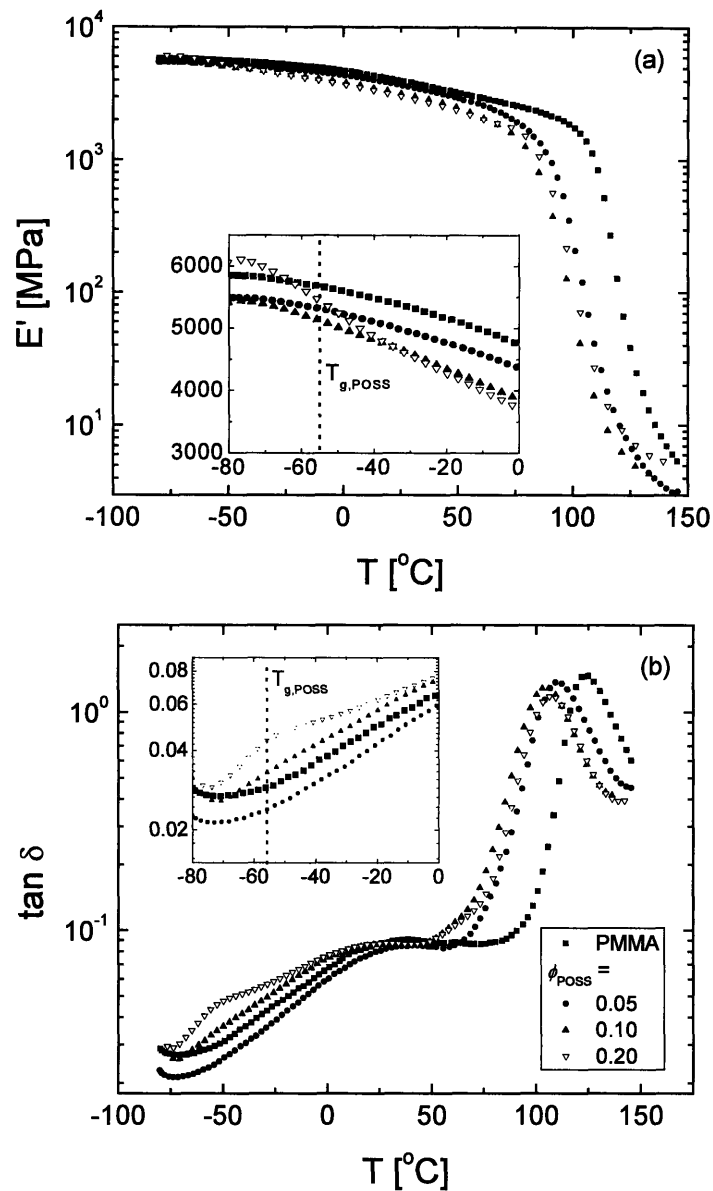


Figure 3.10 DMA curves at a frequency of 1 Hz for (a) the storage modulus E' and (b) the loss tangent $\tan \delta$ for blends of unmodified acrylic-POSS and PMMA.

POSS–PMMA blends, which were more miscible than the hydrogenated-POSS–PMMA blends. The storage modulus E' and the loss tangent $\tan \delta = E''/E'$ measured at a frequency of 1 Hz are plotted as a function of temperature in Figure 3.10. The trend observed in E' with increasing POSS loading is a decrease in the magnitude of the glassy

modulus and a transition into the rubbery region at lower temperatures, consistent with a plasticizing effect.

When focusing more closely on the low temperature region $-80^{\circ}\text{C} \leq T \leq 0^{\circ}\text{C}$ [see inset to Figure 3.10(a)], the effect of the plasticizer in the T_g region of the POSS can be observed. The $\phi = 0.05$ blend has a lower modulus than the unfilled PMMA but the two curves show no discernable difference in shape. The absence of any stiffening in the T_g region of the POSS is clear evidence that the POSS is dispersed on a molecular scale at a loading of $\phi = 0.05$. The $\phi = 0.10$ blend has the same value of the storage modulus as the $\phi = 0.05$ blend at $T = -80^{\circ}\text{C}$ but the modulus diverges to lower values as the temperature increases, indicating some aggregation of the POSS. The most significant difference is in the $\phi = 0.20$ blend, which has the highest modulus below the T_g of the POSS ($T_{g,\text{POSS}} = -55^{\circ}\text{C}$) but when the temperature is increased to $T = -25^{\circ}\text{C}$, it has the lowest modulus of any of the samples tested. This low temperature stiffening is caused by vitrified domains of phase-separated POSS that reinforce the sample like a rigid filler and make it stiffer than the pure matrix material. Above the T_g of the POSS, however, these hard POSS domains soften into sub-micron sized pools that reduce the stiffness of the material. Not surprisingly, this behavior also significantly affects the loss tangent E''/E' shown in Figure 3.10(b). Not only is the β -relaxation of the PMMA shifted to lower temperatures with the addition of POSS, but in the glass transition region of the POSS, a conspicuous shoulder is present in the $\phi = 0.20$ blend.

A practically important property that is often adversely affected by plasticizers is the coefficient of thermal expansion (CTE). Common plasticizers like dioctyl phthalate are liquids at room temperature and they consequently increase the CTE of glassy

polymers. The methacryl-POSS used in this study also acts like a plasticizer, thus we would expect it to increase the CTE of PMMA, however it is unclear how much in a quantitative sense. Comparing the effects of methacryl-POSS and DOP on the CTE of PMMA would be instructive and would indicate whether POSS, with its silica core, is better, worse, or the same as the organic DOP with regard to its effect of this important property.

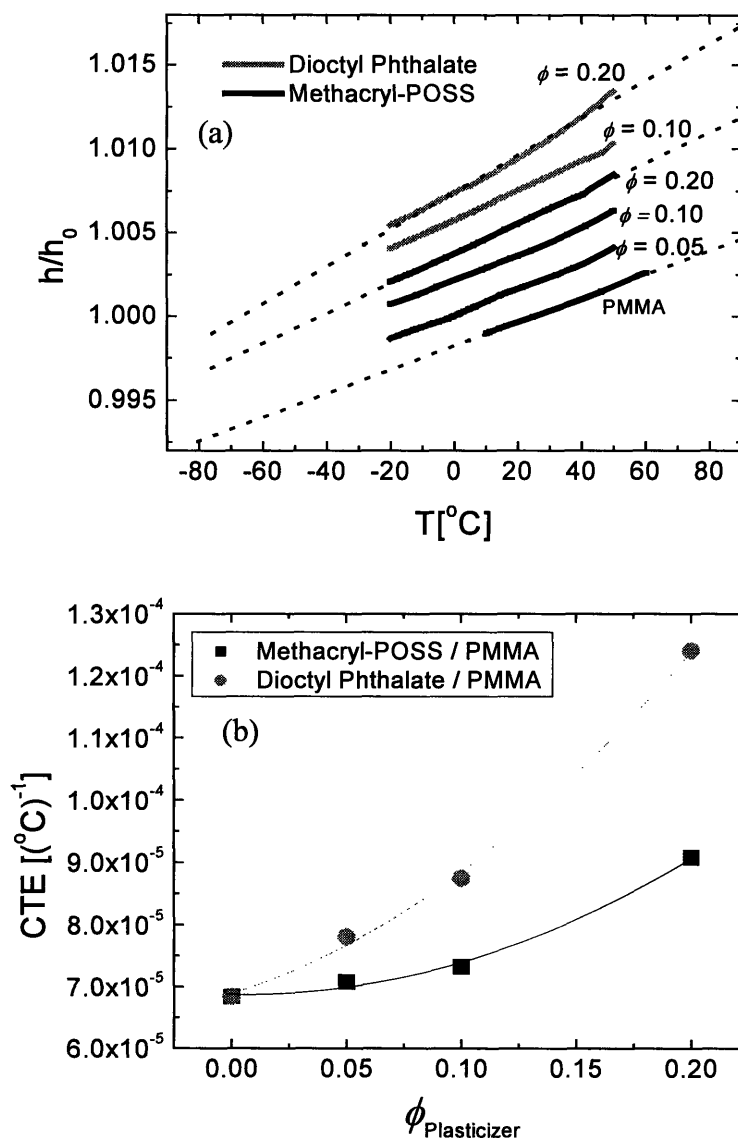


Figure 3.11 Coefficient of thermal expansion (CTE) measurements for both methacryl-POSS in PMMA and diethyl-phthalate (DOP) in PMMA. (a) Normalized height of sample as a function of temperature; (b) CTE as function of diluent content.

In Figure 3.11(a), the normalized heights of the cylindrical samples used to determine CTE are plotted against temperature over the range $-20^{\circ}\text{C} \leq T \leq 60^{\circ}\text{C}$ (bracketing room temperature). The data show good linearity in this temperature region. This plot is ineffective at resolving the differences in the CTE (taken from the slope of the data) between the samples containing $\phi \leq 0.10$. However, by fitting a straight line to the $\phi = 0.20$ blends it is apparent that the slope of 20 vol%-filled DOP blend does in fact have a noticeably high slope than the 20 vol%-filled methacryl-POSS blend. By calculating the slopes of the linear fits to these data sets the values of the linear CTE were determined. These are plotted in Figure 3.11(b) for both the DOP blends and the methacryl-POSS blends. Here a significant difference between the behavior of the POSS-PMMA and DOP-PMMA blends is apparent. The DOP-PMMA blends have much higher CTE values than the corresponding methacryl-POSS-PMMA blends at all loadings. Even at 5 vol%, at which point WAXD and DMA both suggest complete dispersion of the POSS, the CTE is significantly lower in the comparably well-dispersed 5% DOP blend. Only a 3.6% increase in CTE is caused by adding 5 vol% POSS, while adding the same volume of DOP causes a 14.2% increase. The 10 vol% POSS blend shows only a small increase as well before a much more significant increase at 20 vol% (at which point a significant fraction of the POSS is in phase-separated pools).

The reason for the more stable coefficient of thermal expansion values in the POSS blends is likely due to two factors. One, the POSS is approximately 35% inorganic by mass. The core of Si-O has a much smaller CTE than the acrylic R-groups and thus a large fraction of the molecule will not contribute significantly to the CTE. A second factor responsible for keeping the increase in CTE small is the fact that the POSS

particles are much larger than the DOP molecules. DOP and other plasticizers are typically a few hundred grams per mol, while the POSS is between 1500 and 2000 g/mol. Thus many fewer POSS cages are added at a given volume fraction than DOP molecules. Plasticizers are known to act largely by penetrating the spaces between chains, reducing interchain interactions and also increasing free volume. The total volume of the interfacial region should relate somewhat quantitatively to the degree of plasticization. This “interphase” will decrease with increasing size of molecules. Thus, in the POSS case, there is much less interfacial region over which plasticization may occur and thus a much smaller increase in CTE.

3.4 Conclusions

Blends of poly(methyl methacrylate)(PMMA) with two acrylic polyhedral oligomeric silsesquioxanes(POSS) were analyzed to determine the effect of well-dispersed POSS nanoparticles on the thermomechanical properties of PMMA. Differential scanning calorimetry (DSC), dynamic mechanical analysis (DMA), and melt rheology all showed that POSS, when molecularly dispersed, behaved like a plasticizer. Differential scanning calorimetry(DSC) showed a larger drop in the glass transition temperature T_g in the blends containing unmodified acrylic-POSS ($\Delta T_g \approx 11^\circ\text{C}$ at $\phi_{POSS} = 0.20$) when compared with hydrogenated acrylic-POSS blends at the same loading ($\Delta T_g \approx 6^\circ\text{C}$). This difference in the degree of plasticization of the glass transition temperature was related to the degree of miscibility of the POSS and PMMA. Analysis of wide-angle x-ray diffraction patterns of both blend systems showed that significant phase separation of the POSS became apparent at loadings of $\phi \geq 0.20$.

Time temperature superposition (TTS) was successfully employed for all blends in order to construct thermorheological master curves and showed that the decrease in T_g was due to a substantial increase in the free volume of the blends. This plasticization resulted in a substantial decrease in the magnitude of the storage modulus G' and the loss modulus G'' in small amplitude oscillatory shear-flow. Analysis of the TTS data indicated that the free volume at the glass transition was virtually the same for all blends tested. Dynamic mechanical analysis of unmodified acrylic-POSS-PMMA blends showed a consistent decrease in the storage modulus with increasing POSS loading at room temperature; however, at a lower temperature range $-80^\circ\text{C} \leq T \leq 0^\circ\text{C}$ that brackets the T_g of the POSS ($T_{g,\text{POSS}} = -55^\circ\text{C}$), loadings of $\phi \geq 0.10$ showed evidence of a stiffening effect caused by vitrification of phase-separated POSS. No stiffening was observed in the $\phi = 0.05$ blend, indicating that molecular scale dispersion was achieved at that loading in the unmodified acrylic-POSS-PMMA blends. Thermomechanical analysis also showed that the linear value of the coefficient of the thermal expansion was only slightly increased by the addition of 5 to 10 vol% methacryl-POSS, much less than the increase for DOP-PMMA blends at the same volume of plasticizer.

References

- (1) Cole, D. H.; Shull, K. R.; Baldo, P.; Rehn, L. *Macromolecules* **1999**, *32*, 771.
- (2) Glotzer, S. C. *Nature Materials* **2003**, *2*, 713.
- (3) Mackay, M. E.; Dao, T. T.; Tuteja, A.; Ho, D. L.; Van Horn, B.; Kim, H. C.; Hawker, C. J. *Nature Materials* **2003**, *2*, 762.
- (4) McCoy, J. D.; Curro, J. G. *Journal of Chemical Physics* **2002**, *116*, 9154.
- (5) Roberts, C.; Cosgrove, T.; Schmidt, R. G.; Gordon, G. V. *Macromolecules* **2001**, *34*, 538.
- (6) Zhang, Q.; Archer, L. A. *Langmuir* **2002**, *18*, 10435.
- (7) Starr, F. W.; Schroder, T. B.; Glotzer, S. C. *Physical Review E* **2001**, *64*, 021802.
- (8) Starr, F. W.; Schroder, T. B.; Glotzer, S. C. *Macromolecules* **2002**, *35*, 4481.

- (9) Phillips, S. H.; Haddad, T. S.; Tomczak, S. J. *Current Opinion in Solid State and Materials Science* **2004**, *8*, 21.
- (10) Carroll, J. B.; Waddon, A. J.; Nakade, H.; Rotello, V. M. *Macromolecules* **2003**, *36*, 6289.
- (11) Gonzalez, R. I.; Phillips, S. H.; Hoflund, G. B. *Journal of Spacecraft and Rockets* **2000**, *37*, 463.
- (12) Huang, J. C.; He, C. B.; Xiao, Y.; Mya, K. Y.; Dai, J.; Siow, Y. P. *Polymer* **2003**, *44*, 4491.
- (13) Kopesky, E. T.; Haddad, T. S.; Cohen, R. E.; McKinley, G. H. *Macromolecules* **2004**.
- (14) Romo-Uribe, A.; Mather, P. T.; Haddad, T. S.; Lichtenhan, J. D. *Journal of Polymer Science Part B-Polymer Physics* **1998**, *36*, 1857.
- (15) Xu, H.; Kuo, S.-W.; Chang, F.-C. *Polymer Bulletin* **2002**, *48*, 469.
- (16) Zheng, L.; Farris, R. J.; Coughlin, E. B. *Macromolecules* **2001**, *34*, 8034.
- (17) Zheng, L.; Hong, S.; Cardoen, G.; Burgaz, E.; Gido, S. P.; Coughlin, E. B. *Macromolecules* **2004**, *87*, 8606.
- (18) Zheng, L.; Waddon, A. J.; Farris, R. J.; Coughlin, E. B. *Macromolecules* **2002**, *35*, 2375.
- (19) Waddon, A. J.; Coughlin, E. B. *Chemistry of Materials* **2003**, *15*, 4555.
- (20) Waddon, A. J.; Zheng, L.; Farris, R. J.; Coughlin, E. B. *Nano Letters* **2002**, *2*, 1149.
- (21) Mather, P. T.; Jeon, H. G.; Romo-Uribe, A.; Haddad, T. S.; Lichtenhan, J. D. *Macromolecules* **1999**, *32*, 1194.
- (22) Larsson, K. *Arkiv for Kemi* **1960**, *16*, 209.
- (23) Hsiao, B. S.; White, H.; Rafailovich, M.; Mather, P. T.; Jeon, H. G.; Phillips, S.; Lichtenhan, J.; Schwab, J. *Polymer International* **2000**, *49*, 437.
- (24) Constable, G. S.; Lesser, A. J.; Coughlin, E. B. *Macromolecules* **2004**, *37*, 1276.
- (25) Barry, A. J.; Daudt, W. H.; Domicone, J. J.; Gilkey, J. W. *Journal of the American Chemical Society* **1955**, *77*, 4248.
- (26) Kim, G. M.; Qin, H.; Fang, X.; Sun, F. C.; Mather, P. T. *Journal of Polymer Science Part B-Polymer Physics* **2003**, *41*, 3299.
- (27) Zhang, W. H.; Fu, B. X.; Seo, Y.; Schrag, E.; Hsiao, B.; Mather, P. T.; Yang, N. L.; Xu, D. Y.; Ade, H.; Rafailovich, M.; Sokolov, J. *Macromolecules* **2002**, *35*, 8029.
- (28) Lamm, M. H.; Chen, T.; Glotzer, S. C. *Nano Letters* **2003**, *3*, 989.
- (29) Fu, B. X.; Gelfer, M. Y.; Hsiao, B. S.; Phillips, S.; Viers, B.; Blanski, R.; Ruth, P. *Polymer* **2003**, *44*, 1499-1506.
- (30) Billmeyer, F. W. *Textbook of Polymer Science*, 3 ed.; John Wiley & Sons: New York, 1984.
- (31) Ferry, J. D. *Viscoelastic Properties of Polymers*, 3 ed.; John Wiley & Sons: New York, 1980.
- (32) Nakajima, N.; Varkey, J. P. *Journal of Applied Polymer Science* **1998**, *69*, 1727.
- (33) Lomellini, P.; Lavagnini, L. *Rheologica Acta* **1992**, *31*, 175-182.
- (34) Wu, S. *Journal of Polymer Science Part B-Polymer Physics* **1989**, *27*, 723-741.
- (35) Fuchs, K.; Friedrich, C.; Weese, J. *Macromolecules* **1996**, *29*, 5893-5901.
- (36) Graessley, W. W. *Advances in Polymer Science* **1974**, *16*, 133.

- (37) Nakajima, N.; Varkey, J. P. *Polymer International* **1998**, *46*, 298.
- (38) Raju, V. R.; Menezes, E. V.; Marin, G.; Graessley, W. W.; Fetters, L. J. *Macromolecules* **1981**, *14*, 1668.
- (39) Colby, R. H.; Fetters, L. J.; Funk, W. G.; Graessley, W. W. *Macromolecules* **1991**, *24*, 3873.
- (40) Isono, Y.; Fujimoto, T.; Takeno, N.; Kjiura, H.; Nagasawa, M. *Macromolecules* **1978**, *11*, 888.
- (41) Fetters, L. J.; Graessley, W. W.; Kiss, A. D. *Macromolecules* **1991**, *24*, 3136.

Chapter 4: Rheological Properties of Blends Containing an Acrylic Polyhedral Oligomeric Silsesquioxane and an Acrylic Oligomer

4.1 – Introduction

The phenomenology of the glass transition has been studied extensively and many theories have been put forth to explain its cause.¹⁻⁴ Some characterize it as a purely kinetic phenomenon caused by the collapse of free volume¹ while others try to explain it in terms of a thermodynamic necessity in light of the precipitous loss of entropy in glass-forming liquids as they approach their glass transition temperatures.³ Regardless of the cause, glasses are non-equilibrium structures that experience varied degrees of enthalpy relaxation (commonly called physical aging⁵) below their glass transition temperatures.

For blends of a diluent in a polymer matrix, assuming free volume to be additive and the glass transition temperature to be an iso-free volume condition leads to the Kelly-Bueche equation:⁶

$$T_g = \frac{[\phi_1 \alpha_{f1} T_{g1} + (1 - \phi_1) \alpha_{f2} T_{g2}]}{\phi_1 \alpha_{f1} + (1 - \phi_1) \alpha_{f2}} \quad (1)$$

where α_{f1} and α_{f2} are the respective thermal expansion coefficients of the free volume, T_{g1} and T_{g2} are the respective glass transition temperatures, and ϕ_1 is the volume fraction of component 1. This equation works quite well for many plasticized polymer systems, predicting the faster dropoff of T_g at low plasticizer content due to the higher α_f of the plasticizer in the temperature range $T_{g1} \leq T \leq T_{g2}$. An important prediction of Equation 1 is that the glass transition temperature of a blend will always have a T_g in between the glass transition temperatures of the pure components. The vast majority of polymer-plasticizer systems follow this trend, with rare exceptions.^{7,8}

It was shown in Chapter 3 that when an acrylic-POSS species was added to poly(methyl methacrylate)(PMMA), a reduction in the glass transition temperature ($\Delta T_g \approx 10^\circ\text{C}$ at $\phi_{\text{POSS}} = 0.10$) occurred. However, the decrease was less than what is usually observed in conventional polymer-plasticizer systems and the level of the glass transition temperature leveled-off at $\phi_{\text{POSS}} = 0.30$ due to extensive phase separation at moderate to high loadings. In this study, the same POSS species was used (methacryl-POSS), however a PMMA of much lower molecular weight ($M_w = 2190$ g/mol) was used to obtain miscibility over the entire composition range. This oligomer was also chosen because its glass transition temperature ($T_g = -42.4^\circ\text{C}$) was close to the glass transition temperature of the POSS ($T_g = -57.6^\circ\text{C}$). The methacryl-POSS cage is different from conventional plasticizers in that it has an inorganic core and an approximately spherical symmetry. This study seeks to examine the effect of adding a hybrid organic-inorganic particle to an oligomeric matrix of similar T_g and chemical affinity.

4.2 – Experimental Section

4.2.1 – Oligomer Synthesis (Stephen Boyes, Neil Treat; School of Polymers and High Performance Materials, University of Southern Mississippi)

The catalytic transfer agent bis(boron difluorodimethylgloximate) cobaltate(II) (COBF) was synthesized according to a modification of the method described by Bakac and Espenson.⁹⁻¹² Methyl methacrylate (MMA) (Fisher) was purified by passing through a column of activated basic alumina. Toluene and MMA were deoxygenated by purging with nitrogen for 1 h before use. 2,2'-Azobisisobutyronitrile (AIBN) (Aldrich) was purified by recrystallization from methanol.

The reaction was performed using standard Schlenk apparatus under oxygen free conditions.¹³ Initially the MMA and solvent solution (100 mL MMA, 50 mL Toluene)

was purged using nitrogen for at least 1 hour. The AIBN (100 mg) and COBF (6 mg) were added to a separate flask, with a magnetic stirrer bar, sealed with a septum, and deoxygenated by repeated vacuum/nitrogen back-filling cycles. The deoxygenated MMA/toluene mixture was then transferred to the flask containing the AIBN and COBF via a cannular, and the flask was heated at 70 °C for 24 hours under an atmosphere of nitrogen. After this time, the reaction solution was passed through a column of activated basic alumina to remove any residual catalyst and then the residual monomer and solvent were removed by heating at 60 °C under vacuum for 24 hours.

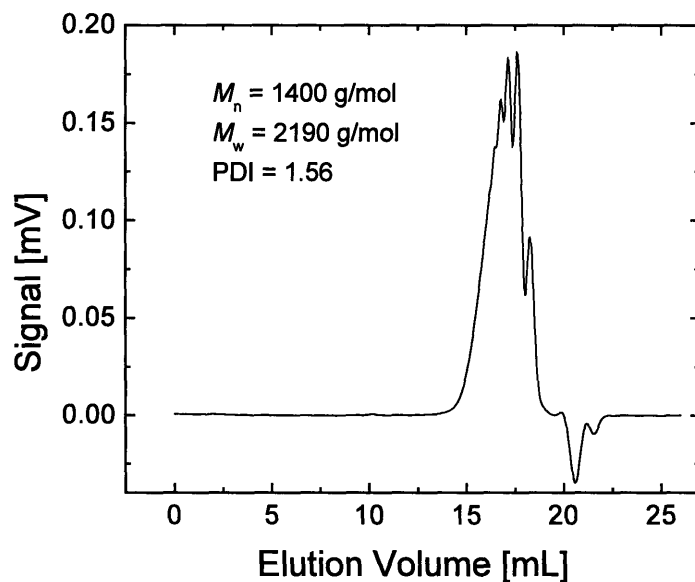


Figure 4.1 – Size-exclusion chromatography curve used to determine molecular weight distribution of oligomer

The molecular weight distribution was determined by size exclusion chromatography (SEC) consisting of a Waters Alliance 2659 Separations Module, an on-line multiangle laser light scattering (MALLS) detector (MiniDAWN™, Wyatt Technology Inc.), an interferometric refractometer (Optilab DSP™, Wyatt Technology Inc.) and two Plgel 3 µm Mixed-E columns in series. The eluent was tetrahydrofuran

(THF) kept at 35°C with a rate of 1.000 mL/min. Sample concentrations were 5 mg/mL in freshly distilled THF, and the injection volume was 100 μ L. The SEC curve for the polymer has been reproduced in Figure 4.1. The weight-average molecular weight $M_w = 2190$ g/mol and the polydispersity index $PDI = 1.56$.

4.2.2 – Blending

Both the oligomeric MMA and the methacryl-POSS were liquids at room temperature. The oligomer had approximately the consistency of honey while the methacryl-POSS was noticeably less viscous, more akin to the consistency of motor oil. These species were blended together by weighing out the oligomer portion first in a glass vial and subsequently adding the methacryl-POSS using a micro spatula. Moderate heating was required ($T = 50^\circ\text{C}$ for 5 minutes) in order to homogenize the mixtures. The methacryl-POSS had a tendency to settle out over a period of days (manifested as a brownish haze at the bottom of the vial) so tests were always begun within 15 minutes of the heating step. Compositions ranged from pure oligomer ($\phi_{\text{POSS}} = 0$) to pure POSS ($\phi_{\text{POSS}} = 1.00$). The POSS had a light brown tint to it compared with a much lighter yellow tint for the oligomer.

4.2.3 – Differential Scanning Calorimetry

Differential scanning calorimetry (DSC) was performed on a TA Instruments Q1000 using hermetic sample pans. Samples were cooled from $T = 50^\circ\text{C}$ to $T \approx -80^\circ\text{C}$ at a rate of $3^\circ\text{C}/\text{min}$, held for five minutes, then heated at $3^\circ\text{C}/\text{min}$ to $T = 50^\circ\text{C}$. The glass transition temperature of the blends was taken as the inflection point in the heat flow versus temperature curve.

4.2.4 – Rheology

Rheological measurements were performed on a TA Instruments AR2000 rheometer using a cone-and-plate geometry (20 mm cone diameter, 2° cone angle, 58 μm truncation height). The temperature was controlled by a Peltier plate system. Linear viscoelastic tests were performed at $T = 0^\circ\text{C}$ at a strain amplitude $\gamma^\circ = 0.05$. Viscometric tests were performed over the range $0^\circ\text{C} \leq T \leq 40^\circ\text{C}$.

4.3 – Results

4.3.1 – Differential Scanning Calorimetry

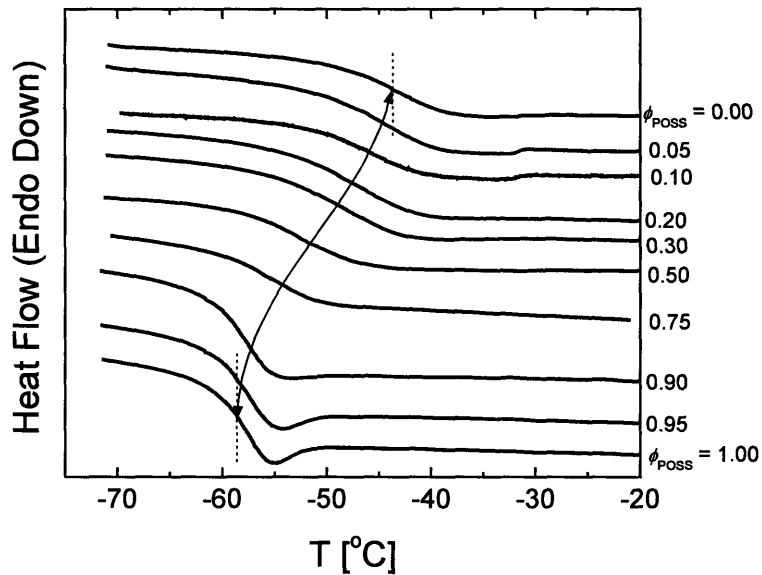


Figure 4.2 – DSC curves for blends of methacryl-POSS in oligomeric MMA

Differential scanning calorimetry (DSC) scans of the methacryl-POSS–oligomer blends are reproduced in Figure 4.2. The heat flow–temperature curves show only one glass transition, indicating complete miscibility over the entire temperature range and the values of the glass transition temperature T_g (Figure 4.3) decrease in a concave-upward fashion with increasing POSS content. From Figure 4.2 it is also apparent that the glass

transition region is sharper at higher POSS contents. This is not surprising considering the vastly different geometries of the two species (despite their similar molecular weights). The methacryl-POSS has an approximately spherical symmetry that should have a far smaller distribution of relaxation modes than the chain structure of the oligomer, which should be described well by the modified Rouse theory for undiluted polymers.^{1,14} However, the blends containing $\phi_{\text{POSS}} \geq 0.90$ show a minimum of increasing depth just beyond the glass transition ($T \approx -58^\circ\text{C}$). This peak is characteristic of physical aging below T_g , which results in enthalpy relaxation as the non-equilibrium glass slowly approaches equilibrium. The size of this peak did not vary with annealing time below T_g , however. This apparent aging along with the large change in heat capacity through the glass transition are signs of a fragile glass-forming material.² It is interesting that the POSS, with its Si-O core, exhibits strong signs of fragile behavior in contrast with the behavior of amorphous silica (SiO_2), which is the classic strong liquid. Fragility will be discussed further in the Discussion section below.

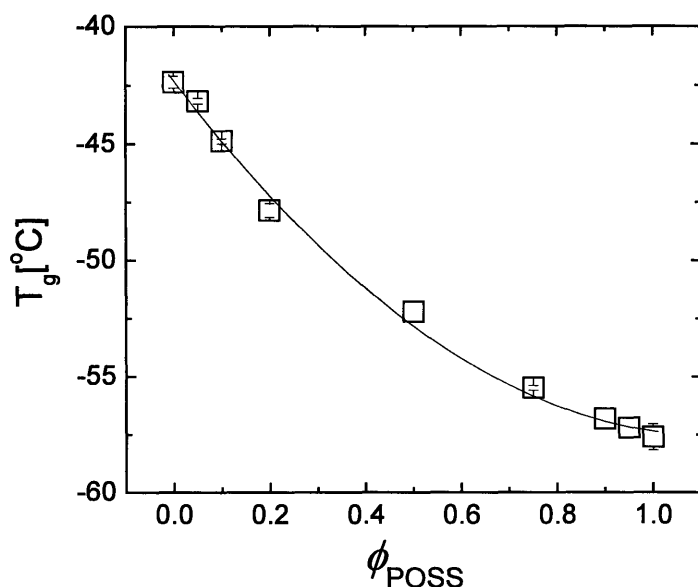


Figure 4.3 – Glass transition temperatures obtained from the inflection points of the DSC curves in Figure 4.2

The decrease in the glass transition temperature of the blends with increasing POSS content agrees with the Kelly-Bueche equation [Eq. (1)], which predicts that the glass transition temperature of a miscible blend should fall between the T_g values of the two components.

4.3.2 – Linear Viscoelastic Properties

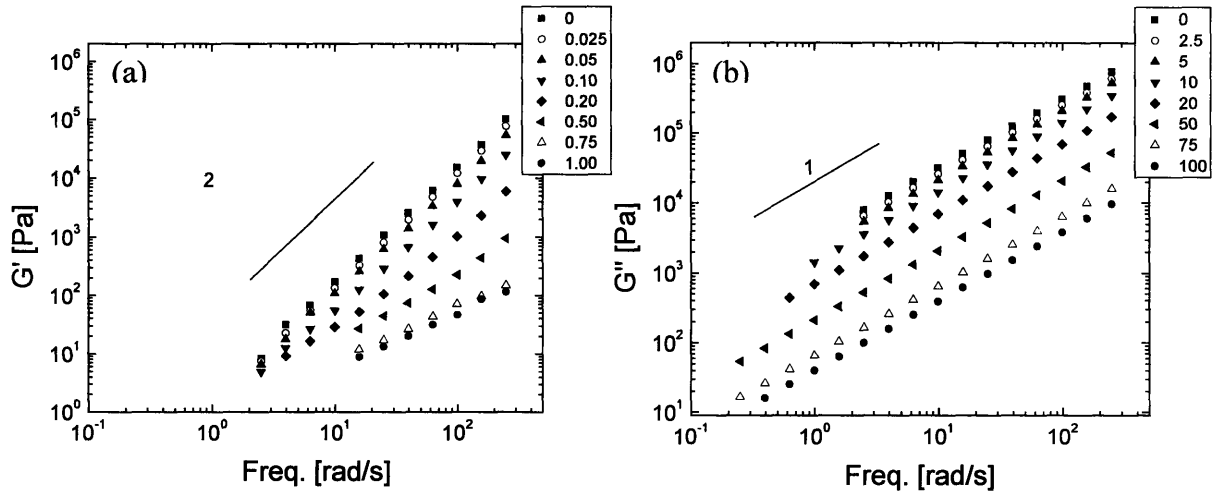


Figure 4.4 – Storage and loss moduli measured at $T = 0^\circ\text{C}$ for blends of methacryl-POSS and oligomeric MMA

The linear viscoelastic properties of the methacryl-POSS–oligomer blends were measured in small amplitude oscillatory shear flow at $T = 0^\circ\text{C}$. The storage moduli G' and the loss moduli G'' are plotted in Figures 4.4(a) and 4.4(b) respectively. The pure oligomer has a measurable amount of elasticity ($G' \approx 10^4$ Pa at $\omega = 10^2$ rad/s) and the storage modulus data show the expected slope of 2 observed in simple viscoelastic fluids. The blends with small loadings of POSS ($\phi < 0.10$) have monotonically decreasing elasticity but retain essentially the same linear slope of 2 on the log-log scale. The elasticity continues to decrease at higher POSS loadings and the slope of G' decreases at loadings $\phi \geq 0.50$, thus at no point in these more highly-filled blends is a slope of 2

observed. The loss modulus data in Figure 4.4(b), on the other hand, have the same slope of 1 for all blends, consistent with the terminal behavior of a linear viscoelastic fluid.

The relaxation modes of the MMA oligomer should be well-characterized by the modified Rouse model for undiluted, unentangled polymers.^{1,14} Because the linear viscoelastic data for the oligomer at $T = 0^\circ\text{C}$ indicate that it is into its terminal relaxation zone, the terminal Rouse relaxation time τ_R should be greater than the highest frequency measured in Figure 4.4. This slowest relaxation mode of the oligomer chain can be calculated using the relation:¹

$$\tau_R = \frac{6\eta_0 M_w}{\pi^2 \rho RT} \quad (2)$$

Using the G'' data in Figure 4.4(b) and the linear viscoelastic identity:

$$\lim_{\omega \rightarrow 0} \left(\frac{G''}{\omega} \right) = \eta_0 \quad (3)$$

the zero shear-rate viscosity of the oligomer can be calculated ($\eta_0 = 3130 \text{ Pa s}$). Using this value for η_0 and the value for the density $\rho = 1.12 \text{ g/cm}^3$, the value of the terminal Rouse time at $T = 0^\circ\text{C}$ is $\tau_R = 1.60 \times 10^{-3} \text{ s}$. This corresponds to a frequency of 627 rad/s, above the range tested ($\omega_{\text{max}} = 250 \text{ rad/s}$).

In Figure 4.5 the loss tangent $\tan \delta = G''/G'$ is plotted to show the relative amounts of viscous and elastic nature in the blends. The pure oligomer is highly viscous in nature over the entire frequency range ($\tan \delta = 7.54$ at $\omega = 250 \text{ rad/s}$). The blends become more viscous in nature as POSS is added, eventually reaching a point at $\phi = 0.75$ where the loss modulus is more than two orders of magnitude greater than the storage modulus over the entire frequency range. Thus the accuracy of the measured storage

modulus values of the high POSS-content blends is questionable. For this reason, the methacryl-POSS was tested at a substantially lower temperature of $T = -40^{\circ}\text{C}$ in an attempt to observe the fluid's linear viscoelastic properties in a more elastic state. These storage and loss moduli are plotted in Figure 4.6(a). As in Figure 4.4(b), the slope of the loss modulus is approximately unity. However, the storage modulus G' shows a greater slope than that observed in Figure 4.4(a) for the pure POSS, with a slope of nearly 2. In Figure 4.6(b), the loss tangent is plotted, showing that the elastic character of the POSS is significantly greater at this lower temperature.

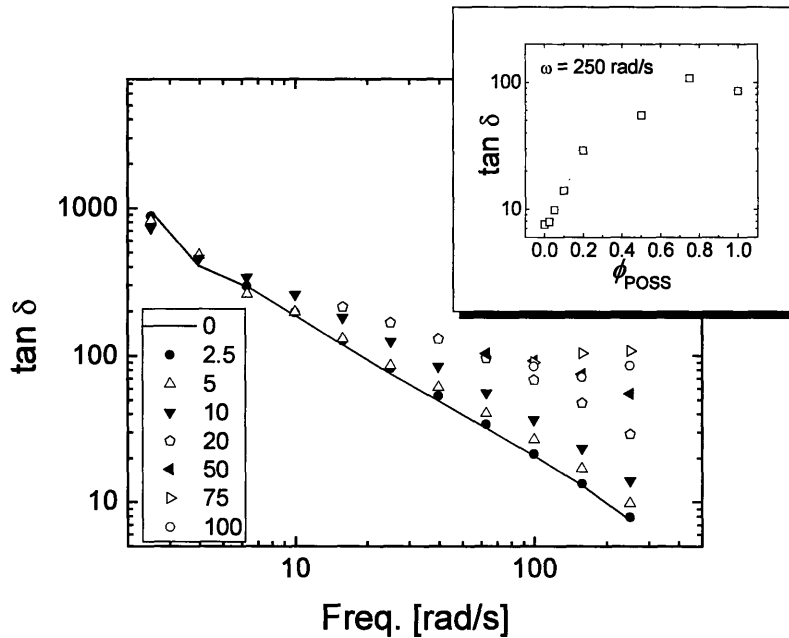


Figure 4.5 – Loss tangent at $T = 0^{\circ}\text{C}$ for blends of methacryl-POSS and oligomeric MMA

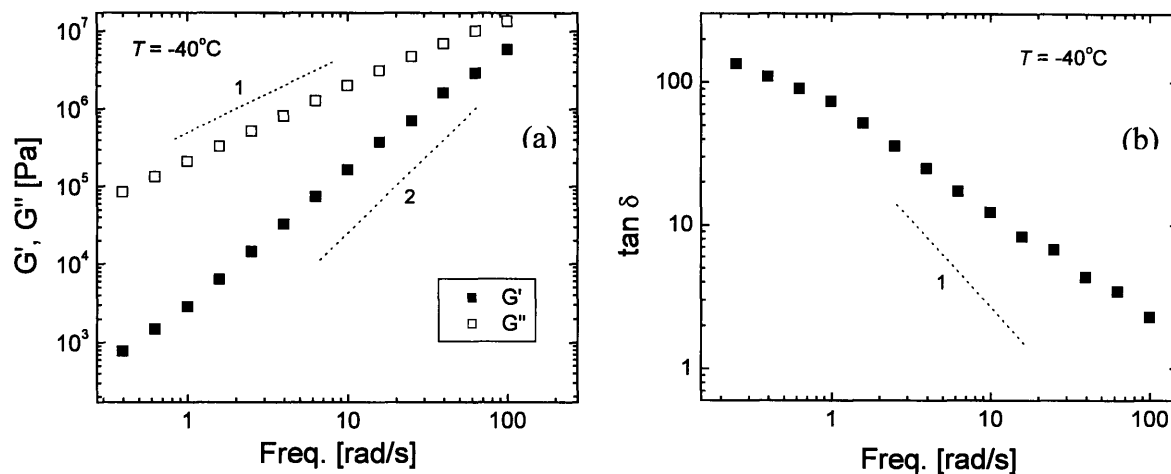


Figure 4.6 – Linear viscoelastic properties of methacryl-POSS at $T = -40^\circ\text{C}$:
 (a) storage modulus G' and loss modulus G'' ; (b) loss tangent

4.3.3 – Viscometric Properties

The shear-rate dependence of the steady shear viscosity at $T = 0^\circ\text{C}$ is shown in Figure 4.7. All blends exhibit a constant Newtonian viscosity over the shear rate range analyzed ($0.001 \leq \dot{\gamma} \leq 10$). The shear viscosity decreases monotonically with increasing POSS content.

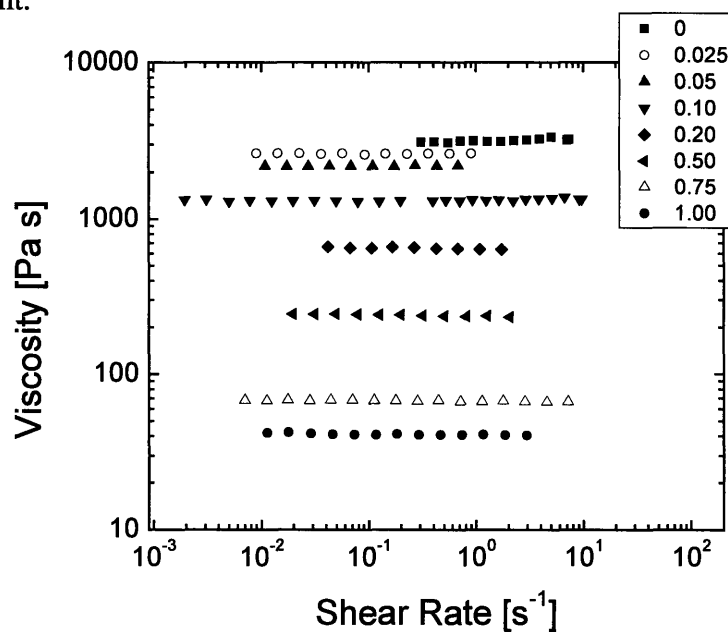


Figure 4.7 – Viscosity vs. shear rate for blends of methacryl-POSS in oligomeric MMA

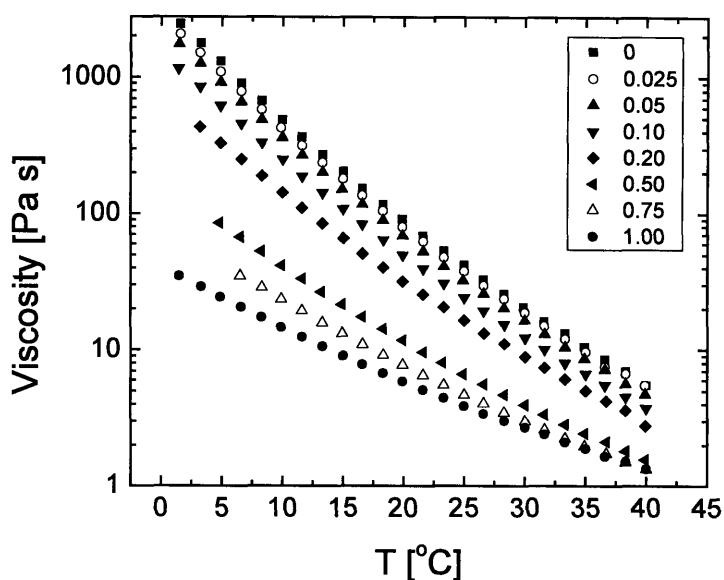


Figure 4.8 – Temperature dependence of the viscosity at a shear rate of 0.1 s^{-1} for blends of methacryl-POSS and oligomeric MMA

In Figure 4.8 the temperature dependence of the viscosity at a shear rate of 0.1 s^{-1} over the range $0 \leq T \leq 40^\circ\text{C}$ is plotted. In addition to the decrease in the level of the curves with methacryl-POSS loading, the curves become less steep as the POSS content is increased as well. The zero shear-rate viscosity η_0 at $T = 20^\circ\text{C}$, taken from the data in Figure 4.8, is plotted against the volume fraction of methacryl-POSS in Figure 4.9. The values of η_0 for the binary mixtures of POSS and oligomer all fall below the log viscosity prediction for mixtures:

$$\log \eta_0 = \phi_{POSS} \log(\eta_{0,POSS}) + (1 - \phi_{POSS}) \log(\eta_{0,oligomer}) \quad (4)$$

The concave upward curvature is consistent with the results for the glass transition temperatures in Figure 4.3, and the degrees of curvature are similar between the data in Figures 4.3 and 4.9.

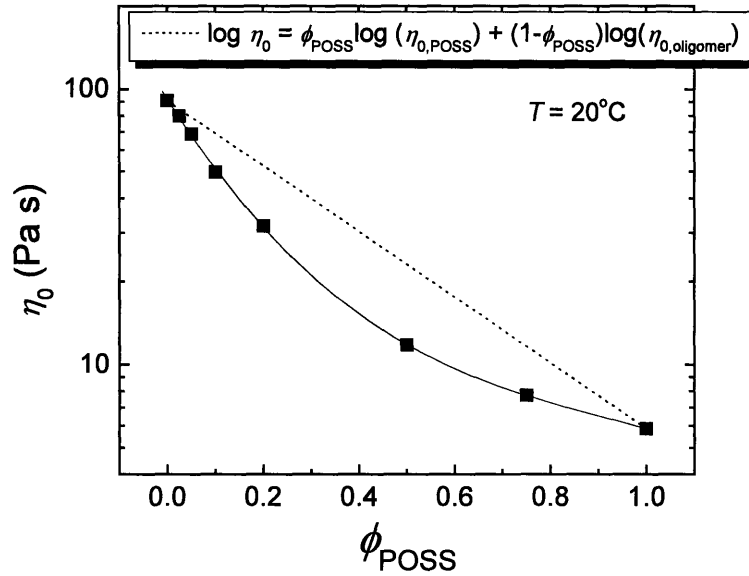


Figure 4.9 – Viscosity of methacryl-POSS–oligomeric MMA blends as a function of POSS content at $T = 20^\circ\text{C}$.

4.4 – Discussion

In Chapters 2 and 3, the principles of time-temperature superposition (TTS)¹ were utilized to construct master curves of linear viscoelastic data over a range of temperatures and the resulting shift factors $a_T(T, T_0)$ were used to shed light on the effect of POSS at the molecular scale. Shift factors containing the same information can be obtained from the temperature dependence of the viscosity (Figure 4.10) using the relation:

$$\log a_T = \log \left(\frac{\eta_0(T)}{\eta_0(T_0)} \right) \quad (5)$$

where $\eta_0(T_0)$ is the zero shear-rate viscosity at the reference temperature T_0 . These data can be fit to the Arrhenius model:

$$\log \eta_0 = A \exp \left(\frac{\Delta H}{RT} \right) \quad (6)$$

$$\log a_T = \frac{\Delta H}{R} \left(\frac{1}{T} - \frac{1}{T_0} \right) \quad (7)$$

where A is a constant, ΔH is a flow activation energy, and R is the universal gas constant. In Figure 4.10 $\log a_T$ has been plotted against the reciprocal of the absolute temperature. The slope of these data sets, which is directly proportional to ΔH , decreases substantially upon the addition of POSS. All samples showed approximately the same correlation coefficients for the linear fits (0.998) to the Arrhenius plot over the temperature range $0 \leq T \leq 40^\circ\text{C}$. The large difference between the flow activation energy of the oligomer and the POSS is interesting considering the small difference between their glass transition temperatures ($\Delta T_g = 14.8^\circ\text{C}$).

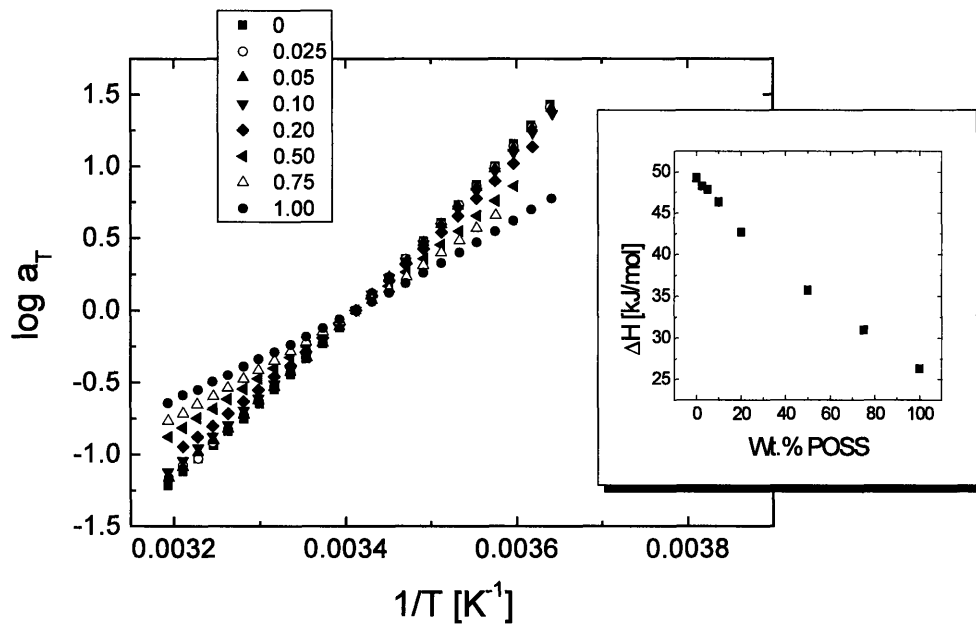


Figure 4.10 – Viscosity shift factors ($T_0 = 20^\circ\text{C}$) plotted against the reciprocal of the absolute temperature. The inset shows the activation energies calculated from the slopes of each data set

The effect of the difference in glass transition temperatures may be essentially removed by instead plotting the zero shear-rate viscosity η_0 against T_g/T , shown in Figure 4.11.² This plot is commonly used to study the properties of glass-forming liquids in the region above T_g .^{2,4,15-18}

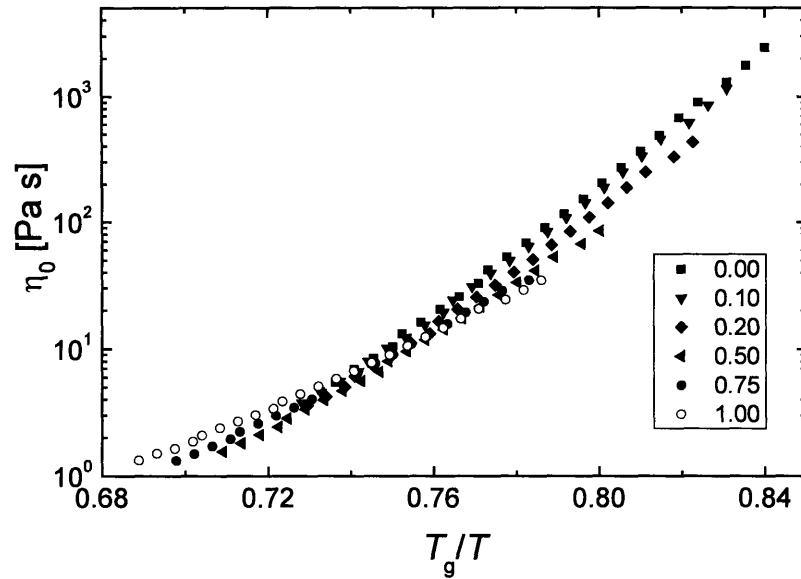


Figure 4.11 – Zero shear-rate viscosity of methacryl-POSS–oligomeric MMA blends plotted against the ratio of the glass transition temperature and the absolute temperature

It is apparent from Figure 4.11 that there is curvature in the viscosity data, even over this small temperature range. This non-Arrhenius behavior must necessarily become more pronounced as the glass transition temperature is approached, and the viscosity behavior can be fitted with the Vogel-Fulcher-Tammann-Hesse (VFTH) Equation:³

$$\eta = A \exp \left[\frac{B}{(T - T^*)} \right] \quad (8)$$

where A , B , and T^* are constants. In Figure 4.12, the viscosity values for both the pure oligomer and the pure POSS (with additional data below $T = 0^\circ\text{C}$) are plotted against the quantity $1/(T - T^*)$. The value of T^* was varied separately for each data set until the best fit was achieved to the data. For the oligomer, $T^* = 171$ K, while for the POSS, $T^* = 175$ K.

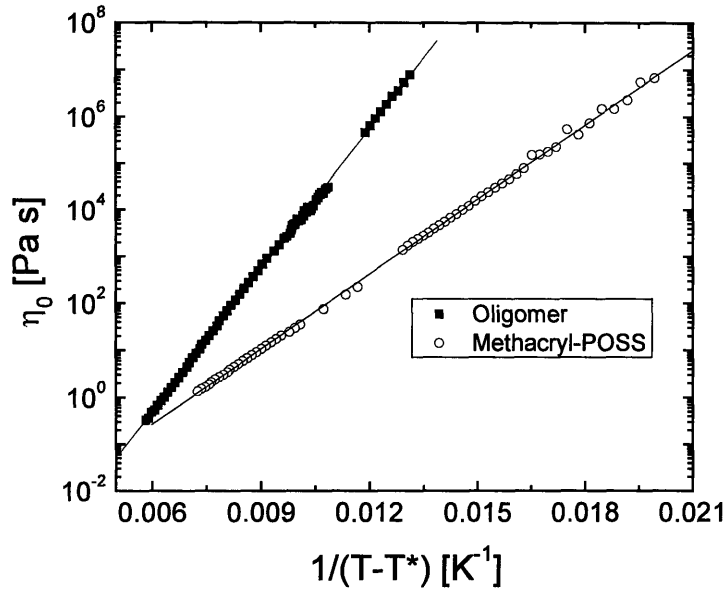


Table 4.1 -- Fragility Parameters

	Oligomer	Methacryl-POSS
B (Eq. 8)	2319	1228
T^* (K)	171	175
D (Eq. 9)	13.56	7.01
m	65.7	90.4

Figure 4.12 – Fits of viscosity data of the oligomer and the methacryl-POSS to the VFTH equation

The VFTH equation may be re-written as:

$$\eta = A \exp\left[\frac{DT^*}{(T - T^*)}\right] \quad (9)$$

where the magnitude of D is an inverse measure of the fragility of the glass-forming liquid. The value of D decreases as the fragility increases. Fragility parameters for the systems are reported in Table 4.1. The value of D is much smaller in the POSS than in the oligomer. This means that the POSS shows a more significant departure from Arrhenius behavior than the oligomer. Fragility is most commonly defined as the slope of the viscosity at T_g .^{19,20}

$$m = \left(\frac{\partial \log \eta_0}{\partial (T_g/T)}\right)_{T_g} \quad (10)$$

where m is the fragility index. The slope of other parameters at T_g , such as a structural relaxation time, can also be used to define m . A way of estimating this fragility index, since the viscosity is difficult to measure near T_g , is using the relation:¹⁶

$$m = \frac{17}{1 - T^*/T_g} \quad (11)$$

where T^* is the value from the fit to the VFTH equation. As expected, the value for the POSS (90.4) is higher than that for the oligomer (65.7). From Equation 11 it is clear that fragility increases as T^* becomes closer to T_g . The value of T^* may approximately be thought of as the Kauzmann temperature T_K , the point at which the entropy of the liquid would equal that of the crystal.²¹ The closer the Kauzmann temperature is to T_g , the more rapidly a liquid approaches an entropy crisis upon cooling. Amorphous SiO_2 is one of the strongest glass-forming liquids known, barely deviating from Arrhenius behavior above T_g . It has an m index of close to 17 (i.e. $T^* \ll T_g$). Polymers, on the other hand, tend to be extremely fragile, because fragility is strongly related to the degree of cooperativity of motion at the glass transition.³ High molecular weight PMMA ($M_w > 50,000$ g/mol) is one of the most fragile polymers with a fragility index $m = 145$.¹⁸ Fragility decreases with decreasing molecular weight in polymers with asymmetric repeat units,¹⁶ much like the glass transition temperature, thus the oligomer in this study has a much smaller fragility index ($m = 65.7$) compared with the $m = 145$ value of high molecular weight PMMA.

In Figure 4.13 a new Arrhenius plot is shown that contains only the viscosity data for the pure oligomer and the POSS. The curves passing through the data sets are the fits to the VFTH equation. It is commonly observed that the viscosity at the glass transition $\eta_g \approx 10^{12}$ Pa s,² and it is also commonly observed that the viscosity at infinite temperature asymptotes to 10^{-5} Pa s, thus the limits on the ordinate scale. Two liquid limits are

represented on the plot: a strong liquid limit and a fragile liquid limit. Strong liquids, like SiO_2 , show only minor deviations from Arrhenius behavior and are characterized by tetrahedrally-coordinated structures with highly directional bonding.^{2,4} Fragile liquids, on the other hand, generally have isotropic bonding like van der Waals forces and have no long range structural order. It is clear that both of the materials under consideration here fall closer to the fragile limit than the strong limit. However, the degree of curvature is more significant in the POSS data over the range of temperatures analyzed. To reach a viscosity of 10^{12} Pa s at T_g , a slightly more abrupt increase in viscosity is required in the POSS.

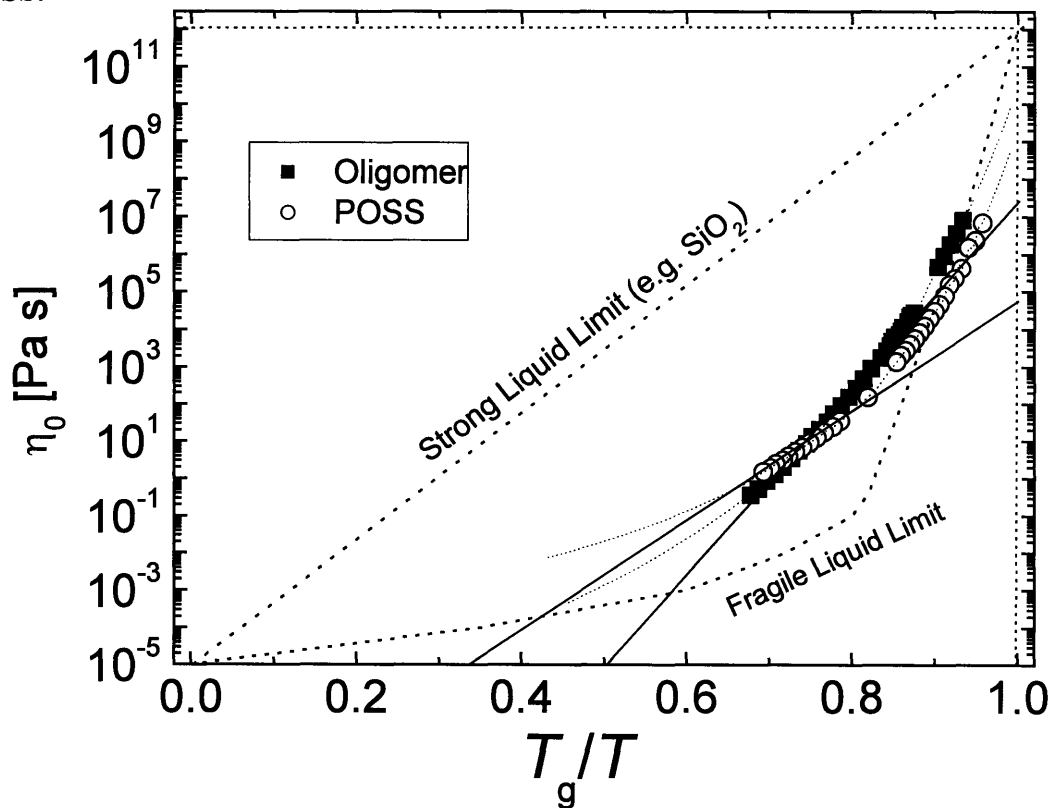


Figure 4.13 – Arrhenius plot showing data for oligomer and methacryl-POSS within the strong/fragile liquid framework

The steepness of the viscosity data near the glass transition temperature makes it unsurprising that the POSS decreases the glass transition temperature of the oligomer.

After the POSS passes through its glass transition its viscosity quickly falls off until it is already relatively low at the T_g of the oligomer ($T = -42.4^\circ\text{C}$).

The VFTH equation is identical in form to the WLF equation when some minor substitutions are made:¹

$$\log a_T = \log \left[\frac{\eta_0(T)}{\eta_0(T_0)} \right] = \frac{B}{2.303} \left[\frac{1}{(T_0 - T^*)} - \frac{1}{(T - T^*)} \right]$$

$$\log a_T = \frac{B}{2.303} \left[\frac{(T - T_0)}{(T_0 - T^*)(T - T^*)} \right]$$

By substituting:

$$c_1^0 = \frac{B}{2.303(T_0 - T^*)} \quad (12)$$

$$c_2^0 = T_0 - T^* \quad (13)$$

the VFTH equation becomes the familiar WLF equation:

$$\log a_T = \frac{-c_1^0(T - T_0)}{c_2^0 + (T - T_0)} \quad (14)$$

where c_1^0 and c_2^0 are constants. By plotting $-(T - T_0)/\log a_T$ against $(T - T_0)$ in Figure 4.14 these two coefficients were obtained for the viscosity data over the temperature range $0 \leq T \leq 40^\circ\text{C}$. Overall, the data show good linearity on both sides of the reference temperature $T_0 = 20^\circ\text{C}$. There is some noise in the data sets, in particular in the pure POSS data set at $(T - T_0) > 0$, however this noise tends to be centered around the best-fit line and thus does not significantly affect the WLF coefficients. The slope is equal to $1/c_1^0$ and the intercept c_2^0/c_1^0 . These values have been tabulated in Table 4.2. In addition, the constants c_1^0 and c_2^0 can be used to determine c_1^g and c_2^g , which are the

WLF coefficients at the glass transition temperature. They may be calculated using the relations:¹

$$c_1^g = \frac{c_1^0 c_2^0}{(c_2^0 + T_g - T_0)} \quad (15)$$

$$c_2^g = c_2^0 + T_g - T_0 \quad (16)$$

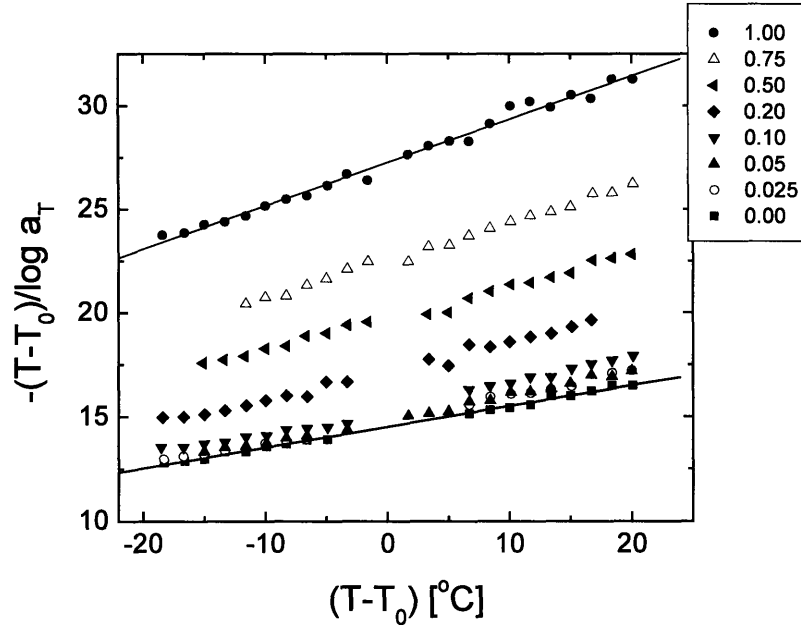


Figure 4.14 – WLF plot for blends of methacryl-POSS and oligomeric MMA ($T_0 = 20^\circ\text{C}$)

Table 4.2 - WLF Parameters for Methacryl-POSS–Oligomer Blends ($T_0 = 20^\circ\text{C}$)

ϕ_{POSS}	c_1^0	c_2^0 (K)	f_g/B	T_g ($^\circ\text{C}$)	α_f (K^{-1})	c_1^g	c_2^g (K)	f_g/B
0.00	10.07	146.16	0.0431	-42.4	0.00030	17.54	83.90	0.0248
0.05	8.88	132.23	0.0489	-43.2	0.00037	16.98	69.16	0.0256
0.10	8.30	127.84	0.0523	-44.9	0.00041	16.82	63.06	0.0258
0.20	7.28	125.28	0.0596	-45.9	0.00048	15.34	59.48	0.0283
0.50	6.61	130.48	0.0657	-50.9	0.00050	14.45	59.73	0.0301
0.75	5.51	123.98	0.0789	-54.4	0.00064	13.74	49.68	0.0316
1.00	4.78	130.24	0.0909	-57.6	0.00070	11.80	52.74	0.0368

These values may be used to approximate the fractional free volume f_g at the glass transition temperature and the thermal expansion coefficient of the free volume α_f :¹

$$f_g = \frac{B}{2.303c_1^g} \quad (17)$$

$$\alpha_f = \frac{B}{2.303c_1^g c_2^g} \quad (18)$$

where B is a constant usually assumed to be unity. The addition of POSS to the oligomer leads to a significant decrease in the first WLF coefficient c_1^g over the entire composition range while the second coefficient c_2^g shows a moderate decrease at low loadings ($\phi_{\text{POSS}} \leq 0.20$) before reaching an apparent minimum at $\phi = 0.75$. The increase in c_2^0 between $\phi = 0.75$ and $\phi = 1.00$ is consistent with Ferry's observations of highly-diluted polymers due to less temperature dependence of the relaxation times.¹ From Table 4.2 it can be seen that f_0 increases at $T_0 = 20^\circ\text{C}$ and α_f increases monotonically from $3.0 \times 10^{-4} \text{ K}^{-1}$ at $\phi_{\text{POSS}} = 0.00$ to $7.0 \times 10^{-4} \text{ K}^{-1}$ at $\phi_{\text{POSS}} = 1.00$. Both of these results are expected based on the decrease in the glass transition temperature caused by the addition of POSS. The free volume at the glass transition temperature f_g also increases monotonically with increasing POSS content. The pure oligomer has $f_g = 0.0248$, about 20% less than the value for high molecular weight PMMA from Chapter 3. At low molecular weights, it has been reported that f_g/B is smaller in polymers of low molecular weight.¹ At very low molecular weights such as that of the oligomer in this study, the friction coefficient is lower than that in a high molecular weight polymer of the same structure.¹ Thus rather than T_g being an iso-free volume condition as is a reasonable approximation in high molecular weight polymers, in low molecular weight polymers it instead corresponds better to a constant viscosity.¹

The decrease in both glass transition temperature and viscosity with POSS content may owe something to the fragility of the POSS liquid. Fragile liquids tend to have sharper glass transitions, resulting in a more abrupt dropoff in the viscosity above T_g .

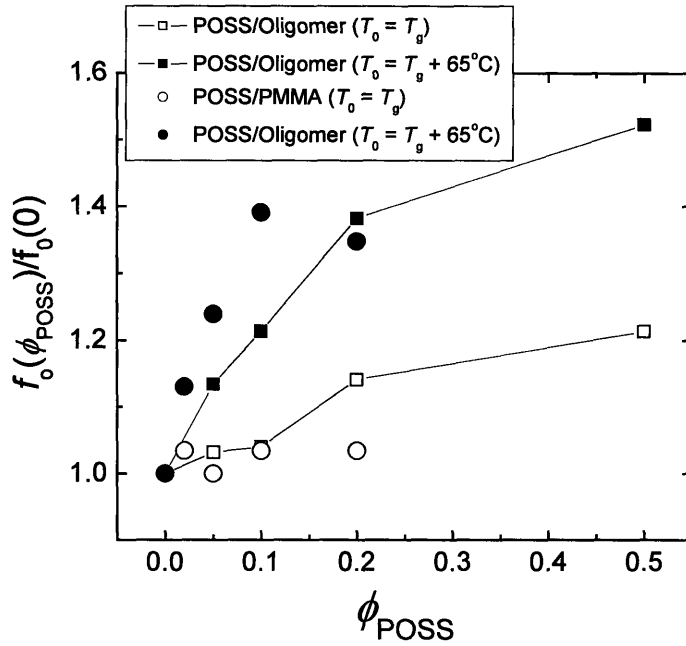


Figure 4.15 – Normalized fractional free volume for both methacryl-POSS in both oligomeric MMA and high molecular weight PMMA

In Figure 4.15 we compare the fractional free volume f_0 of the oligomer-POSS and the high molecular weight PMMA-POSS systems at two separate reference temperatures. The open symbols represent value of the fractional free volume at T_g for each blend, and the filled symbols represent f_0 at $T = T_g + 65^\circ\text{C}$. The values of f_g , the fractional free volume at $T = T_g$, when normalized by the values for the unfilled samples, are similar at loadings of $\phi \leq 0.10$. However, at $\phi = 0.20$, the free volume at T_g is significantly greater in the oligomer-POSS blends, while the value in the high molecular weight PMMA-POSS blends is relatively constant. At $T = T_g + 65^\circ\text{C}$, the fractional free volume values follow similar trends between the two systems. Both show significant

increases in fractional free volume up to a POSS loading of $\phi = 0.10$. However, above this loading in the high molecular weight PMMA-POSS system, phase separation sets in and the free volume value plateaus.

4.5 – Conclusion

Blends of oligomeric methyl methacrylate and methacryl-POSS have monotonically varying values of viscosity, linear viscoelastic moduli, and glass transition temperature over the entire spectrum of composition. Both the values of the glass transition temperature and the zero shear-rate viscosity have a concave upward shape when plotted against POSS loading. Both the oligomer and the POSS are highly fragile liquids, with the POSS surprisingly having the higher fragility index. This higher fragility is due to the spherical shape of the POSS molecules, which require more cooperativity at the glass transition than the linear oligomeric methyl methacrylate chains.

References

- (1) Ferry, J. D. *Viscoelastic Properties of Polymers*, 3rd ed.; John Wiley & Sons: New York, 1980.
- (2) Angell, C. A. *Science* **1995**, *267*, 1924.
- (3) Ngai, K. L. In *Physical Properties of Polymers*, 3rd ed.; Mark, J. E., Ed.; Cambridge University Press: Cambridge, 2004; pp 72-152.
- (4) Debenedetti, P. G.; Stillinger, F. H. *Nature* **2001**, *410*, 259.
- (5) Struick, L. C. E. *Physical Aging in Amorphous Polymers and Other Materials*; Elsevier: New York, 1978.
- (6) Kelly, F. N.; Beuche, F. *Journal of Polymer Science* **1961**, *50*, 549.
- (7) Santangelo, P. G.; Roland, C. M.; Ngai, K. L.; Rzos, A. K.; Katerinopoulos, H. *Journal of Non-crystalline Solids* **1994**, *172-174*, 1084.
- (8) Rzos, A. K.; Ngai, K. L. *Physical Review B* **1992**, *46*, 8127.
- (9) Bakac, A.; Espenson, J. H. *Journal of the American Chemical Society* **1984**, *106*, 5197.
- (10) Bakac, A.; Brynildson, M. E.; Espenson, J. H. *Inorganic Chemistry* **1986**, *25*, 4108.
- (11) Suddaby, K. G.; Maloney, D. R.; Haddleton, D. M. *Macromolecules* **1997**, *30*, 702.

- (12) Sanayei, R. A.; O'Driscoll, K. F. *Journal of Macromolecular Science: Pure and Applied Chemistry* **1989**, *A26*, 1137.
- (13) Shriver, D. F.; Drezdzon, M. A. *The Manipulation of Air Sensitive Compounds*, 2nd ed.; Wiley-Interscience: New York, 1986.
- (14) Rouse, P. E. *Journal of Chemical Physics* **1953**, *21*, 1272.
- (15) Angell, C. A. **1997**.
- (16) Ding, Y.; Novikov, V. N.; Sokolov, A. P.; Cailliaux, A.; Dalle-Ferrier, C.; Alba-Simionesco, C.; Frick, B. *Macromolecules* **2004**, *37*, 9264.
- (17) Green, J. L.; Ito, K.; Xu, K.; Angell, C. A. *Journal of Physical Chemistry B* **1999**, *103*, 3991.
- (18) Bohmer, R.; Ngai, K. L.; Angell, C. A.; Plazek, D. J. *Journal of Chemical Physics* **1993**, *99*, 4201.
- (19) Bendler, J. T.; Fontanella, J. J.; Shlesinger, M. F. *Journal of Chemical Physics* **2003**, *118*, 6713.
- (20) Scopigno, T.; Ruocco, G.; Sette, F.; Monaco, G. *Science* **2003**, *302*, 849.
- (21) Kauzmann, W. *Chemical Reviews* **1948**, *43*, 219.

Chapter 5: Mechanical Properties of POSS-PMMA

Nanocomposites

5.1 – Introduction

Amorphous polymers such as poly(methyl methacrylate)(PMMA), polystyrene(PS), and polycarbonate(PC) are attractive for many engineering applications due to their excellent transparencies(PMMA is more transparent than glass), high moduli, and relative ease of processing. However, these polymers all exhibit shortcomings in their mechanical properties. PMMA and PS tend to be brittle materials that break at small strains when unoriented.¹ PC is usually very ductile but is highly notch-sensitive.² A vast number of studies have attempted to toughen these materials with varying degrees of success.²⁻¹⁰

Both PMMA⁸ and PS¹⁰ has been toughened successfully with rubber particles, but high rubber contents (> 30 wt%) are generally required. These studies have shown higher toughness values but at the cost of reducing the yield stress by 50-75% and the modulus by 50-60%. The rubber-toughened PMMA study of Jansen et al.⁸ showed superior toughness values when the particle size in a 70/30 PMMA/rubber blend was 50 nm. In the case of polystyrene, particles of at least 1 μm in diameter were required to achieve the toughening, thereby robbing the polymer of its intrinsic transparency. A study by Qin et al.⁷ on a ternary blend of PS/high-impact polystyrene(HIPS)/low molecular weight polybutadiene showed improved modulus, yield, and flow stress over the HIPS resin, however a 50% reduction in yield stress was still observed when compared with the unfilled PS. The toughening imparted by the polybutadiene diluent was ascribed to a lowering of the craze flow stress by the mobile diluent.^{5,7}

A recent study of PMMA filled with alumina nanoparticles by Ash et al.⁴ showed a significant improvement in the tensile toughness when particles with average diameter $d = 38$ nm were blended with PMMA along with the help of a methacrylic acid dispersant. A particle loading of 2.2 wt% was optimum. Representative stress-strain curves are shown in Figure 5.1. The strain-at-break increased from $\epsilon_{br} = 0.05$ to $\epsilon_{br} = 0.30$ while the modulus and yield stress decreased by 20-25%. The glass transition temperature of the PMMA was also suppressed 20°C by the alumina nanoparticles. The use of smaller ($d = 17$ nm) nanoparticles produced no improvement in toughness. Electron microscopy showed that the toughness increase was due to void formation around the larger ($d = 100$ -200 nm) particles. Poor interfacial adhesion was also necessary for toughening to be observed.

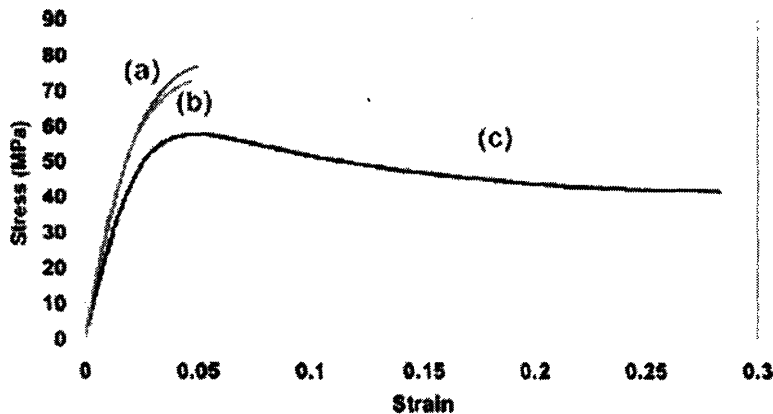


Figure 5.1 – Stress-strain curves taken from study by Ash et al. (Macromolecules, 2004) of alumina-filled PMMA

Figure 5. Typical stress–strain curves for (a) neat PMMA, (b) 2 wt % as-received micrometer-sized alumina filled/PMMA composite, and (c) 2.2 wt % 38 nm (MAA) alumina/PMMA nanocomposite. The crosshead speed was 1 mm/min, which translates to a 0.04 min^{-1} rate.

These toughening studies generally show that in order to toughen amorphous polymers like PMMA, a significant sacrifice in the modulus and yield stress is required. A specific size range of nanoparticles ($d = 50$ -200 nm) also seems to be important. In the present study, three different types of particles have been tested. All are polyhedral

oligomeric silsesquioxanes. One, cyclohexyl-POSS, is a monodisperse, crystallizable T₈ cage containing a cyclohexyl group on each corner. It shows rather poor miscibility in PMMA¹¹(see Chapter 2) and thus phase separates into highly polydisperse crystallites. The second, methacryl-POSS, is a non-crystallizable POSS species composed primarily of T₁₀ and T₁₂ cages. It is a liquid at room temperature and disperses on a molecular level at loadings less than 10 wt%¹²(see Chapter 3). The third species, trisilanol-phenyl-POSS, is an incompletely condensed T₈ cage [see Figure 1.7] with a phenyl group on seven of the corners of the cage and the remaining corner open. It is crystallizable yet extremely miscible with PMMA, dispersing to loadings of 20 wt%. This study aims to compare and contrast the mechanical properties of POSS-filled PMMA containing varied nanoparticle morphologies.

5.2 – Experimental Section

5.2.1 – Notes on Nomenclature

In Table 5.1 the nomenclature of the POSS-PMMA blends analyzed in this chapter are shown. For each binary blend containing one type of POSS and PMMA, the name consists of a number followed by an abbreviation representing the type of POSS. The abbreviations for each type of POSS are: *Acryl* (methacryl-POSS), *Cy* (cyclohexyl-POSS), and *tsP* (trisilanol-phenyl-POSS). Thus, a blend named 5Acryl contains 5 wt% Methacryl-POSS. For the ternary blends that contain two types of POSS, the abbreviations and weight fractions for each type of POSS are indicated in the blend name.

Table 5.1 Nomenclature of POSS-PMMA Blends

Blend Name	Blend Composition
PMMA	No POSS (Pure PMMA)
2.5Acryl	2.5 wt% Methacryl-POSS
5Acryl	5 wt% Methacryl-POSS
10Acryl	10 wt% Methacryl-POSS
2.5Cy	2.5 wt% Cyclohexyl-POSS
5Cy	5 wt% Cyclohexyl-POSS
10Cy	10 wt% Cyclohexyl-POSS
2.5Cy/2.5Acryl	2.5 wt% of both Cyclohexyl-POSS and Methacryl-POSS
5Cy/5Acryl	5 wt% of both Cyclohexyl-POSS and Methacryl-POSS
5tsP	5 wt% trisilanol-phenyl-POSS
10tsP	10 wt% trisilanol-phenyl-POSS
15tsP	15 wt% trisilanol-phenyl-POSS

5.2.2 – Materials

A commercial PMMA resin from Atofina Chemicals (Atoglas V920, HP) was used as the matrix. Three different nanoparticles were blended with PMMA: cyclohexyl-POSS, methacryl-POSS, and trisilanol-phenyl-POSS, all obtained from Hybrid Plastics.

5.2.3 – Blending and Sample Preparation

Each blend was produced by first dissolving the required amount of POSS and PMMA in THF at approximately 10 wt%. The solutions were cast onto glass dishes, covered with aluminum foil (vented slightly), and the solvent was allowed to evaporate over a period of 48 hours. The films were then placed in a vacuum oven at $T = 110^{\circ}\text{C}$ for 48 hours to remove residual solvent. The dried films were then ground into a powder and processed for three minutes at $T = 225^{\circ}\text{C}$ in a DACA instruments micro-compounder.

Tensile dogbones with a gauge region $20\text{ mm} \times 4.0\text{ mm} \times 1.6\text{ mm}$ were injection-molded from a melt kept at $T = 250^{\circ}\text{C}$ into a mold held at $T = 60^{\circ}\text{C}$ in a DACA Instruments injection molder. Bar-shaped specimens of size $63\text{ mm} \times 10.2\text{ mm} \times 3.2\text{ mm}$ were also injection molded in the same apparatus using a different mold. Split-Hopkinson pressure

bar (SPHB) specimens were cylinders with heights of approximately 5 mm and diameters of approximately 3 mm. These were machined from compression-molded bars.

5.2.4 – Mechanical Tests

Tensile tests were performed on the dogbone specimens using a Zwick Z010 mechanical tester using a crosshead speed of 2 mm/min. This corresponded to an engineering strain rate $\dot{\epsilon} = 3.3 \times 10^{-3} \text{ s}^{-1}$. IZOD bars were notched using a TMI notching cutter. Notch depths were 0.4 mm. IZOD impact tests were performed on a TMI Model 43-1 IZOD impact testing device using a 2 ft-lb pendulum.

Split-Hopkinson pressure bar (SPHB) tests were performed on an apparatus designed by Physics Applications, Inc. (Dayton, Ohio).¹³ The solid aluminum pressure bars had a length of 2.3 meters and a diameter of 19.05 mm. The pressure used to create the stress wave was 40 psi.

5.3 - Results

5.3.1 – Slow-speed Tension Tests of PMMA and POSS-filled PMMA

The stress-strain behavior of the unfilled PMMA in slow-speed tension at $T = 20^\circ\text{C}$ is shown in Figure 5.2. The curves have been offset from each other on the ordinate by a factor of 2 MPa and on the abscissa by a strain of 0.004 for clarity. The modulus E and yield stress σ_y remain relatively constant throughout the five samples, however the strain at break ϵ_{br} shows significant scatter, varying between 0.02 and 0.12. These samples show the expected stress-strain behavior for PMMA, a fairly brittle material that is often able to reach its plastic yield point before fracture but unable to draw much further. In this section, the most ductile sample has been chosen as the representative

curve when comparing to the POSS-filled systems in order to analyze the least-flawed samples. Average properties and reproducibility will be addressed in Section 5.3.2.

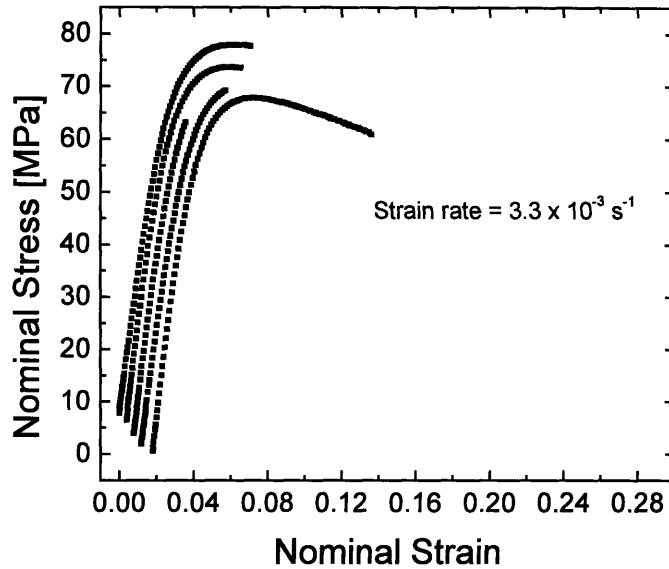


Figure 5.2 – Stress-strain behavior of unfilled PMMA in tension

The PMMA was filled separately with three different types of POSS: cyclohexyl-POSS, methacryl-POSS, and trisilanol-phenyl-POSS. The cyclohexyl-POSS is a crystallizable-POSS species that is relatively incompatible with PMMA (Chapter 2); methacryl-POSS is non-crystallizable and compatible with PMMA at loadings less than 20 wt% (Chapter 3); trisilanol-phenyl-POSS is a crystallizable species like cyclohexyl-POSS, but it shows good compatibility with PMMA and disperses on a molecular scale at loadings up to 20 wt%. The degree of dispersion can, to a first order, be estimated from the optical clarity of the material upon addition of the nanofiller. In Figure 5.3 the absorbances of these POSS-filled blend systems at $\lambda = 550$ nm are plotted against the weight fraction of each component in the blend. Both the methacryl-POSS and the trisilanol-phenyl-POSS have approximately the same absorbance as PMMA up to 20

wt% loading. On the other hand, cyclohexyl-POSS shows a monotonic and substantial increase in absorbance with filler loading.

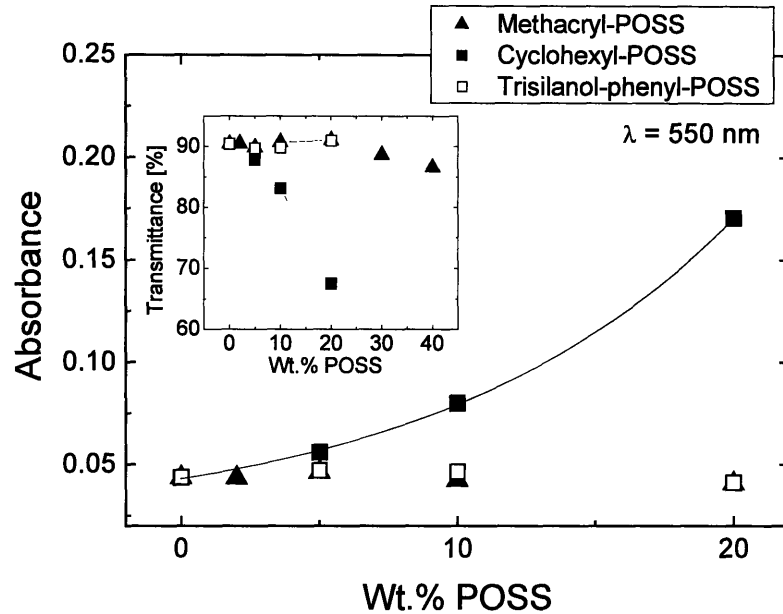


Figure 5.3 – Optical Properties of POSS-PMMA Blends

In Figures 5.4(a)-(c) we compare the stress-strain behaviors of PMMA when filled with the three different types of POSS. In Figure 5.4(a) the stress-strain behavior of cyclohexyl-POSS–PMMA blends is shown for cyclohexyl-POSS loadings between 0 and 10 wt%. The cyclohexyl-POSS has little effect on the modulus but it does significantly decrease the yield stress, even at a loading of only 2.5 wt%. The strain-at-break ϵ_{br} is significantly improved in the 2.5 wt% blend, nearly doubling from 0.12 to 0.23. This improvement in ϵ_{br} is lost at the larger loadings of 5 wt% and 10 wt%. The cyclohexyl-POSS dogbones showed significant whitening in the gauge region (Figure 5.5) during the test, with the onset of whitening occurring at the yield point.

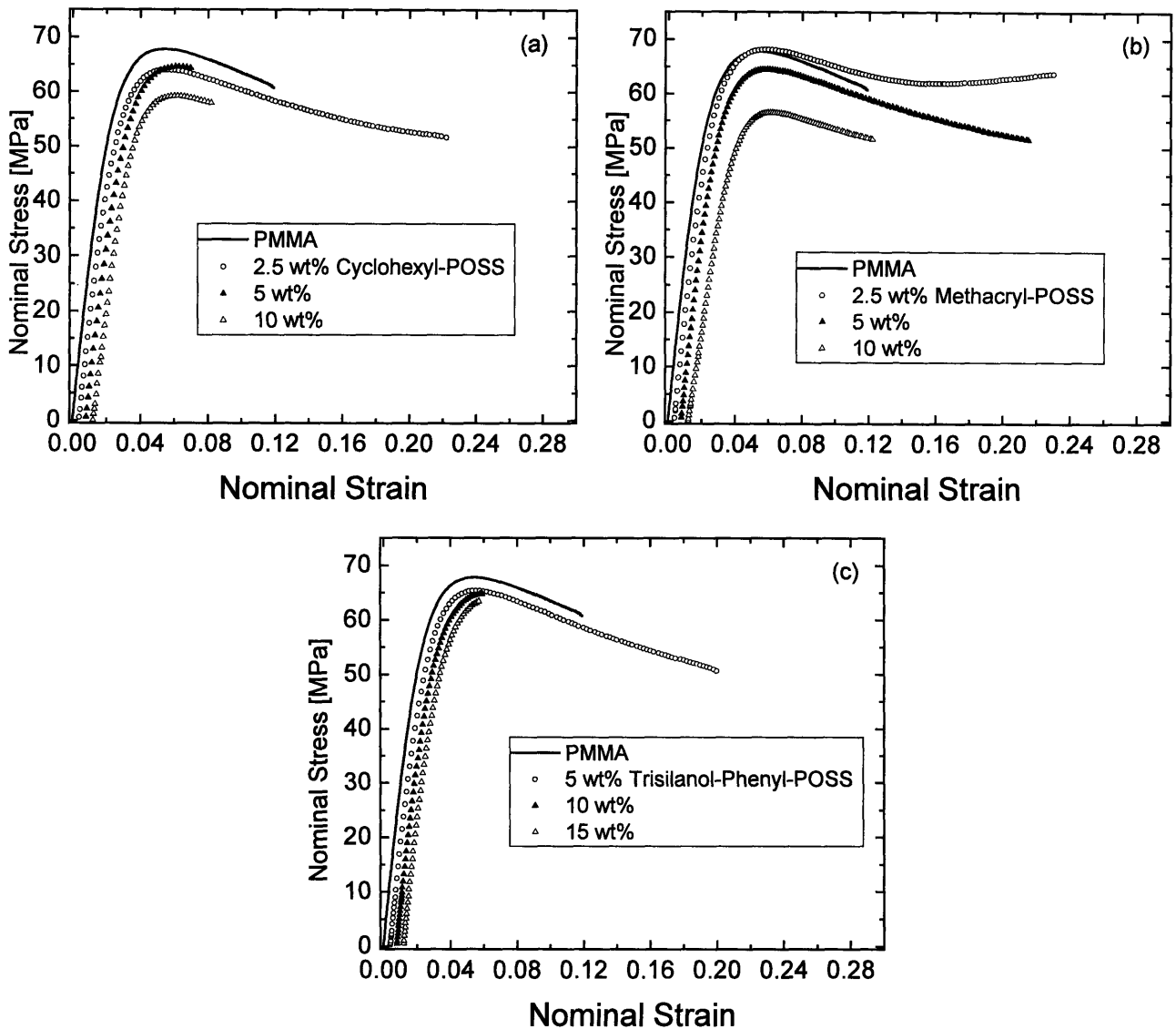


Figure 5.4 – Tensile Properties of PMMA filled with: (a) cyclohexyl-POSS; (b) methacryl-POSS; (c) trisilanol-phenyl-POSS. Curves have been offset horizontally for clarity.

In Figure 5.4(b) the stress-strain behavior of the methacryl-POSS–PMMA blends is shown for POSS loadings between 0 and 10 wt%. In this system, there is a noticeable decrease in the modulus at the highest loading of 10 wt%, and unlike the cyclohexyl-POSS–PMMA system, there is no decrease in the yield stress at a loading of 2.5 wt%. The softening after the yield point is also decreased at 2.5 wt% methacryl-POSS, but

similar softening is seen at 5 wt%. The strain-at-break ϵ_{br} increases significantly in both the 2.5 wt% and the 5 wt% blends, but at 10 wt% ϵ_{br} falls to less than that of the unfilled PMMA. The methacryl-POSS-filled samples, unlike the cyclohexyl-POSS-filled samples, showed no stress-whitening in the gauge region during testing. However, at the lowest loading of 2.5 wt%, the more ductile samples showed moderate haziness in the gauge region (Figure 5.5).

In Figure 5.4(c) the stress-strain behavior of the trisilanol-phenyl-POSS-PMMA blends is shown for POSS loadings between 0 and 10 wt%. As in the cyclohexyl-POSS blends, no apparent change in the modulus is observed when the POSS is added. The yield stress decreases moderately at 5 wt% but overall the decrease is much less than in the cyclohexyl-POSS and methacryl-POSS systems. The only sample to improve on the properties of the PMMA is the 5 wt% sample. No stress-whitening was observed in the trisilanol-phenyl-POSS-filled samples, only moderate haziness in the more ductile samples, much like the behavior of the methacryl-POSS-filled blends.

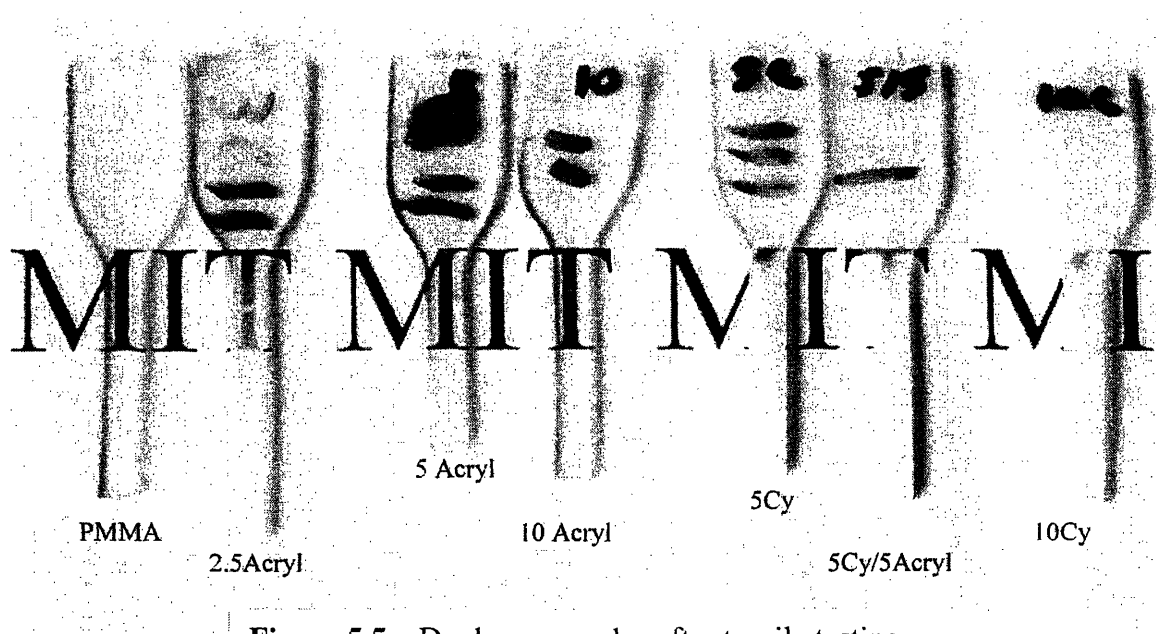


Figure 5.5 – Dogbone samples after tensile testing

All three types of POSS increase the tensile toughness of PMMA when added in very small amounts (≤ 5 wt%). The cyclohexyl-POSS loses its toughening effect above 2.5 wt%, while methacryl-POSS and trisilanol-phenyl-POSS, both of which show good miscibility with the POSS to moderate loadings, can improve the properties of PMMA at 5 wt%. In all cases, any toughening effect is lost above 5 wt%.

The different deformation mechanisms between the stress-whitened cyclohexyl-POSS blends and the methacryl-POSS blends suggested the use of both these types of POSS might allow these disparate mechanisms to be present and have a synergistic effect. The stress-strain behavior of PMMA blended with equal amounts of methacryl-POSS and cyclohexyl-POSS is shown in Figure 5.6. The combination of these two dissimilar POSS species leads to the greatest strain-at-break ϵ_{br} observed in any of the compositions analyzed. The blend containing 2.5 wt% of each POSS species yields and draws to a strain of 0.30. The blend with 5 wt% of each POSS species draws to a strain of 0.22. From the low-strain data in Figure 5.6 it is also clear that there is virtually no change in the modulus of these blends. From Fig. 5.5 it is also apparent that the combined methacryl-POSS and cyclohexyl-POSS system leads to more stress-whitening than when cyclohexyl-POSS is used alone. The 5Cy blend in Figure 5.5 is not completely opaque in the gauge region, however the 5Cy/5Acryl blend is.

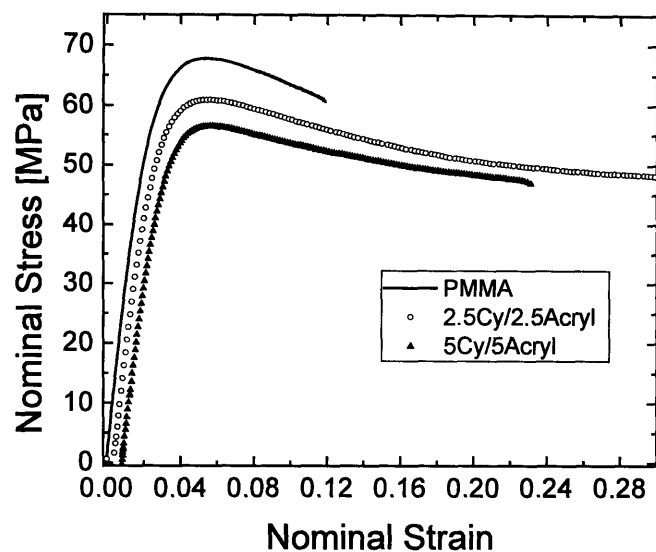


Figure 5.6 – Stress-strain behavior of blends containing both cyclohexyl-POSS and methacryl-POSS. Curves have been offset horizontally for clarity.

In Table 5.2 important stress-strain parameters are tabulated along with their standard deviations where pertinent. The Young's Modulus of the methacryl-POSS-PMMA blends decreases monotonically with increasing POSS loading, with a 25% decrease at 10 wt%. The decrease, however, is negligible at the lowest loading of 2.5 wt%. Both the cyclohexyl-POSS and the trisilanol-phenyl-POSS-filled systems show non-monotonic changes in the modulus. The cyclohexyl-POSS-PMMA system has a slightly smaller modulus at 2.5 wt%. This may be due to a small amount of molecularly-dispersed cyclohexyl-POSS at this low loading. The modulus is slightly larger than that of PMMA at 5 wt%, likely due to the onset of phase separated crystallites with relatively small diameter. The modulus then becomes significantly smaller at 10 wt%. The trisilanol-phenyl-POSS-PMMA system shows no significant change in modulus for the loadings 5, 10, and 15 wt%.

Table 5.2 Tensile Properties of POSS-PMMA Nanocomposites

Composition	Young's Modulus, ¹ <i>E</i> (GPa)	Yield Stress, σ_y (MPa)	Strain-to-break ϵ_{br} [%]	Tensile Toughness [MJ/m ³]	Percent of Samples Yielded ²
PMMA	2.89	67.7	6.32 (+/- 2.81)	3.24 (+/- 1.84)	17
2.5Acryl	2.87	67.3	16.28 (+/- 15.96)	8.85 (+/- 9.04)	50
5Acryl	2.59	64.6	14.71 (+/- 9.31)	7.64 (+/- 5.11)	60
10Acryl	2.18	56.1	8.93 (+/- 3.25)	3.99 (+/- 1.73)	50
2.5Cy	2.76	63.9	13.07 (+/- 8.60)	7.03 (+/- 4.95)	67
5Cy	3.00	64.7	7.74 (+/- 3.07)	3.86 (+/- 1.87)	25
10Cy	2.58	58.6	6.27 (+/- 1.11)	2.83 (+/- 0.65)	0
2.5Cy/2.5Acryl	2.87	61.8	25.30 (+/- 6.65)	13.29 (+/- 3.05)	100
5Cy/5Acryl	2.77	60.9	23.70 (+/- 6.89)	11.28 (+/- 3.17)	90
5tsP	2.84	65.5	11.30 (+/- 6.54)	6.15 (+/- 3.84)	75
10tsP	2.93	67.5	6.80 (+/- 3.67)	3.69 (+/- 2.56)	33
15tsP	2.86	64.0	3.30 (+/- 1.70)	1.33 (+/- 0.97)	0

¹Young's Modulus measured by fitting stress-strain data between 10 MPa and 20 MPa

²A sample was determined to have yielded if it reached a strain of 8% before failure

The results for the modulus show the importance of the POSS R-group and cage size even when the same degree of dispersion is achieved. Both methacryl-POSS and trisilanol-phenyl-POSS disperse completely in the PMMA matrix at these low loadings. The methacryl-POSS is composed of T₁₀ and T₁₂ cages that are less rigid than the incompletely-condensed T₈ cages of the trisilanol-phenyl-POSS. In addition, the phenyl R-group is much stiffer than the flexible propylmethacryl R-groups on the methacryl-POSS. It is also possible that the pendant hydroxyl groups on the uncondensed corner of the trisilanol-phenyl-POSS cage hydrogen bond with the ester groups of the PMMA backbone.

The effect of POSS on the modulus shows clearly that at no concentration does POSS significantly increase the modulus. The addition of both cyclohexyl-POSS and methacryl-POSS, interestingly, allows the modulus to be maintained quite well. The modulus of the 5Cy/5Acryl blend (which contains 10 wt% POSS total) is 2.77 GPa,

larger than both the 10 wt% methacryl-POSS blend (2.18 GPa) and the 10 wt% cyclohexyl-POSS blend (2.58 GPa).

The effect of POSS on the yield stress is qualitatively similar to the effect on the modulus for the three POSS types tested. All samples lower the yield stress, with the drop in the methacryl-POSS system being the largest.

5.3.2 – Reproducibility of Stress-Strain Results

While six blend compositions in Figures 5.4 and 5.6 showed the ability to improve the tensile toughness of PMMA, these compositions showed widely varied degrees of reproducibility. Figures 5.7(a) and (b) show the entire set of tensile stress-strain curves for the 5 wt% methacryl-POSS–filled samples and six of the 5 wt% methacryl/5 wt% cyclohexyl-POSS–filled samples, respectively. The samples containing only methacryl-POSS [Figure 5.7(a)] show a widely varying degree of elongation. Two samples draw beyond a strain of 0.20 while two samples fail at a strain of less than 0.06. Therefore while the tensile toughness of 7.64 MJ/m^3 reported in Table 5.2 for the 5Acryl sample set is on average more than double that of PMMA, it has a standard deviation (5.11 MJ/m^3) that is two-thirds the average value.

In Figure 5.7(b), however, it is clear that the combination of both methacryl and cyclohexyl-POSS leads to excellent reproducibility. All samples show the ability to yield before breaking and only one sample out of six fails before reaching a strain of 0.20. The average tensile toughness increases by a factor of 3.5 over PMMA with a standard deviation that is only 28% of the average value. Perhaps most telling of all is that in the blends containing both cyclohexyl-POSS and methacryl-POSS (2.5Cy/2.5Acryl and 5Cy/5Acryl), over 90% of the samples yielded before fracture. Across the board these

ternary blends showed the best properties: retaining the modulus, increasing the tensile toughness, and reducing the flaw sensitivity of the PMMA. The reasons for this synergistic effect are discussed in Section 5.4 below.

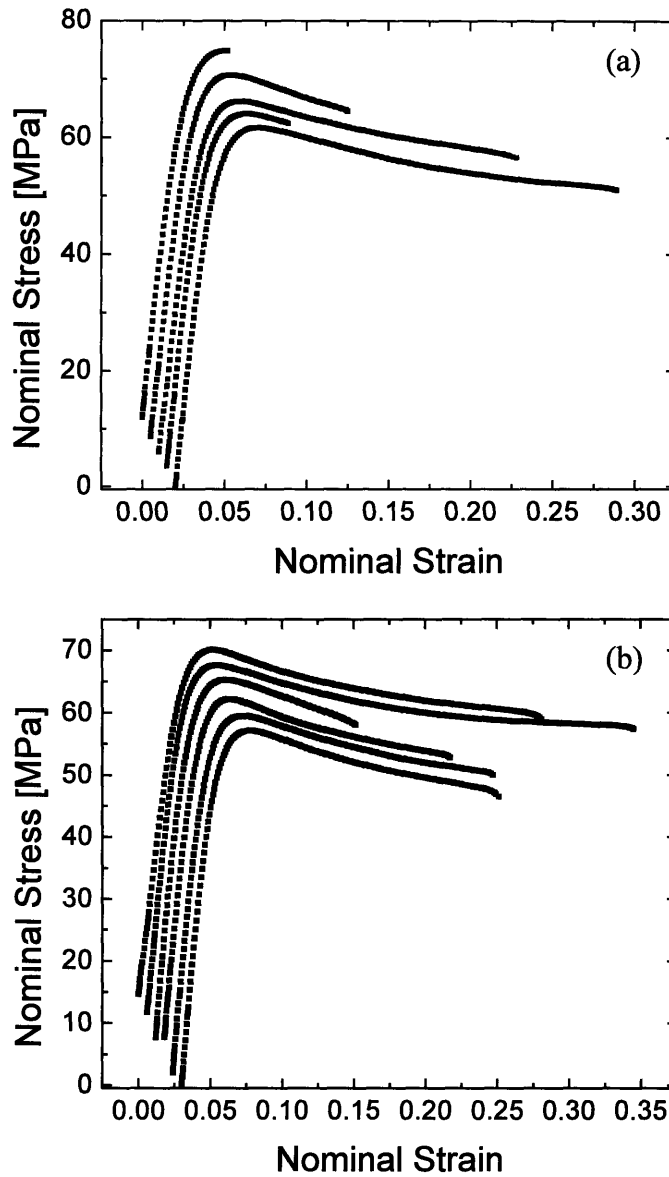


Figure 5.7 – Stress-strain properties of (a) 5 wt% methacryl-POSS in PMMA; (b) 5 wt% methacryl-POSS and 5 wt% cyclohexyl-POSS in PMMA. Curves have been offset both vertically and horizontally for clarity.

5.3.3 – Split-Hopkinson Pressure Bar (SHPB) and Notched IZOD Impact Testing

In addition to the slow-speed tension experiments, high-rate tests were performed using both a Split-Hopkinson pressure bar (SPHB) apparatus and a notched IZOD impact apparatus.

The stress-strain results from the SPHB tests are shown in Figures 5.8 and 5.9. The stress-strain curves in Figure 5.8 show that the PMMA did not pass through its yield process fully before fracturing in the compressive Hopkinson bar test. The peak stress of 305 MPa is close to the yield stress of PMMA reported by Mulliken and Boyce using the same apparatus.¹³ In that previous study the PMMA was able to yield but it fractured at a strain $\epsilon \approx 0.15$. All of the PMMA samples in this study were destroyed by the test, leaving behind only small, shredded pieces.

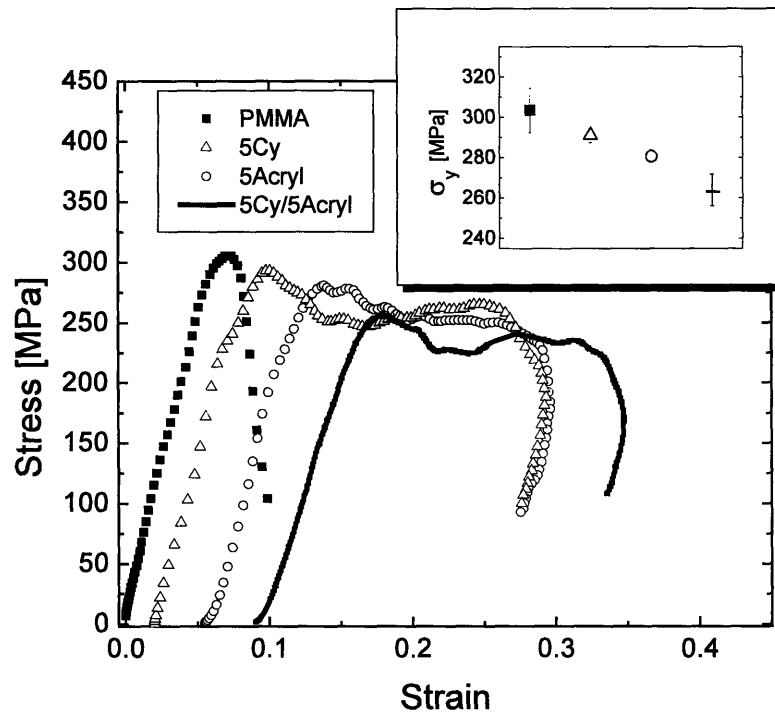


Figure 5.8 – Split-Hopkinson Pressure Bar Stress-Strain Data for PMMA and POSS-PMMA Blends. Curves have been offset by a strain of 0.03 for clarity.

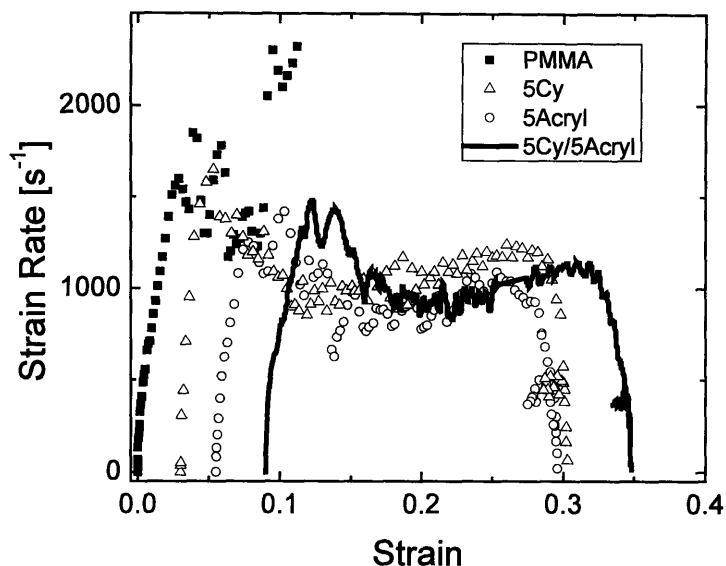


Figure 5.9 – Strain Rate as a function of True Strain in Split-Hopkinson Pressure Bar Tests. Curves have been offset by a strain of 0.03 for clarity.

The POSS-filled samples, however, all showed the ability to deform well past the yield point. These samples also had the ability to decrease the yield stress as well, even at these high rates of strain. Figure 5.9 shows a plot of strain rate as a function of strain for each of the samples tested. As the plot shows, the strain rate is not constant in the Hopkinson bar test, but for all the samples the average strain rate was centered around 1000 s^{-1} .

The reproducibility of the yielding observed in the split-Hopkinson bar tests (Figure 5.10a) was similar to that observed in the slow-speed tension experiments discussed in Section 5.3.1-5.3.2. Only one of four samples containing 5 wt% cyclohexyl-POSS showed the ability to fully yield; three of five 5 wt% methacryl-POSS-filled samples yielded; and all four samples containing both 5 wt% methacryl-POSS and 5 wt% cyclohexyl-POSS yielded.

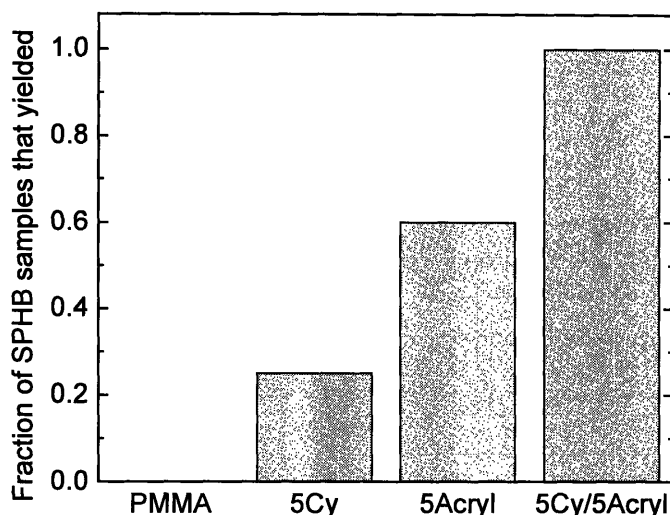


Figure 5.10a – Fraction of samples that yielded and avoided fracture in split-Hopkinson pressure bar tests

The results were different in the notched-IZOD impact tests, summarized in Figure 5.10b. While the ternary blends 2.5Cy/2.5Acryl and 5Cy/5Acryl were reproducibly tougher than pure PMMA in slow-speed tension and split-Hopkinson pressure bar tests, this same toughening effect is not observed in the notched-IZOD impact tests. One trend in the tensile tests that is repeated in the IZOD tests is that the samples with the least amount of POSS filler have the highest toughness. This is shown most clearly in the cyclohexyl-POSS-filled samples. The samples containing 2.5 wt%, 5 wt%, and 10 wt% cyclohexyl-POSS show a smoothly decreasing impact strength as POSS content is increased.

The lack of toughening in the notched-IZOD tests may be partially attributable to the poor sample preparation. The mold for the IZOD bars was not designed well, and thus the rather than molten polymer entering the mold in the desired fountain flow regime, it instead jetted in, causing the polymer to fold over on itself and produce several weld lines in each sample.

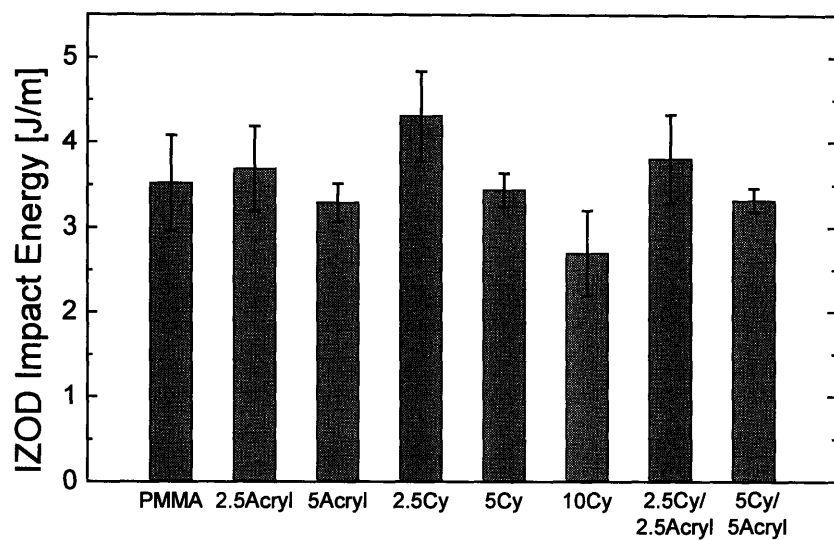


Figure 5.10b – Notched IZOD Impact Energy for Blends of PMMA and POSS

5.4 – Discussion

In both slow-speed tension (strain rate = 0.0033 s^{-1}) and high-rate split Hopkinson pressure bar tests (strain rate = 1000 s^{-1}), POSS has been shown to toughen PMMA significantly over the unfilled polymer's value. In particular, a combination of the crystallizable cyclohexyl-POSS with the non-crystallizable, plasticizing methacryl-POSS leads to not only the highest toughness values but also excellent reproducibility of the toughening. The reason for the synergistic toughening effect of these dissimilar POSS species can be understood by analyzing the microscopic cause of the enhanced stress-whitening (Figure 5.5) in the tougher blends.

The micrographs in Figure 5.11(a) and (b) show fracture surfaces for blends containing 5 wt% methacryl-POSS and 5 wt% trisilanol-phenyl-POSS, respectively. Neither of these images contains evidence of phase-separated POSS domains, indicating molecular-level dispersion, consistent with the high transmittance values of these materials from Figure 5.2. Both of these blend compositions showed improvements in toughness over unfilled PMMA in slow-speed tension tests (Figure 5.3) but showed no stress-whitening in the gauge region after yield. The samples that drew past $\epsilon = 0.15$ did, however, develop moderate haziness in the gauge region. From Figure 5.12, which shows side views of the samples in Figure 5.11 near the fracture surface, a high concentration of microcracks are present in these samples. The formation of these cracks during deformation eventually led to a critical flaw that initiated fracture. These cracks are also responsible for the haziness in the gauge region of the deformed methacryl-POSS and trisilanol-phenyl-POSS samples. Crack formation and haziness were not observed in the more brittle methacryl-POSS and trisilanol-phenyl-POSS specimens.

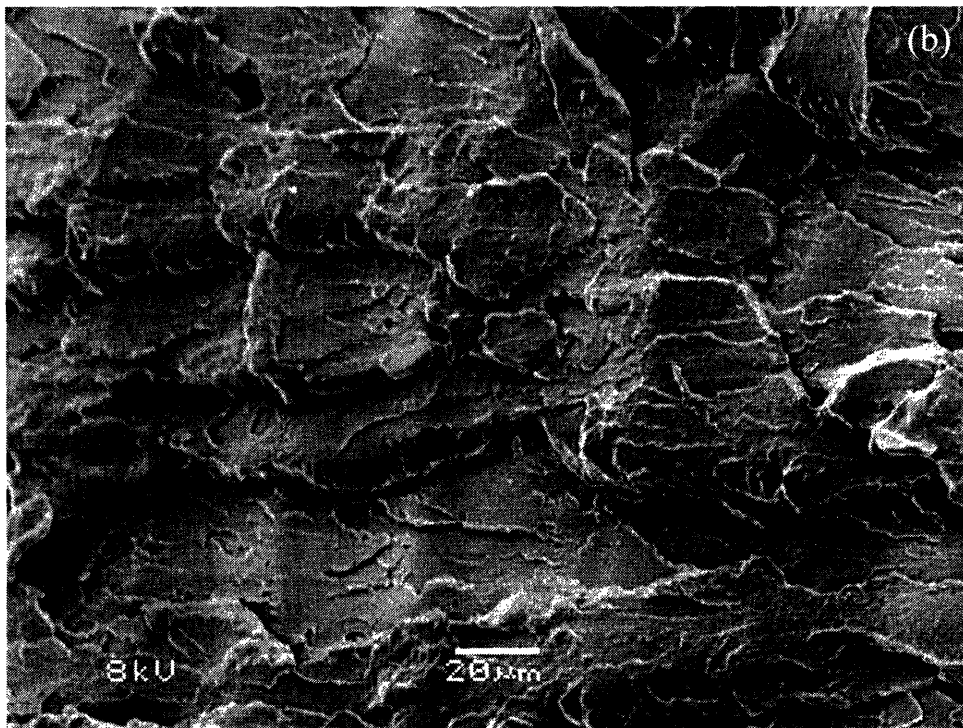
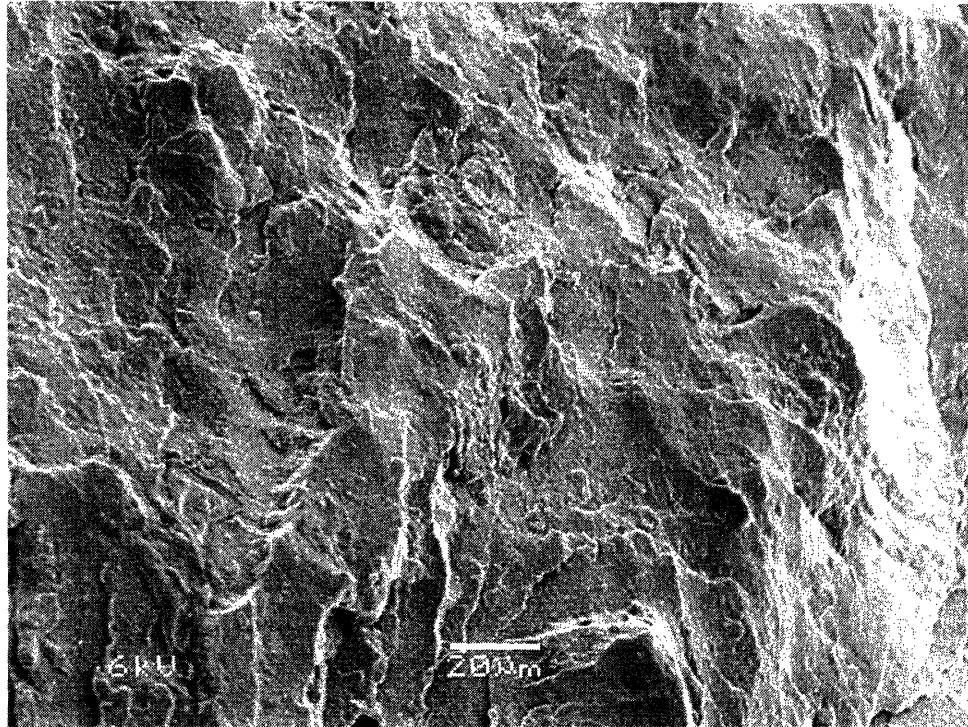


Figure 5.11 – Fracture surfaces of tensile specimens for blends containing (a) 5 wt% methacryl-POSS ($\epsilon_{br} = 0.21$) and (b) 5 wt% trisilanol-phenyl-POSS ($\epsilon_{br} = 0.20$). In both cases there is no evidence of phase separation of the POSS from the matrix.

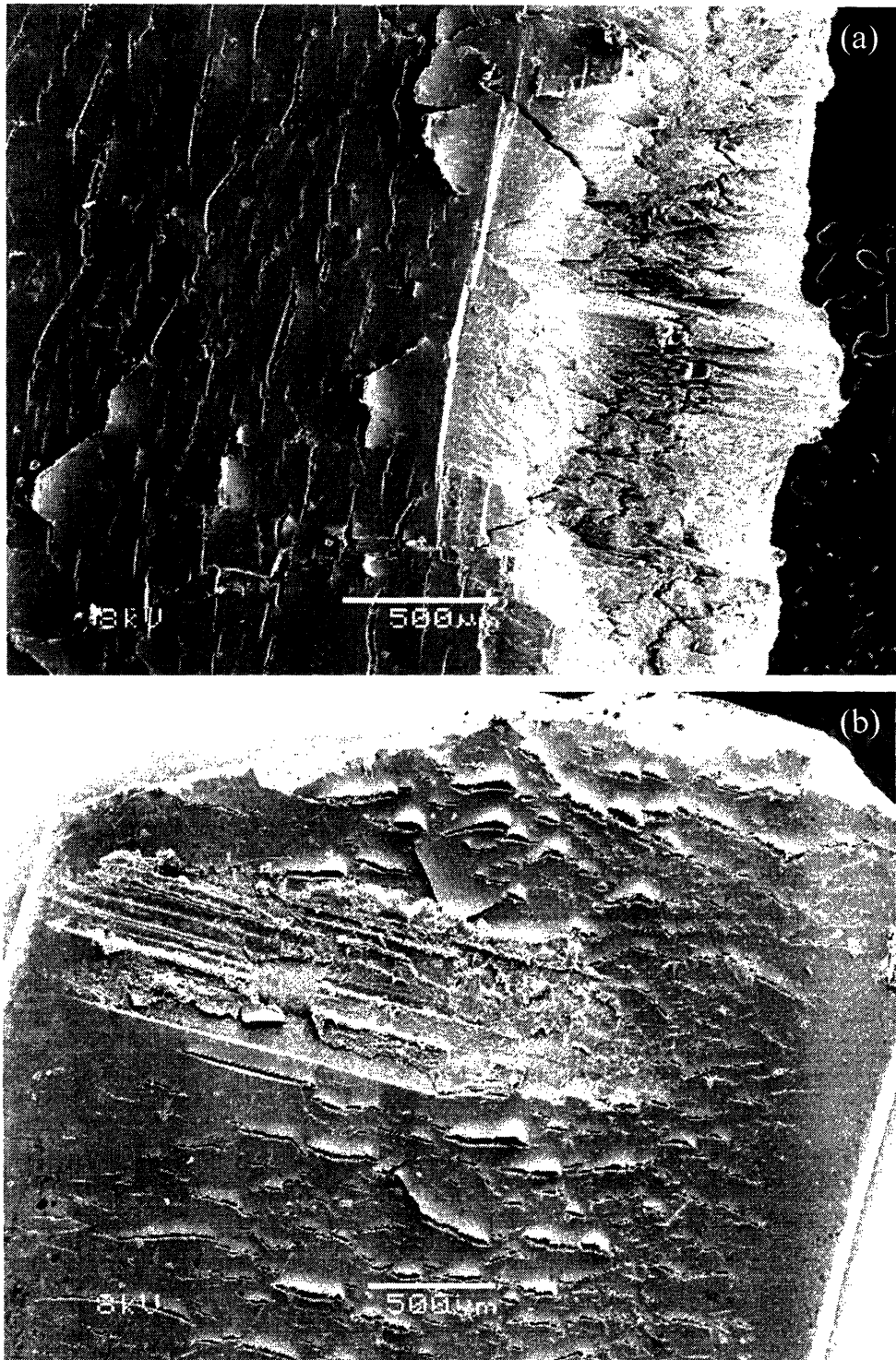


Figure 5.12 Side view of deformed tensile specimens for blends containing (a) 5 wt% methacryl-POSS ($\epsilon_{br} = 0.21$) and (b) 5 wt% trisilanol-phenyl-POSS ($e_{br} = 0.20$). A high concentration of surface cracks is present in both specimens.

In Figure 5.13(a) we show a fracture surface for a blend containing 5 wt% cyclohexyl-POSS. Crystallites of cyclohexyl-POSS are visible, with many small crystallites in the range $50 \text{ nm} \leq d \leq 250 \text{ nm}$, and a few micron-sized crystallites as well. There are several nanoscopic voids throughout the sample surface and two large ($d \approx 5 \mu\text{m}$) voids, consistent with debonding of the particles from the matrix during deformation. This debonding is the cause of the stress-whitening in the gauge region of the cyclohexyl-POSS blends (Figure 5.5). Many of the sub-micron-sized particles have failed to debond, however. In Figure 5.13(b) a fracture surface for a blend containing 5 wt% of both cyclohexyl-POSS and methacryl-POSS is shown. This micrograph shows a much higher concentration of voids than those observed in Figure 5.13(a). The voids on average are also larger than those observed in 5.13(a). This is again consistent with debonding of the particles from the matrix. In this case, the addition of methacryl-POSS allows virtually all particles to debond irrespective of size and also allows the polymer between particles to deform well past the yield point before fracture. This extensive void formation is the cause of the intense stress-whitening observed in these ternary blends.

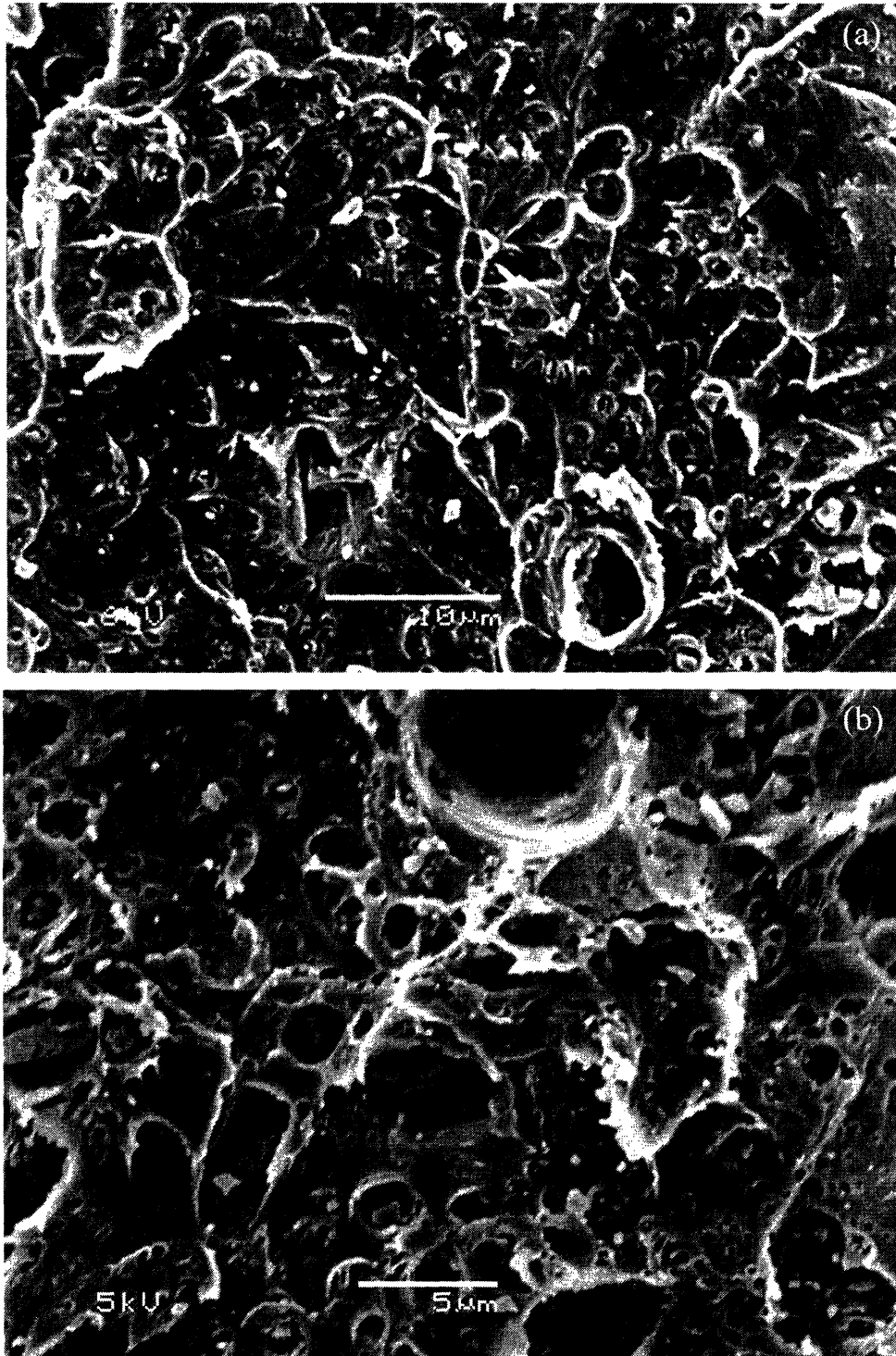


Figure 5.13 Fracture surfaces of tensile specimens for blends containing (a) 5 wt% cyclohexyl-POSS ($\epsilon_{br} = 0.10$) and (b) 5 wt% of both cyclohexyl-POSS and methacryl-POSS ($\epsilon_{br} = 0.22$).

The wide-angle x-ray diffraction patterns in Figure 5.14 allow further comparison of the morphologies of the cyclohexyl-POSS–PMMA blends and the (cyclohexyl-POSS + methacryl-POSS)–PMMA blends. Blends containing both 2.5 wt% cyclohexyl-POSS and 5 wt% cyclohexyl-POSS were analyzed. When comparing either the 2.5Cy and 2.5Cy/2.5Acryl or the 5Cy and the 5Cy/5Acryl blends, little difference in crystalline structure of the cyclohexyl-POSS is apparent. The location of the primary peak at $2\theta = 7.8^\circ$ is the same for all blends. This indicates that in the ternary blends there is no significant interpenetration of the methacryl-POSS into the cyclohexyl-POSS crystallites. This does not preclude the possibility that a portion of the methacryl-POSS preferentially segregates at the interface between the cyclohexyl-POSS crystallites and the matrix. In fact, the extensive debonding observed in Figure 5.13(b) suggests that this is likely the case. While the majority of the methacryl-POSS is distributed throughout the PMMA matrix, a minority fraction is likely present at the particle-matrix interface, helping to facilitate debonding of the cyclohexyl-POSS crystallites from the matrix. The debonded matrix ligaments, plasticized by the methacryl-POSS, are then able to deform before fracture.

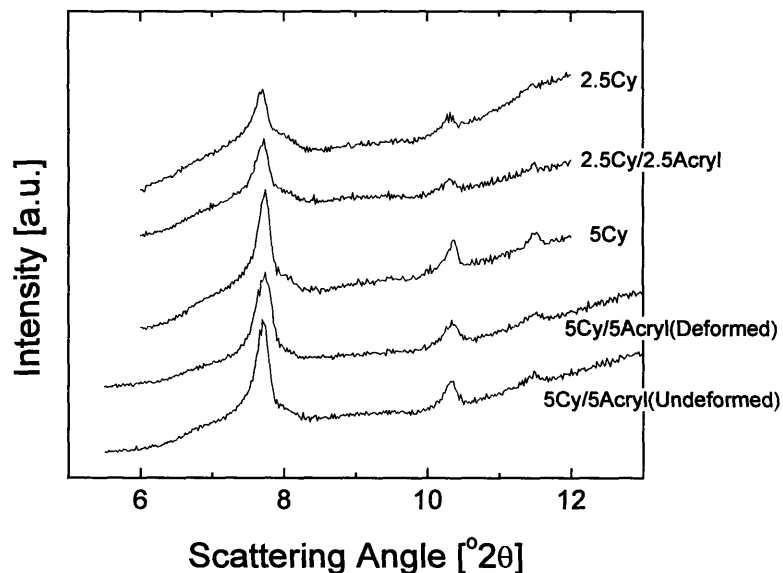


Figure 5.14 Wide-angle x-ray diffraction patterns comparing blends containing only cyclohexyl-POSS and blends containing both cyclohexyl-POSS and methacryl-POSS.

In Figure 5.15(a) and (b) we show analogous micrographs to those in Figure 5.12, where a side view of the gauge region near the fracture surface is presented for blends containing 5 wt% cyclohexyl-POSS and 5 wt% cyclohexyl-POSS + 5 wt% methacryl-POSS. The micrograph in Figure 5.15(a) contains no evidence of surface crack formation. This sample, which fractured at a strain of $\varepsilon = 0.10$, was only able to deform slightly past its yield point. The poor ductility did not allow it to reach the regime in which surface cracks became prevalent. The sample did, however, show a significant amount of stress-whitening in the gauge region, indicating that the onset of debonding occurs at a far lower strain than surface cracking in this filled system.

In Figure 5.15(b), the microcrack structure is similar to those in Figure 5.12, but the concentration of cracks is much less. Thus it appears that crack nucleation is suppressed somewhat in these ternary blends due to the addition of debonding cyclohexyl-POSS crystallites. The brittle appearance of the cracks indicates that this blend composition is not successful at deflecting cracks, however. Thus once cracks are nucleated, the sample becomes much more flaw sensitive and is prone to fracture. The micrograph in Figure 5.16 shows a less ductile sample containing 5 wt% of both cyclohexyl-POSS and methacryl-POSS, which fractured at a strain $\varepsilon = 0.13$. Only one small crack is present near the center of this image, and a large dirt or dust particle is present at the fracture point in the upper left corner of the image. This large flaw led to premature fracture just as the sample entered the range where surface cracks began to form.

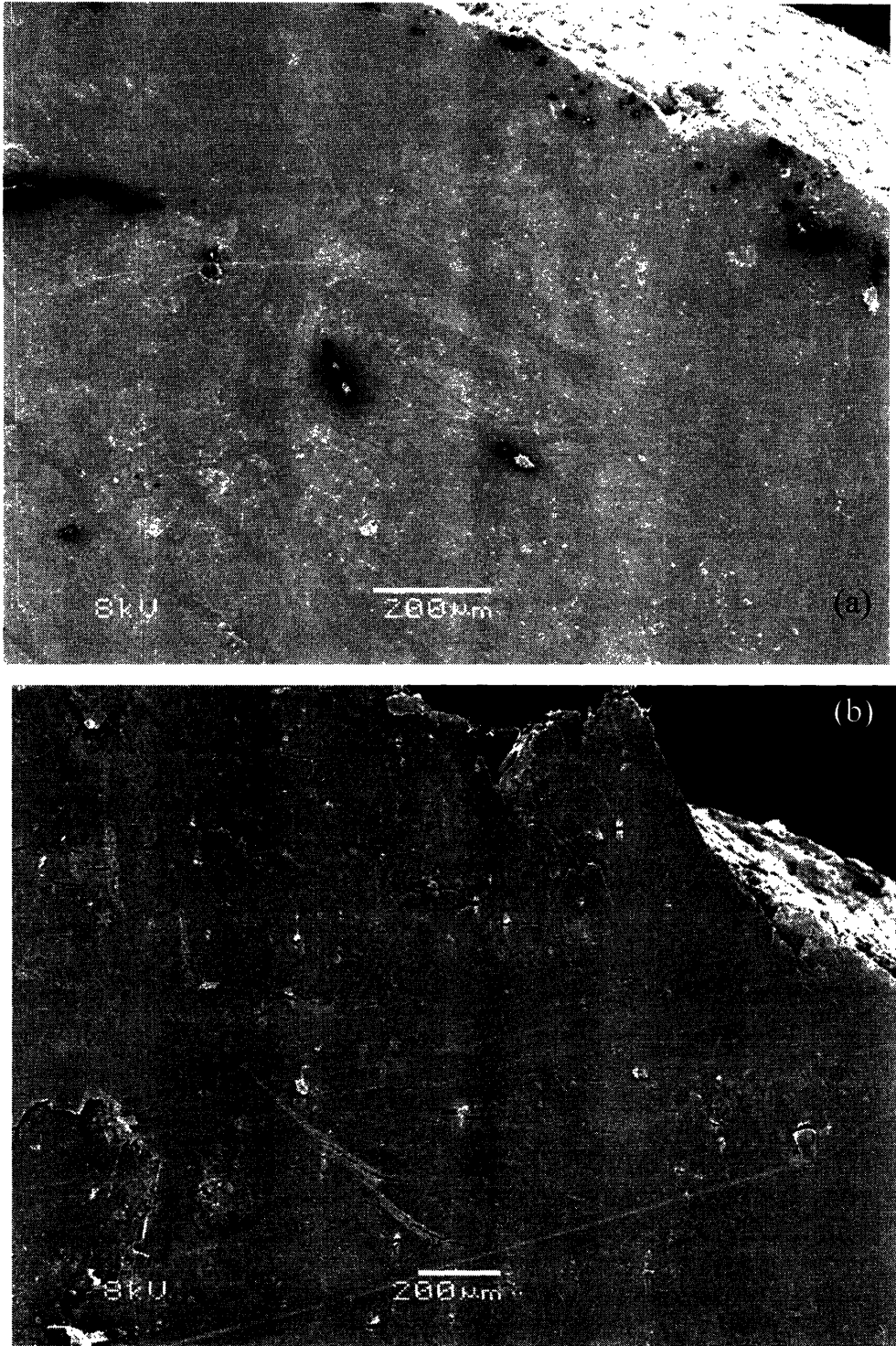


Figure 5.15 Side view of deformed tensile specimens for blends containing (a) 5 wt% cyclohexyl-POSS ($a_{br} = 0.10$) and (b) 5 wt% of both cyclohexyl-POSS and methacryl-POSS ($a_{br} = 0.22$). No surface cracks are visible in (a) but cracks are present in (b).

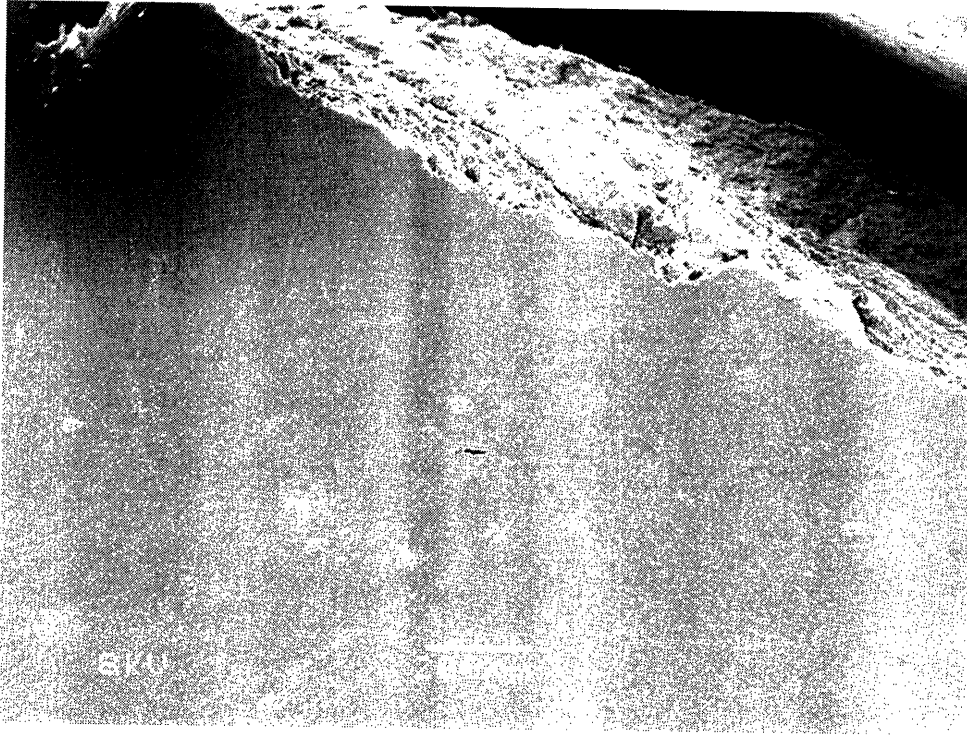


Figure 5.16 Side view of deformed tensile specimen containing 5 wt% of both cyclohexyl-POSS and methacryl-POSS. This less ductile sample ($\epsilon_{br} = 0.13$) did not draw into the regime where surface cracks nucleate and propagate, but instead fractured at the site of the large flaw in the upper left corner just as the crack regime was reached.

In Figure 5.17 (a) and (b) we show a fracture surface and a side view of a sample containing 2.5 wt% of both cyclohexyl-POSS and methacryl-POSS. The fracture surface in Figure 5.17(a) contains extensive voids formed by debonded particles, even more than that observed in the blend containing 5 wt% of both cyclohexyl-POSS and methacryl-POSS in Figure 5.13(b). The crack structure in Figure 5.17(b) is far different from that observed in Figure 5.15(b). Rather than possessing brittle cracks that propagate perpendicular to the direction of load, these cracks tend to propagate at an angle relative to the perpendicular, indicating that the cracks are deflected. In addition, a large flaw in the upper left corner of the image has not initiated fracture despite being surrounded by a highly voided sample. By zooming in more closely on this region [Figure 5.18(a)], the massive amounts of plastic deformation around these void regions is apparent. Many small circular voids are also apparent at the surface, which suggest that these surface void structures may not be cracks as much as voids caused by debonded particles. Comparing these plastic voids to the brittle voids in Figure 5.18(b) for the 5 wt% cyclohexyl POSS + 5 wt% methacryl-POSS blend it is clear that the lower-filled ternary blend is much more successful at suppressing crack propagation, which explains why it shows the greatest resistance to flaws of any of the samples tested.

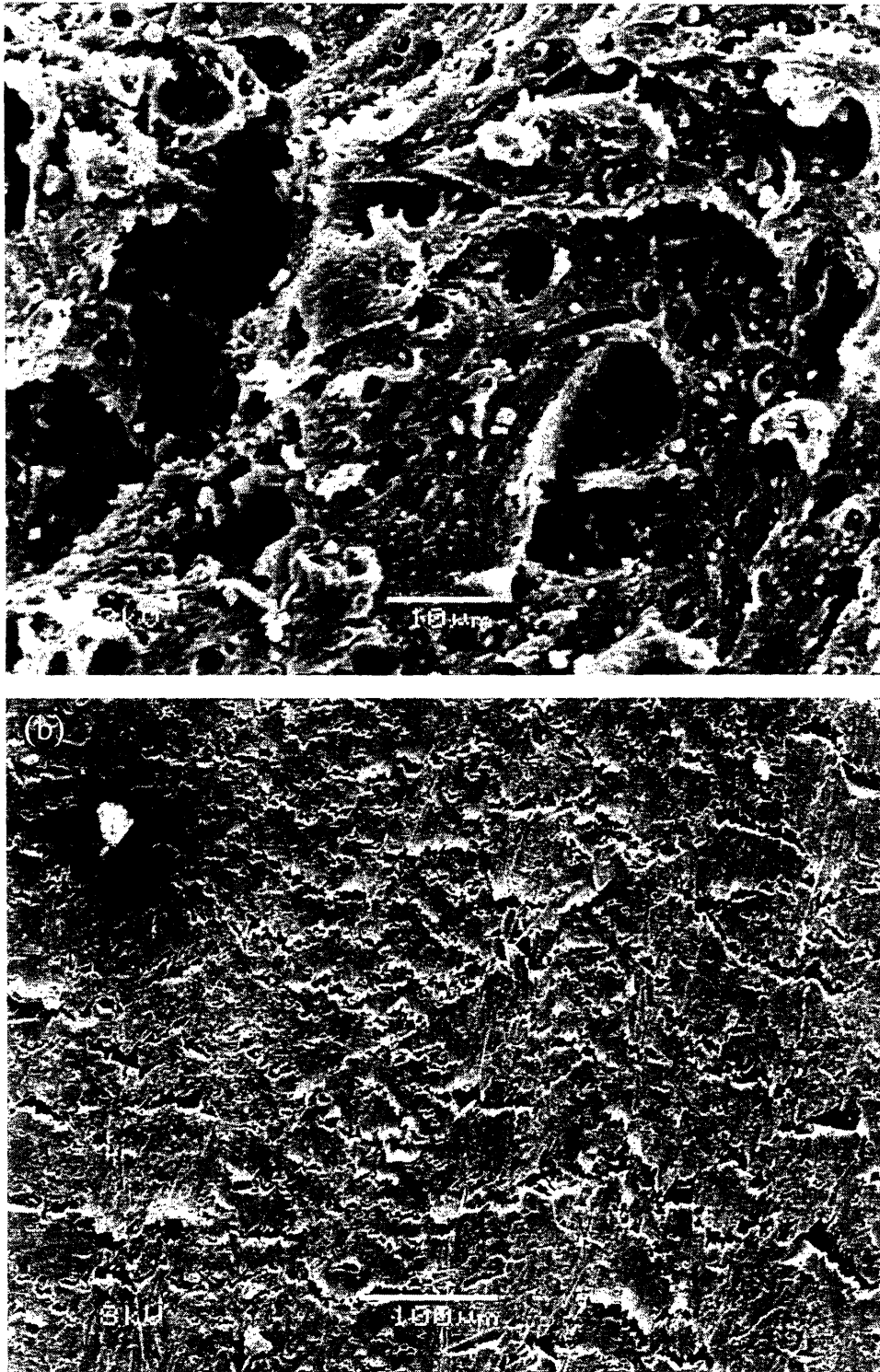


Figure 5.17 (a) Fracture surface of deformed tensile specimen ($\epsilon_{br} = 0.30$) containing 2.5 wt% of both cyclohexyl-POSS and methacryl-POSS. (b) Side view. The cracks are unable to propagate exactly perpendicular to the direction of load. In addition, the large flaw in the upper left corner does not initiate fracture in this ductile sample.

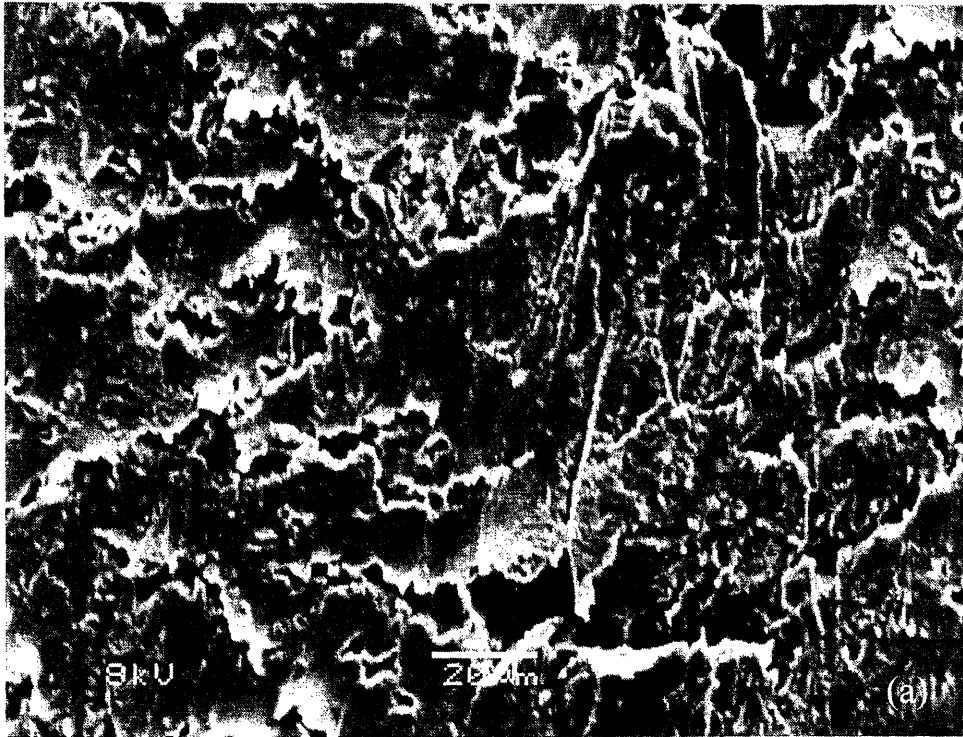


Figure 5.18 High magnification of surface cracks in deformed tensile specimens containing (a) 2.5 wt% of both cyclohexyl-POSS and methacryl-POSS and (b) 5 wt% of both cyclohexyl-POSS and methacryl-POSS. Extensive plastic deformation around the cracks is apparent in (a) while the crack in (b) has a brittle appearance.

To investigate further the role of interfacial adhesion between particles and matrix an additional blend composition was prepared with an adhesion promoting polymer. A blend containing 5 wt% cyclohexyl-POSS in PMMA was blended with a PMMA copolymer containing 15 wt% cyclohexyl-POSS tethered to the chain. The copolymer constituted 10 wt% of the blend. This well-entangled copolymer ($M_w \approx 250,000$ g/mol) was added with the expectation that it would preferentially migrate to the interface between the cyclohexyl-POSS crystallites and the PMMA matrix and suppress debonding. The stress-strain behavior of this blend, compared with the 5 wt% cyclohexyl-POSS blend, is shown in Figure 5.19. While the 5 wt% cyclohexyl-POSS samples could often reach their yield point before fracturing, the blends containing the adhesion-promoting copolymer were unable to reach a yield point and fractured before any stress-whitening could be observed. The micrograph in Figure 5.20 shows that no voids have formed around the particles due to debonding or poor adhesion. In Figure 5.13(a), a number of the voids are likely due to the poor adhesion of the crystallites to the matrix, and would be present even if debonding-induced cavitation had not occurred. The complete absence of voids in Figure 5.20 is a strong sign of the adhesion between the particles and the matrix. This strong particle-matrix bond is actually a negative in this case, however, as it reduces the toughness significantly and gives no improvement to the Young's Modulus.

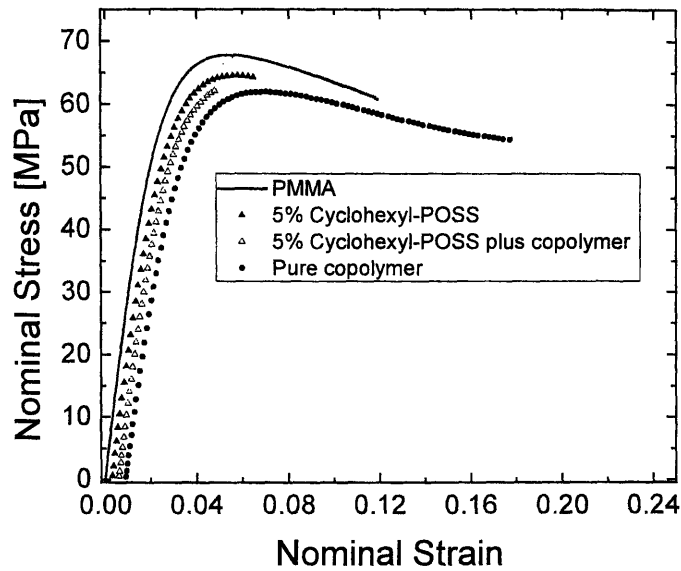


Figure 5.19 Tensile stress-strain curves comparing a 5 wt% cyclohexyl-POSS blend with a 5 wt% cyclohexyl-POSS blend containing 10 wt% of a cyclohexyl-POSS–PMMA copolymer to improve adhesion between POSS particles and the matrix. In addition, the stress-strain behavior of the PMMA and the pure copolymer have been plotted. The curves are offset by a strain $\Delta\varepsilon = 0.003$ for clarity.

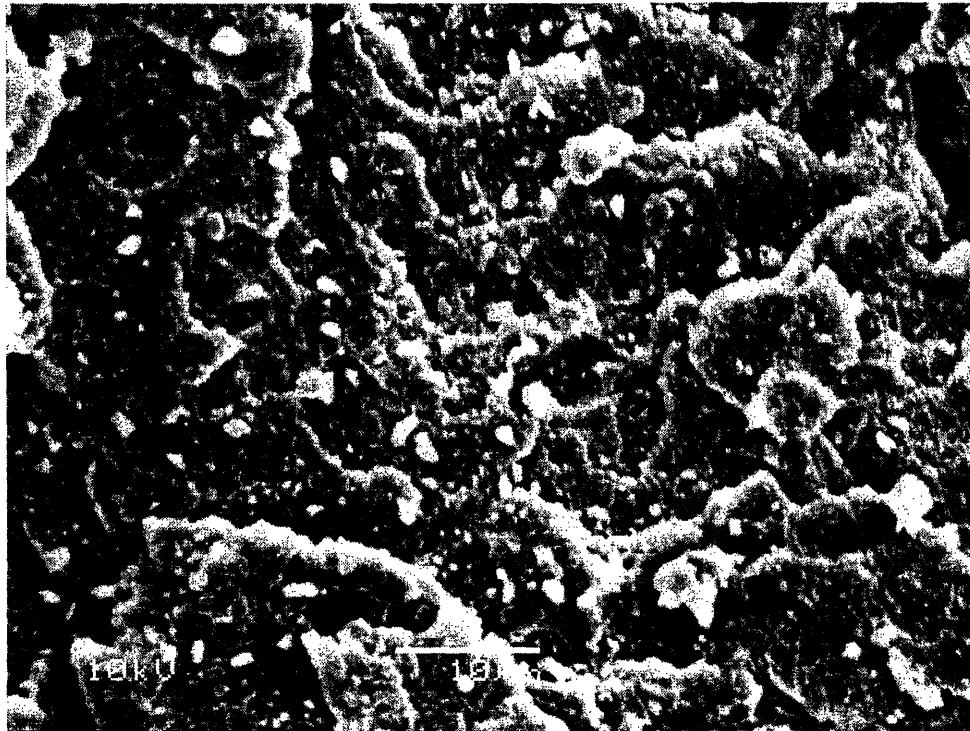


Figure 5.20 Fracture surface of a 5 wt% cyclohexyl-POSS blend containing 10 wt% cyclohexyl-POSS–PMMA copolymer. No voids are present, indicative of a strong particle-matrix bond facilitated by the copolymer.

The overall picture obtained from the entire range of compositions analyzed shows that there is a correlation between reproducible toughening and particle-matrix debonding during deformation. A weak interfacial bond is a necessity. The blends containing only cyclohexyl-POSS in PMMA meet this requirement, but without an additional plasticizing component no toughening is observed. The blends containing only methacryl-POSS or trisilanol-phenyl-POSS are able to toughen PMMA but show high flaw sensitivity because they contain no particles and thus there is no nothing from which the matrix can debond. By adding a cyclohexyl-POSS-containing copolymer to a 5 wt% cyclohexyl-POSS blend, the particle-matrix bond is significantly increased but the material is very brittle in tension. Only the combination of cyclohexyl-POSS and methacryl-POSS leads to reproducible toughening. The cyclohexyl-POSS crystallites are able to debond from the matrix more easily by adding methacryl-POSS and this debonding allows interparticle matrix ligaments to deform and shows signs of crack deflection at the surface of the specimens. A particularly encouraging result is that blends containing the smallest amounts of POSS had the highest toughness values. This is important for applications where good transparency is required. Keeping the nanoparticle content low ensures less scattering of light by the nanocomposites than in conventional composite systems.

5.5 – Conclusion

Other attempts to toughen PMMA have achieved significant improvements in tensile toughness but have significantly sacrificed other properties like modulus and yield stress.^{4,8} The present study shows that PMMA can be toughened in both slow-speed tension and impact-rate compression tests without sacrificing more than a few percent of

the modulus, even when particles greater than a micron are incorporated into the matrix. The reason for this toughening appear to be partially attributable to debonding of nano-to-micron-sized particles, however molecularly-dispersed POSS particles also show the ability to toughen PMMA. The addition of a molecularly-dispersed component and a particulate component provides the most reproducible toughening observed. Further SEM work is required to fully understand the mechanisms for this enhanced toughening.

None of the POSS species was able to toughen in notched-IZOD impact tests. Poor sample preparation keeps a conclusion from being drawn, however, about whether well-produced samples could show a toughening effect.

An overarching result from the tests is that small amounts of POSS are superior to large amounts of POSS. This is an encouraging result in light of the high cost of POSS and the desire for optically transparent materials. In the ternary blends of PMMA with cyclohexyl-POSS and methacryl-POSS, further work can be done to try to optimize the ratio of the cyclohexyl-POSS and the methacryl-POSS. It also may be possible that using a conventional plasticizer in place of the methacryl-POSS in conjunction with cyclohexyl-POSS may produce a similar toughening effect.

References

- (1) Brown, H. R.; Argon, A. S.; Cohen, R. E.; Gebizlioglu, O. S.; Kramer, E. J. *Macromolecules* **1989**, *22*, 1002.
- (2) Cho, K.; Yang, J.; Kang, B. I.; Park, C. E. *Journal of Applied Polymer Science* **2003**, *89*, 3115.
- (3) Cho, K.; Yang, J.; Yoon, S.; Hwang, M.; Nair, S. V. *Journal of Applied Polymer Science* **2005**, *95*, 748.
- (4) Ash, B. J.; Siegel, R. W.; Schadler, L. S. *Macromolecules* **2004**, *37*, 1358.
- (5) Argon, A. S. *Journal of Applied Polymer Science* **1999**, *72*, 13.
- (6) Piorkowska, E.; Argon, A. S.; Cohen, R. E. *Polymer* **1993**, *34*, 4435.
- (7) Qin, J.; Argon, A. S.; Cohen, R. E. *Journal of Applied Polymer Science* **1999**, *71*, 2319.

- (8) Jansen, B. J. P.; Rastogi, S.; Meijer, H. E. H.; Lemstra, P. J. *Macromolecules* **2001**, *34*, 3998.
- (9) Gorga, R. E.; Cohen, R. E. *Journal of Polymer Science Part B: Polymer Physics* **2004**, *42*, 2690.
- (10) Gilbert, D. G.; Donald, A. M. *Journal of Materials Science* **1986**, *21*, 1819.
- (11) Kopesky, E. T.; Haddad, T. S.; Cohen, R. E.; McKinley, G. H. *Macromolecules* **2004**, *37*, 8992.
- (12) Kopesky, E. T.; Cohen, R. E.; McKinley, G. *Polymer* **2005**, submitted.
- (13) Mulliken, A. D.; Boyce, M. C. *International Journal of Solids and Structures* **2005**, Submitted.
- (14) Ward, I. M.; Hadley, D. W. *An Introduction to the Mechanical Properties of Solid Polymers*; John Wiley & Sons: New York, 1993.
- (15) Kramer, E. J. *Advances in Polymer Science* **1983**, *52-53*, 1.
- (16) van der Sanden, M. C. M.; Meijer, H. E. H.; Lemstra, P. J. *Polymer* **1993**, *34*.
- (17) Argon, A. S.; Cohen, R. E.; Gebizlioglu, O. S.; Brown, H. R.; Kramer, E. J. *Macromolecules* **1990**, *23*, 3975.
- (18) Gebizlioglu, O. S.; Beckham, H. W.; Argon, A. S.; Cohen, R. E.; Brown, H. R. *Macromolecules* **1990**, *23*, 3968.
- (19) Bartczak, Z.; Argon, A. S.; Cohen, R. E.; Weinberg, M. *Polymer* **1999**, *40*, 2347.

Chapter 6: In-situ Polymerized Acrylates Containing Isobutyl-POSS: Effect of Glass Transition Temperature on Self-Assembly and Properties (w/ Dr. Alex Hsieh)

6.1 – Introduction

Copolymers containing high percentages of tethered-POSS (as high as 100 mol%¹) have been synthesized often over the past decade.¹⁻¹² For the most part, POSS has been shown to have very little effect on the properties of polymers at low to moderate loadings (< 30 wt%), and only at very high loadings is a significant change seen in properties such as glass transition temperature,¹ thermo-oxidative stability,⁷ or linear viscoelastic properties.^{3,12} This is because at low loadings the POSS is usually in a randomly dispersed state throughout the matrix and thus has little impact on the overall matrix properties. On the other hand, at high POSS loadings, the tethered moieties are able to crystallize into rafts⁸ or cylinders¹³ with thicknesses $d < 10$ nm. These POSS domains lead to confinement of the polymer matrix (which often times is a minority component) and thus the properties of the matrix and the polymer itself are significantly altered. A significant enhancement in thermal and viscoelastic properties is observed at this point.^{1,7,12} However, it has also been observed that POSS can cause a decrease in the glass transition temperature with increasing POSS loading, even at very high loadings.⁹ It was also shown in Chapter 2¹⁴ that incorporation of moderate loadings (25 wt%) of either isobutyl-POSS or cyclopentyl-POSS on a PMMA backbone leads to a significant decrease in the plateau modulus G_N^0 . One potential problem with these past studies is that they have typically focused on polymers such as polystyrene,¹ polyethylene,⁵ polynorbornene,^{4,13} and poly(methyl methacrylate),² all of which have relatively high moduli at room temperature (≈ 1 GPa). Still more work has been done trying to toughen

and reinforce thermosets with tethered-POSS.¹⁵⁻²² Relatively little work has been done on incorporating POSS into elastomeric matrices.^{10,11,23,24} A recent study incorporated POSS into a triblock copolymer with structure isobutyl-POSS–poly(*n*-butyl acrylate)–isobutyl-POSS,¹⁰ however it may have been possible to achieve similar properties using a PMMA-PBA-PMMA triblock copolymer.

What these results show is that there is no universal behavior in POSS-polymer systems, and that a sweeping generalization may not be drawn in order to capture completely the behavior of POSS-polymer systems. The effect that a given POSS cage will have on a polymer matrix, when covalently tethered to the backbone, is a function of the R-group on the seven non-reactive corners of the POSS cage, the type of matrix (glassy, rubbery, leathery), and also the rigidity of the attachment of the POSS to the backbone. Different POSS cages have different melting points. Those with fairly rigid R-groups (e.g. cyclohexyl, phenyl, cyclopentyl) tend not to melt below their organic components burn off, though they can exhibit low *T* transitions at which point their R-groups become mobile.⁴ Other POSS cages with more flexible R-groups (e.g. isobutyl) exhibit phase transitions before their R-groups degrade.¹⁴ Polymers also have widely varying transition points. Many commercial polymers are glassy at room temperature (PMMA, polystyrene, polycarbonate) while others are rubbery [polyisoprene, polyisobutylene, polybutadiene, poly(*n*-butyl acrylate)] and still others are somewhere in between [poly(butyl methacrylate)]. Quantitatively, PMMA has a glass transition temperature near 105°C while PBA has a *T_g* of approximately –50°C. Tethered-POSS cages would find vastly different environments when tethered separately to these two polymers. In a PMMA matrix, POSS cages would need to crystallize at high

temperatures, likely closer to the α -transition measured in DMA ($T_\alpha \approx 130^\circ\text{C}$) than the T_g of 105°C as measured in DSC. Only the POSS cages with very rigid R-groups will experience a strong enough thermodynamic driving force to crystallize, and in many cases even these will have difficulty achieving good self-assembly. In the poly(*n*-butyl acrylate), on the other hand, the matrix will not vitrify until well below room temperature. This should allow POSS cages to self-assemble, even the low-melting ones such as isobutyl-POSS.

For this study, POSS-PMMA copolymers and POSS-PBA copolymers were synthesized in order to analyze the ability for isobutyl-POSS, a relatively low-melting POSS cage, to self-assemble within a high T_g polymer and a low T_g polymer. Recent work has shown that high POSS contents can lead to a thermoplastic elastomer when incorporated into a rubbery matrix.¹¹ Previous work by Pyun et al.¹⁰ on PBA incorporating POSS dealt with triblock copolymers of POSS-PBA-POSS, in which the POSS formed micro-phase separated domains between the connecting domains of PBA. Our present work uses a much simpler synthesis technique that randomly polymerizes the POSS macromer with PBA. Comparison with the results of Pyun et al. will help shed light on the benefits of our more practical synthetic technique.

6.2 – Experimental Section

6.2.1 – Polymer Synthesis

The synthesis procedure for the POSS-PMMA copolymers is described below in Section 6.3.1 and the synthesis of the POSS-PBA copolymers is summarized in Section 6.3.4.

6.2.2 – Polymer Characterization

Differential scanning calorimetry was performed in a TA Instruments Q1000 DSC. PMMA-based polymers were heated and cooled at 3°C/min over the range $-50^{\circ}\text{C} \leq T \leq 200^{\circ}\text{C}$; PBA-based polymers were heated and cooled at the same rate over the range $-80^{\circ}\text{C} \leq T \leq 100^{\circ}\text{C}$. Data were taken on the second heating run in each case.

Dynamic mechanical analysis was performed using a TA Instruments Q800 in tension. Samples were rectangular with approximate dimensions of 20 mm × 3 mm × 1 mm. Samples were heated at 3°C/min over the temperature range $-100^{\circ}\text{C} \leq T \leq 175^{\circ}\text{C}$.

Dielectric measurements were performed on a TA Instruments 2970 Dielectric Analyzer over the temperature range $-50^{\circ}\text{C} \leq T \leq 175^{\circ}\text{C}$ at frequencies ranging from $1 \text{ Hz} \leq \omega \leq 10^4 \text{ Hz}$.

Stress-strain measurements were performed using a Zwick Z010 mechanical tester. A 500 N load cell was used and the crosshead speed was 12 mm/min. The gauge length of the samples was 20 mm.

6.3 – Results

6.3.1 – In-situ polymerization of poly(methyl methacrylate)-co-propylmethacryl-isobutyl-POSS

Prior to polymerization, the solubility limit of the isobutyl-POSS macromer [propylmethacryl-isobutyl-POSS, Hybrid Plastics, M.W. = 943.64 g/mol] in methyl methacrylate (MMA)[Aldrich] was determined. As the POSS macromer was added to MMA in increasing amounts the solution became progressively more cloudy but showed complete solubility up to a weight fraction of 0.50. Different batches of the macromer

had different degrees of solubility. The batch used for the present study showed the best solubility, with excellent miscibility to greater than 50 wt% macromer.

The three PMMA samples produced for this study are listed in Table 6.1 and the reaction scheme is shown in Figure. 6.1.

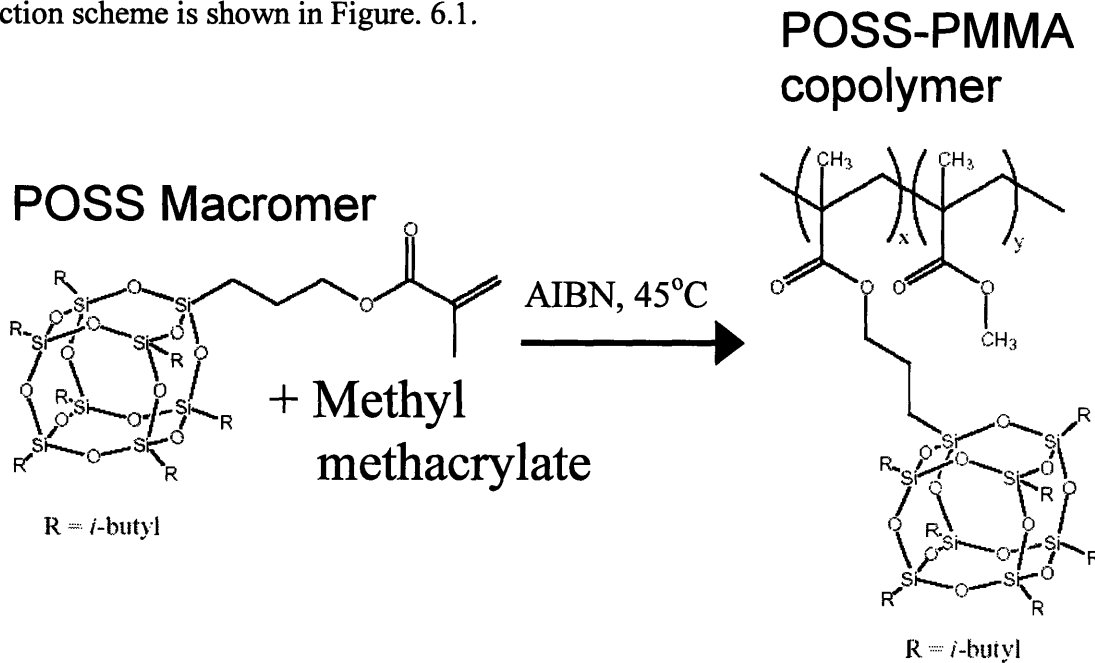


Figure 6.1 – Reaction scheme for in-situ polymerization of POSS-PMMA copolymers

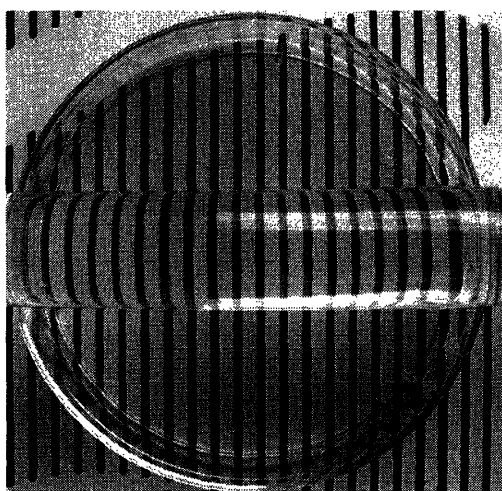
Table 6.1 Composition and Properties of POSS-PMMA Copolymers

	Wt.% POSS	M_w (g/mol)	PDI (M_w/M_n)	T_g (°C) [DSC]	T_g (°C) [DMA]
Control	0.0	3.2×10^6	2.1	109.7	133.2
5 mol%	33.2	1.5×10^6	2.6	102	120.1
10 mol%	50.0	1.6×10^6	2.3	87.7	106.1

A PMMA control was synthesized, as were two copolymers: one containing 5 mol% POSS macromer in the mixture (33 wt% POSS) and the other containing 10 mol% POSS (50 wt% POSS). The initiator (AIBN) was added at 0.5 mol% and the reaction mixture was stirred at room temperature for five minutes with the aid of a magnetic stir bar. The solution was then poured into the reaction vessel, which consisted of two glass plates with non-stick sealant clamped to a makeshift rubber gasket approximately 3 mm

thick. The gasket had a rectangular section carved out with a total volume of approximately 10 mL. The gasket was sealed by placing a rubber strip over the opening where the mixture was poured into the vessel. A second clamp was placed over the vessel to ensure proper sealing before it was placed into a water bath held at a constant temperature $T = 45^{\circ}\text{C}$. The sample was held at this temperature for 24 hours before the temperature was raised to $T = 60^{\circ}\text{C}$ for another 24 hours. The vessel was then removed from the water bath and the polymers were post-cured at a temperature $T = 120^{\circ}\text{C}$ to polymerize any unreacted components.

After post-curing all samples exhibited outstanding optical clarity. In Figure 6.2 a picture of the 10 mol% polymer after post-curing shows its excellent transparency. The



50 wt% POSS (10 mol%)

Figure 6.2 – Image showing optical clarity of high POSS-content copolymer

mechanical properties were affected substantially by the POSS, however. The PMMA control and the 5 mol% polymer both made a robust sound when tapped against a hard surface, but the 10 mol% sample made only a weak “click” that was clear evidence of its poor mechanical properties. The 10 mol% sample was difficult to machine due to its inherent brittleness.

The molecular weights of the samples (Table 6.1) were measured in GPC using THF as the eluent and a polystyrene standard. The GPC traces are reproduced in Figure

6.3. The molecular weights achieved were extremely high, with the peaks of the GPC traces occurring at greater than 10^6 g/mol for each polymer composition.

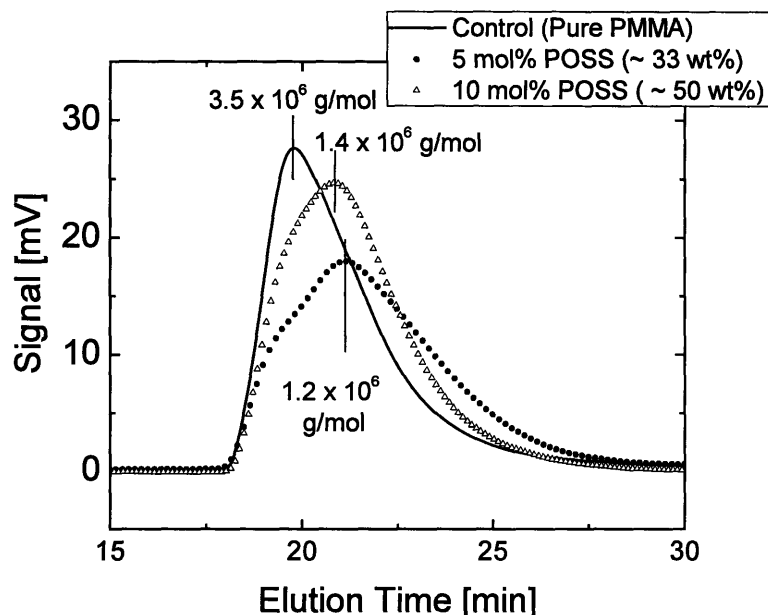


Figure 6.3 – GPC curves for POSS-PMMA copolymers

6.3.2 – Wide Angle X-ray Diffraction of POSS-PMMA copolymers

Wide angle x-ray diffraction was performed on the samples and also on the POSS macromer to observe the degree of POSS aggregation in the sample. These traces are shown in Figure 6.4. The macromer is a highly crystalline powder at room temperature, exhibiting sharp peaks, with the tallest peak at $2\theta = 8.04^\circ$ ($d = 1.10$ nm). The PMMA control has only a broad amorphous peak at $2\theta = 14.12^\circ$ ($d = 0.63$ nm). The copolymers, on the other hand, show no sign of the amorphous spacing of the PMMA, instead exhibiting two widely spaced amorphous peaks. The 5 mol% sample has a low-angle peak at $2\theta = 9.40^\circ$ ($d = 0.94$ nm) and a high-angle peak at $2\theta = 17.42^\circ$ ($d = 0.51$ nm). The peak positions for the 10 mol% sample are farther apart: the low-angle peak is at $2\theta = 9.02^\circ$ ($d = 0.98$ nm) while the high-angle peak is at $2\theta = 18.00^\circ$ ($d = 0.49$ nm). The trend

observed in the peak locations is typical of POSS-copolymers.³ The low-angle peak of the POSS macromer around $2\theta = 8^\circ$ is typically shifted to around $2\theta = 9^\circ$ (a smaller d -spacing) upon polymerization. As the POSS content of the copolymer is increased, this peak shifts back to more closely approximate that of the crystalline macromer. However, in this case, even at 50 wt% POSS in the copolymer, the 10 mol% sample's low-angle peak is nearly one full degree offset from the highest peak of the macromer spectrum. This is due to the poor order in the copolymer, the reasons for which will be analyzed in the Discussion section below.

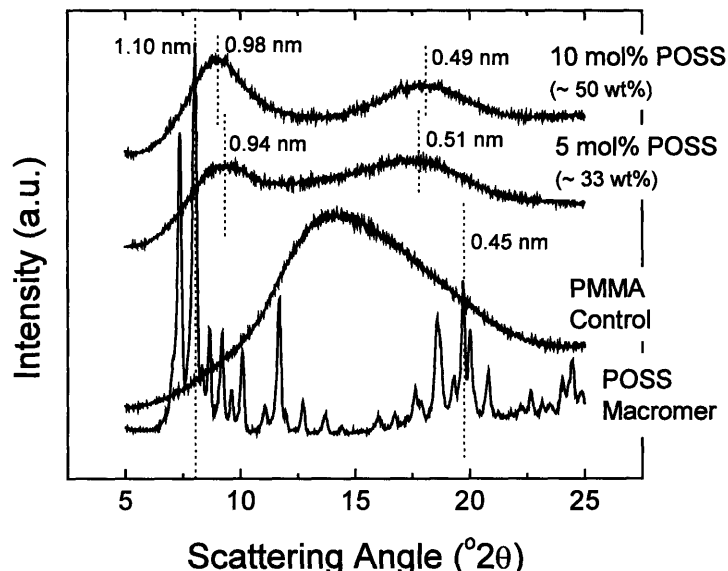


Figure 6.4 – Wide angle x-ray diffraction patterns for POSS, PMMA, and POSS-PMMA copolymers

6.3.3 – Thermomechanical Properties of POSS-PMMA Copolymers

The effect of the isobutyl-POSS on the thermomechanical properties of PMMA was analyzed using differential scanning calorimetry(DSC), dynamic mechanical analysis(DMA), dielectric analysis(DEA), and small amplitude oscillatory shear flow. Figure 6.5 is a plot of DSC curves for the three polymers synthesized in the study. A

monotonic and significant decrease in the glass transition temperature T_g is observed with increasing POSS content (see Table 6.1). The decrease in the T_g is more significant between 5 mol% and 10 mol% ($\Delta T_g = 14.3^\circ\text{C}$) than between the PMMA and the 5 mol% sample ($\Delta T_g = 7.7^\circ\text{C}$). In general, copolymerization with POSS usually leads to an increase in the glass transition temperature T_g , but in a study by Mather et al. it was observed that isobutyl-POSS copolymerized with styrene caused a decrease in the glass transition temperature.⁹

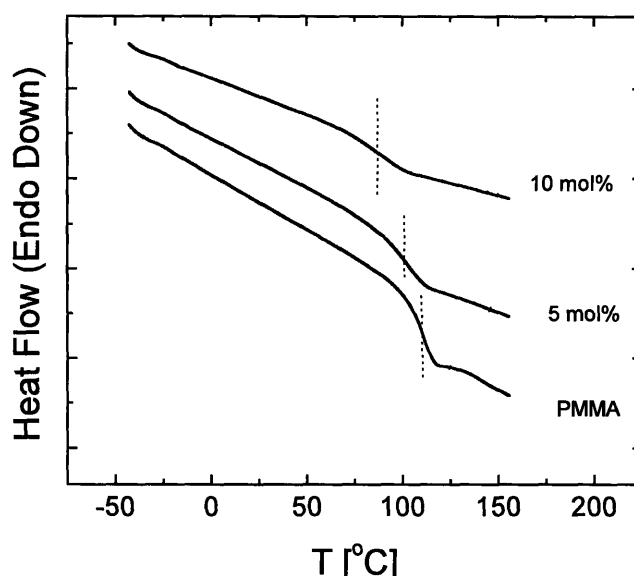


Figure 6.5 – DSC curves for PMMA and POSS-PMMA copolymers

A similar plasticizing effect is observed in the dynamic mechanical behavior of the polymers in Figures 6.6(a)-(b). Significant decreases in both the glassy and rubbery moduli are observed with POSS content, as well as decreases in the temperatures at which the α - and β -transitions occur. The α -transition, characterized by the peak in $\tan \delta$ and associated with segmental relaxations at the glass transition,²⁵ peaks at $T = 133.2^\circ\text{C}$ in the PMMA control and falls to $T = 106.1^\circ\text{C}$ in the 10 mol% sample. The difference in

the α -transition values is slightly larger than the difference in the glass transition temperatures measured in DSC. The observed decrease in the modulus is again somewhat atypical for POSS-copolymers,⁴ however it is expected based on the lower T_g .

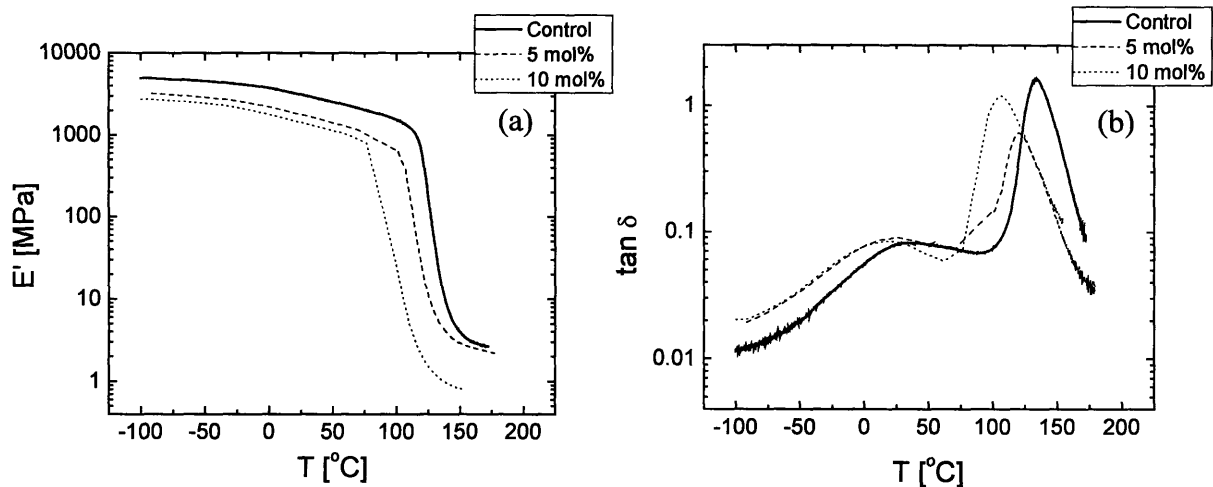
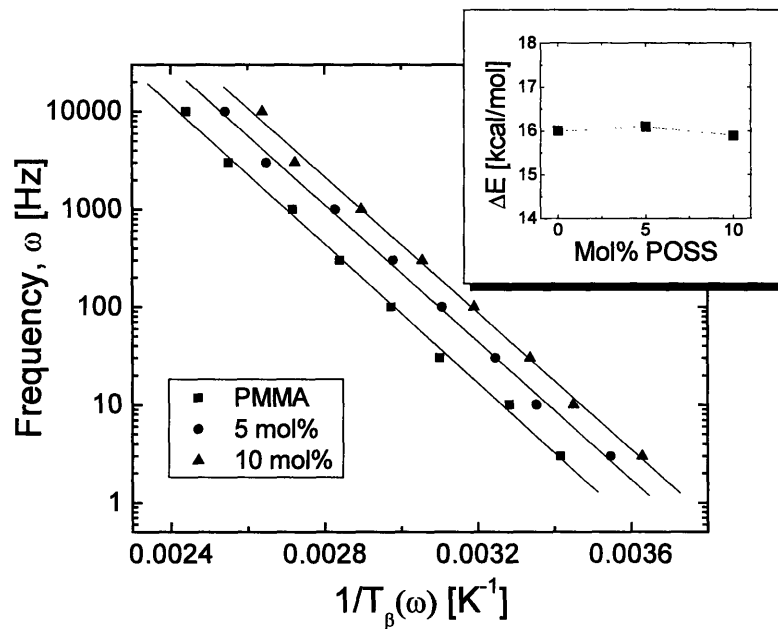


Figure 6.6 – Dynamic mechanical analysis curves for POSS-PMMA copolymers: (a) storage modulus; (b) loss tangent

Dielectric analysis (DEA) was performed on the three different polymers to determine the temperature dependence of the β -transition. In Table 6.2 the measured β -transition values are tabulated as a function of frequency. These frequencies are plotted in Arrhenius fashion against the reciprocal of the measured β -transition temperatures in Figure 6.7 to determine activation energies for this transition. From the fits to these data, it is clear that the addition of POSS to the PMMA chain does not affect the activation energy for the β -transition, it simply shifts the β -transition to lower temperatures. This shift is similar in magnitude to the shift in the α -transition.

Table 6.2 Beta Transition Temperatures Measured in DEA

Frequency (Hz)	PMMA	5 mol%	10 mol%
	T_{β} ($^{\circ}\text{C}$)	T_{β} ($^{\circ}\text{C}$)	T_{β} ($^{\circ}\text{C}$)
3	19.6	8.8	2.4
10	31.5	25.1	16.7
30	49.3	34.9	26.5
100	63.2	48.8	40.3
300	79.1	62.6	54.2
1000	95	80.5	72.1
3000	118.9	104.4	94
10000	136.8	120.3	105.9

**Figure 6.7** – Arrhenius plot of frequency vs. the reciprocal of the beta transition temperature measured in the dielectric analyzer

The final tool for analysis of the polymers was rheological characterization in small amplitude oscillatory shear flow. The storage modulus G' and the loss modulus G'' are plotted in Figure 6.8 at a temperature of $T = 170^{\circ}\text{C}$. These polymers all have quite flat storage modulus profiles, indicative of very highly entangled polymers. The variation of the rubbery plateau modulus G_N^0 with POSS content of these in-situ-polymerized

polymers is similar to the results for the solution-polymerized polymers from Chapter 2. In both cases, the plateau modulus decreased monotonically with POSS content.

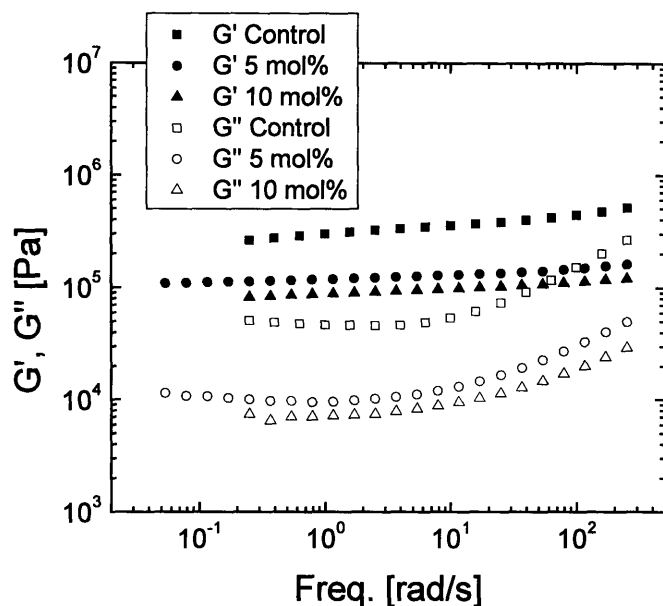


Figure 6.8 – Storage and loss moduli of POSS-PMMA copolymers measured in small amplitude oscillatory shear flow at $T = 170^\circ\text{C}$

6.3.4 - In-situ polymerization of poly(*n*-butyl acrylate)-co-propylmethacryl-isobutyl-POSS

The reaction scheme for the synthesis of the POSS-PBA copolymers is shown in Figure 6.9. Butyl acrylate monomer [Aldrich] was used as received. The isobutyl-POSS macromer was highly soluble in butyl acrylate, though fully dissolving high concentrations (50 wt%) required heating the solution to $T = 45^\circ\text{C}$ to homogenize the mixture. Once the macromer had fully dissolved, the initiator (AIBN) was added at 0.3 mol%. (The low initiator concentration was required to avoid bubble formation during polymerization.) Each solution was then poured into an 8 mL glass vial, sealed, and placed in a water bath at $T = 45^\circ\text{C}$ for 24 hours. The temperature of the water bath was

then increased to $T = 60^{\circ}\text{C}$ for 24 hours. The samples were subsequently removed from the water bath and post-cured at $T = 120^{\circ}\text{C}$ for 24 hours. The resulting polymers were mildly crosslinked, thus GPC analysis could not be performed. The samples simply swelled even at very low concentrations. Analysis using ^1H NMR on the swelled polymers did not reveal quantitative estimates of the POSS content, but they did show that there was no residual olefin content in the samples and thus full conversion of the monomer and macromer had been achieved.

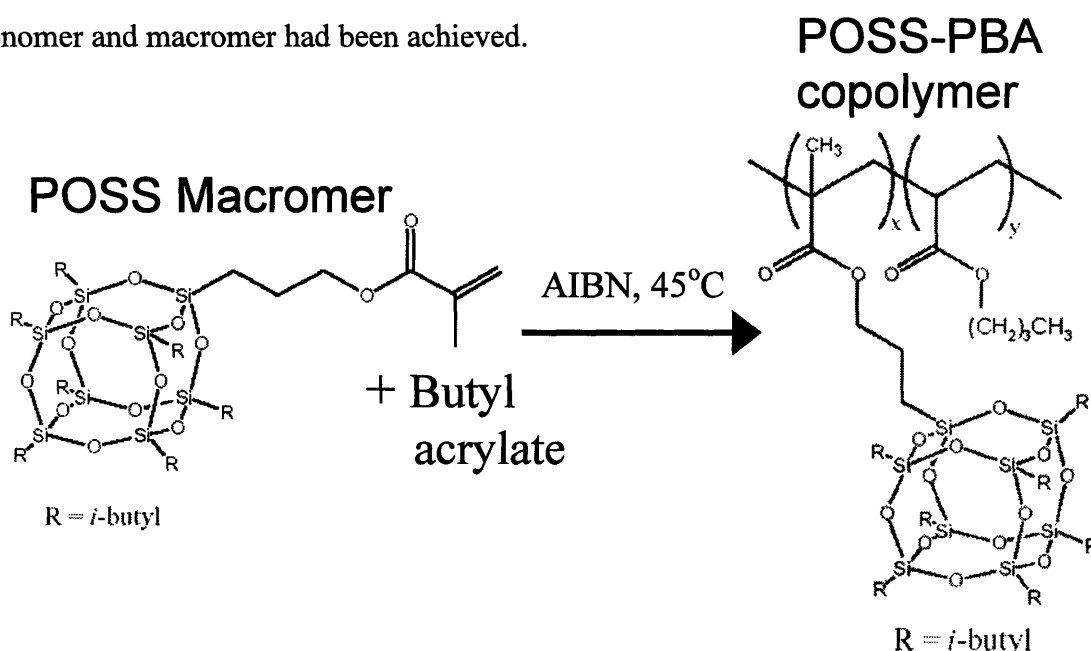


Figure 6.9 – Reaction scheme for in-situ polymerization of POSS-PBA copolymers

6.3.5 - Wide Angle X-ray Diffraction of POSS-PBA copolymers

In Figure 6.10 wide angle x-ray diffraction (WAXD) spectra are plotted for the PBA control and for copolymers containing 26, 40, and 50 wt% POSS on the chain. When comparing the POSS-PBA copolymer spectra to the POSS-PMMA spectra in Figure 6.4 it is clear that the POSS groups are significantly more ordered in the POSS-PBA copolymers. The POSS-PBA copolymers exhibit sharp peaks of increasing height as the POSS content increases. At 26 wt% POSS, there is a short but relatively sharp peak at

$2\theta = 8.2^\circ$ ($d = 1.06$ nm). This peak shows a dramatic increase in intensity as the POSS content in the polymer increases to 40 wt% and then further to 50 wt%. The location of the peak is also much closer to the highest crystalline peak in the macromer ($d = 1.10$ nm, Figure 6.4) than the analogous peak in the POSS-PMMA copolymers. Clearly the POSS has the ability to crystallize in the butyl acrylate matrix whereas this phenomenon is significantly hindered in the PMMA matrix.

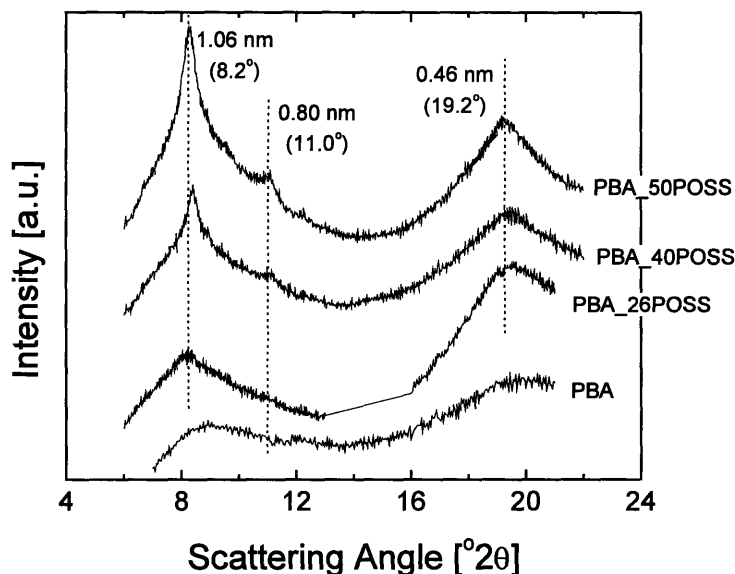


Figure 6.10 – Wide angle x-ray diffraction patterns for POSS-PBA copolymers

6.3.6 - Thermomechanical Properties of POSS-PBA Copolymers

The effect of these crystalline POSS domains on the thermomechanical properties of the polymers was analyzed using both DSC and DMA. In Figure 6.11 DSC traces for the POSS-PBA copolymers are shown. The PBA curve shows a glass transition centered at $T = -52^\circ\text{C}$. The 26 wt% copolymer also shows no thermal events other than the glass transition, which is slightly higher at $T = -48^\circ\text{C}$. The 40 wt% POSS copolymer has a substantially higher T_g of $T = -42^\circ\text{C}$ and also shows an endotherm at $T = 55^\circ\text{C}$

corresponding to the melting of the crystallites in the POSS matrix. The magnitude of the endotherm is 2.2 J/g. The 50 wt% POSS copolymer has a slightly higher melting point ($T = 62^{\circ}\text{C}$) and a slightly greater heat of fusion (2.6 J/g). From the WAXD spectra in Figure 6.10 there appears to be only minimal crystalline content at 26 wt% but significant crystalline content at 40 wt% and 50 wt%, thus it is not surprising that no melting endotherm is observed in the 26 wt% POSS-PBA copolymer.

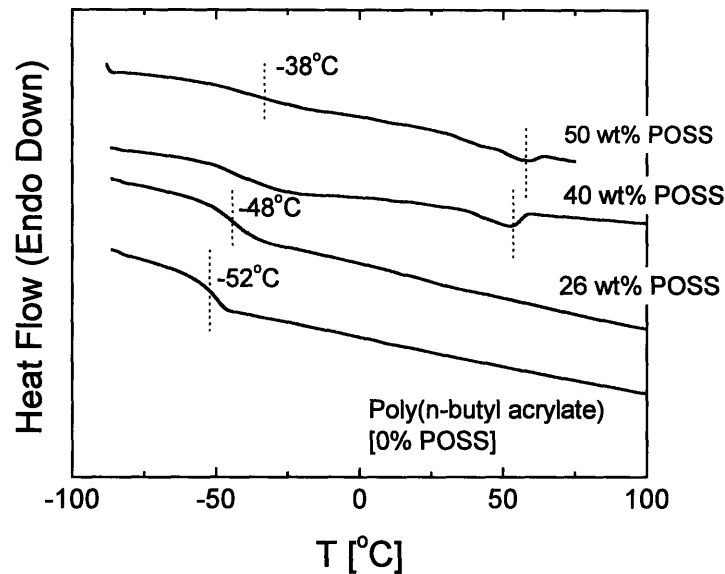


Figure 6.11 – DSC curves for POSS-PBA copolymers

The DMA results in Figures 6.12 and 6.13 are even more intriguing. The storage modulus E' is shown in Figure 6.12 for samples containing between 0 and 50 wt% POSS. The pure PBA sample and the specimen containing 13 wt% POSS were both tacky rubbers that were difficult to cut into well-defined geometries, thus the absolute magnitudes of the storage moduli for these samples is not very accurate. However, the horizontal location of the thermal transitions should not be affected by this problem. The shape of the pure PBA curve shows only one significant feature: the glass transition

which begins around $T = -40^{\circ}\text{C}$. A similar shape is observed in the 13 wt% POSS sample, however the onset of the T_g occurs at a slightly lower temperature. At this low POSS loading, the POSS is unable to crystallize to any significant degree and thus it behaves as an internal plasticizer as it does in the POSS-PMMA copolymers discussed earlier. At 26 wt% a secondary plateau begins to appear over the range $0^{\circ}\text{C} \leq T \leq 60^{\circ}\text{C}$. This plateau increases in magnitude as the POSS content is further increased. The magnitude of the plateau at 50 wt% POSS (34 MPa) is more than two orders of magnitude greater than the plateau of the pure PBA (0.1 MPa).

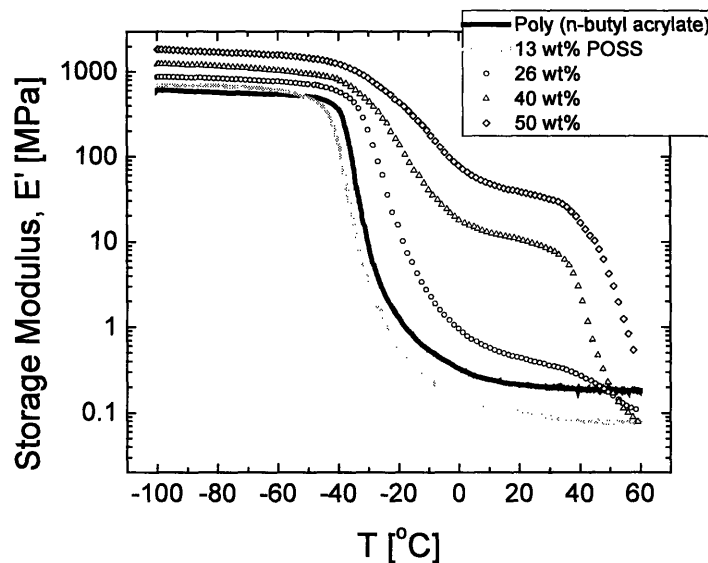


Figure 6.12 – Tensile storage moduli of POSS-PBA copolymers measured in dynamic mechanical analysis

The α -transitions of the copolymers with 26 wt% POSS or greater, visible in Figure 6.13, shift to significantly higher temperatures compared with the PBA homopolymer. An expanded view of the temperature range $30^{\circ}\text{C} \leq T \leq 60^{\circ}\text{C}$ shows a second loss peak in the high POSS content polymers. The melting of the isobutyl-POSS

nanocrystals leads to a peak at $T = 41^\circ\text{C}$ in the 40 wt% blend and a peak at $T = 50^\circ\text{C}$ in the 50 wt% blend.

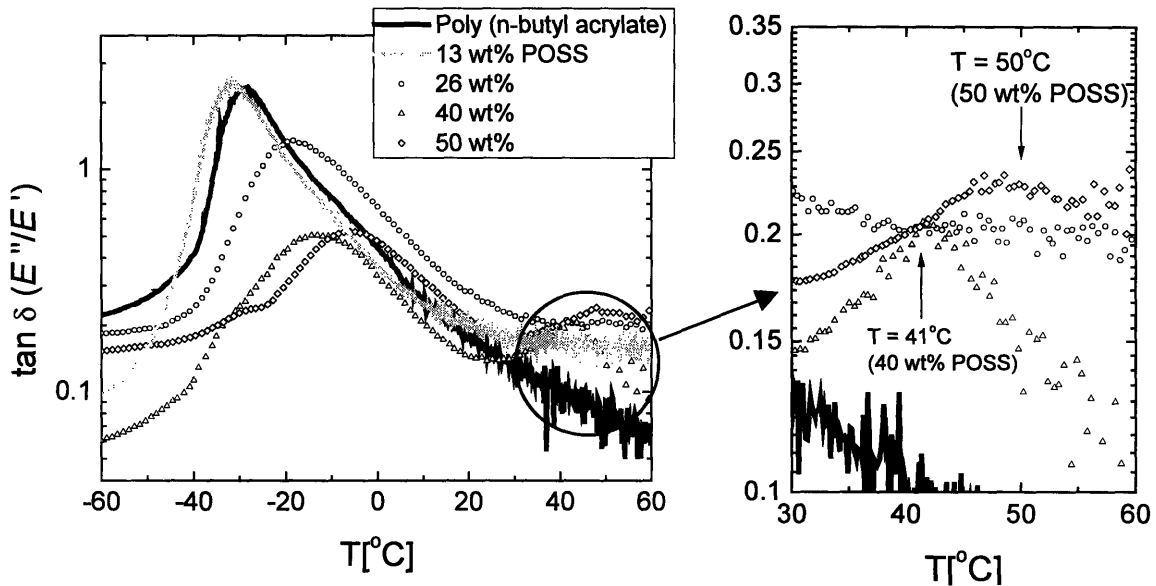


Figure 6.13 – Loss tangent of POSS-PBA copolymers showing the α -transition of the butyl acrylate (left) and the peak associated with melting of tethered-POSS crystals (right)

6.3.7 - Tensile Properties of POSS-PBA Copolymers

The tensile properties of the POSS-PBA copolymers are plotted in Figure 6.14. As with the DMA measurements, well-defined samples were difficult to make for the pure PBA and the 13 wt% sample, thus the absolute accuracy of these two (particularly on the horizontal axis), is difficult to gauge. However, it can be easily observed that these two samples have an extremely low modulus (≈ 0.2 MPa) and thus they deform freely with virtually no resistance and are able to regain their original shapes after strains of greater than 500%. The 26 wt% POSS sample, which showed a minor effect of crystallinity of the POSS domains in WAXD and DMA, has a significantly higher modulus ($E = 0.6$ MPa), however it still retains some tack at room temperature. The sample at 40 wt% POSS is where the sample takes on a more rigid constitution and no

longer retains a noticeable amount of tack. The modulus jumps by an order of magnitude over that at 26 wt% and a moderate drop in the strain-at-break is observed. The 50 wt% POSS sample increases further in stiffness to a room temperature modulus of $E = 34$ MPa. This material does not deform and fracture in the same fashion as the more rubbery polymers. It is stiff and difficult to deform by hand and thus when deformed in the tensile experiment most of the deformation is plastic in nature and thus is retained when the stress is released. The polymer fractures more like a solid than like a rubber.

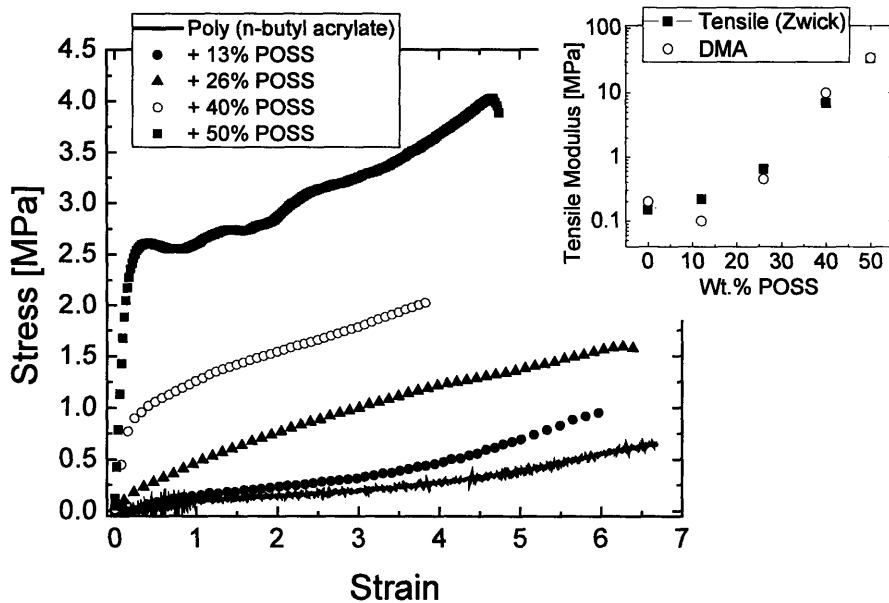


Figure 6.14 – Tensile properties of POSS-PBA copolymers taken at a strain rate of 0.02 s^{-1}

Figure 6.15 shows qualitative differences between four of the polymers: pure PBA, 26 wt% POSS, 40 wt%, and 50 wt%. The pictures show that both the PBA and the 26 wt% sample deform easily with only minor applied tension, and upon the release of the tension they retain their original shape. The 40 wt% sample does not deform as easily, but can still be pulled to small strains with a significant tensile stress. The polymer does

then return to near its original shape, however a small amount of plastic deformation occurs. The 50 wt% sample is too stiff to deform by hand but the 1 mm thick film shown in Figure 6.15 can be bent back and forth without requiring high bending stresses.



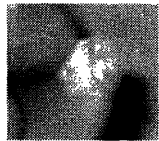







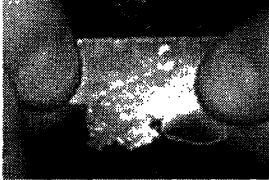
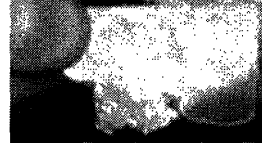
	Before stress	Stressed	After stress
Pure PBA		Easily deformable 	
26 wt% POSS		Easily deformable 	
40 wt% POSS		Much stiffer 	
50 wt% POSS		Doesn't deform 	

Figure 6.15 – Qualitative pictures showing deformability and retraction in POSS-PBA copolymers

6.4 – Discussion

There is a fundamental difference between the POSS-PMMA copolymers and the POSS-PBA copolymers discussed above. The tethered-POSS groups are able to order into nanocrystallites in the PBA-based polymers but not in the PMMA-based ones. The reason is simple: PBA has a glass transition temperature significantly lower than the temperature at which the POSS groups can crystallize whereas PMMA has a T_g that is significantly higher.

In the POSS-PBA copolymers, the unreacted macromer is initially randomly dispersed throughout the solution. As polymerization progresses at $T = 45^\circ\text{C}$, the system loses significant configurational entropy as the molecular weight increases over time²⁶ and the POSS and the butyl acrylate segments develop a thermodynamic tendency to phase separate. They are unable to macrophase separate, however, and the POSS moieties are thus restricted to forming nanoscopic crystallites.⁷ The shape of these domains is a point of debate¹³ (see Chapter 1) and not important to the current discussion; the important point is that this self-assembly has been repeatedly shown to occur at high volume fractions of POSS. At no point does the reaction mixture vitrify, thus the POSS units are free to associate once the loss in configurational entropy due to the assembly is offset by the enthalpic gain from the POSS crystallization. The mild crosslinking in the POSS-PBA polymers does not allow the chains to reptate over long distances, however this is not necessary in order for the POSS to crystallize. The chains need only locally rearrange. These motions will be governed by Rouse modes and thus the self-assembly should not be heavily dependent on molecular weight. It will, however, depend on crosslink density.

The POSS-PMMA copolymerization, on the other hand, is far different. The same loss in configurational entropy occurs due to the huge increase in molecular weight, but as the number average molecular weight of the system M_n increases beyond a critical value ($M_n \approx 10,000$ g/mol), the matrix vitrifies, kinetically locking the tethered POSS cages in place. The POSS cannot assemble into crystallites beyond this point. It is possible that the isobutyl-POSS groups could crystallize during the in-situ reaction process before vitrification, however the post-curing process at $T = 120^\circ\text{C}$ ensures that both the POSS ($T_m \approx 55^\circ\text{C}$) and the PMMA ($T_g = 110^\circ\text{C}$) are above their primary thermal transition temperatures. Thus upon cooling the PMMA matrix vitrifies long before the POSS can crystallize, locking the unassembled POSS cages in place.

In light of these points, the opposite effect of the isobutyl-POSS on the glass transition temperature of the copolymers makes sense. The POSS-PBA copolymers have large concentrations of ordered POSS domains. To accommodate these crystallites, the PBA segments between POSS groups (which on average are approximately 10 segments long) will be confined between the crystallites. The confinement effect in this case causes an increase in the glass transition temperature, likely due to the connectivity between the POSS and the PBA. In the POSS-PMMA system, the POSS is not contained in nanocrystallites, yet there is still evidence for POSS association from the broad peaks in the WAXD spectra in Figure 6.4. It is likely that the PMMA will be confined at the high POSS weight fractions analyzed in the current study, however in this case the POSS cages are above their melting point when T_g is reached, thus these inclusions will tend to plasticize rather than reinforce, and the glass transition temperature decreases as POSS content is increased, and the increase is considerably larger as the loading is increased.

It is possible, based on the precipitous drop in the glass transition temperature with increasing isobutyl-POSS content, that if the POSS content in a copolymer with PMMA were increased to a high enough level (≥ 60 wt%) that the glass transition temperature would drop below the crystallization point of the POSS nanocrystals and self-assembly could occur in the PMMA matrix. In Figure 6.16, it is apparent that the decrease in the glass transition temperature with weight fraction of POSS accelerates with increasing POSS content. Depending on the trajectory of the system above 50 wt%, it is conceivable that a POSS-PMMA copolymer containing 60 wt% POSS on the chain would have a $T_g \leq 55^\circ\text{C}$, which is the melting point of the POSS crystals in PBA. It is unclear whether the POSS crystals would melt or crystallize at the same point in a PMMA matrix as they do in a PBA matrix. It is possible that the POSS would crystallize at a higher temperature in the PMMA due to the loss of entropy as the polymer approaches its glass transition. This would allow a self-assembled system to be produced in a PMMA matrix using a POSS species with melting point below the T_g of the polymer matrix.

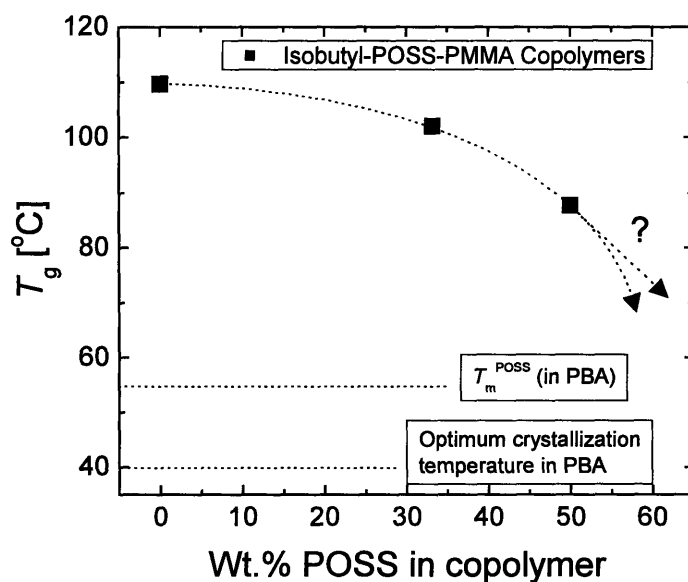


Figure 6.16 Glass transition temperature of POSS-PMMA copolymers showing potential trajectories of higher POSS content copolymers

A separate way in which self-assembly of the POSS could be achieved in the PMMA matrix would utilize results from Waddon and Coughlin.⁷ In their study, polyethylene(PE) was copolymerized with a norbornyl-cyclopentyl-POSS macromer to create what was essentially a cyclopentyl-POSS-PE copolymer. At high POSS contents (≥ 37 wt%), both the PE and the cyclopentyl-POSS on the copolymer chain had a tendency to form separate crystal domains. This can be observed in the WAXD spectra for the polymer PE-POSS4 (56 wt% POSS) (curve (ii) in Figure 6.17). However, by dissolving the copolymers in xylene and then precipitating with acetone (a non-solvent for PE but a good solvent for the POSS macromer), the crystallization of the POSS was frustrated due to the fact that the PE was able to crystallize first, thereby locking the POSS in a nearly amorphous configuration. Curve (iii) in Figure 6.17 shows the effect of this precipitation procedure on the WAXD spectrum for the PE-POSS4 copolymer. Whereas a sharp peak is apparent at $2\theta = 8.2^\circ$ in curve (ii), only a very broad and shallow peak is present in the spectrum in curve (iii). The copolymers from curve (ii), with enhanced POSS crystallinity, showed substantially better thermo-oxidative stability than the copolymers in curve (iii).

While Waddon and Coughlin showed the ability to suppress crystallization of POSS by precipitating with a non-solvent for the polymer that solvated the POSS, it seems reasonable that the reverse process could be attempted on the POSS-PMMA copolymers of the present study. One could imagine dissolving the 10 mol% (50 wt%) POSS-PMMA copolymer in a good solvent (e.g. THF) and then precipitate with a non-solvent for the isobutyl-POSS that is a good solvent for the PMMA. This would allow a

route around the problem of the polymer having a higher glass transition temperature than the melting temperature of the POSS.

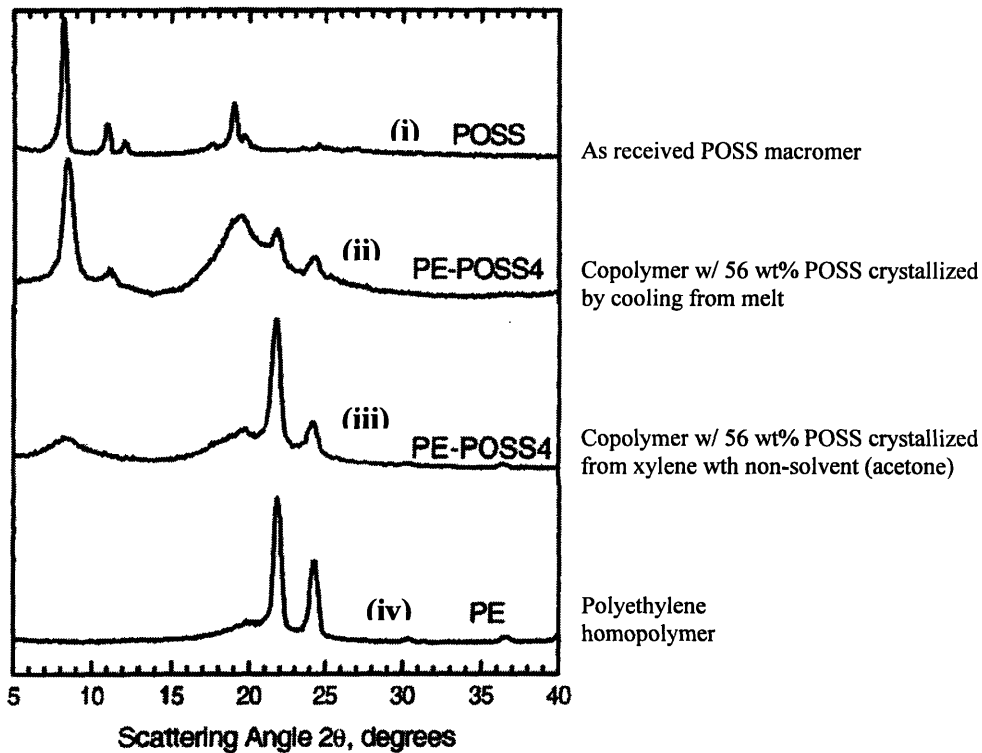


Figure 6.17 – Wide angle x-ray diffraction patterns of PE-POSS copolymers taken from paper by Coughlin et al. (Nano Letters, 2002)

6.5 – Conclusions

The relation of the polymer's glass transition temperature was shown to be the dominant factor in determining whether tethered-isobutyl-POSS cages could form nanocrystallites within acrylic polymer matrices. Incorporation of isobutyl-POSS into PMMA led to a decrease in the glass transition temperature and significant embrittlement at high weight fractions of POSS. Adding the same POSS cage to a poly(*n*-butyl acrylate) matrix instead led to an increase in the glass transition temperature of the matrix, an increase in the tensile modulus, and completely removed the inherent tackiness of the

PBA matrix. A future study producing random copolymers of butyl acrylate and methyl methacrylate (with high POSS content) would shed light on whether the mechanical properties can be optimized at a given ratio of BA to MMA. This optimized ratio should allow the POSS to self-assemble (T_g should be $< 50^\circ\text{C}$) yet would also have a higher modulus than the pure POSS-PBA polymers.

References

- (1) Haddad, T. S.; Lichtenhan, J. D. *Macromolecules* **1996**, *29*, 1996.
- (2) Lichtenhan, J. D.; Otonari, Y. A.; Carr, M. J. *Macromolecules* **1995**, *28*, 8435-8437.
- (3) Romo-Urbe, A.; Mather, P. T.; Haddad, T. S.; Lichtenhan, J. D. *Journal of Polymer Science Part B-Polymer Physics* **1998**, *36*, 1857-1872.
- (4) Mather, P. T.; Jeon, H. G.; Romo-Urbe, A.; Haddad, T. S.; Lichtenhan, J. D. *Macromolecules* **1999**, *32*, 1194-1203.
- (5) Zheng, L.; Farris, R. J.; Coughlin, E. B. *Macromolecules* **2001**, *34*, 8034-8039.
- (6) Zheng, L.; Farris, R. J.; Coughlin, E. B. *Journal of Polymer Science Part a-Polymer Chemistry* **2001**, *39*, 2920-2928.
- (7) Waddon, A. J.; Zheng, L.; Farris, R. J.; Coughlin, E. B. *Nano Letters* **2002**, *2*, 1149-1155.
- (8) Zheng, L.; Waddon, A. J.; Farris, R. J.; Coughlin, E. B. *Macromolecules* **2002**, *35*, 2375-2379.
- (9) Mather, P. T.; Wu, J.; Haddad, T. S. In *Society of Rheology Annual Meeting*: Pittsburgh, PA, 2003.
- (10) Pyun, J.; Matyjaszewski, K.; Wu, J.; Kim, G. M.; Chun, S. B.; Mather, P. T. *Polymer* **2003**, *44*, 2739-2750.
- (11) Zheng, L.; Hong, S.; Cardoen, G.; Burgaz, E.; Gido, S. P.; Coughlin, E. B. *Macromolecules* **2004**, *37*, 8606.
- (12) Lee, A.; Xiao, J.; Feher, F. J. *Macromolecules* **2005**, *38*, 438.
- (13) Jeon, H. G.; Mather, P. T.; Haddad, T. S. *Polymer International* **2000**, *49*, 453.
- (14) Kopesky, E. T.; Haddad, T. S.; Cohen, R. E.; McKinley, G. H. *Macromolecules* **2004**, *37*, 8992.
- (15) Matejka, L.; Strachota, A.; Plestil, J.; Whelan, P.; Steinhart, M.; Slouf, M. *Macromolecules* **2004**, *37*, 9449.
- (16) Constable, G. S.; Lesser, A. J.; Coughlin, E. B. *Macromolecules* **2004**, *37*, 1276.
- (17) Choi, J.; Yee, A. F.; Laine, R. M. *Macromolecules* **2004**, *37*, 3267.
- (18) Kim, G.-M.; Qin, H.; Fang, X.; Sun, F. C.; Mather, P. T. *Journal of Polymer Science Part B: Polymer Physics* **2003**, *41*, 3299.
- (19) Fu, B. X.; Namani, M.; Lee, A. *Polymer* **2003**, *44*, 7739.
- (20) Choi, J.; Yee, A. F.; Laine, R. M. *Macromolecules* **2003**, *36*, 5666.

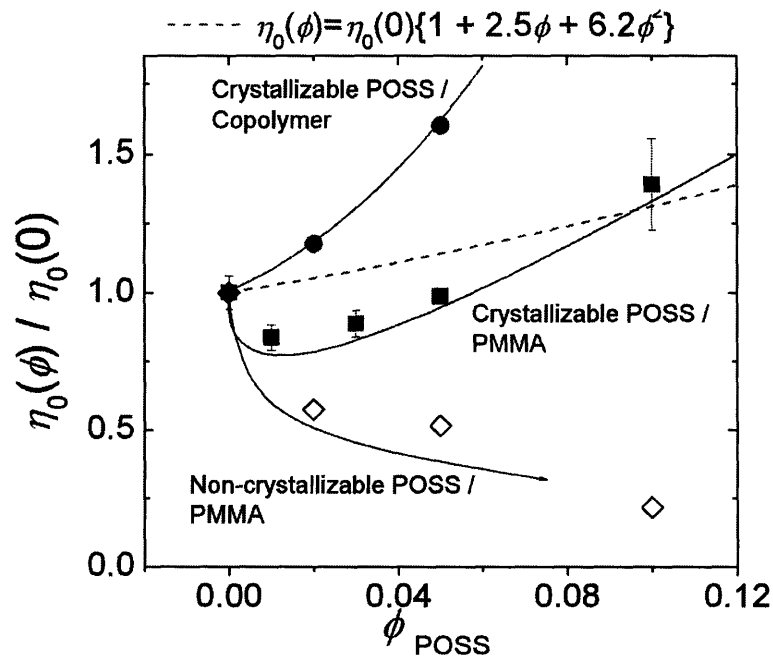
- (21) Li, G. Z.; Wang, L. C.; Toghiani, H.; Daulton, T. L.; Koyama, K.; Pittman, C. U. *Macromolecules* **2001**, *34*, 8686.
- (22) Lee, A.; Lichtenhan, J. *Macromolecules* **1998**, *31*, 4970.
- (23) Liu, H.; Zheng, S. *Macromolecular Rapid Communications* **2005**, *26*, 196.
- (24) Pan, G.; Mark, J. E.; Schaefer, D. W. *Journal of Polymer Science Part B: Polymer Physics* **2003**, *41*, 3314.
- (25) Ferry, J. D. *Viscoelastic Properties of Polymers*, 3 ed.; John Wiley & Sons: New York, 1980.
- (26) Flory, P. J. *Principles of Polymer Chemistry*; Cornell University Press: Ithaca, 1953.

Chapter 7: Conclusions and Future Work

7.1 – Conclusions

The linear viscoelastic results from Chapters 2 and 3 show that POSS can reinforce or plasticize PMMA melts, depending on the degree of dispersion of the POSS and the interaction between the PMMA and the POSS. In the case of a well-dispersed POSS cage with an essentially athermal interaction with the PMMA matrix (Chapter 3), plasticization of the melt occurs, along with a decrease in the glass transition temperature. In melts containing the crystallizable cyclohexyl-POSS (Chapter 2), an initial decrease in the viscosity occurs followed by a significant increase at high loadings (> 5 vol%). For blends of a POSS-PMMA copolymer blended with POSS filler (Chapter 2), a significant increase in viscosity is observed at all loadings.

The combination of two different types of POSS species was shown to lead to significant toughening of PMMA in Chapter 5. The toughening was observed in slow-speed tension tests and high-rate split Hopkinson pressure bar tests. The tensile toughening was due to significant debonding of particles from the PMMA matrix which



made crack propagation more difficult.

The results from Chapter 6 show that the glass transition temperature of the polymer matrix is an important factor in determining whether the POSS moieties in a copolymer can crystallize. POSS particles were unable to self-assemble in a PMMA matrix, which had a T_g above the melting point of the POSS, while the same POSS particles were able to self-assemble in a polybutyl acrylate matrix. The randomly-dispersed POSS had a detrimental effect on the properties of the PMMA while the self-assembled POSS had a beneficial effect on the properties of the PBA.

7.2 – Future Work

7.2.1 – Optimization of Mechanical Properties

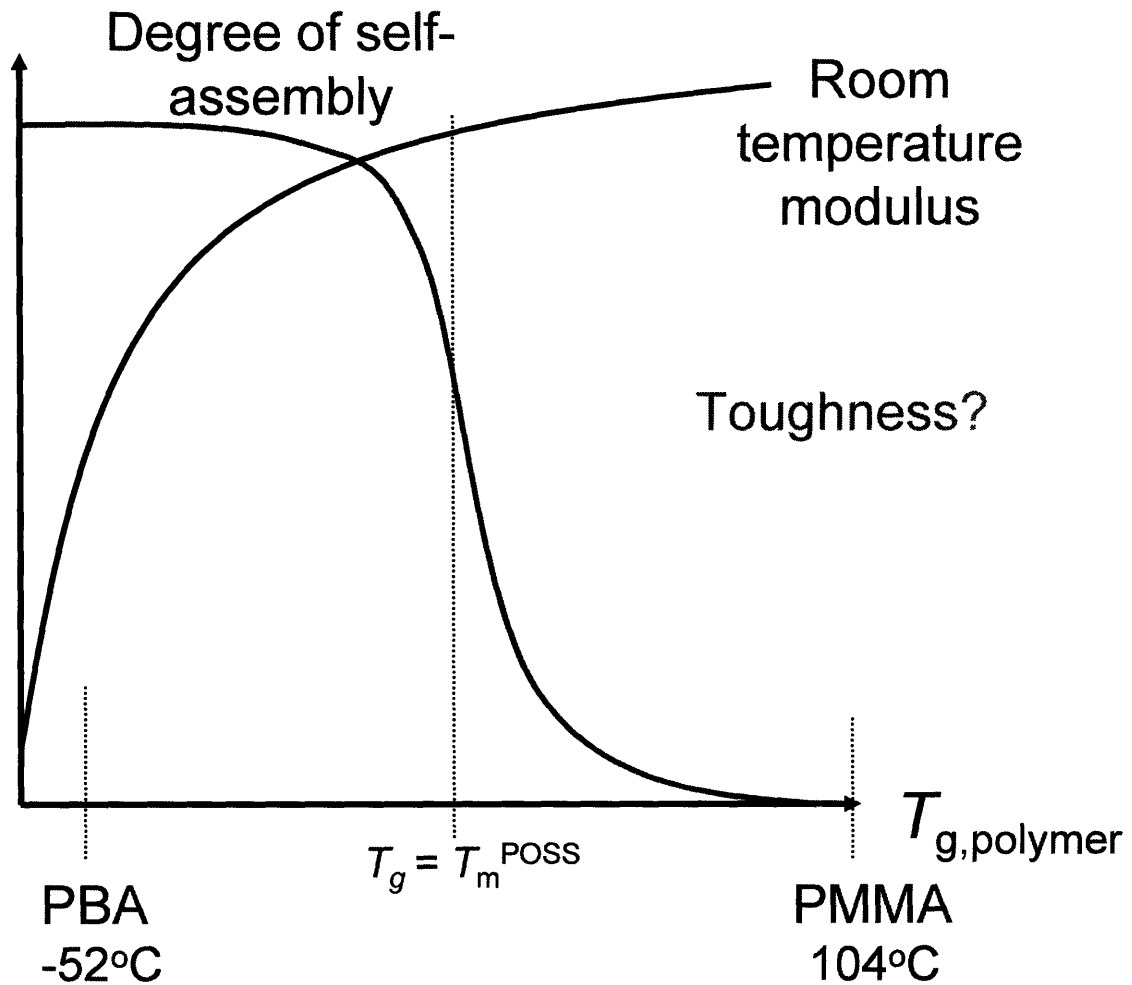
In Chapter 5, the mechanical testing results showed that POSS filler had the ability to toughen PMMA, particularly when a combination of a molecularly-dispersed POSS component and a phase-separated POSS component was used. However, the optimum amounts of the dispersed and phase separated components is still not clear. Smaller amounts of POSS appeared to be better, but the ratios of the two POSS components would be an interesting optimum to pursue. In addition, use of a more common plasticizer like DOP in place of the dispersed POSS phase would help shed light on whether this toughening is unique to the two POSS system or is instead a more general property of phase-separated-POSS/plasticizer systems.

7.2.2 –Use of POSS in Elastomers for Shape Memory Applications

Too much work to this point has focused on using POSS in rigid, glassy polymers and too little has focused on incorporating POSS into elastomeric matrices and using its self-assembly properties to enhance the mechanical properties of rubbers. Future studies

should recognize that POSS is not a particularly good reinforcing agent [as can be seen in Chapter 5 for glassy polymers] but can be a significant reinforcing agent for rubbers.

An interesting application for POSS in elastomers is in the field of shape memory polymers. It is important in designing shape memory materials that the glass transition temperature and the rubbery modulus be controlled independently. POSS –based materials offer this possibility: the rubbery modulus can be controlled by the POSS content and the glass transition temperature can be controlled by the polymer matrix (e.g. butyl acrylate, methyl methacrylate, butyl methacrylate, or a copolymer).



7.2.3 – Adhesive Applications

The results from Chapter 6 show that POSS can enhance the mechanical properties of the normally tacky poly(*n*-butyl acrylate). Qualitative observations from POSS-copolymer films cast on glass have shown that there is a tremendous adhesive strength between the copolymer and the glass. On the other hand, cast films of POSS-filled homopolymer do not adhere well to glass. Further studies on these POSS-PBA copolymers would be useful to determine whether improvements in properties such as creep resistance, adhesive strength, and dimensional stability can be improved over non-hybrid PBA adhesives. The enhanced adhesion to glass may be useful in interlayer glass laminates like those used in car windshields.

Appendices

A-1: Stress-Strain Properties of a Cyclohexyl-POSS-PMMA copolymer containing Cyclohexyl-POSS filler

A side study was performed to complement the results of Chapter 5, particularly the results in Figure 5.19 that showed the effect of adding a small amount (10 wt%) of a cyclohexyl-POSS-PMMA copolymer to a blend of 5 wt% cyclohexyl-POSS filler in PMMA. The copolymer was added in order to improve the adhesion between the cyclohexyl-POSS filler particles and the PMMA matrix. The effect observed in Figure 5.19 was that the enhanced adhesion due to the copolymer actually embrittled the samples. All of these samples broke before yielding.

Samples of cyclohexyl-POSS filler blended with only the copolymer (no PMMA homopolymer) were also prepared. Cyclohexyl-POSS loadings of 5, 10, and 20 wt% were analyzed. Representative stress-strain curves in slow-speed tension (strain rate = $3.3 \times 10^{-3} \text{ s}^{-1}$) are shown in Figure A.1. The curves for the unfilled copolymer and the PMMA homopolymer are also plotted. The yield stress of the PMMA is significantly higher than the yield stress of the copolymer, which contains 15 wt% cyclohexyl-POSS on the chain. At the lowest loading of 5 wt% cyclohexyl-POSS filler in the copolymer, the yield stress decreases and the modulus also decreases significantly (from $E = 2.54 \text{ GPa}$ to $E = 2.23 \text{ GPa}$, see inset to Figure A.1). Increasing the filler loading to 10 wt% leads to a slight increase in the modulus (to $E = 2.39 \text{ GPa}$) and also maintains the same level of the yield stress as that observed in the 5 wt% blend. Further addition of filler to 20 wt% causes a significant decrease in both the yield stress and the modulus. In Figure 5.4(a), the cyclohexyl-POSS-filled PMMA homopolymer blends showed a similar trend with increasing POSS loading: a slight decrease in modulus at the lowest loading (2.5 wt%)

followed by an increase at the next highest loading (5 wt%), and finally a significant decrease at the highest loading (10 wt%). The trend in the yield stress was also similar.

The loadings analyzed in the present study are higher, however.

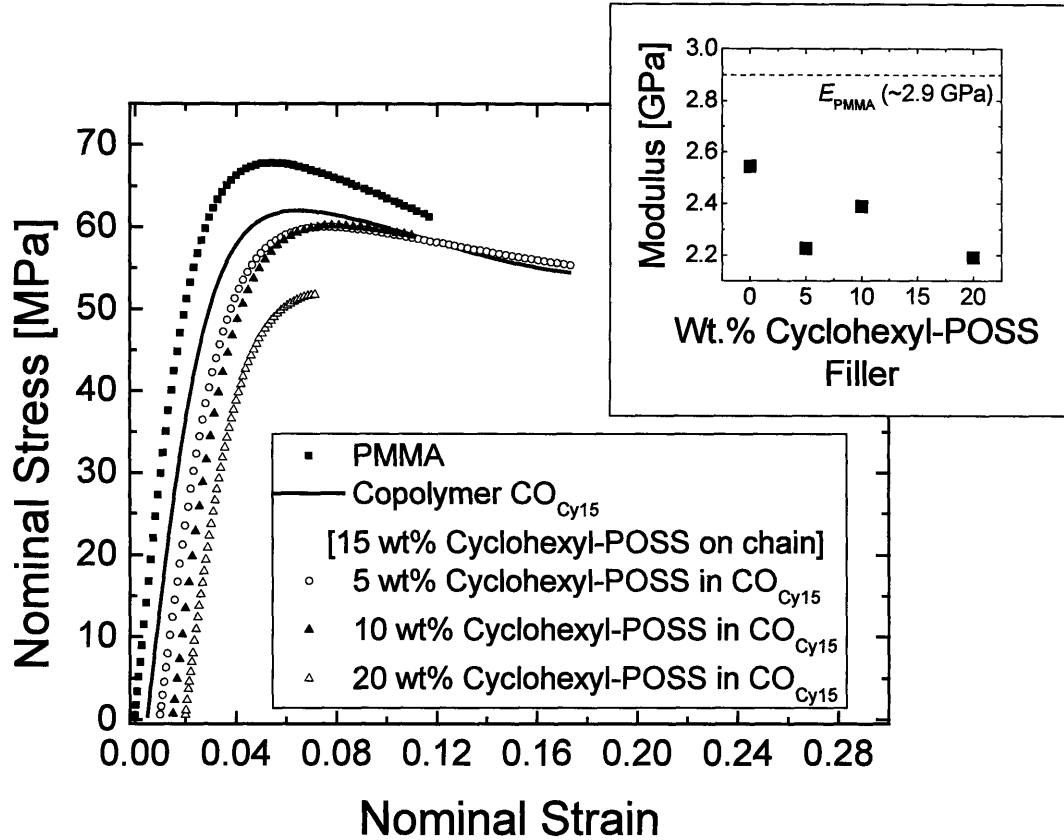


Figure A.1 Tensile stress-strain behavior of a POSS-PMMA copolymer CO_{Cy15} containing 15 wt% cyclohexyl-POSS tethered to the chain blended with different amounts of cyclohexyl-POSS filler. The stress-strain behavior of the PMMA homopolymer used throughout the thesis research has been plotted for comparison. Curves have been offset horizontally by a factor of $\epsilon = 0.005$.

The reason for this non-monotonic trend is due to the two states of dispersion present in the POSS-PMMA blends. In both the filled homopolymer and the filled copolymer blends, the cyclohexyl-POSS has a tendency to phase-separate into crystallites at moderate to high loadings. At low loadings, however, a significant fraction of the

POSS is present in a molecularly-dispersed state. When dispersed on these extremely small scales, the POSS has a plasticizing effect on the modulus, thus the decrease in modulus at low loadings. When the POSS begins to phase-separate out at moderate loadings (5-10 wt%), many nanocrystallites form ($d = 50-250$ nm). These larger particles still contain relatively high surface area and are able to provide reinforcement to the polymer. At high loadings (10-20 wt%), the POSS forms micron-sized crystallites, which weaken the polymer matrix, reducing the modulus and causing embrittlement.

The reason that the non-monotonic trend in the modulus and the yield stress is observed over a wider range of filler loadings in the filled copolymer system (0-20 wt%) compared with the filled homopolymer system (0-10 wt%) is due to the better particle dispersion in the filled copolymer system. The regime of nanodispersion of the POSS is extended to higher filler loadings by the compatibilizing effect that the tethered-POSS on the copolymer has on the thermodynamics of the system.

It is interesting to note that the trend in the strains-at-break is also similar between the data in Figure A.1 and Figure 5.4(a). In the regime of good dispersion [≤ 5 wt% in Figure A.1; ≤ 2.5 wt% in Figure 5.4(a)], both samples are able to yield and draw to strains $\epsilon > 0.15$.

A-2: Rheological Properties of PMMA containing Trisilanol-Phenyl-POSS

In Figure A.2, the storage modulus G' and the loss modulus G'' are shown for unfilled poly(methyl methacrylate) and for blends containing 5 vol% and 10 vol% trisilanol-phenyl-POSS (an incompletely-condensed POSS cage like the one shown in Figure 1.7). This particular POSS species disperses completely in PMMA to loadings as high as 20 vol%, so the loadings investigated in Figure A.2 are well within the completely-dispersed regime. At 5 vol%, there is only a minimal effect of the POSS on the linear viscoelastic properties. At reduced frequencies $a_T\omega > 10^2$ rad/s, the storage moduli of the PMMA and the 5 vol% blends are virtually identical. At lower frequencies the POSS-filled sample is slightly less elastic. In particular, it enters the terminal flow regime (characterized by slope 2 in G' and slope 1 in G'') at a higher frequency, indicating a lower zero shear rate viscosity. The 10 vol% blend has lower values of the linear viscoelastic moduli over the entire reduced frequency range investigated.

The decrease in the plateau modulus G_N^0 is less pronounced in the trisilanol-phenyl-POSS–PMMA blends than in the methacryl-POSS–PMMA blends (Figures 3.5 and 3.6). This has two root causes. First, the three pendant hydroxyl groups on the trisilanol-phenyl-POSS cages can hydrogen-bond with the ester groups on the PMMA chains. In addition, the phenyl R-groups on the trisilanol-phenyl-POSS cages are much stiffer than the acrylic R-groups on the methacryl-POSS cages. This more rigid nanoparticle, with a more thermodynamically attractive interaction with the polymer chains, would thus be expected to decrease the plateau modulus and the viscosity less significantly.

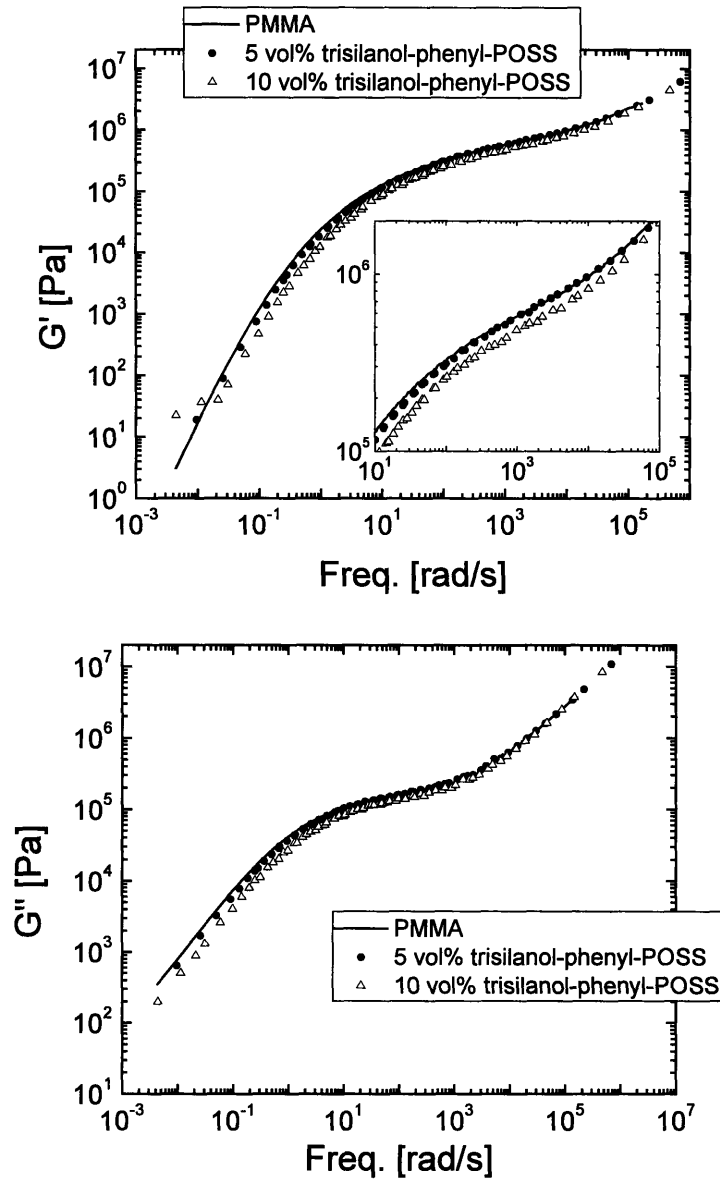


Figure A.2 – Storage modulus and loss modulus of PMMA and trisilanol-phenyl-POSS–PMMA blends

Information can be obtained from the shift factors $a_T(T, T_0)$ that were determined using the WLF framework. In Table A.1 the WLF coefficients c_1^0 and c_2^0 are reported, along with values of the fractional free volume (which is inversely proportional to c_1^0) at the reference temperature $T_0 = 190^\circ\text{C}$ and at the glass transition temperature $T_g(\phi)$. The effect of the POSS is clearly to increase the fractional free volume at a given temperature,

as can be seen by the increase from $f_0/B = 0.050$ for PMMA to $f_0/B = 0.056$ for 10 vol% trisilanol-phenyl-POSS. This explains the decrease in viscosity in the trisilanol-phenyl-POSS blends. Despite the rigidity of the POSS cage and the polar hydroxyl groups on one corner, the geometry of the dispersed POSS cages causes free volume to be generated within the sample. This additional free volume causes a decrease in the glass transition temperature T_g (which, according to Table A.1, occurs at a constant free volume $f_g = 0.029$) as well.

These linear viscoelastic data agree with the trends observed in the tensile properties of POSS–PMMA blends in Chapter 5 [see Figure 5.4(b) and (c)]. The trisilanol-phenyl-POSS blends maintain a nearly constant modulus up to 15 wt% POSS loading (≈ 15 vol%), while the methacryl-POSS–PMMA blends lose approximately 20% of their modulus at a loading of 10 wt%. These results help shed light on the differences between rigid and flexible dispersed POSS cages.

Table A.1 WLF Parameters for PMMA containing trisilanol-phenyl-POSS ($T_0 = 190^\circ\text{C}$)

ϕ_{POSS}	c_1^0	c_2^0 (K)	f_0/B	f_g/B	T_g ($^\circ\text{C}$)
0	8.60	207	0.050	0.029	104
0.05	8.36	203	0.052	0.029	100
0.10	7.76	190	0.056	0.029	98